ASSEMBLED DIBENZYLIDENE SORBITOL DERIVATIVES: AS A CONFINED REACTION MEDIA AND FUNCTIONAL MATERIALS

A THESIS SUBMITTED TO

NATIONAL INSTITUTE OF TECHNOLOGY WARANGAL

DOCTOR OF PHILOSOPHY

IN

CHEMISTRY

BY

REBAKA VARA PRASAD

(Roll No. 701970)

Under the supervision of

Prof. S. NAGARAJAN

Associate Professor

DEPARTMENT OF CHEMISTRY

NATIONAL INSTITUTE OF TECHNOLOGY WARANGAL

HANUMAKONDA-506004

TELANGANA, INDIA.

(July-2024)

Dr. S. NAGARAJAN ‖ डॉ. एस. नागराजन
Associate Professor ‖ सह - प्राध्यापक
Department of Chemistry ‖ रसायनिकी विभाग
e-mail: snagarajan@nitw.ac.in
Phone: 08702462660 (office) ‖ 9940430715 (mobile)

राष्ट्रीय प्रौद्योगिकी संस्थान वारंगल
National Institute of Technology Warangal
An Institute of National Importance
Hanumakonda – 506 004, Telangana State, India

CERTIFICATE

This is to certify that the research work presented in this thesis entitled **"Assembled Dibenzylidene Sorbitol Derivatives: As a Confined Reaction Media and Functional Materials"** submitted by **Mr. Rebaka Vara Prasad** for the degree of Doctor of Philosophy in Chemistry, National Institute of Technology Warangal (Telangana), under my supervision and that the same has not been submitted elsewhere for a degree.

Date: 24.07.2024
Place: NIT Warangal

Dr. S. Nagarajan
Supervisor

DECLARATION

I hereby declare that the work embodied in this thesis entitled **"Assembled Dibenzylidene Sorbitol Derivatives: As a Confined Reaction Media and Functional Materials"** is based entirely on the results of the investigations and research work carried out by me under the supervision of **Prof. S. Nagarajan**, Department of Chemistry, National Institute of Technology Warangal. I declare that this work is original and has not been submitted in part or full, for any degree or diploma to this or any other University.

Date: 24.05.2024 **(Rebaka Vara Prasad)**

Place: NIT Warangal

ACKNOWLEDGEMENTS

The work presented in this thesis would not have been possible without my close association with many people. I take this opportunity to extend my sincere gratitude and appreciation to all those who made this Ph.D. thesis possible.

It gives me immense pleasure and delight to express my deep sense of gratitude to my research supervisor ***Prof. S. Nagarajan*****,** Associate Professor, Department of Chemistry, National Institute of Technology Warangal for his constant unwavering support throughout my Ph.D. His inspiring and valuable guidance made my Ph.D. journey successful. His unfailing attention, unmitigated encouragement, and cooperation have helped me in attaining my goal. It would have been impossible to achieve this goal without his able support and valuable advice. I consider myself fortunate that he has given me a decisive tune, a significant acceleration to my career. I will be thankful to him throughout my lifetime.

I am greatly indebted to ***Prof. Bidyadhar Subudhi*****,** Director, National Institute of Technology Warangal for allowing me to submit my research work in the form of a thesis. I express my gratitude to ***Prof. N. V. Ramana Rao*****,** former Director, National Institute of Technology Warangal for giving me the opportunity to carry out the research work.

My special words of thanks to ***Prof. Santhosh Penta,*** Head, Department of Chemistry, and ***Prof. D. Kashinath, Prof. Vishnu Shanker, Prof. P. V. Srilakshmi,*** former Heads, Department of Chemistry, National Institute of Technology Warangal for their valuable advice, help and support.

I express my sincere thanks to the Doctoral Scrutiny Committee (DSC) members, ***Prof. K. Hari Prasad, Prof. Raghu Chitta, Prof. V. Rajeswar Rao*** (former member), Department of Chemistry and ***Prof. Asim Bikas Das,*** Department of Biotechnology for their support and valuable suggestions.

I take this opportunity to express thanks to ***Prof. A. Ramachandraiah (Retd), Prof. K. Laxma Reddy (Retd)***, ***Prof. K. V. Gobi***, ***Prof. Venkatathri Narayanan, Dr. Raghu Chitta, Dr. B. Srinivas, Dr. M. Raghasudha, Dr. C. Jugun Prakash, Dr. Ravinder Pawar, Dr. Mukul Pradhan, Dr. G. Rajesh Khanna*** and ***Dr. V. Rajesh Kumar*** for their suggestions and encouragement.

Financial assistance from the Government of India, **Ministry of Education (MoE)** in the form of fellowship is gratefully acknowledged.
My sincere thanks to ***Prof. V Sridharan***, University of Hyderabad, Hyderabad, Telangana, ***Dr. C. Uma Maheswari,*** *and* ***Dr. K. Lalitha,*** SASTRA University, Thanjavur, Tamil Nadu for their help in characterization studies.

My special thanks to ***Dr. K. Hari Prasad,*** Associate Professor, faculty in charge (Bruker-400 MHz NMR instrument) for rendering uninterrupted services to run the instrument.

I am very delighted to work with my colleagues ***Mr. Arun Kumar, Ms. Tohira Banoo, Mr. Yogendra Kumar, and Mr. Barath Kumar*** for their support and encouragement during my Ph.D. and this thesis would not have come to a successful completion without the help of these labmates.

Throughout these trying years, a lot of colleagues have supported me and kept me sane. I'm grateful for the jovial help from all of my research colleagues, whom I appreciate with great pleasure, ***Dr. Vinay Pogaku, Dr. A. Bhargava Sai, Dr. Dhanujaya Rao, Dr. Shiva Parvathy, Dr. Suman Chirra, Dr. T. Sanjeeva, Dr. P. Sowmya, Dr. N. Satyanarayana, Dr. P. Babji, Dr. Ch. Raju, Dr. G. Sripal Reddy, Mr. G. Srinath Mr. K. Sampath, Mrs. T. Shirisha, Dr. M. Shireesha, Dr. P. Venkatesham, Dr. A. Naveen Reddy, Mrs.B. Sravanthi, Mr. V Rukya Naik, Dr. Prashanth, Mr. Kancharana Madhu, Ms. Akanksha, Mr. B. Anjaiah, Mr. Ch. Vijay, Mr. N. Nagaraju Yadav, Mr. I. Madhu, Mrs. J. Swathi, Mr. K. Rambabu, Ms. Anshu Kari***, ***Mr. B. Srikanth Goud, Mrs. B. Gayathri, Ms. Nitika, Ms. C. Shruthilaya, Ms. Khushboo Agarwala, Ms. Gargi, Mr. Subir, Ms. Sasi Sree, Ms. Pooja, Mr. Avinash Sharma, Mr. Akash Kumar, Mr. B. Apurba, Mr. Faizan, Mr. Arokiaraj. Mr. K. Ramakrishna, Mr. N. Sumit, Mr. B. Thirupathi, Mr. Anindya Roy, Mr. P. Vijay, Ms. P. Amala***, ***Ms. Amulya, Mr. D. Ravinder,*** and research scholars of various departments.

My special thanks to the non-teaching and technical supporting staff of the chemistry department ***G. Santhosh, K. Sreenivas, P. Heerulal, Md. Shaheen begum, T. Kiran Kumar, J. Praveen, A. Rajini, K. Keshavulu, B. Sadanandam, Ch. Ramesh Babu (late), P. S. Sunil Kumar, P. Abhivardhan, Shirshendu Mondal,*** and ***Atanu Sahoo*** for their help in need.

I take immense pleasure to be grateful to my parents **Rebaka Nageshwara Rao, Venkata Laxmi,** and brother **Srikanth Kumar** for being my support system and pillars of strength. It would be an

understatement to say that I would not be the person I am today without my family. I owe everything to them.

(Rebaka Vara Prasad)

Table of contents

Abstract

Low molecular weight gels (LMWG) undergo self-assembly to form 3D networks that are capable of immobilizing the solvent to form a gel. Over a century, Dibenzylidene sorbitol (DBS), a versatile carbohydrate-based LMWG is well known for its gelation abilities in numerous solvents. It is widely applicable in many industries from personal care to pharmaceuticals. The versatility of DBS stems from its unique combination of hydrophilic hydroxy groups and hydrophobic phenyl groups. By modifying these functional units, various DBS derivatives have been synthesized, and have displayed distinct properties and applications. This study aims to synthesize a new class of DBS derivatives and investigate their potential applications across multiple fields, as well as their utility in organic reactions as a confined reaction media.

An oligomeric dialdehyde derivative of DBS (HBSD) displayed gelation in NMP solvent. Utilizing high solubility for H_2S gas in NMP, a pH-responsive H_2S drug delivery system has been developed. In addition, by adopting the co-gelation process, polyphenylene sulfide is generated in a confined reaction media.

Eutectogel is derived from 4-(hydroxymethyl)-1,3:2,4-dibenzylidene-D-sorbitol (HMDBS) and utilized as a confined media for photochemical reaction for the regioselective synthesis of 4-arylamino-1,2-naphthoquinones in good yield.

Mono- and di-tetrazole DBS derivatives were generated from 4-(cyano)-1,3:2,4-dibenzylidene-D-sorbitol (DNDBS) and sodium azide in confined reaction media by adopting a co-gelation process. Among metallogels prepared from di-tetrazole DBS (DTZDBS), Eu^{3+}-DTZDBS metallogel displayed potential in the fabrication of stimuli-responsive, self-healing Schottky diode.

Furthermore, the research highlights the versatility of DBS as a building block for designing advanced materials with tailored properties and it demonstrates the potential of gel derived from DBS derivatives in organic reactions as a confined media.

List of abbreviations

2D : Two-dimentional

3D : Three-dimensional

ACS14 : 2-acetyloxybenzoic acid 4-(3-thioxo-3H-1,2-dithiol-5-yl) phenyl ester

ADT : 5-(4-hydroxyphenyl)-3H-1,2-dithiole-3-thione

AR : Analytical reagwnt

CGC : Critical gelation concentration

ChCl : Choline chloride

Cys : Cysteine

DBS : 1,3:2,4-dibenzylidene-D-sorbitol

DBS-$CONHNH_2$: 1,3: 2,4-dibenzylidene-D-Sorbitol *p,p'*-dihydrazide

DBS-COOH : 1,3: 2,4-Dibenzylidene-D-Sorbitol-*p,p'*-dicarboxylic acid

DBS-COOMe : 1,3:2,4-dibenzylidene-D-Sorbitol-*p,p'*-dimethylester

DBS-NH_2 : 1,3:2,4-di-(*p*-aminobenzylidene)-D-Sorbitol

DBS-NO_2 : 1,3:2,4-di-(*p*-nitrobenzylidene)-D-Sorbitol

DBS-OMe : 1,3:2,4-di-(*p*-methoxybenzylidene)-D-Sorbitol

DBS-Pyrene : 1,3:2,4-dipyrenylidene-D-sorbitol

DCB : *p*-dichlorobenzene

DCBSD : Deca[1,3:2,4-(O-benzylidine)-D-sorbitol]-dialdehyde

DCC : *N*,*N*′-Dicyclohexylcarbodiimide

DCM : Dichloromethane

DES : Deep eutectic solvent

DMDBS : 1,3:24-Bis-(3,4-dimethylobenzyliden)sorbitol

DMF : *N,N'*-Dimethyl formamide

DMSO : Dimethyl sulfoxide

DNA : Deoxyribonucleic acid

DNDBS : 1,3:2,4-dibenzylidene-D-Sorbitol-*p, p'*- dinitrile

DTZDBS : 1,3:2,4-dibenzylidene-D-Sorbitol-*p,p'*- ditetrazole

EG : Ethylene glycol

EMA : European Medical Agency

EuDTZDBS : metallogel of Eu^{3+} metal with DTZDBS

FDA : Food and Drug Administration

FTIR : Fourier Transform Infrared

GRAS : Generally Recognised as Safe

GSH : Glutathione

GYY4137 : Morpholin-4-ium 4-methoxyphenyl (morpholino) phosphinodithioate

HBA : Hydrogen bond acceptor

HBD : Hydrogen bond donor

H-bonding : Hydrogen bonding

HBSD : Hexa[1,3:2,4-(O-benzylidine)-D-sorbitol]-dialdehyde

HMDBS : 4-(hydroxymethyl)-1,3:2,4-dibenzylidene-D-sorbitol

HUVEC : Human umbilical vein endothelial cells

IEM-DBS : 1,3:2,4-bis-(benzylidene)- 5,6-bis-(carbonylaminoethylmethymethacrylate)-D-Sorbitol

IH : Intimal hyperplasia

ITO : Indium titanium oxide

JK1 : H_2S donor

LCD : Liquid crystal display

LED : Light-emitting diode

LMWG : Low Molecular Weight Gel

LR : Laboratory reagent

MBS : 1,3-Mono benzylidene-D-sorbitol

MOF : Molecular organic framework

MRI : Magnetic resonance imaging

MTZDBS : 1,3:2,4-dibenzylidene-D-Sorbitol-*p*- tetrazole

NADES : Natural deep eutectic solvents

NIR : Near-Infrared

NMDA : N-methyl-D-aspartate

NMP : N-methyl pyrrolidone

NMR : Nuclear magnetic resonance

NPs : Nanoparticles

NTA : N-Thiocarboxyanhydride

OBSD : Octa[1,3:2,4-(O-benzylidine)-D-sorbitol]-dialdehyde

OBSDA : Oligo[1,3:2,4-(O-benzylidene)-D-sorbitol]-dialdehyde

PEG : Polyethylene glycol

PPS : Polyphenylene sulfide

SATO : S -aroylthiooxime

SEM : Scanning electron microscope

SMAB	: Sodium N-methyl-4-aminobutyrate
S_NAr	: Aromatic nucleophilic substitute reaction.
SPRC	: S-propargyl-cysteine
$S_{RN}1$	: Unimolecular Radical Nucleophilic Substitution
TBS	: 1,3:2,4:5,6-Tri benzylidene-D-sorbitol
TBSD	: Tetra[1,3:2,4-(O-benzylidine)-D-sorbitol]-dialdehyde
TEA	: Triethyl amine. Hydrochloride
TEMPO	: 2,2,6,6-tetramethyl-1-piperidinyloxy
TFA	: Trifluoroacetic acid
THF	: Tetrahydrofuran
TLC	: Thin layer chromatography
TTA-UC	: Triplet-triplet annihilation upconversion
UV	: Ultraviolet
VT ^{1}H-NMR	: Variable temperature NMR
XRD	: X-ray diffraction

List of Figures

List of Tables

List of Schemes

CHAPTER-1

INTRODUCTION

1.1 INTRODUCTION

1.1.1 Supramolecular low molecular weight gelators

Supramolecular Low Molecular Weight Gels (LMWG) are a class of fascinating and useful soft materials.[1] Most gels are based on either entangled polymers or covalently cross-linked networks. Recently, LMWG has gained significant interest from researchers worldwide because of their applications in various fields. Gels are formed due to the bottom-up self-assembly of small molecules into 3D structures by means of non-covalent interactions like H-bonding, π-π interactions, donor-acceptor interactions, and weak van der Waal forces, which, at sufficient concentration, entangle themselves to form a crosslinking network that can immobilize a solvent.[2] (Figure 1.1)

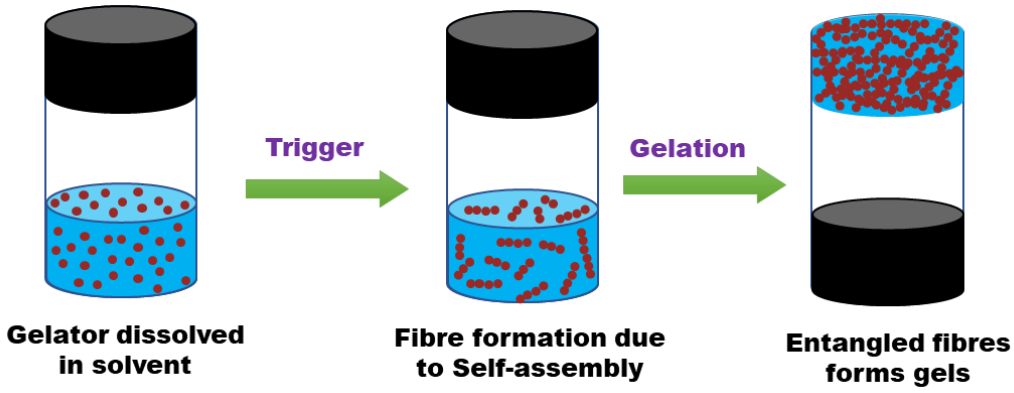

Figure 1.1. Pictorial representation of the formation of a gel.

Gels formed in water, referred to as hydrogels; in organic solvents, referred to as organogels; and in oils, referred to as oleogels. Gels formed by small molecules are different from polymers because the non-covalent interactions in the gels can easily break when external energy, such as heat, mechanical stress, pH, and additives, are applied. Generally, gels are two-component systems comprising a high volume of solvent gelled by a low concentration of a structuring agent. This structuring agent creates a skeleton-type network that entraps the solvent, preventing flow in a steady state. The physical appearance of the gels, whether it is transparent, opaque, or translucent, is decided by the molecular disparity of the gels.[3]

The supramolecular self-assembly of LMWG proceeds in a hierarchical manner, encompassing three distinct levels of organization: (i) the molecular level, where individual gelator molecules interact and assemble; (ii) the fiber level, where these assembled molecules form supramolecular

fibers; and (iii) the network level, where these fibers entangle and intersect to generate the three-dimensional gel network. This hierarchical self-assembly process governs the structural and functional properties of LMWG.[4,5] Gels are ubiquitous materials with substantial applications across various fields (**Figure 1.2**), including food technology,[6] cosmetics,[7] agriculture,[8] catalysis,[9] environmental remediation,[10] pharmaceuticals,[11] batteries materials,[12] and electronics.[13] A wide range of compounds can be used as gelators, including peptides[14], urea derivatives[15], Carbohydrates[16], steroids[17], bile acids[18], lipids[19], nucleobases[20], oligoarenes,[21] and higher alkanes.[22]

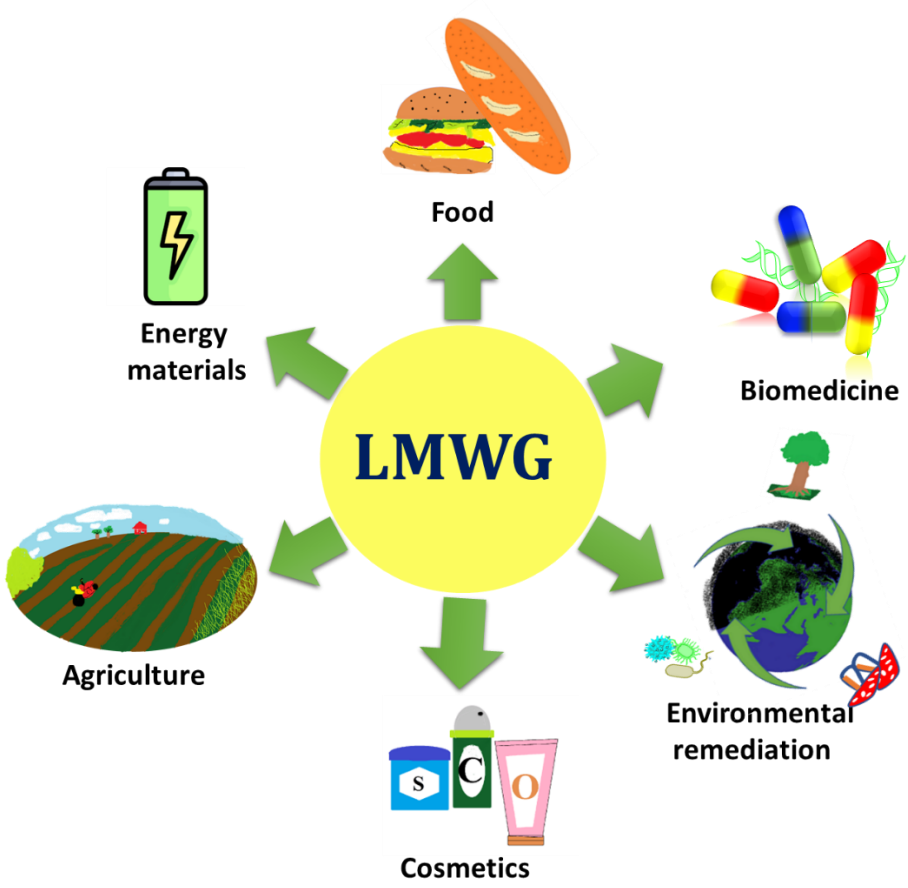

Figure 1.2. Pictorial representation displaying the applications of gels.

1.1.2 Carbohydrates-based LMWG

Carbohydrates have emerged as a promising feedstock for designing and synthesizing LMWG's, owing to their attractive features such as renewability, cost-effectiveness, and biocompatibility, with minimal environmental footprint.[23,24] The structural diversity of natural monosaccharides has

substantially enriched the molecular libraries for gelator design. Consequently, researchers have largely adopted a bottom-up strategy for developing LMWG's with tailored properties, leveraging the versatility of these natural precursors to create application-specific gelators. Carbohydrates are distinguished from other biomolecules by their exceptional structural complexity, rich stereochemical diversity, and vital biological roles.[25] Researchers have extensively investigated carbohydrates as gelators over the past two decades. The self-assembly of sugar derivatives into gels renders diverse applications such as biomolecule separation, liquid crystal formation, optical device development, and controlled drug release, to name a few.[26–30] The abundance of hydroxyl groups in carbohydrates makes them an ideal choice for gelation, as they promote the generation of extensive H-bonding networks. Numerous sugar-based LMWG have been designed and used for various applications (Figure 1.3).

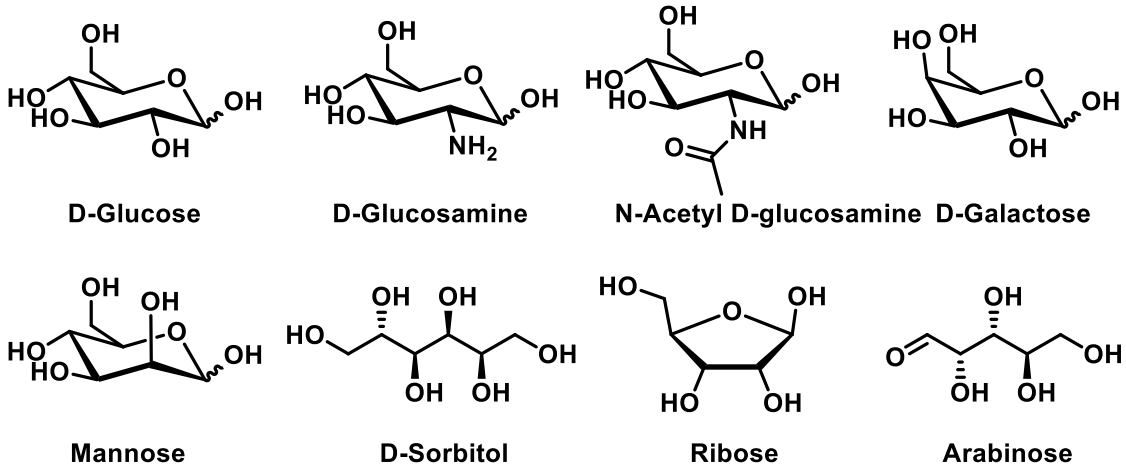

Figure 1.3. Structures of common sugar based LMWG's.

1.1.3 1,3:2,4-Dibenzylidene sorbitol

Meunier, in 1891, synthesized 1,3:2,4-dibenzylidene sorbitol (DBS), a protected version of sorbitol with benzaldehyde.[31] For over a century, DBS has intrigued scientists as a model chiral gelator with its remarkable ability to form gels in various solvents. The synthesis of DBS employs a simple condensation reaction of D-sorbitol, a naturally occurring sugar alcohol known for its water-thickening properties, and benzaldehyde (Scheme 1.1). The molecular structure of DBS exhibits a distinct configuration reminiscent of a butterfly, where the sorbitol moiety forms the central core, analogous to the body, while the delocalized π-electron systems of the benzylidene groups projected outwards, resembling wings. The presence of hydroxyl groups present on the

sorbitol backbone of DBS suggests, potential for intermolecular hydrogen bonding. Additionally, the aromatic rings in DBS offer π-π stacking interactions. These non-covalent interactions are believed to significantly affect DBS's overall supramolecular structure and properties.[32]

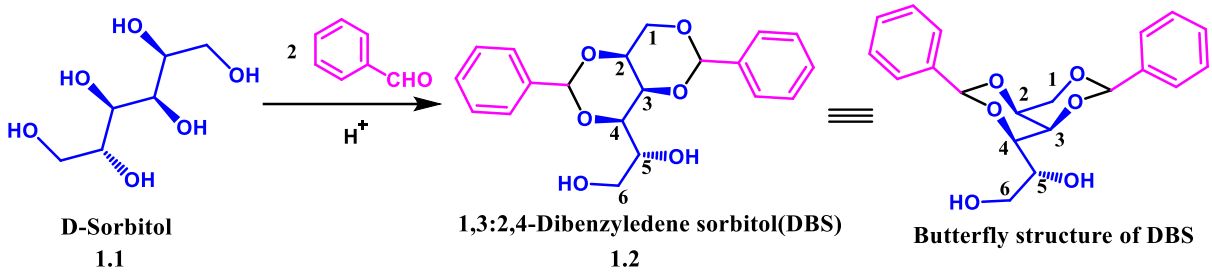

Scheme 1.1. Synthesis of DBS.

1.1.3.1 Unveiling the Isomeric Mystery of DBS

Meunier, in the early 20th century, proposed a condensation reaction between D-sorbitol and benzaldehyde under acidic conditions, which yielded the formation of two isomeric diacetals. Both of them displayed distinctive properties like solubility in water and melting point. During the course of the investigation, one of the isomers displayed gelation.[31]. After its discovery, extensive research was carried out on molecular structure and supramolecular chemistry. Thomas et al. investigated the gelation behavior of DBS in various organic solvents and water.[33] In 1942, Wolfe et al. has performed investigation the synthesis of DBS again and found that along with DBS, mono benzylidene sorbitol (MBS) and tri benzylidene sorbitol (TBS) byproducts were formed (Figure 1.4).[34]

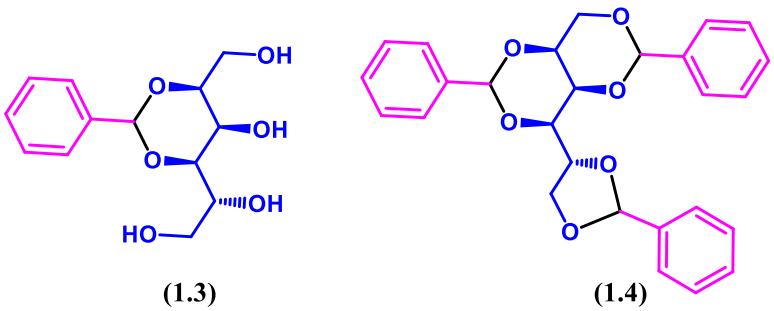

Figure 1.4. Structure of MBS and TBS.

Later in 1944, Angyal et al. performed careful hydrolysis of DBS to give 2,4-mono benzylidene-D-sorbitol, which confirms the 1,3;2,4 diacetal pattern for DBS molecule.[35] An intriguing aspect of DBS lies in the newly formed chiral centers within its ring structure due to cyclization. Since

this process is likely thermodynamically controlled, the bulky phenyl groups can be presumed to occupy the more spacious equatorial positions to minimize steric hindrance. Building upon prior structural investigations, Brecknell et al. employed NMR spectroscopy to elucidate the definite structure of DBS. Their comprehensive analysis gave a conclusion to interpret the assignment of DBS as 1,3(*R*):2,4(*S*)-dibenzylidene-D-sorbitol.[36]

1.1.3.2 Synthetic Strategies for DBS Derivatives

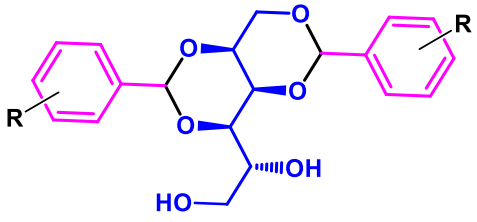

(1.5)

R = -H, -OH,-OMe, -NO_2, -F, -Cl

Figure 1.5. Structure of phenyl ring modified DBS derivatives

Numerous patents filed on DBS are clear evidence of commercial significance. Various protocols have been devised to reduce the side-product in the DBS synthesis.[37–46] From the application point of view, derivatives of the DBS are synthesized by modifying the phenyl rings and carbohydrate moiety. Feng et al.have investigated the synthesis of various DBS derivatives from D-sorbitol and substituted aromatic aldehydes and studied the effect of substituents on the reaction rate (Figure 1.5).[47]

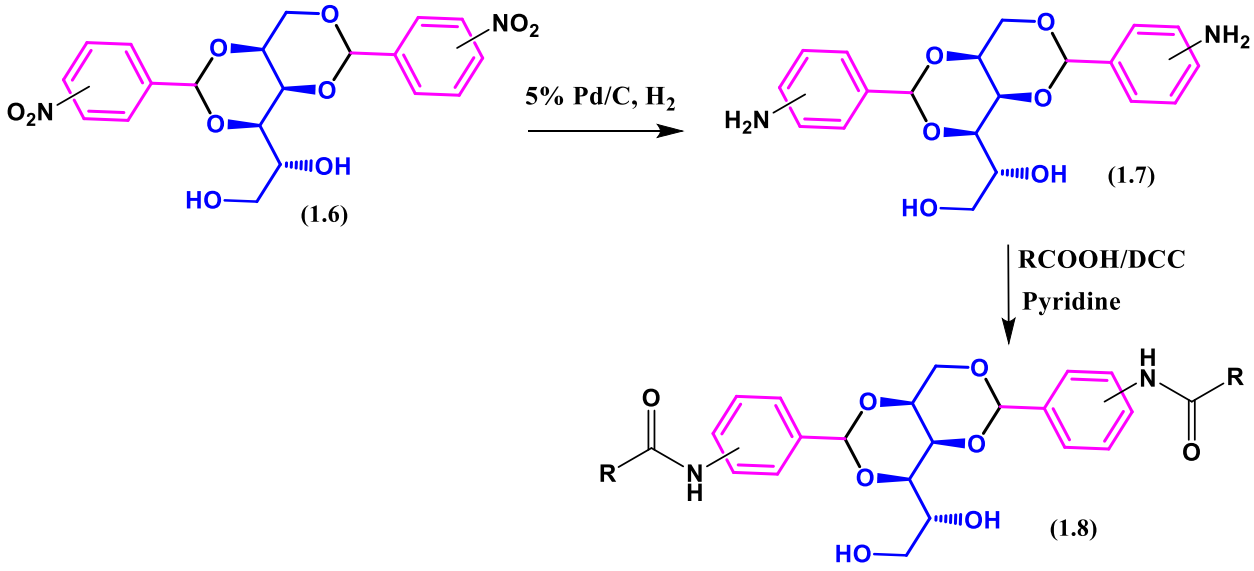

Scheme 1.2. Synthesis of amino and amido derivatives of DBS

The acetal unit in the DBS is quite stable and displays tolerance to various reaction conditions. For example, DBS-NO_2 is reduced to DBS-NH_2 by hydrogenation reaction using palladium on carbon, and the formed amine is further converted into amides by coupling reaction with allyl or alky acids in the presence of DCC (Scheme 1.2)[48].

To increase DBS gelators' water solubility, the corresponding methyl esters were initially synthesized and further transformed to DBS-COOH and DBS-$CONHNH_2$ using simple reaction conditions (Scheme 1.3).[49,50]

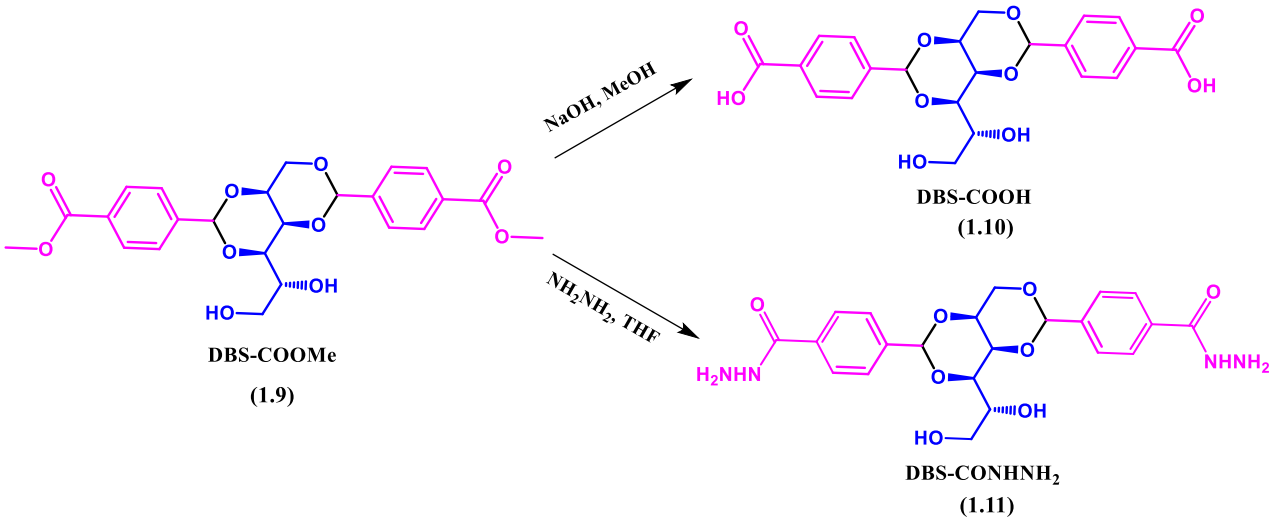

Scheme 1.3. Synthesis of DBS-COOH and DBS-$CONHNH_2$

Extensive research has been performed on the functionalization of the free hydroxy groups of DBS in addition to the modification in the substituents of phenyl groups of DBS. Feng et al. have reported the modification of free hydroxyl groups of DBS through esterification using acid halides (Scheme 1.4).[47]

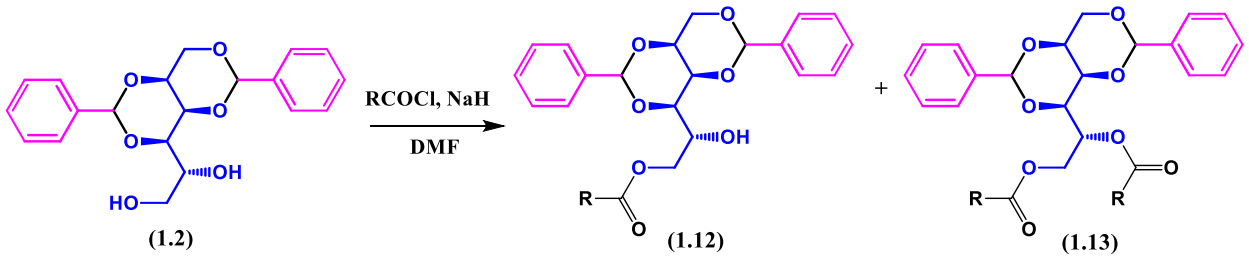

Scheme 1.4. Esterification of free hydroxyl groups of DBS.

Further, significant effort has been made to functionalize the hydroxyl groups of DBS, such as acrylates, higher fatty esters, and bola-amphiphiles (Figure 1.6).[51–55] Most of the DBS derivatives displayed potential in pharmaceutical and personal care product formulations.

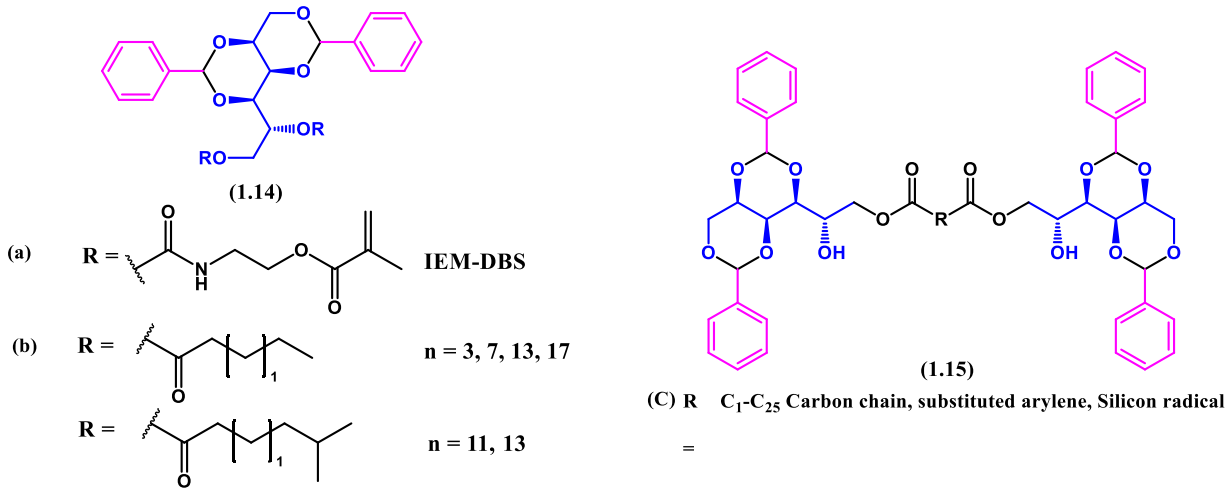

Figure 1.6. Molecular structures of acrylates, higher fatty esters, and bola-amphiphiles.

1.1.3.3 Self-assembly of DBS

Extensive studies have been performed to investigate the self-assembly mechanism of DBS, employing both experimental and computational approaches. A detailed investigation revealed that intermolecular H-bonding occurs between C5-OH/C6-OH groups of DBS or acetal hydrogens. The π-π stacking interactions occurs between phenyl groups. Yamasaki et al. revealed that solvent polarity profoundly impacts the hydrogen bonding interactions governing DBS self-assembly.[56] Yamasaki et al. proposed that the C5-OH group of DBS is involved in intramolecular hydrogen bonding with an acetal oxygen or intermolecular hydrogen bonding with the surrounding solvent but does not participate in the molecular recognition pathways that result in gelation. In contrast, the C6-OH group of DBS displays intermolecular hydrogen bonds with acetal oxygens, playing a crucial role in supporting self-assembly and gelation. Moreover, the phenyl groups exhibit a highly ordered arrangement, aligning side by side along the aggregate axis, which likely contributes to the stability and structure of the gel (Figure 1.7).[57,58]

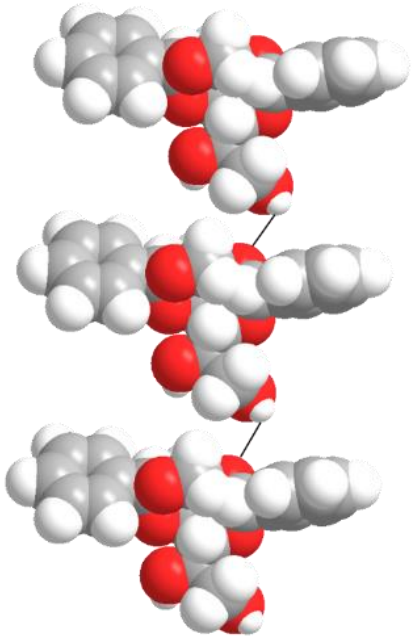

Figure 1.7. Self-assembly model proposed by Yamasaki and co-workers.[57]

Conformational studies revealed the existence of four different energy-minimized structures of DBS that can switch (Figure 1.8).[59,60]

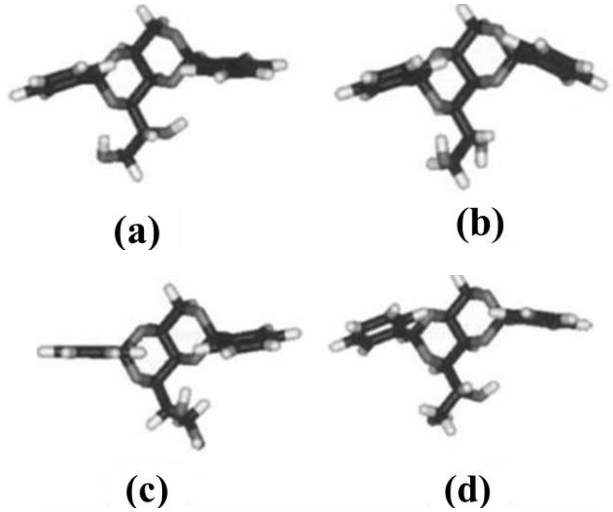

Figure 1.8. Energy minimized structures of DBS obtained through conformational studies by Wilder et al.[image reproduced from ref 59]

It is worth mentioning that the position of the substituents in the aromatic ring of DBS and the surrounding solvent plays a crucial part in determining morphology of assembled structure of DBS derivatives.[61,62] These findings highlight the crucial role of solvent and molecular design in governing supramolecular structure and gelation behaviour.

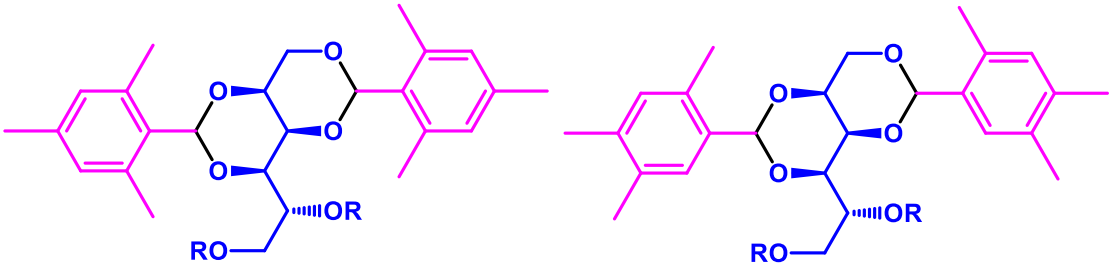

Figure 1.9. Structures of 2,4,6-TMDBS and 2,4,5-TMDBS

1.1.3.4 Applications of DBS derivatives

DBS is a promising candidate for forming soft materials and supramolecular systems with potential applications in pharmaceuticals, food chemistry, cosmetics, environmental remediation, drug delivery, molecular recognition, crystal engineering, and battery applications. Each DBS derivative has unique properties, making them useful in diverse fields.

Eutectogel derived from DBS displayed potential as solid electrolytes for flexible battery fabrication,[63] ionic thermo-electronic devices,[64] and stimuli-responsive systems.[65,66] DBS-based gels are used as antiperspirant sticks and lipsticks in the cosmetic industry.[67,68] The thickening property of DBS derivatives in oil-water emulsions makes it an ideal ingredient for the formulation of lotions, creams, sunscreen, and cosmetics.[69] Marine oil spill recovery using phase selective gelation,[70] electro-responsive and thermo-reversible liquid crystals for fabricating LCDs,[71,72] and nucleating agent in crystallography[73] are the remarkable applications displayed by DBS derivatives.[50,74] DBS derivatives also show footprints in dye remediation,[75] drug delivery,[76] organic semiconductors,[77] catalysis,[78,79,80,27] anti-microbial agents,[81] and stem cell research.[82–86] Thermo-reversible nanofillers architecture derived from DBS derivatives improved the mechanical properties of vitrimers.[87] It has also been used as a nucleating and clarifying agent for polypropylene[88,89,90] and polyethylene, which are commercially used in food packaging under the name of Millad® 3988.[91,92] DMDBS is used as an electret additive to polypropylene filaments, which led to their rapid decay. Moreover, charging at elevated temperatures significantly improved charge density and stability for both additives, enhancing the overall performance of the filaments for their application as electret filters.[93] DMDBS has been used to form strong-standing solid electrolytes when incorporated with Fumed silica, a nanoparticulate material suspended in propylene carbonate with $LiClO_4$ for lithium-ion batteries.[94] Increase in the tensile strength and

tensile modulus, a decrease in the crystallization is observed when polylactic acid is nucleated with DMDBS.[95]

DBS-Pyrene has been used to form a cellulose-based cartridge for the absorption of dyes using an intercalation mechanism.[96] DBS-OMe gels have displayed self-healing and stimuli-responsive properties, which exhibited multiple visual molecular recognition abilities. The multifunctionality of DBS-OMe includes an efficient lubricator, safe fuel, dye absorbent, and propellant.[97] The extensive research on DBS has laid a solid foundation, paving the way for innovations. As the investigations to uncover the full potential of DBS derivatives are underway, their impact and scope are likely to increase in the years to come.

1.2 Objectives

The objectives of this thesis are

- **Design and synthesis of DBS derivatives:** To develop a simple and efficient protocol for the synthesis of new DBS derivatives with varying functional groups and architectures. and to establish a versatile synthetic route to access a library of DBS derivatives.
- **Comprehensive investigation of self-assembly behaviour:** To systematically investigate the self-assembly properties of DBS derivatives, exploring the effects of solvent variation, temperature, and concentration on their supramolecular organization, with the goal of elucidating the complex relationships between molecular structure, solvent interactions, and self-assembly behaviour.
- **DBS derivatives as a confined media:** To evaluate the potential of DBS derivatives as confined media for organic synthesis, focusing on enhancing reaction rates, Solvent-free or minimal solvent conditions, recyclability and regioselectivity control.
- **Applications of DBS derivatives:** To explore the potential applications of the synthesized DBS derivatives, especially in the fields of drug delivery, eutectogels, metallogels and as a reaction medium.

1.3 References

1 D. J. Lloyd, *The problem of gel structure*, 1926.

2 G. C. Maity, *J. Phys. Sci.*, 2007, **11**, 156–171.

3 D. J. Adams, *J. Am. Chem. Soc.*, 2022, **144**, 11047–11053.

4 P. S. Kubiak, S. Awhida, C. Hotchen, W. Deng, B. Alston, T. O. McDonald, D. J. Adams and P. J. Cameron, *Chem. Commun.*, 2015, **51**, 10427–10430.

5 G. M. Whitesides, J. P. Mathias and C. T. Seto, *Science.*, 1991, **254**, 1312–1319.

6 N. E. Hughes, A. G. Marangoni, A. J. Wright, M. A. Rogers and J. W. E. Rush, *Trends Food Sci. Technol.*, 2009, **20**, 470–480.

7 S. C. C. Sanches, M. Ines Ré, J. O. Carrera Silva-Júnior and R. M. Ribeiro-Costa, *Gels*, 2023, **9**,150.

8 W. Maatar, S. Alila and S. Boufi, *Ind. Crops Prod.*, 2013, **49**, 33–42.

9 D. Giuri, P. Ravarino and C. Tomasini, *Gels*, 2023, **9**, 932.

10 B. Mondal, D. Bairagi, N. Nandi, B. Hansda, K. S. Das, C. J. C. Edwards-Gayle, V. Castelletto, I. W. Hamley and A. Banerjee, *Langmuir*, 2020, **36**, 12942–12953.

11 B. Anand, S. S. Pisal, A. R. Paradkar and K. R. Mahadik, *J. Sci. Ind. Res.*, 2001, **60**, 311–318.

12 K. Aruchamy, S. Ramasundaram, S. Divya, M. Chandran, Y. Kyusik and Tae H Oh, *Gels*, 2023, **9**, 585.

13 J. M. Galindo, C. Tardío, B. Saikia, S. Van Cleuvenbergen and I. Torres-Moya, *Gels*, 2023, **9**, 875.

14 B. Pramanik, *Gels*, 2002, **8**, 569.

15 M. Yamanaka, *J. Incl. Phenom. Macrocycl. Chem.*, 2013, **77**, 33–48.

16 O. Gronwald and S. Shinkai, *Chem. Eur. J.*, 2001, **7**, 4328–4334.

17 J. H. Jung, Y. Ono, K. Sakurai, M. Sano and S. Shinkai, *J. Am. Chem. Soc.*, 2000, **122**, 8648–8653.

18 D. Bariya, V. Anand and S. Mishra, *Steroids*, 2021, **165**, 108769.

19 K. F. Chaves, D. Barrera-Arellano and A. P. B. Ribeiro, *Food Res. Int.*, 2018, **105**, 863–

872.

20 E. Snip, S. Seiji and D. N. Reinhoudt, *Tetrahedron Lett.*, 2001, **42**, 2153–2156.

21 L. Wu, C. Han, X. Jing and Yong Yao, *Chinese Chem. Lett.*, 2021, **32**, 3322–3330.

22 M. A. Rogers and Richard G. Weiss, *New J. Chem.*, 2015, **39**, 785-799.

23 R. I. Hollingsworth and G. Wang, *Chem. Rev.*, 2000, **100**, 4267–4282.

24 S. Datta and S. Bhattacharya, *Chem. Soc. Rev.*, 2015, **44**, 5596–5637.

25 K. Soundarajan, R. Periyasamy and T. Mohan Das, *RSC Adv.*, 2016, **6**, 81838–81846.

26 P. K. Vemula, J. Li and G. John, *J. Am. Chem. Soc.*, 2006, **128**, 8932–8938.

27 Z. Yang, G. Liang, M. Ma, A. S. Abbah, W. W. Lu and B. Xu, *Chem. Commun.*, 2007, 843–845.

28 P. V. Bhavya, K. Soundarajan, J. G. Malecki and T. Mohan Das, *ACS Omega*, 2022, **7**, 39310–39324.

29 A. Vidyasagar, K. Handor and K. M. Sureshan, *Angew. Chemie - Int. Ed.*, 2011, **50**, 8021–8024.

30 T. Kato, Y. Hirai, S. Nakaso and M. Moriyama, *Chem. Soc. Rev.*, 2007, **36**, 1857–1867.

31 M. J. Meunier, *ann.chim. phys.*, 1891, **22**, 412.

32 E. A. Wilder, R. J. Spontak and C. K. Hall, *Mol. Phys.*, 2003, **101**, 3017–3027.

33 P. Thomas and M. sibi, *compt. Rend.*, 1926, **183**, 282–284.

34 R. M. Hann. and C. S. H. John K. Wolfe, *J. Am. Chem. Soc.*, 1942, **64**, 1493–1497.

35 S. J. Angyal And Lawler J. V., *J Am Chem Soc*, 1944, **66**, 837–838.

36 J. J. K. and a. L. T. N. R. M. C. Douglas J. Brecknell, *Aust. J. Chem.*, 1976, **29**, 5.

37 G. Akazome, Y. Choshi, T. Kobayashi, K. Murai and A. Tsuji, US Patent 3721682 A, 1973.

38 H. Uchiyama, US Patent 4131612 A, 1978.

39 G. Machell, US Patent 4562265 A, 1985.

40 K. Murai, T. Kobayashi and K. Fujitani, US Patent 4429140 A, 1984.

41 J. P. Salome and G. Fleche, US Patent 5023354A, 1991.

42 T. Kobayashi, US Patent 5120863 A, 1992.

43 W. A. Scrivens and J. M. Salley, US Patent 5731474 A, 1998

44 J. G. Lever, D. L. Dotson, J. D. Anderson, J. R. Jones and S. R. Sheppard, US Patent 6500964 B2, 2002.

45 B. Chien, J. Strobel, M. Strobel, C. Jones, J. Getschel and E. Bosl, US Patent 20060093845, 2006.

46 P. V. Uppara, P. Aduri, M. Sakhalkar and U. Ratnaparkhi, US Patent 20130281716, 2014

47 R. Feng, L. Chen, Z. Hou and J. Song, Trans. Tianji Univ., 2007, 13, 6.

48 C. Villa, S. Rum, E. Russo and P. Kirilov, *Mater. Lett.*, 2023, **340**, 134170.

49 V. M. P. Vieira, L. L. Hay and D. K. Smith, *Chem. Sci.*, 2017, **8**, 6981–6990.

50 D. J. Cornwell and D. K. Smith, *Chem. Commun.*, 2020, **56**, 7029–7032.

51 R. Stan, C. Ott, N. Sulca, A. Lungu and H. Iovu, *Mater. Plast.*, 2009, **46**, 230–235.

52 Gérard Malle and T. Luukas, US Patent 20130039862, 2013

53 M. Fariya, A. Jain, V. Dhawan, S. Shah and M. S. Nagarsenker, *Adv. Pharm. Bull.*, 2014, **4**, 483–491.

54 L. A. Estroff and A. D. Hamilton, *Chem. Rev.*, 2004, **104**, 1201–1217.

55 C. Xie, L. R. Rieth and T. D. Danielson, US Patent 7662978, 2010.

56 B. S. Yamasaki and H. Tsutsumi, *Chem. Soc. Jpn.*, 1995, **68**, 123–127.

57 S. Yamasaki, Y. Ohashi, H. Tsutsumi and B. K. Tsujii, *Chem. Soc. Jpn.*, 1995, **68**, 146–151.

58 M. Watase, Y. Nakatani and H. Itagaki, *J. Phys. Chem. B.*, 1999, **103**, 2366–2373.

59 E. A. Wilder, R. J. Spontak and C. K. Hall, *Mol. Phys.*, 2003, **101**, 3017–3027.

60 D. Knani and A. D, *Polym. Adv. Technol.*, 2013, **24**, 391–397.

61 Y. Y. and J. S. J. Li, K. Fan, X. Guan, *Langmuir*, 2014, **30**, 13422–13429.

62 P. F. Deng, Y. Q. Feng, F. H. Xu and J. Song, *Fine. Chem.*, 2007, **24**, 1056–1060.

63 J. Ruiz-Olles, P. Slavik, N. K. Whitelaw and D. K. Smith, *Angew. Chemie Int. Ed.*, 2019, **58**, 4173–4178.

64 Z. Dong, Q. Xiang, Z. Zhang, J. Tang, F. Li, K. Sun and S. Chen, *CCS Chem.*, 2024, 1–17.

65 V. Vanoli, J. Pietrowska, G. de Araujo Lima e Souza, M. E. Di Pietro, F. Briatico Vangosa, A. Mele and F. Castiglione, *ACS Appl. Eng. Mater.*, 2024, **2**, 388–396.

66 N. M. Şulcă, A. V. Munteanu, R. G. Popescu, A. Lungu, R. Stan and H. Iovu, *UPB Sci. Bull. Ser. B Chem. Mater. Sci.*, 2010, **72**, 25–36.

67 A. Urrutia, J. Albanese, Joseph, J. Bianchini, Robert And L. Fantano, Steven, 2000, EU patent 1035830B1.

68 C. L. Esposito and P. Kirilov, Gels, 2021, **7**, 97.

69 T. Saito, T. Teshigawara, M. Reger, H. Hoffmann, Y. Sugiyama and M. Kitajima, US Patent 2014/0134255, 2014.

70 T. Kobayashi, Y. Kawashima, M. Yoshimura, M. Sugiura, T. Nobe and S. Fujimoto, US Patent 4502975, 1985.

71 K. Steck and C. Stubenrauch, *Langmuir*, 2019, **35**, 17132–17141.

72 R. H. C. Janssen, V. Stümpflen, M. C. W. Van Boxtel, C. W. M. Bastiaansen, D. J. Broer, T. A. Tervoort and P. Smith, *Macromol. Symp.*, 2000, **154**, 117–126.

73 B. Chien, J. Strobel, M. Strobel, C. Jones, J. Getschel and E. Bosl, US Patent 20060093845, 2006

74 D. J. Cornwell, B. O. Okesola and D. K. Smith, *Angew. Chemie - Int. Ed.*, 2014, **53**,

12461–12465.

75 B. O. Okesola and D. K. Smith, *Chem. Commun.*, 2013, **49**, 11164–11166.

76 E. J. Howe, B. O. Okesola and D. K. Smith, *Chem. Commun.*, 2015, **51**, 7451–7454.

77 B. O. Okesola, S. K. Suravaram, A. Parkin and D. K. Smith, *Angew. Chemie - Int. Ed.*, 2016, **55**, 183–187.

78 P. Slavík, D. W. Kurka and D. K. Smith, *Chem. Sci.*, 2018, **9**, 8673–8681.

79 P. Slavik and D. K. Smith, *Tetrahedron*, 2020, **76**, 131344.

80 C. C. Piras, C. S. Mahon and D. K. Smith, *chem. Eur.J.*, 2020, **26**, 8452–8457.

81 C. C. Piras and and D. K. S. Petr Slavik, *Angew. Chemie - Int. Ed.*, 2020, **59**, 853–859.

82 C. C. Piras, A. G. Kay, P. G. Genever, J. Fitremann and D. K. Smith, *Chem. Sci.*, 2022, **13**, 1972–1981.

83 C. C. Piras, A. K. Patterson and D. K. Smith, *Chem. - A Eur. J.*, 2021, **27**, 13203–13210.

84 A. K. Patterson and D. K. Smith, *Chem. Commun.*, 2020, **56**, 11046–11049.

85 T. T. Vadukoote, A.-J. Avestro and D. K. Smith, *Angew. Chemie Int. Ed.*, 2024, e202409757.

86 C. C. Piras, C. S. Mahon, P. G. Genever and D. K. Smith, *ACS Biomater. Sci. Eng.*, 2022, **8**, 1829–1840.

87 A. Quinteros-Sedano, B. Bresson, N. J. Van Zee and R. Nicolaÿ, *ACS Mater. Lett.*, 2024, **6**, 877–884.

88 Y. F. Zhang, X. Li and X. S. Wei, *J. Therm. Anal. Calorim.*, 2010, **100**, 661–665.

89 J. Lipp, M. Shuster, A. E. Terry and Y. Cohen, *Polym. Eng. Sci.*, 2008, **48**, 705–710.

90 M. Shokrollahi, B. T. Marouf and R. Bagheri, *Polyolefins J.*, 2023, **10**, 21–26.

91 J. Hernández-Fernández, J. Martinez-Trespalacios and E. Marquez, *Foods*, 2024, **13**, 1200.

92 Y. Zhao, C. Yao, T. Chang and Y. Zhu, *Polymers*, 2019, **11**, 1–12.

93 Ali Kilic, E. Shim, B. Y. Yeom and B. Pourdeyhimi, *J. Appl. Polym. Sci.*, 2013, 2068–2075.

94 V. R. Basrur, J. Guo, C. Wang and S. R. Raghavan, *ACS Appl. Mater. Interfaces*, 2013, **5**, 262–267.

95 N. Petchwattana, P. Naknaen, J. Sanetuntikul and B. Narupai, *Plast. Rubber Compos.*, 2018, **47**, 147–155.

96 V. Singh, K. Lalitha, C. Uma Maheswari, V. Sridharan, D. Pradhan, S. Batra and S. Nagarajan, *ACS Omega*, 2024, **9**, 5695–5704.

97 F. Wen, J. Li, L. Wang, F. Li, H. Yu, B. Li, K. Fan and X. Guan, *RSC Adv.*, 2021, **11**, 32459–32463.

CHAPTER 2A

STIMULI-RESPONSIVE OLIGOBENZYLIDENE-D-SORBITOL DIALDEHYDES GELS: DIRECT ENCAPSULATION AND DELIVERY OF H_2S

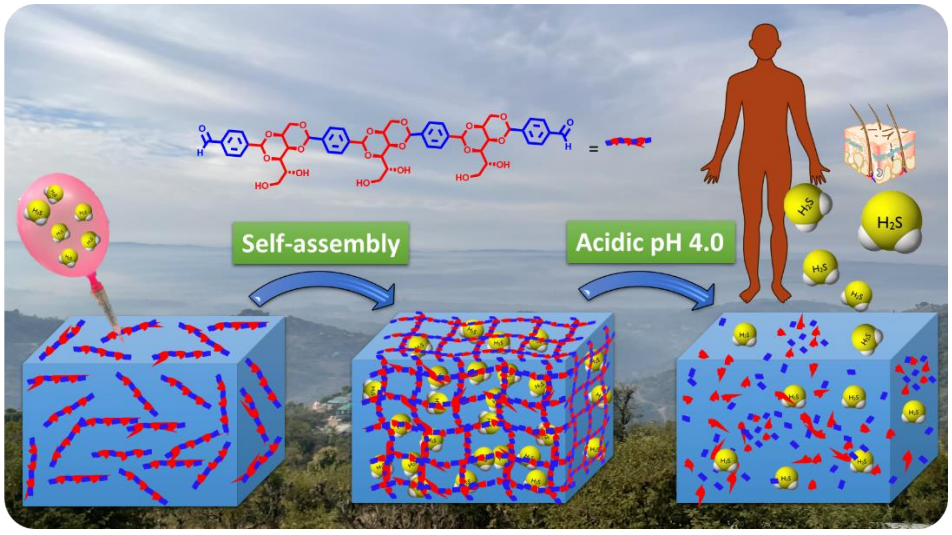

2A.1 Objective

This chapter aims to design, synthesize, and evaluate a new oligo[1,3:2,4-(O-benzylidene)-D-sorbitol]-dialdehyde (OBSDA) based organogelator as a pH-responsive drug delivery system for controlled release of hydrogen sulfide (H_2S), a crucial biological signalling gasotransmitter, overcoming the limitations of existing H_2S delivery methods.

2A.2 Abstract

Over the past two decades, stimuli-responsive drug delivery systems have garnered significant attention. Hydrogen sulfide (H2S) has emerged as a crucial endogenous molecule promoting tissue regeneration, angiogenesis, and antioxidant effects. However, its gaseous nature and reactivity pose challenges for therapeutic administration. This study reports the development of a smart, biocompatible H2S delivery system using oligo[1,3:2,4-(O-benzylidene)-D-sorbitol]-dialdehyde (OBSDA), synthesized from FDA-approved, environmentally benign resources. OBSDA self-assembles into supramolecular gels in N-methyl pyrrolidone (NMP), an FDA-approved solvent with anti-inflammatory properties. The gel's molecular interactions, mechanism, morphology, and strength were characterized using NMR, FTIR, XRD, SEM, and rheology. A novel, stimuli-responsive H2S delivery system was achieved through direct encapsulation and pH-triggered gel-to-sol transition, enabling precise H2S release for future physiological studies.

2A.3 Introduction

Supramolecular chemistry, aptly described as “chemistry beyond molecules”, mainly focuses on exploring higher-order self-assemblies and dynamic molecular recognition through non-covalent interactions.[1] Supramolecular chemistry, as observed in biological systems, has served as a source of inspiration for scientists to develop innovative, smart materials. Particularly, advanced drug-delivery systems leverage supramolecular concepts to create efficient and targeted treatments for various diseases. Notably, molecular self-assembly, recognition, and foldamers have garnered significant attention and offer a promising solution for addressing the challenges of drug delivery, enabling the development of finite and effective therapies. The use of supramolecular chemistry in drug delivery has shown great promise in improving the efficacy and reducing the toxicity of therapeutic agents.[2] By harnessing the power of molecular self-assembly and recognition, scientists can design drug delivery systems that are tailored to specific diseases and can target specific sites of action, thereby enhancing the overall effectiveness of the treatment.

Supramolecular delivery systems offer a targeted and controlled release of active pharmaceutical ingredients, including drugs, enzymes, peptides, vaccines, and nutrients, over an extended period. The advantages of these systems include reduced side effects, controlled dosage, increased bioavailability, improved solubility, and enhanced drug efficiency, with various administration methods.[3] In pharmaceutical formulations, various drug delivery systems including liposomal formulations,[4] micelles,[5] nanoparticles,[6] implantable systems,[7] biopolymers,[8] and LMWG,[9] have been used for treating various diseases. Clinical trials have shown that nanomedicine is pharmacologically and pharmacokinetically more efficient than the simple drug-alone formulations.[10] Over 100 nanomedicine-based formulations have been approved by the US FDA and the EMA. Doxil®, Somavert®, Avinza®, Venofer®, and Abraxane® are representative examples of commercial lipid, polymer, nanocrystal, inorganic nanoparticles, and protein-based nanomedicine, respectively.[11] To meet the high pharmaceutical market demand, there is a rapid growth in research and development of nanomedicine-based advancements.

This chapter aims to design, synthesize, and evaluate a novel oligo[1,3:2,4-(O-benzylidene)-D-sorbitol]-dialdehyde (OBSDA) based organogelator as a pH-responsive drug delivery system for controlled release of hydrogen sulfide (H2S), exploring its potential as a therapeutic agent for various diseases, and overcoming the limitations of existing H2S delivery methods.

2A.3.1 H_2S as a Therapeutic agent

Hydrogen Sulfide (H_2S), despite of its reputation as a toxic swamp gas with corrosive and flammable properties, it is an important biological signalling gasotransmitter generated by various enzymes within our body.[12] Abe and Kimura made a significant discovery in 1996, revealing that H_2S at physiological concentrations, selectively enhances NMDA receptor-mediated responses. This finding implicated the role of H_2S in the modulation of synaptic activity, which is regulated by hormones and neurotransmitters.[13] H_2S plays a crucial role in cardiovascular, gastrointestinal, excretory, nervous, and immune-responsive biological processes.[12] Exogenous delivery of H_2S aided in treating various diseases such as diabetes, Alzheimer's, Parkinson's, stroke, and Arthritis.[14–18] In biomedical research, various H_2S donors have been employed to investigate the biological effects of H_2S. These donors serve not only as valuable research tools but also as potential therapeutic agents, offering a promising platform for the treatment of various diseases. The oral administration of H_2S is the most straightforward approach, however, its toxicity,

unpleasant odour, and rapid oxidation limit its practical applications.[19,20] Hence, it is required to develop methods for more targeted and controlled H_2S delivery methods.

2A.3.2 H_2S donors and drug delivery systems

The effects of H_2S are deeply rooted in its redox chemistry, and rapid single-dose administration may disrupt cellular redox states,[21] leading to far-reaching consequences beyond H_2S-specific functions. To achieve a sustained release, various H_2S donors were generated and used as drug delivery systems (Table 1). All the reported methods displayed various limitations such as tedious synthetic procedures, less loading capacity, bio-compatibility, and complex delivery mechanisms.

Table 2A.1. List of H_2S drug delivery systems and H_2S donors

S.No	Delivery system	H_2S Donor	Advantage	Limitation
1	Caged thiocarbamates[22]	Thiocarbamates	Organelle targeted delivery, Resolving organelle stress	Multiple steps for H_2S delivery from donor
2	*N*-Thiocarboxyanhydrides (NTAs) and poly-NTAs[23]	Carbonyl Sulfide	Controlled release, Endothelial cell Proliferation	Multiple steps for H_2S delivery from donor
3	Mesoporous silica nanoparticles[24]	Diallyl trisulfide	Controlled release, enhanced endothelial cell proliferation and migration, Alleviates inflammation	Toxic effects of silica nanoparticles, Multiple steps for H_2S delivery from donor
4	Hypromellose hydrogels[25]	ADT	Transdermal delivery, enhanced mitochondrial function in HUVEC cells	Multiple steps for H_2S delivery from donor
5	Epoxide functional Polymeric nanoparticles[26]	Perthiols	Thiol triggered delivery	Multiple steps for H_2S delivery from donor
6	Microfluidics assisted large porous microspheres[27]	ACS14	Inhalable donor deposits on lungs, treats pulmonary artery endothelial cells,	Multiple steps for H_2S delivery from donor
7	Peptide Hydrogel[28]	SATO	Thiol triggered controlled release, in vitro HUVEC proliferation and transmigration, treat IH	Multiple steps for H_2S delivery from donor

8.	Mesoporous iron oxide nanoparticles[29]	Diallyl trisulfide	Controlled release, heart and brain targeting, myocardial and cerebral protection from ischemic injury	Toxic effects of metal oxide nanoparticles, Multiple steps for H_2S delivery from donor
9	Large porous microspheres[30]	ACS14	Lung accumulation, Relief of pulmonary arterial	Multiple steps for H_2S delivery from donor
10	Conductive hydrogel[31]	2-Aminopyridine-5-thiocarboxamide	Thiol responsive and treats Myocardial infarction treatment	Multiple steps for H_2S delivery from donor
11	Polymeric micelles[32]	ADT	protecting cardiomyocytes from ischemic cell death	Multiple steps for H_2S delivery from donor
12	PEG and lactoferrin modified mesoporous iron oxide nanoparticles[33]	Diallyl trisulfide	Magnetic guided, blood-brain barrier transporting, brain-targeting, MRI Cerebral and myocardial protection after cardiac arrest	Multiple steps for H_2S delivery from donor
13	Polymeric hydrogel[34]	α-Thioetherketone	UV responsive, Antithrombosis	Multiple steps for H_2S delivery from donor
14	SDS and SBC loaded gelatin capsule[35]	Diallyl trisulfide	in situ self-spray, thiol-responsive, Inflammatory bowel disease treatment	Multiple steps for H_2S delivery from donor
15	Collagen hydrogel[36]	JK1	pH and enzyme dual-responsive, Disc degeneration treatment	Multiple steps for H_2S delivery from donor
16	Poly(lactic acid) microspheres[37]	SPRC	Rheumatoid arthritis alleviation	Multiple steps for H_2S delivery from donor
17	Polymeric micelles[38]	ADT	Promoting inflammation	Multiple steps for H_2S delivery from donor
18	Polycaprolactone nanofibers[39]	JK1	pH responsive, Wound healing	Multiple steps for H_2S delivery from donor
19	Hyaluronic acid hydrogel[40]	JK1	pH responsive, Wound healing	Multiple steps for H_2S delivery from donor

20	Sodium alginate sponge[41]	JK1	pH responsive, Wound healing	Multiple steps for H_2S delivery from donor
21	Silk fibroin porous scaffolds[42]	GYY4137	Bone tissue engineering	Multiple steps for H_2S delivery from donor
22	Enzyme-functionalized albumin[43]	Thiosulfate cyanide sulphur transferase	In-situ enzymic H2S generation, Cardiac tissue repair	Multiple steps for H_2S delivery from donor
23	PEG-cholesteryl conjugate[44]	Trisulfide	Thiol responsive, Anticancer effects	Multiple steps for H_2S delivery from donor
24	Magnetic nanoliposomes[45]	ADT	Magnetic guided, US and MRI dual model imaging, Anticancer effects	Multiple steps for H_2S delivery from donor
25	BSA modified MnS nanoparticles[46]	Metastable-phase MnS	pH responsive, MRI imaging, Anticancer effects	Multiple steps for H_2S delivery from donor
26	FeS embedded BSA nanoclusters[47]	FeS	pH responsive, MRI imaging, Anticancer effects	Multiple steps for H_2S delivery from donor
27	Polymeric nanoparticles[48]	SATO	Cys responsive, bioimaging	Multiple steps for H_2S delivery from donor
28	Polymeric micelles[49]	Aryl thioamide	Thiol responsive	Multiple steps for H_2S delivery from donor
29	Polycaprolactone microfibers[50]	*N*-(benzoylthio)benzamide	Thiol responsive, Protecting cell from oxidative damage, cells proliferation	Multiple steps for H_2S delivery from donor
30	Polymeric hydrogels[51]	SATO	Elastase-degradable, Cys responsive	Multiple steps for H_2S delivery from donor
31	Crescent-shaped peptide assemblies[52]	SATO	Cys responsive, enhanced cell internalization, Reducing ROS levels in macrophages	Multiple steps for H_2S delivery from donor
32	Aggregates of mPEG and cholesteryl conjugates[53]	Trisulfide	Mitigating ROS generation	Multiple steps for H_2S delivery from donor

33	PEG brush polymers[54]	Trisulfide	Ameliorating cellular oxidative stress	Multiple steps for H_2S delivery from donor
34	Polymersomes[55]	SATO	Bacteria-targeted, Cys responsive, Healing of the infectious diabetic wound	Multiple steps for H_2S delivery from donor
35	Zwitterionic nanoparticles[56]	L-Cys	GSH responsive, Cancer treatment	Multiple steps for H_2S delivery from donor
36	Hyaluronated liposomes[57]	Phenyl substituent ADT-doxorubicin conjugate	Tumour-targeted, Cancer treatment	Multiple steps for H_2S delivery from donor
37	PEG-modified conjugated polymer nanoparticles[58]	Polysulfide	GSH responsive, NIR fluorescence imaging, Cancer treatment, wound healing	Multiple steps for H_2S delivery from donor

Among these various nanomedicine-based delivery systems, gels formed by low molecular weight gelators have attracted a broad range of interest because of their 3D-porous network, extensive loading capability, ease of tunability, biocompatibility, and stimuli-responsiveness.[59] Matson and co-workers have developed a hydrogel using *S*-aroylthiooxime conjugated peptides, which can deliver H_2S by the decomposition of *S*-aroylthiooxime moiety[60–63,51]. Liang et al. have generated a H_2S prodrug by grafting 2-aminopyridine-5-thiocarboxamide on partially oxidized alginate, which upon decomposition releases H_2S endogenously.[64] Recently, Nagarajan and co-workers have developed an enolizable amphiphilic gel from renewable resources and used it for the direct delivery of H_2S, wherein the reaction of Na_2S and water generated H_2S.[65] Hyaluronic acid-based hydrogel has been used as a matrix for encapsulating H_2S donors, which are released through pH response for repairing wounds on skin.[66]

In the recent past, various polymer conjugated H_2S prodrug such as dithiolethiones, aryl thioamides, acyl protected perthiols, dialkyl trisulfide, dialkyl tetrasulfide, polysulfides, *N*-benzoylthiobenzamides *N*-thiocarboxyanhydrides, Na_2S, SATOs, Lawesson reagents (phosphonamidoodithiolates), geminal dithiols, thioether ketones thiocarbamates, and carbamothioates have been developed.[67] However, the controlled release is achieved by a complex chemical/enzymatic process. The main reason for the evolution of the prodrug concept in H_2S delivery is because of the poor encapsulation of H_2S in solid, liquid, and gel phases. A careful analysis of the molecular structure of the H_2S prodrug and the release mechanism shows that the

overall release of H_2S would be much less. To achieve the desired concentration of H_2S release, a huge amount of H_2S prodrug loading is necessitated. To overcome the existing limitations, Oligo[1,3:2,4-(O-benzylidene)-D-sorbitol]-dialdehyde (OBSDA) based organogelator as H_2S drug delivery system has been developed. The idea of developing OBSDA originated from DBS, which is one of the well-known chiral amphiphiles that could able to gelate numerous solvents for over a century. In particular, DBS-based gelators have gained attention among researchers because of its bio-compatibility, facile bottom-up assembly in a broad range of solvents, multi-functionality, and multi-responsive behaviour.[68] For the synthesis of OBSDA, Sorbitol is used as one of the starting materials because of its natural abundance, biodegradability, biocompatibility, and eco-friendliness. Sorbitol is a sugar substitute providing dietary energy with an E number of E420 and is also classified as GRAS by the FDA. Sorbitol is often used in medical, health care, food, and cosmetics.[69] Another starting material, terepthalaldehyde, used for the synthesis of OBSDA facilitates $\pi-\pi$ stacking interactions. In this thesis, OBSDA is synthesized from biologically significant starting materials using a simple protocol in good yield. Bottom-up assembly of OBSDA in polar solvent furnished a 3D network structure, wherein the polar solvents are trapped. To our fortunate, OBSDA formed gel in N-methyl pyrrolidone (NMP), a widely used pharmaceutical solvent displaying bioactive and anti-inflammatory properties. In addition, NMP is a widely preferred solvent for solubilizing many commercial drugs and it has the tendency to enhance the drug penetration in humans as well as animals.[70] The famous Purisol process is adopted in petrochemical industries to selectively remove H_2S from syn gas using NMP solvent.[71] By getting the idea from the Purisol process, H_2S is directly encapsulated in the OBSDA gel formed in NMP solvent and demonstrated the controlled stimuli-responsive delivery. A plausible self-assembly and pH as stimuli-responsive H_2S release mechanism, have been investigated.

2A.4 Results and Discussions

DBS gels derived from sorbitol display potential applications in pharmaceuticals, food industries, and personal care products. In pharmaceuticals, DBS-based gels act as a stimuli-responsive drug delivery system for the controlled release of Naproxen, Rosuvastatin, Ibuprofen, and Mesalazine.[72,73,74] To extend the current research of this study in the field of fabrication of assembled organic materials and also by considering the potential application of DBS, an analogue of DBS, i.e. OBSDA is synthesized using a simple protocol. The chemistry of hydroxyl

functionalization of monosaccharides has been prevalent for over a century and displayed a significant scope because of its sustainable and smart material applications which are mostly useful in pharmaceuticals, environmental chemistry, and the fabrication of optical and electronic materials. The chemistry of OBSDA synthesis is in a similar line with DBS, where the formation of acetal is the key step. Traditionally, Lewis acids such as $AlCl_3$, $ZnCl_2$, $SnCl_2$, $FeCl_3$, and BF_3, and Brønsted acids such as *p*-toluene sulfonic acid, phosphoric acid, etc. were typically used for the formation of sugar acetal.[75] An extensive literature search revealed that the use of Brønsted acids in excess during the reaction lowers the yield by forming impurities and enhances the purification process. In addition, the use of metal-based Lewis acids allows the traces of metal ions in the product because of the strong interaction of sugar acetals with metal ions, which limits its applications on an industrial scale. Even though DBS is commercially available, the reported procedure for the synthesis of DBS did not work well in the case of OBSDA, because of the involvement of simultaneous formation of more than two acetals.

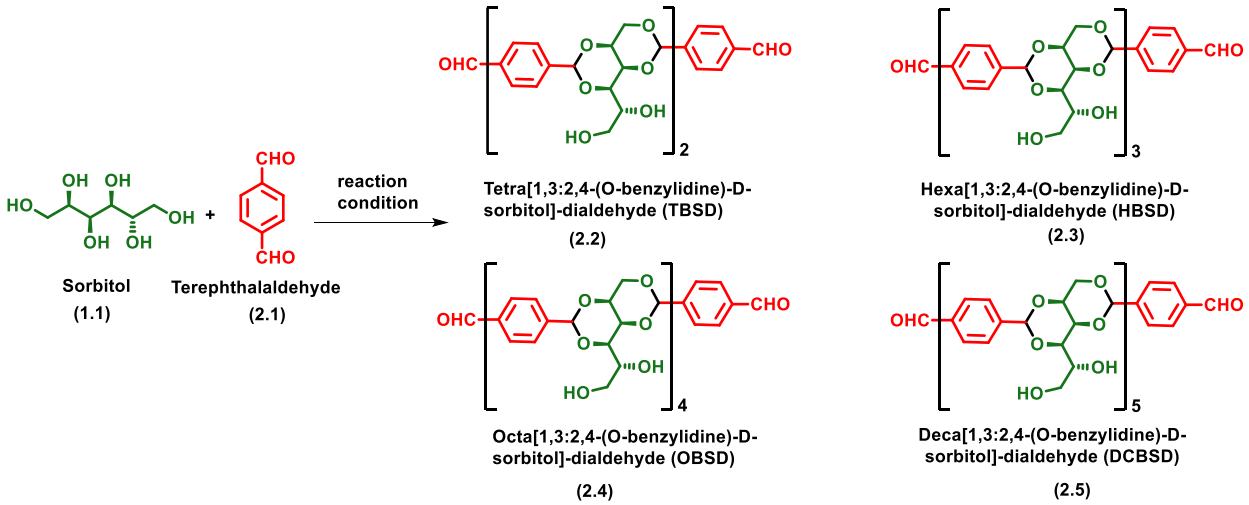

Scheme 2A.1. Synthesis of oligo[1,3:2,4-(O-benzylidene)-D-sorbitol]-dialdehyde (OBSDA)

In the process of identifying a suitable reaction condition to synthesize OBSDA (**2.2-2.5**) in good yield, various Lewis and Brønsted acids as a catalyst and a broad range of solvents have been selected. Based on the literature, our initial attempts with the use of 0.2 mol% of Lewis acids such as $AlCl_3$, $ZnCl_2$, $SnCl_2$, $FeCl_3$, and $BF_3.OEt_2$ as catalysts in MeCN at rt furnished tetrabenzylidene-disorbitol (**2.2**) in low to moderate yields (31-67%). In carbohydrate chemistry, it is well known that the use of Brønsted acids can facilitate the acetal formation by the protonation of the carbonyl group of aldehydes followed by the attack of a hydroxyl nucleophile. Among the various Brønsted

acids used, *p*-TSA rendered tetrabenzylidene-sorbitol dialdehyde (**2.2**) in moderate yield (55 %). Interestingly, the use of heterogeneous catalysts such as Dowex and Amberlyst at room temperature furnished the HBSD **2.3** with 72 and 78 % yield respectively (Table 1). To enforce the reaction, the reactivity of all the catalysts was studied at elevated temperatures and prolonged reaction time. Unfortunately, the Lewis acids selected for the investigation did not render a satisfactory result. A careful analysis of a reaction mechanism of acetal formation in sorbitol, metal ions in the Lewis acid are entrapped in the benzylidene sorbitol moiety utilizing weak van der Waals forces and hence are not readily available for the further activation of the carbonyl group of pendant aldehyde groups. It is worth mentioning that there is no further progress in the reaction in the case of increasing mol% of Lewis acid. Subsequently, acetal formation in sorbitol using terepthalaldehyde in heterogeneous catalysts at 50 ^{o}C delivered encouraging results. Interestingly, the reactions at elevated temperatures furnished the higher analogues of benzylidene sorbitol product.

Having optimized the catalysts, Dowex and Amberlyst, the increase in temperature and time render HBSD **2.3** and OBSD **2.4**. The change of solvents did not provide satisfactory results. Altogether, the use of heterogeneous catalysts such as Dowex and Amberlyst at different temperatures and varying times can furnish one of the TBSD, HBSD or OBSD as a major product.

During the progress of the reaction, the acetal product formed is separated as a precipitate or gelatinous substance. The precipitate is dissolved in a hot cyrene solvent, and the heterogeneous catalyst is separated by filtration. The cyrene solution containing the desired compound is kept under refrigeration for crystallization. The yield denoted in Table 1 are after recrystallization. To identify the number of oligomeric units formed during the reaction, ^{1}H-NMR and mass spectral techniques were used. Altogether, OBSDA oligomers of 3,4,5, and 6 units were successfully synthesized using Dowex and Amberlyst catalysts (Table 2A.1).

Table 2A.2. Optimization for the synthesis of oligo[1,3:2,4-(O-benzylidene)-D-sorbitol]-dialdehyde (OBSDA).

S.NO	catalyst	Mol%	Temp (˚C)	solvent	Time (h)	DBSD	TBSD (2.2)	HBSD (2.3)	OBSD (2.4)	DCBSD (2.5)
1	$AlCl_3$	0.2	rt	MeCN	12	traces	31	-	-	-
2	$ZnCl_2$	0.2	rt	MeCN	12	traces	45	-	-	-

3	$SnCl_2$	0.2	rt	MeCN	12	traces	14	-	-	-
4	$FeCl_3$	0.2	rt	MeCN	12	traces	23	-	-	-
5	$BF_3.OEt_2$	0.2	rt	MeCN	12	traces	62			
6	*p*-TSA	0.2	rt	MeCN	12	traces	55			
7	H_3PO_4	0.2	rt	MeCN	12	traces	traces			
8	CH_3COOH	0.2	rt	MeCN	12	traces	traces			
9	HCl	0.2	rt	MeCN	12	-	-			
10	Dowex	-	rt	MeCN	12	traces	72	traces		
11	Amberlyst	-	rt	MeCN	12	traces	78	traces		
12	$AlCl_3$	0.2	50	MeCN	12	traces	25	12	-	-
13	$ZnCl_2$	0.2	50	MeCN	12	traces	32	traces	-	-
14	$SnCl_2$	0.2	50	MeCN	12	traces	traces	traces	-	-
15	$FeCl_3$	0.2	50	MeCN	12	traces	traces	traces	-	-
16	$BF_3.OEt_2$	0.2	50	MeCN	12	traces	52	16		
17	*p*-TSA	0.2	50	MeCN	12	traces	38	23		
18	H_3PO_4	0.2	50	MeCN	12	traces	traces			
19	CH_3COOH	0.2	50	MeCN	12	traces	traces			
20	HCl	0.2	50	MeCN	12	-	-			
21	Dowex	-	50	MeCN	12	traces	63	17		
22	Amberlyst	-	50	MeCN	12	traces	59	15		
23	Dowex	-	70	MeCN	12	traces	45	36		
24	Amberlyst	-	70	MeCN	12	traces	39	40		
25	Dowex	-	reflux	MeCN	12	traces	35	42	traces	
26	Amberlyst	-	reflux	MeCN	12	traces	31	48	traces	
27	Dowex	-	reflux	MeCN	16	traces	16	53	traces	
28	Amberlyst	-	reflux	MeCN	16	traces	24	57	traces	
29	Dowex	-	reflux	MeCN	20	traces	traces	64	traces	
30	Amberlyst	-	reflux	MeCN	20	traces	traces	67	traces	
31	Dowex	-	reflux	MeCN	24		traces	77	traces	traces
32	Amberlyst	-	reflux	MeCN	24		traces	79	traces	traces
33	Dowex	-	reflux	MeCN	32			65	traces	traces
34	Amberlyst	-	reflux	MeCN	32			59	traces	traces
35	Dowex	-	reflux	MeCN	60			18	37	traces
36	Amberlyst	-	reflux	MeCN	60			16	45	traces
37	Dowex	-	reflux	MeOH	60			18	21	traces

38	Amberlyst	-	reflux	MeOH	60			16	27	traces
39	Dowex	-	reflux	cyrene	60				67	13
40	Amberlyst	-	reflux	cyrene	60				72	11

The number of units present in the OBSDA oligomer is obtained from the integration of the number of aromatic protons, acetal protons, and protons attached to the sorbitol backbone. In a single unit of OBSDA, there are 8 aromatic protons, 2 acetal protons, and 10 sorbitol protons. When one more unit is attached, the aromatic protons are increased by 4 protons, the acetal protons are increased by 2 protons, and the sorbitol protons are increased by 10 protons relatively.

Table 2A.3. Number of units in OBSDA oligomer

Aromatic protons	Acetal proton	Sorbitol proton	No of units (n)
12H	4H	20H	2
16H	6H	30H	3
20H	8H	40H	4
24H	10H	50H	5

Generally, the reaction of hexose sugar, sorbitol with various aldehydes furnishes the corresponding acetal-based amphiphiles displaying a butterfly-like conformation. The sorbitol moiety is considered as backbone and the pendant groups attached to it are considered as wings. Bottom-up assembly of butterfly-shaped amphiphiles depends upon the wings, which significantly expands the potential and scope of materials applications. In the current research, the wings were systematically expanded by conjugation with suitable sorbitol or sorbitol acetals. To further investigate the bottom-up assembly process of the newly synthesized compound HBSD **2.3**, Gelation studies have been performed in various solvents and vegetable oils. Gelation behaviour of the sorbitol acetals bearing varying degrees of H-bonding and π–π stacking units was studied by the stable-to-inversion method, which proceeds through the dissolution of the gelator in a suitable solvent by heating followed by cooling to room temperature. While cooling, bottom-up assembly of molecules generates the required microstructures with greater precision and error rectification ability by means of H-bonding and π–π interactions. (Table 2A.3).

Table 2A.4. Gelation studies of OBSDA with different solvents and oils

S.No	Solvent	Critical Gelation Concentration Observed (CGC wt/vol%)			
		TBSD	**HBSD**	**OBSD**	**DCBSD**
1	Water	NS	NS	NS	NS
2	Methanol	NS	NS	NS	NS
3	Glycerol	NS	NS	NS	NS
4	Ethylene glycol	NS	NS	NS	NS
5	Tetrahydrofuran	NS	NS	NS	NS
6	Dimethyl sulfoxide	G (1.2)	G (0.8)	G (1)	G (1)
7	Dimethyl sulfoxide + H_2O	G (1)	G (0.6)	G (1)	G (1)
8	Acetone	NS	NS	NS	NS
9	1,4-dioxane	NS	NS	NS	NS
10	Dimethyl formamide	G (1)	G (1)	G (1)	G (1)
11	Poly(ethylene glycol)	NS	NS	NS	NS
12	Acetic acid	NS	NS	NS	NS
13	N-methyl pyrrolidone	G (1.5)	G (1.0)	G (1.5)	G (1.5)
14	1,2-Dichlorobenzene	NS	NS	NS	NS
15	pyridine	NS	NS	NS	NS
16	Ethanol	NS	NS	NS	NS
17	n-Butanol	NS	NS	NS	NS
18	Toluene	NS	NS	NS	NS
19	Diesel	NS	NS	NS	NS
20	Hazel nut oil	NS	NS	NS	NS
21	Olive oil	NS	NS	NS	NS
22	Linseed oil	NS	NS	NS	NS
24	Dimethyl carbonate	NS	NS	NS	NS
25	Cyrene	NS	NS	NS	NS

NS–Not soluble, G-gel.

Interestingly, these compounds display gelation in polar aprotic solvents such as DMSO, DMF, and NMP with the critical gelation concentration (CGC) of 0.6-1.5% (wt/v). Representative images of gel formed in DMSO, DMF, and NMP are given in Figure 2A.1. NMP is one of the well-known pharmaceutical solvents used for commercial drug formulations. Investigation of the gelation behaviour of compounds 3-6 revealed that the tuning of the wing portion by conjugation with benzylidene sorbitol influences the gelation behaviour and assembly pattern. Furthermore,

compounds 3-6 were insoluble in most of the non-polar solvents and vegetable oils, whereas a complete or partial dissolution was observed in polar protic solvents. To our fortunate, compounds 3-6 displayed excellent gelation in polar aprotic solvents such as DMSO, DMF, and NMP. The use of a mixture of solvents such as DMSO, DMF and NMP along with water in 1:1 ratio for the gelation studies substantially alters the intermolecular interactions, thereby molecules failed to form supramolecular architecture by means of bottom-up assembly process. These results reveal that while forming the gel, the introduction of a proton donor interferes with the molecular aggregation which results in precipitation. At this point, this class of molecules is prone to form a gel in a specific range of solvents, where it can achieve dissolution because of intermolecular interactions and solvent balancing in the bottom-up assembly process. Among the various solvents displaying gelation, NMP is widely used in various industries and pharmaceuticals, and it is a versatile water-miscible polar aprotic solvent displaying drug solubilization and penetration in humans and animals. NMP solvent exhibits a well-established safety profile and anti-inflammatory properties.[70] Hence, our further research focuses on the gel formed in a pharmaceutical solvent, NMP. Purisol is a physical absorption process employed in chemical industries to remove H_2S and CO_2 from various natural gas streams, crude oil, etc., by using NMP solvent. The high absorption capacity and high boiling point of NMP solvent allow the removal of acid gases at high pressure and high temperature. The Literature review revealed that the Purisol process utilizing NMP is one of the important methods adopted for the purification of syngas at high pressure because of its high selectivity towards H_2S. By gaining clue from the literature, H_2S is encapsulated into the gel matrix and studied its release profile.

It is worth mentioning that the organogel formed by HBSD is stable under the heating and cooling cycle from rt to 70 ˚C. Upon heating of the gel above 120 ˚C resulted in precipitation, which is attributed to the cleavage of the acetal moiety of HBSD The existence of intermolecular interactions in the process of self-assembly can be studied by using Fourier Transform Infrared Spectroscopy (FTIR), X-ray diffraction (XRD), and nuclear magnetic resonance (NMR) studies.

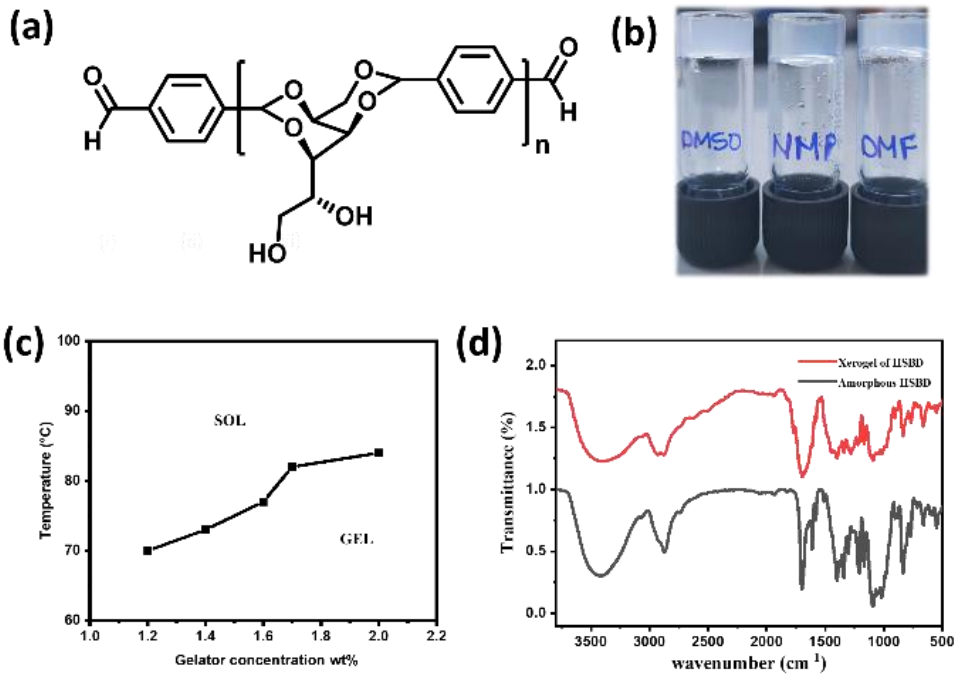

Figure 2A.1. (a) Butterfly conformation of gelator; (b) Images of gel formed by HBSD in DMSO, NMP, and DMF solvents (i-iii); (c) Phase diagram of HBSD gel formed in NMP with respect to the concentration of gelator in wt/v%. (d) FTIR spectra of HBSD in xerogel and amorphous state.

FTIR spectroscopy provides insights into various molecular interactions that give rise to self-assembled 3D supramolecular architectures. The FTIR spectrum of amorphous HBSD and HBSD xerogels in NMP solvent are shown in Figure 2A.1. HBSD in an amorphous state displays O-H stretching vibrations at 3428 cm^{-1} and aldehyde carbonyl (C=O) stretching at 1699 cm^{-1}. After undergoing self-assembly in NMP solvent, the HBSD xerogels displayed O–H stretching vibrations at 3410 cm^{-1}, and aldehyde (C=O) stretching at 1695 cm^{-1}, which implies the involvement of hydroxy groups and aldehyde carbonyl groups in the process H-bonding-mediated self-assembly of molecules into 3D architectures.

Further evidence of the self-assembly process is probed from variable temperature ^{1}H-NMR spectral studies. ^{1}H-NMR of HBSD in DMSO at various temperatures is displayed in Figure 2A.2. Variable temperature ^{1}H-NMR spectral studies revealed that upon the increase in temperature, an upfield shift in signals corresponding to the proton of the methylene and free hydroxy groups from δ = 4.84, 4.68, 4.41 ppm to δ = 4.41, 4.30 and 4.05 was observed. In a complex system like carbohydrates, it is very difficult to understand the electronic nature of various groups in free and assembled states.

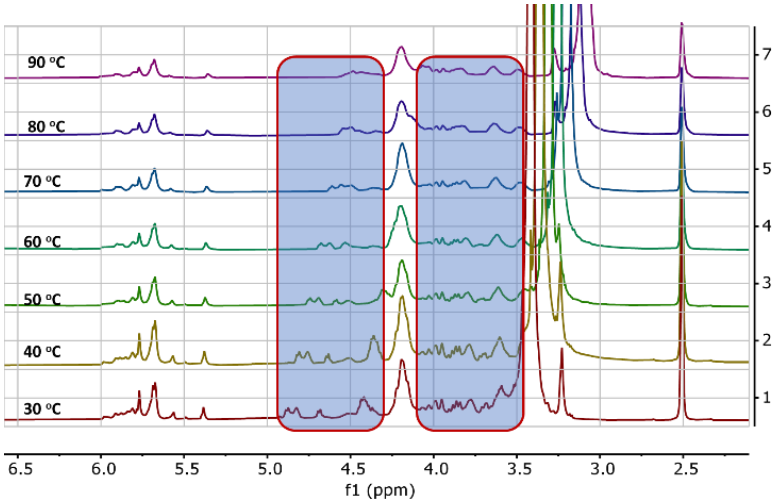

Figure 2A.2. Variable temperature ^{1}H-NMR spectra of gel formed by HBSD in DMSO-d_6. The shift of proton peaks is highlighted in the blue box.

In the assembled state, because of the involvement of –OH groups in intermolecular H-bonding, the electron density decreases, and hence the respective proton generates a relatively lesser induced magnetic field. Owing to the consequences of the induced magnetic field, the protons of methylene and hydroxyl groups feel a higher magnitude of the applied magnetic field and hence relatively higher frequency is required for the resonance. However, upon disassembly, these protons display an upfield shift because of the disturbance in the intermolecular interaction. Increased electron density in the aggregated π-conjugated systems is fairly known in the literature and is considered as one of the basic criteria for the development of organic electrons and sensors. However, the influence of aggregation in π -system is not known till to date, and such investigation is very important to study the structure-function activity of complex biological systems. VT ^{1}H-NMR studies revealed that upon molecular assembly, CH protons of carbohydrate moiety resonated at a lower frequency and upon gel-to-sol transition influenced by the heating displayed a downfield shift in protons (Figure 2A.2). This demonstrates the involvement of hydroxy groups in the self-assembly process utilizing H-bonding.

The mechanical characteristics of the HBSD gel formed in NMP are understood by studying its viscoelastic properties using a Rheometer. Gels undergo deformation in response to stress or strain, which depends upon the intermolecular interactions governing the supramolecular architecture. Investigation of flow characteristics of gel with respect to strain amplitude sweep and angular frequency sweep in terms of storage modulus(G') and loss modulus(G'') is very crucial for

biomedical applications. In Figure 2A.3, throughout the frequency sweep measurements of the HBSD gel, it was consistently observed that the storage modulus G' remained higher than the loss modulus G''; this indicates that the HBSD gel exhibits stability and resilience towards external forces. The amplitude sweep measurements distinctly demonstrate that the HBSD gels show gel-like behaviour (G'>G'') up to a critical strain level 0.02%. After this point, a decrease in G' and G'' indicates the onset of fluid-like behaviour in the gels. After assessing the gel's capacity to endure external forces, evaluation of the processability of the gels through continuous temperature ramp-up and ramp-down experiments was conducted within the temperature range of 23°C to 45°C.

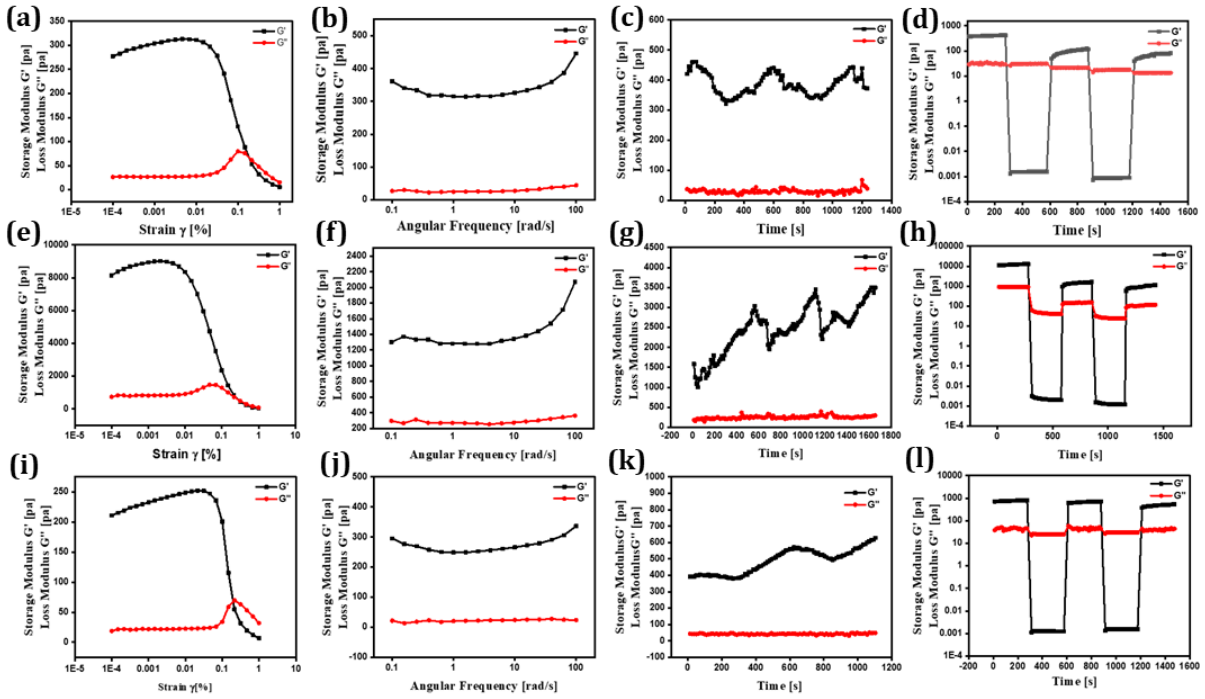

Figure 2A.3. Amplitude sweep, Frequency sweep, temperature ramp-up and Thixotropy studies of HBSD gel formed in NMP (a-d), DMSO (e-h) and DMF (i-j) respectively.

This study demonstrates that these gels undergo disassembly upon heating and then reassemble the gel network upon cooling, driven by reversible non-covalent interactions. Typically, the thixotropic nature of gels provides insight into their capacity to restore the structural integrity that may have been compromised due to the application of different strains to the gel. After applying a constant strain of 100%, the HBSD gel experienced a reduction in strength. However, upon decreasing the strain to 0.1%, the viscosity of the gels returned to their initial state. Through a

sequence of three successive cycles of continuous strain ramp-up and ramp-down experiments, a gradual deterioration in gel structural integrity is observed, as the strain increases. However, the original state promptly recovered as the strain was eased back to 0.1%.

During the process of self-assembly, how individual molecules are interconnected to create well-ordered 3D architectures such as fibers, tubules, helices, lamellae, twisted fibers, micelles, and vesicles is of utmost significance. These organized patterns contributed distinctive attributes to the resulting soft materials. Scanning electron microscopy is employed to investigate the morphology of the self-assembled gels. Figure 2A.4 shows that HBSD gels in NMP display fibre-like structures in a self-assembled state.

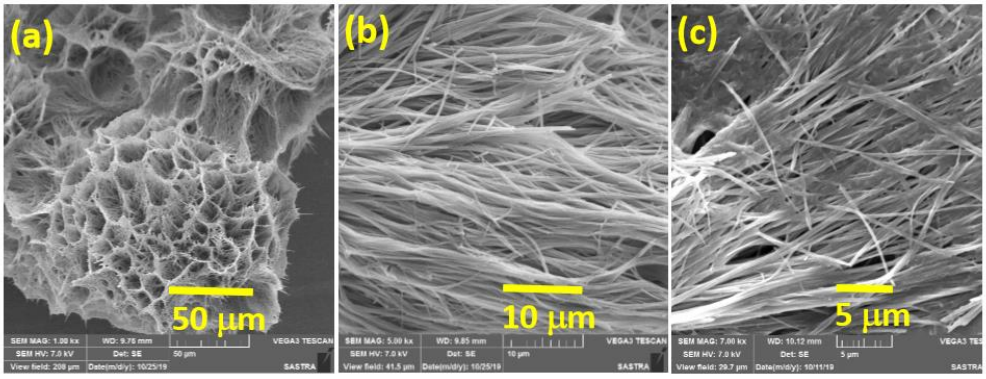

Figure 2A.4. SEM images of xerogels of HBSD in NMP at (a) 50µm (b) 10 µm and (c) 5 µm

Regardless of its foul-smelling and toxic nature, H_2S is an important gasotransmitter in the neurosystem. Initially, the biological properties of H_2S were investigated by direct administration of NaHS and Na_2S, but the main drawback in direct administration is the rapid increase in the concentration of H_2S which then declines rapidly, which causes an inflammatory response.

The Development of H_2S-based drugs is quite challenging because of their volatility and rapid metabolism. Hence, a controlled H_2S delivery system is necessary. Regulation of H_2S delivery has become a prominent area for research in the last few decades. Many types of drug delivery systems from complex macromolecular architectures to nanofiber systems have been used to deliver H_2S. Among these drug delivery systems, gels have attracted a wide range of interest because of their 3D-porous network, biodegradability, and stimuli-responsive gel-sol transition. In a recent study, Arunan and his colleagues utilized microwave spectroscopy to confirm the

existence of hydrogen bonding in H_2S,[76] which made us curious to establish a new method to encapsulate H_2S through an in situ gelation process.

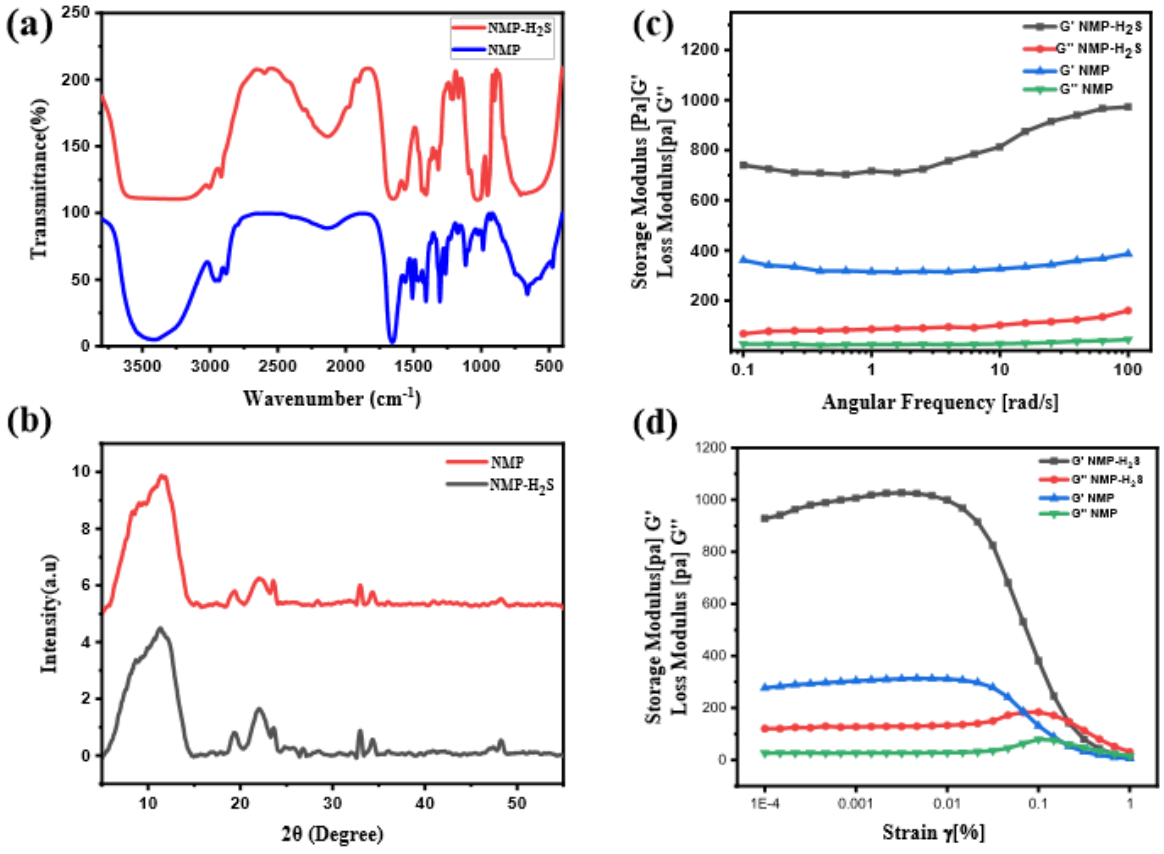

Figure 2A.5. a) FTIR spectra of HBSD xerogel and H_2S encapsulated gel; (b) XRD of xerogels of HBSD in NMP before and after loading H_2S; (c &d) A comparative rheology of HBSD gel formed in NMP and H_2S encapsulated gel respectively.

By considering its solubility with H_2S gas, a drug delivery protocol is engineered in which H_2S is directly injected into a solution of HBSD dissolved in NMP. This results in a self-assembly process that leads to gel formation, effectively entrapping the H_2S gas. Entrapment of H_2S is greater in HBSD gel formed in NMP because of dipole-dipole interaction, acid-base interaction, and size and polarizability of H_2S with NMP, in addition to the complementary H-bonding extended by the gelator and NMP. Injecting H_2S into HBSD solution in NMP has accelerated the self-assembly process and the gel formed quickly. The entrapment of H_2S can be visually confirmed by the colour change of HBSD gel from white to yellow. To investigate the self-assembly mechanism after the injection of H_2S, FTIR spectra is recorded for the xerogel of HBSD before and after the Injection

of H_2S (Figure 2A.5a). In FTIR spectra, the peak observed at 2602 cm^{-1} represents the S–H stretching frequency, confirms the encapsulation of H_2S in the gel matrix, which is absent in HBSD xerogel. A comparison of O–H stretching vibrations in HBSD and H_2S encapsulated xerogels revealed the engagement of hydroxyl groups in H-bonding with H_2S. It is worth mentioning that the increase in H-bonding with H_2S substantially increases the strength of the gels, which is demonstrated by angular frequency and amplitude sweep experiments (Figure 2A. 5c&d). The storage modulus of the H_2S encapsulated gel is higher than the storage modulus of HBSD gel inferring the increase in strength of the gel upon forming H-bonding with H_2S.

Molecular packing of HBSD and H_2S encapsulated gels were identified using XRD analysis HBSD xerogels displayed peaks at 2θ = 8.28, 10.80, 12.5, 19.29, 22.10, 23.59, 32.97, 34.29, 28.36, 36.48 and 48.19, corresponds to the d-spacing (interplanar spacing) of 10.66, 8.17, 7.15, 4.59, 4.01, 3.76, 2.71, 2.61, 3.14, 2.46 and 1.88 nm respectively. However, xerogels of HBSD-H_2S displayed peaks at 2θ = 8.85, 11.79, 19.37, 22.08, 23.63, 32.97, 34.30, 47.03, 47.51 and 48.24, which corresponds to the d-spacing of 9.97, 7.49, 4.57, 4.021, 3.76, 2.71, 2.61, 1.93, 1.91 and 1.88 nm respectively. The notable variation in the d-spacing of molecular structures, observed before and after H_2S injection, provides strong evidence for the interaction between H_2S and HBSD (Figure 2A.5b).

Having established the interactions of H_2S in the HBSD gel, the stability studies of these gels have been performed at different pH conditions. Initial H_2S release studies at neutral pH displayed the stability of HBSD gel towards distilled water. It is worth mentioning that a little release in H_2S is observed because of the exchange of entrapped NMP in HBSD gel by water molecules rather than a rapid disintegration. It is observed that at pH = 4.0, the gel slowly disintegrates and releases the H_2S, whereas at neutral and basic pH levels, the gel retains its stability. Visual observation and NMR spectral studies revealed that the release of H_2S is due to disruption of H-bonding, visualized by the conversion of translucent gel into opaque soft gel and the slow hydrolysis of acetal groups present in the HBSD gelator, and the disruption of H-bonding interactions in the gel caused to lose its structural integrity of the Self-assembled fibrillar network and the gel collapses.

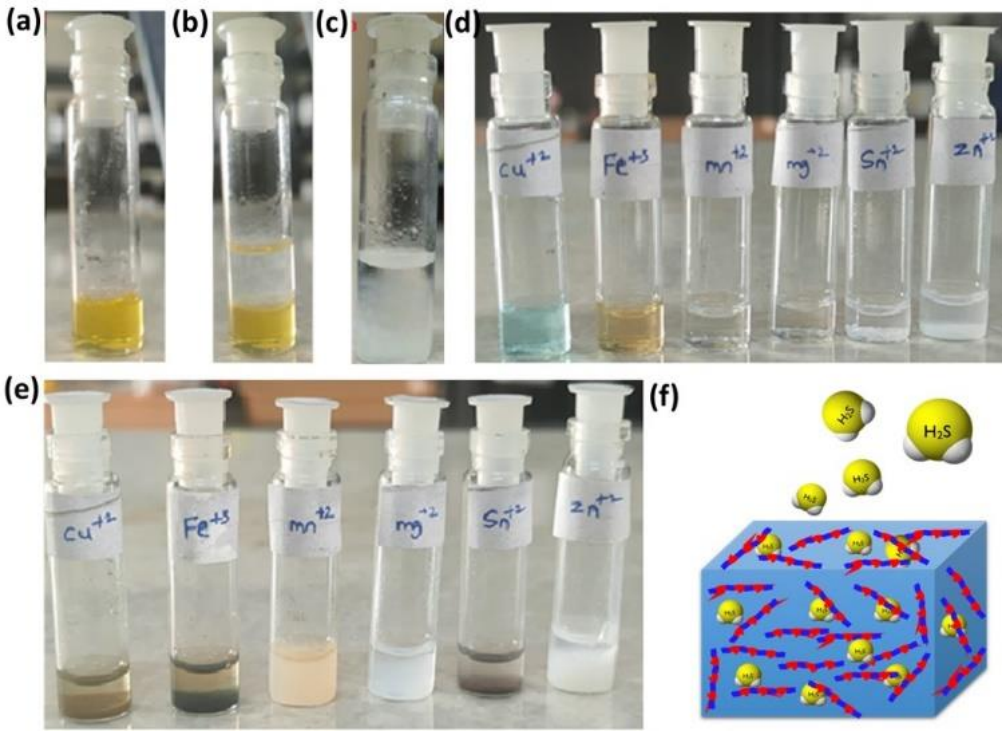

Figure 2A.6. (a) H_2S entrapped gel. (b) H_2S entrapped gel in acidic medium (pH-4.0), (c) H_2S entrapped gel in acidic medium after 12h, (d). Different metal ion solutions (e) metal sulfides formed after the addition of released H_2S. (f) pictorial representation of H_2S release from HBSD gel.

During the process of disassembly of H_2S entrapped HBSD gel, H_2S gas trapped in the fibrillar network is released. Acetyl-based gels have great potential in the controlled delivery of drugs and active pharmaceutical ingredients. As shown in figure 2A.6, when a buffer solution of pH 4.0 is added on top of the HBSD-H_2S gel, disassembly of the gel occurs, thereby gradual release of the H_2S is observed. The deformation of the gel with a significant colour change in buffer solution is physically visible, however, the release of H_2S is systematically assessed by converting it into respective metal sulphides. It is well known that under normal room temperature, the interaction between various metal ions and H_2S often gives rise to the formation of the corresponding metal sulfides. Specifically, Group II cations exhibited a tendency to form less soluble metal sulfides (with a solubility product constant, Ksp, of less than 10^{-30}) when exposed to lower amounts of H_2S. The supernatant liquid from the buffer solution is retrieved and further added to a vial containing the solution of different metal ions such as Cu^{+2}, Fe^{+3}, Mn^{+2}, Mg^{+2}, $Sn^{+2,}$ and Zn^{+2} at 0.1M concentration. The minimum concentration of H_2S present in the aliquots react with the respective metal ions in turn generating an insoluble metal sulphide which is confirmed by the change in

colour (Figure 2A.6). To quantify the loaded H_2S in HBSD gel and their release profile, a linear regression analysis is performed by taking the absorbance values obtained from methylene blue assay (Figure 2A7a&b).[77] To the 1 mL of H_2S entrapped HBSD gel, pH = 4 buffer solution is added, and aliquots of 0.5 mL are collected every 30-minute intervals and performed methylene blue assay.

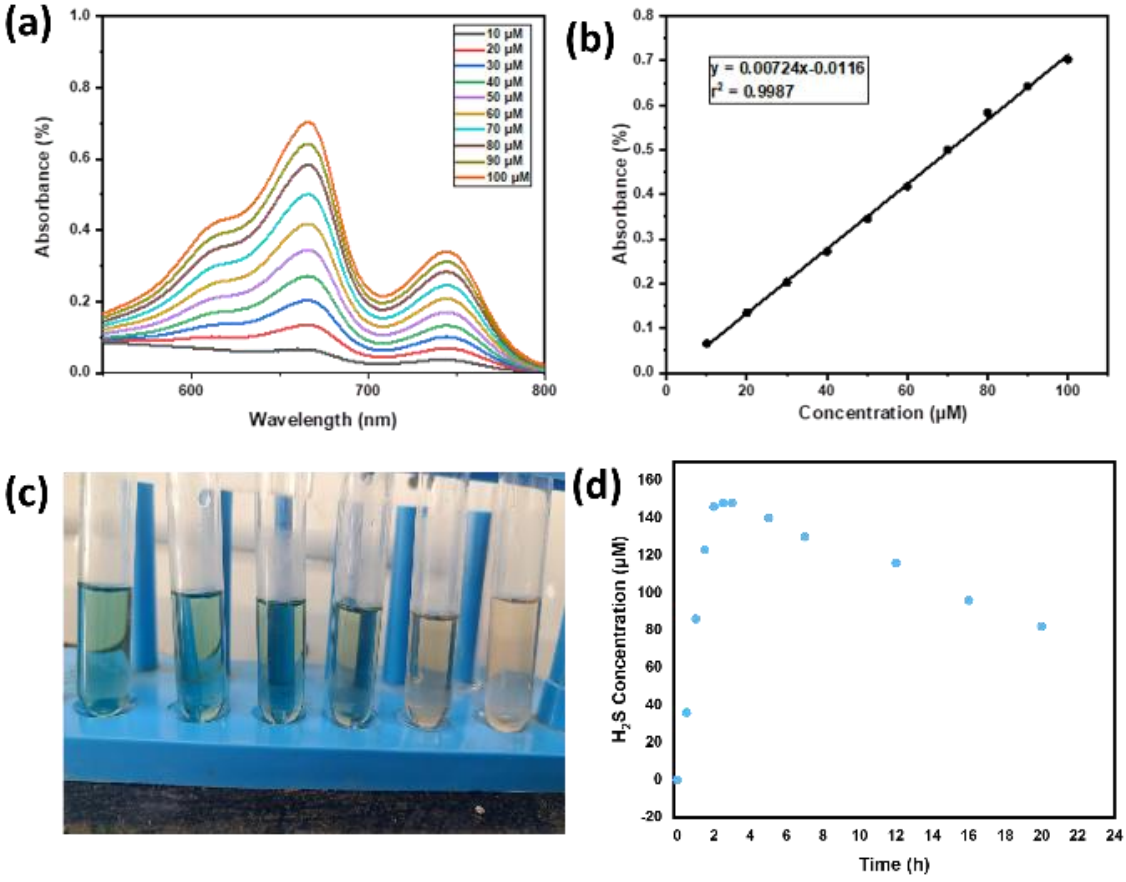

Figure 2A.7. (a) Methylene blue assay at different concentrations of Na_2S. (b) Linear regression analysis of concentration vs absorbance. (c) photograph of the formation of methylene blue by the released H_2S from HBSD gel at different time intervals (d) H_2S release profile displayed by HBSD gel at different time intervals

The interpolation of obtained UV data with the linear regression plot revealed a slow release of H_2S with respect to time and reached a maximum release after 3h. It is also observed that a slow decline in the concentration of H_2S is observed due to its volatile nature. The total amount of H_2S loaded in the gel is observed as 148 mm. In contrast to other H_2S donors or H_2S delivery materials documented in the reported literatures, the HBSD-NMP gel offers numerous advantages, such as

uncomplicated entrapment of H_2S in the gel matrix, without necessitating any covalent bonding, achieved through a self-assembling process. There is no requirement for additional H_2S donors. Furthermore, the HBSD gel exhibits pH-triggered H_2S delivery.

2A.5 Experimental

2A.5.1 Materials and Methods

All the solvents and chemicals utilized for the synthesis of Diformyl dibenzylidene sorbitol were purchased from commercial suppliers such as Merck, Aldrich, Himedia and Avra chemicals and were used without purification. LR grade solvents for recrystallization and AR grade solvents for gelation studies have been used. The progress of the reactions was monitored by thin-layer chromatography (TLC) using pre-coated Merck silica gel 60 F254 plates and visualized by UV detection or using sulfuric acid spray or molecular iodine. Melting points were recorded on Stuart SMP30 melting point apparatus in capillaries and are uncorrected. ^{1}H- and ^{13}C- NMR spectra were recorded on a Bruker Avance 300 MHz instrument in deuterated solvents such as DMSO-d_6 at room temperature. TMS is used as an internal standard and chemical shifts in NMR spectra (δ) is reported in parts per million (ppm) Multiplicity in ^{1}H NMR spectra of the synthesized compounds were referred as singlet (s), doublet (d), triplet (t), quartet (q), multiplet (m) and coupling constants (J) are given in Hz. Infrared (IR) spectra were recorded using Perkin Elmer spectrum 100 spectrophotometer from 400 – 4000 cm^{-1} using KBr. High-resolution MS analysis was performed on an Agilent Q-TOF 6230 instrument by dissolving the solid sample in methanol or acetonitrile. To obtain the morphology of the gel, scanning electron microscopy is used with a JEOL JSM-6701F ultrahigh resolution field emission scanning electron microscope. The XRD measurements were taken by keeping a small portion of the xerogel in the X pert-PRO Diffractometer system.

2A.5.2 General Procedure for the synthesis of HBSD oligomers

To a stirred solution of D-Sorbitol (1 mmol) in acetonitrile (10 mL) at rt under N_2 atmosphere, terepthalaldehyde (2 mmol) and Dowex 50WX8/Amberlyst were added. The reaction mixture was stirred for another 24 h at reflux condition. After completion of the reaction confirmed by TLC, the reaction mixture was allowed to cool down to room temperature. The formed precipitate is dissolved in hot cyrene and separate the catalyst by filtration. The cyrene solution is refrigerated for crystallization. The catalyst was further reused in other reactions.

2A.5.3 Gelation Studies

To the known amount of HBSD solid taken in a glass vial, appropriate quantity of solvent is added, and sealed tightly, and the glass vial was heated till the complete dissolution of solid. The clear solution that formed is allowed slolwly to cool room temperature. The gel forming ability of HBSD can be visually identified by inverting the glass vial. In the inverted glass vial, the solvent demosntrating no gravitational free flow is called as gel "G," if it is remained in the solution state, then it is referred as "S." If the compound is insoluble, it is denoted as "I." If there is any Precipitation is observed in the glass vial, it is denoted as "P"

2A.5.4 Morphological analysis

The nature of morphology of the HBSD gel was investigated using a Carl Zeiss AXIO ScopeA1 fluorescent/phase contrast microscope, JEOL JSM-6701F ultrahigh resolution field emission scanning electron microscope. To analyze the morphology of HBSD gel, a small portion of hydrogel is placed on a glass slide and sputter coating has been applied on its surface and subjected to a Phase Contrast Microscope.

2A.5.5 Rheological measurements

The viscoelastic nature and deformation under external forces behaviour of HBSD gel was studied using an Anton Paar 302 rheometer. Experiments were performed on a 25 mm diameter steel-coated parallel-plate geometry, on which, a 1 mm gap is maintained inbetween two plates. Amplitude sweep experiment was performed to determine the linear viscoelastic range, which determines the mechanical strength of the gel sample. Thixotropy, frequency sweep and temperature ramp-up and down were perfomed 28 °C to further understand the properties of the gel.

2A.5.6 Encapsulation of H_2S

Na_2S flakes are taken into a double neck Round bottom flask fitted with a rubber septum. Into the round bottom flask, 40% H_2SO_4 is added through a glass syringe. When H_2SO_4 is reacted with Na_2S, it generates H_2S gas. The released gas is trapped in a rubber balloon attached to the round bottom flask through a syringe. Then the H_2S gas is injected directly into the HBSD solution in NMP and leave it to form the gel.

2A.5.7 Methylene blue assay

To quantify the loaded H_2S in HBSD gel and their release profile, a standard plot was arrived at by preparing 1.0 mM Na_2S as a stock solution. 5 mL of Na_2S at varying concentrations ranging from 10 to 100 μM were prepared from the stock solution. Samples for the assay are prepared by taking 0.5mL of each concentration of Na_2S solution and mixing it with 0.5mL of $FeCl_3$ solution, followed by 0.5 mL of *N*,*N*-Dimethyl phenylene diamine sulfate solution. The samples are incubated at room temperature for 3 h, and the absorbance of each sample is recorded using a UV-Vis Spectrometer.[52] During this process, the formation of methylene blue displayed absorbance at 667 nm, and the intensity increased with the increase in the concentration of Na_2S. Linear regression analysis is performed by taking the absorbance values at 667 nm.[53] The quantification of H_2S release from HBSD gel has been performed in duplicate. To the H_2S entrapped HBSD gel, pH = 4 buffer solution is added, and aliquots of 0.5 mL are collected every 30-minute time intervals. To these aliquots, 0.5 mL of $FeCl_3$ solution, followed by 0.5 mL of *N*,*N*-Dimethyl phenylene diamine sulfate solution, was added and incubated for 3 h at room temperature. The formation of methylene blue was confirmed by the absorbance at 667 nm using UV-Vis spectroscopy and interpolated with the linear regression plot to obtain the concentration of H_2S released at different time intervals.

2A.6 Characterisation data

2A.6.1 ^{1}H-NMR, ^{13}C-NMR, HRMS data of synthesized compounds

TBSD (3): The product is obtained as a white solid with 78% yield.

^{1}H NMR (400 MHz, DMSO-d_6) δ 10.04 (s, 2H, C<u>H</u>O), 7.95 (d, J = 6.4 Hz, 4H, Ar<u>H</u>), 7.70 (t, J = 8.6 Hz, 4H, Ar<u>H</u>), 7.57-7.42 (m, 4H, Ar<u>H</u>), 6.03 – 5.65 (m, 4H, C<u>H</u>(OR)$_2$), 4.97 – 4.81 (m, 1H), 4.60 – 4.32 (m, 3H), 4.30 – 4.10 (m, 6H), 4.09 – 3.95 (m, 2H), 3.94 – 3.84 (m, 1H), 3.80 (s, 1H), 3.62 (d, J = 4.9 Hz, 1H), 3.49 (dt, J = 11.9, 5.9 Hz, 1H), 3.67-3.52 (m, 1H), 3.29 – 3.16 (m, 3H).

^{13}C NMR (100 MHz, DMSO-d_6) δ 193.45, 144.66, 137.23, 136.75, 130.48, 129.78, 127.82, 127.36, 126.29, 102.56, 99.54, 98.99, 78.05, 69.81, 69.02, 68.10, 63.03, 48.96, 30.58, 29.48, 17.69.

ESI-MS: *m/z* calculated for $C_{36}H_{38}O_{14}$ $[M+Na]^+$ is 717.2159: found *m/z* = 717.2135.

HBSD (4): The product is obtained as a white solid with 79% yield.

^{1}H NMR (400 MHz, DMSO-d_6) δ: 10.03 (s, 2H, C<u>H</u>O), 7.94 (d, J = 7.8 Hz, 4H, Ar<u>H</u>), 7.77 – 7.65 (m, 4H, Ar<u>H</u>), 7.58 – 7.38 (m, 8H, Ar<u>H</u>), 5.99 – 5.75 (m, 3H, C<u>H</u>(OR)$_2$), 5.74-5.63 (3, 3H, C<u>H</u>(OR)$_2$), 4.59 – 4.09 (m, 8H), 4.07 – 3.94 (m, 2H), 3.93 – 3.82 (m, 2H), 3.82-3.73(m, 2H), 3.72-3.52(m, 4H), 3.52-3.37 (m, 9H), 3.26-3.14(m, 3H)

^{13}C NMR (100 MHz, DMSO-d_6) δ: 193.44, 145.00, 136.80, 129.87, 129.79, 127.39, 126.28, 102.81, 99.56, 78.12, 70.55, 69.59, 68.91, 68.14, 63.04.

ESI-MS: *m/z* calculated for $C_{50}H_{54}O_{20}$ $[M+Na]^+$ is 997.3101: found *m/z* = 997.3100.

OBSD (5): The product is obtained as a white solid with 72% yield.

^{1}H NMR (400 MHz, DMSO-d_6) δ 10.03 (s, 2H, C<u>H</u>O), 7.94 (d, J = 7.9 Hz, 4H, Ar<u>H</u>), 7.70 (q, J = 7.1 Hz, 4H, Ar<u>H</u>), 7.59-7.36(m, 12H, Ar<u>H</u>), 6.00 – 5.89 (m, 1H, C<u>H</u>(OR)$_2$), 5.83 (d, J = 10.9 Hz, 1H, C<u>H</u>(OR)$_2$), 5.77 (s, 1H, C<u>H</u>(OR)$_2$), 5.69 (q, J = 6.8 Hz, 4H, C<u>H</u>(OR)$_2$), 5.60-5.44 (m, 1H, C<u>H</u>(OR)$_2$), 4.52 (s, 1H), 4.38 (s, 1H), 4.19 (q, J = 11.6 Hz, 10H), 4.05-3.94 (m, 4H), 3.90-3.74 (m, 6H), 3.73-3.65 (m, 2H), 3.59 (m,6H), 3.45 (m, 9H), 3.17(s,1H).

DBSD (6): The product is obtained as a white solid with 13% yield.

^{1}H NMR (400 MHz, DMSO-d$_6$) δ 10.03 (s, 2H, C<u>H</u>O), 7.94 (d, J = 7.0 Hz, 4H, Ar<u>H</u>), 7.69 (t, J = 8.3 Hz, 4H, Ar<u>H</u>), 7.60 – 7.35 (m, 16H, Ar<u>H</u>), 6.00 – 5.33 (m, 10H, C<u>H</u>(OR)$_2$), 4.94 – 4.80 (m, 2H), 4.74-4.63 (m, 1H), 4.50-4.22 (m, 6H), 4.27-4.09 (m, 13H), 4.07-3.92 (m,5H), 3.92 – 3.73 (m, 6H), 3.69 (d, J = 11.4 Hz, 1H), 3.59 (s, 4H), 3.54 – 3.46 (m, 6H), 3.23 (s, 6H).

2A.6.2 ^{1}H-NMR, ^{13}C-NMR, HRMS spectra of synthesized compounds

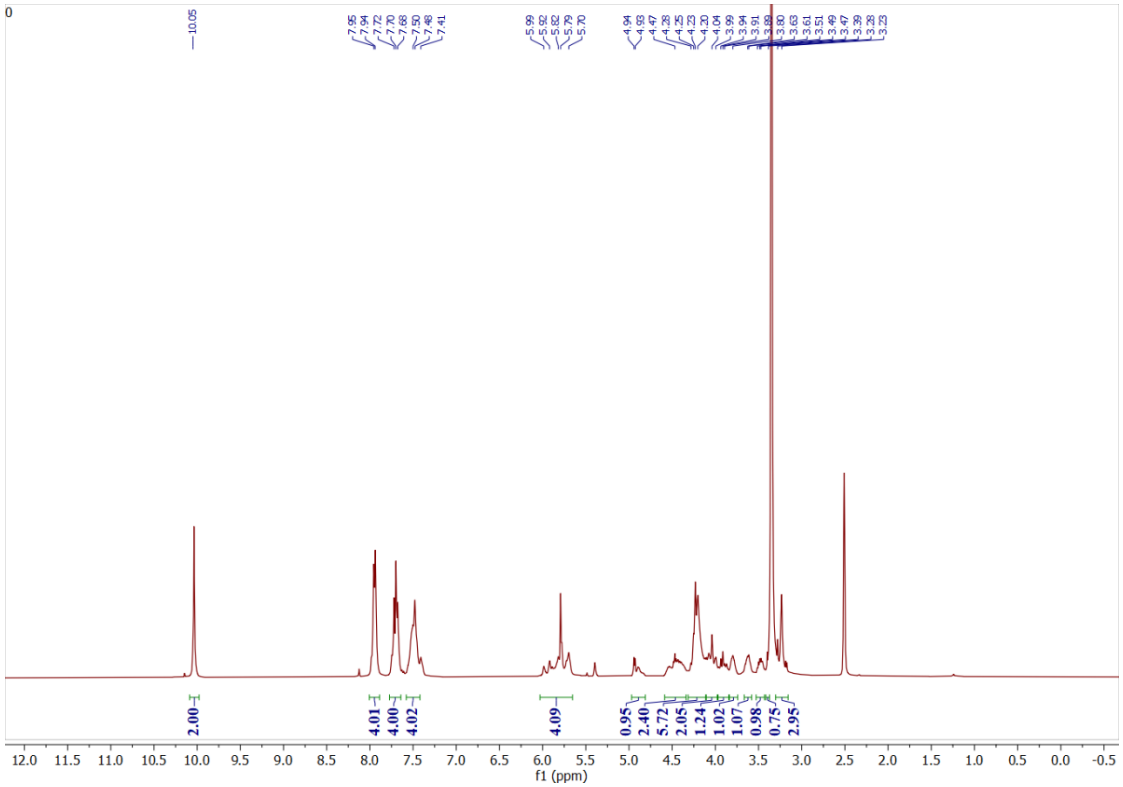

Figure 2A.8. ^{1}H NMR (400MHz) of compound 2.2 in DMSO-d_6 at 28 °C.

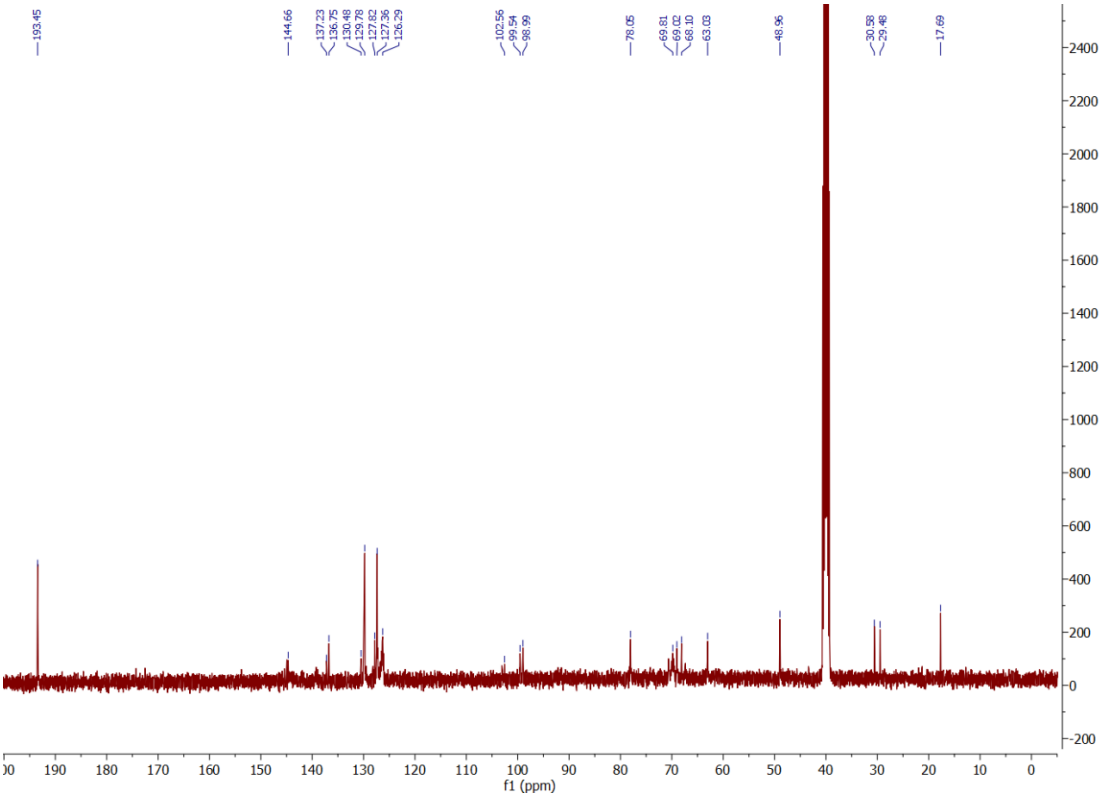

Figure 2A.9. ^{13}C NMR (100MHz) of compound 2.2 in DMSO-d_6 at 28 °C.

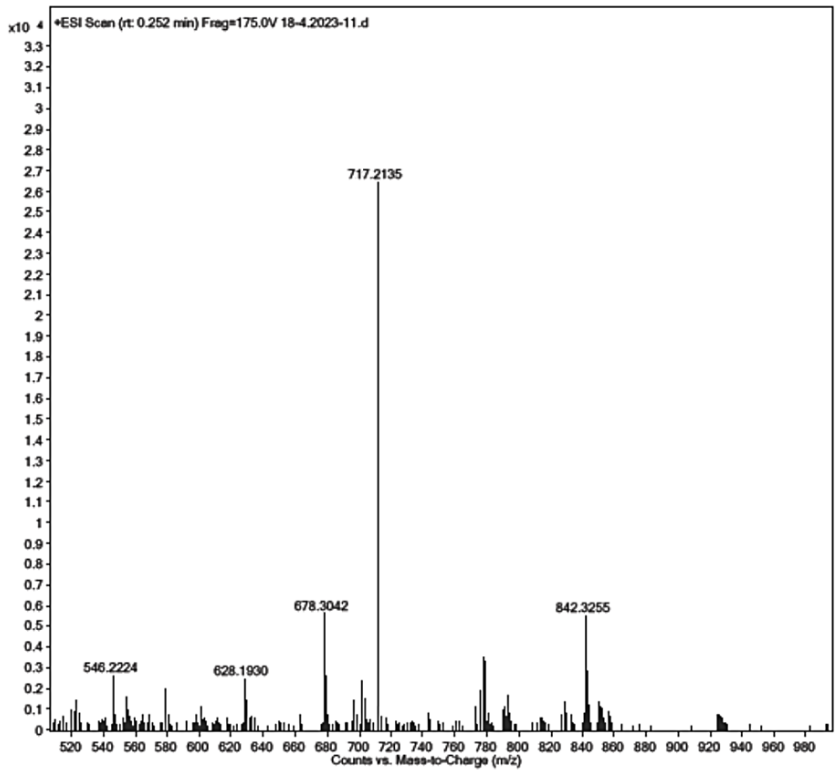

Figure 2A.10. HRMS Spectra of compound 2.2 dissolved in methanol.

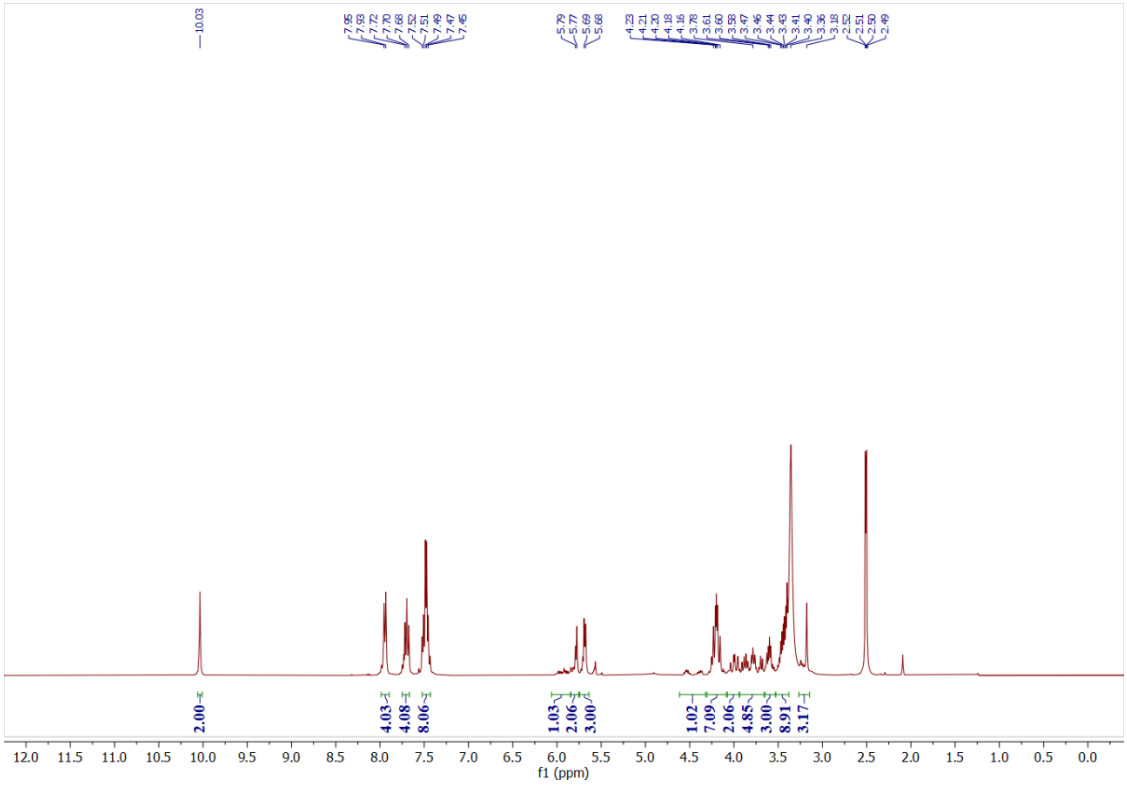

Figure 2A.11. ^{1}H NMR (400MHz) of compound 2.3 in DMSO-d_6 at 28 °C.

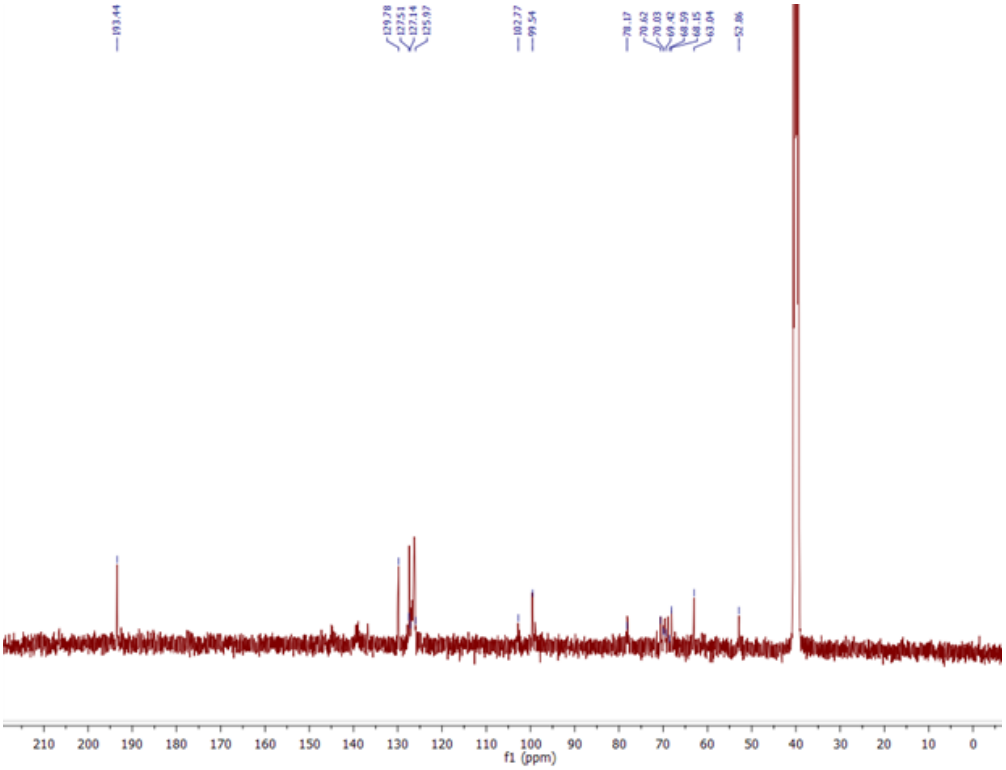

Figure 2A.12. ^{13}C NMR (100MHz) of compound 2.3 in DMSO-d_6 at 28 °C.

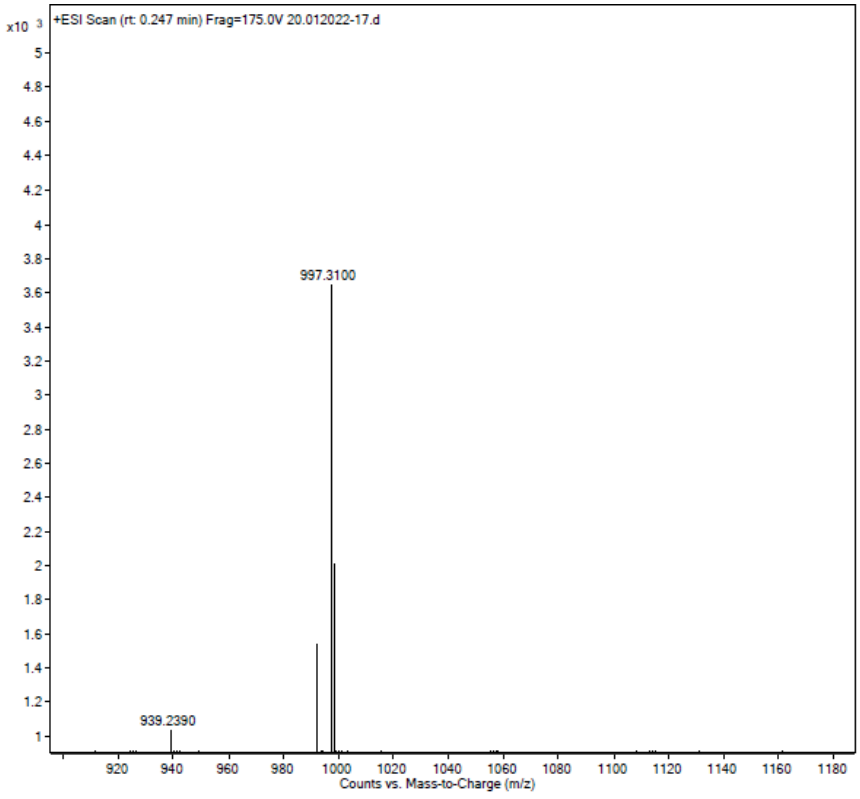

Figure 2A.13. HRMS Spectra of Compound 2.3 dissolved in methanol.

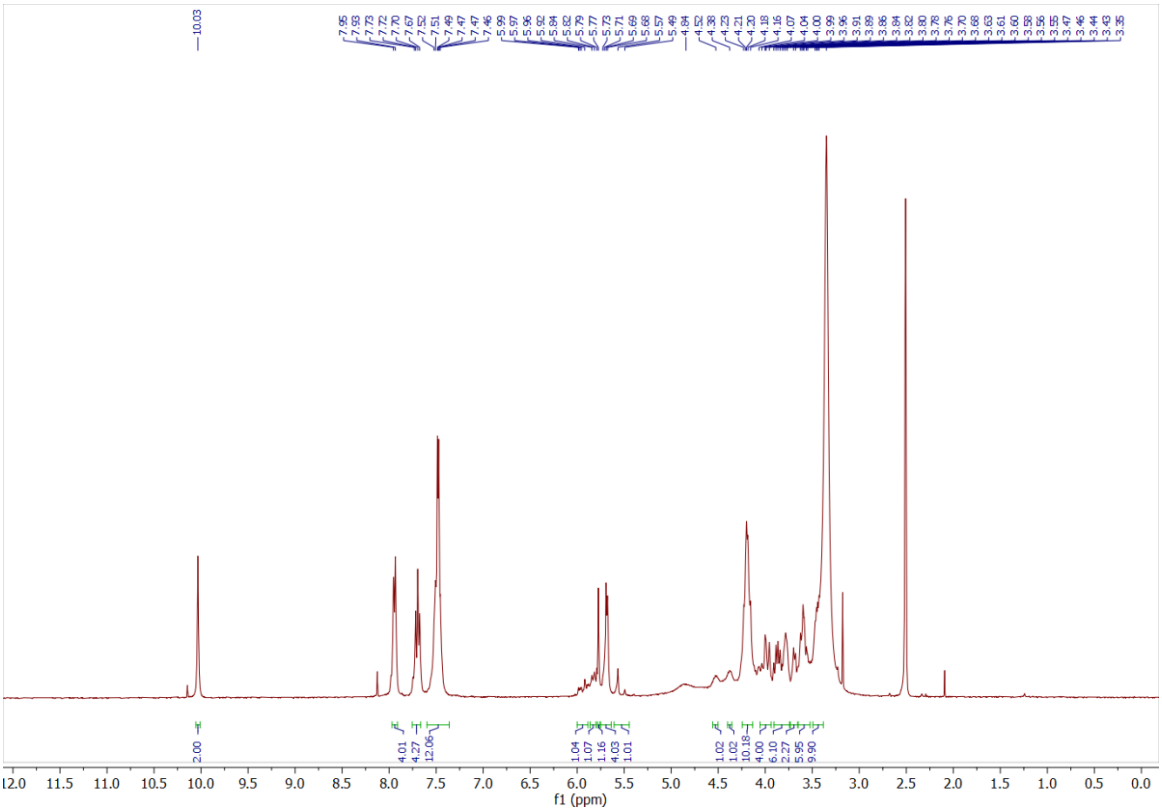

Figure 2A.14. ^{1}H NMR (400MHz) of compound 2.4 in DMSO-d_6 at 28 °C.

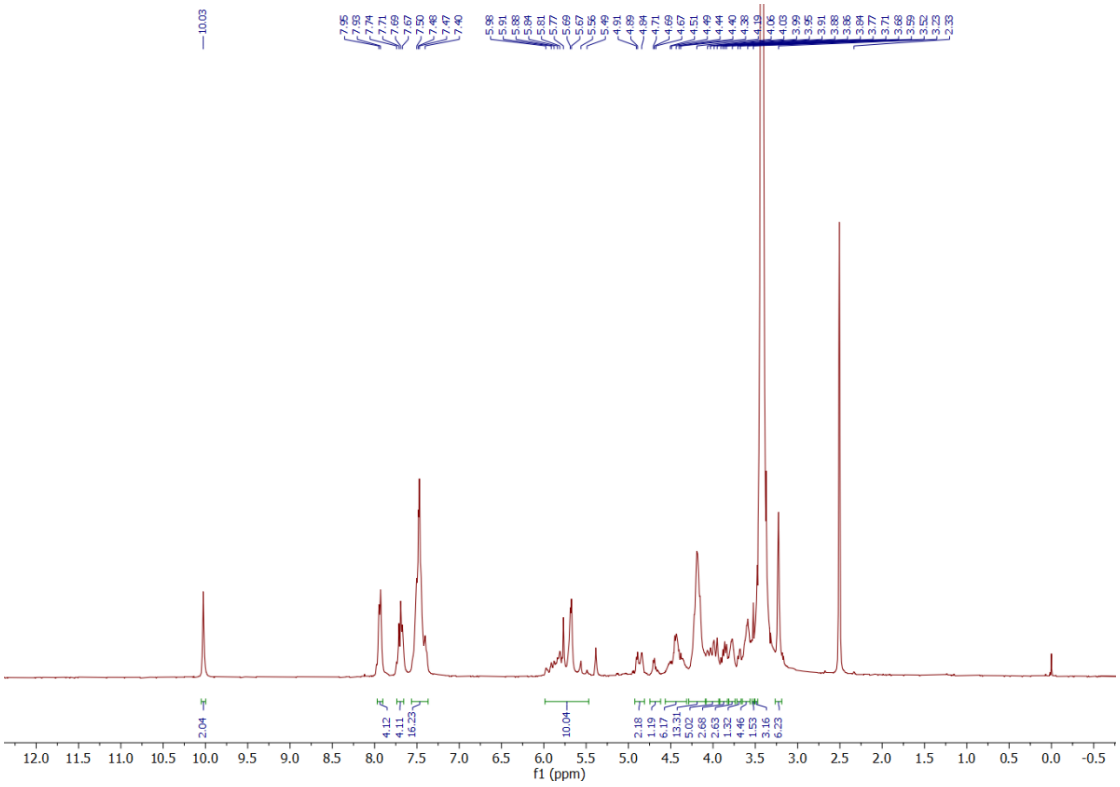

Figure 2A.15. ^{1}H NMR(400MHz) of compound 2.5 in DMSO-d_6 at 28 °C.

2A.7 Conclusion

In summary, oligo[1,3:2,4-(O-benzylidene)-D-sorbitol]-dialdehydes (OBSDA) are synthesized using environmentally benign protocol in good yields. Supramolecular gelation of HBSD, one of the OBSDA compounds displayed gelation in FDA-approved pharmaceutical solvents, N-methyl pyrrolidone (NMP). Molecular level interactions such as H-bonding and π- π stacking responsible for the formation of supramolecular architecture have been identified using NMR and FTIR analysis. Morphology and mechanical strength analysis establish the suitability of gel for pharmaceutical applications. Owing to the volatile nature of H_2S, till to date researchers utilized additional H_2S donors in fabricating drug delivery systems. This chapter deals with the direct encapsulation of H_2S gas into the gel matrix and stimuli-responsive delivery via gel-to-sol transition and demonstrates the suitability of NMP gel in evaluating the physiological role of H_2S in various biological processes. It also has scope in transdermal drug delivery applications, as NMP has a high penetrating capacity on the skin.

2A.8 References

1 F. Huang and E. V. Anslyn, *Chem. Rev.*, 2015, **115**, 6999.

2 B. X. Jie Zhou, Jie Li, Xuewen Du, *Biomaterials*, 2017, **129**, 1–27.

3 A. Hardenia, N. Maheshwari, S. S. Hardenia, S. K. Dwivedi, R. Maheshwari and R. K. Tekade, *Scientific rationale for designing controlled drug delivery systems*, Elsevier Inc., 2018.

4 D. Yadav, K. Sandeep, D. Pandey and R. K. Dutta, *J Biotechnol Biomater*, 2017, **7**, 1000276.

5 H. S. Kapare and S. R. Metkar, *Pharm. Reson. 2020, 2 ,2.*

6 A. Z. Wilczewska, K. Niemirowicz, K. H. Markiewicz and H. Car, *Pharmacol. rep.*, 2012, **64**, 1020–1037.

7 E. Chappel, *Implantable drug delivery devices*, Elsevier Inc., 2021.

8 W. B. Liechty, D. R. Kryscio, B. V. Slaughter and N. A. Peppas, *Annu Rev Chem Biomol Eng.*, 2010, **1**, 149–173.

9 Z. Li, J. Cao, H. Li, H. Liu, F. Han, Z. Liu, C. Tong and S. Li, *Drug Deliv*, 2016, **23**, 3168–3178.

10 E. Beltrán-Gracia, A. López-Camacho, I. Higuera-Ciapara, J. B. Velázquez-Fernández and A. A. Vallejo-Cardona, *Nanomedicine review: Clinical developments in liposomal applications*, Springer Vienna, 2019, vol. 10.

11 R. K. Thapa and J. O. Kim, *J. Pharm. Investig.*, 2023, **53**, 19–33.

12 R. Wang, *FASEB J.*, 2002, **16**, 1792–1798.

13 K. Abe and H. Kimura, *The Possible Role of Hydrogen Sulfide as an Endogenous Neuromodulator*, 1996, vol. 76.

14 A. Katsouda, S.-I. Bibli, A. Pyriochou, C. Szabo and A. Papapetropoulos, *Pharmacol. Res.*, 2016, **113**, 175–185.

15 D. Wu, N. Luo, L. Wang, Z. Zhao, H. Bu, G. Xu, Y. Yan, X. Che, Z. Jiao, T. Zhao, J. Chen, A. Ji, Y. Li and G. D. Lee, *Sci. Rep.*, 2017, **7**, 455.

16 R. C. O. Zanardo, V. Brancaleone, E. Distrutti, S. Fiorucci, G. Cirino and J. L. Wallace, *FASEB J.*, 2006, **20**, 2118–2120.

17 R. Wang, *Physiol. Rev.*, 2012, **92**, 791–896.

18 D. J. Lefer, *Proc. Natl. Acad. Sci. U. S. A.*, 2007, **104**, 17907–17908.

19 W. Rumbeiha, E. Whitley, P. Anantharam and D. Kim, *Ann. N.Y. Acad. Sci.*, 2016, **1378**, 5–16.

20 H. Ali, C. Opere and S. Singh, *AAPS PharmSciTech*, 2014, **15**, 910–919.

21 Omer Kabil, N. Motl and and R. Banerjee, *Biochim Biophys Acta*, 2014, **1844**, 1355–1366.

22 A. K. Gilbert and M. D. Pluth, *J. Am. Chem. Soc.*, 2022, **144**, 17651–17660.

23 C. R. Powell, J. C. Foster, B. Okyere, M. H. Theus and J. B. Matson, *J. Am. Chem. Soc.*, 2016, **138**, 13477–13480.

24 W. Wang, X. Sun, H. Zhang, C. Yang, Y. Liu, W. Yang, C. Guo and C. Wang, *Int. J. Nanomedicine*, 2016, **11**, 3255–3263.

25 M. K. Marwah, H. Shokr, L. Sanchez-Aranguren, R. K. S. Badhan, K. Wang and S. Ahmad, *Pharm. Res.*, 2022, **39**, 341–352.

26 S. H. Yu, L. Esser, S. Y. Khor, D. Senyschyn, N. A. Veldhuis, M. R. Whittaker, F. Ercole, T. P. Davis and J. F. Quinn, *J. Polym. Sci. Part A Polym. Chem.*, 2019, **57**, 1982–1993.

27 H. Zhang, L. Z. Hao, J. A. Pan, Q. Gao, J. F. Zhang, R. K. Kankala, S. Bin Wang, A. Z. Chen and H. L. Zhang, *J. Control. Release*, 2021, **329**, 286–298.

28 A. Longchamp, K. Kaur, D. Macabrey, C. Dubuis, J. M. Corpataux, S. Déglise, J. B. Matson and F. Allagnat, *Acta Biomater.*, 2019, **97**, 374–384.

29 X. Sun, Y. Wang, S. Wen, K. Huang, J. Huang, X. Chu, F. Wang and L. Pang, *J. Nanobiotechnology*, 2021, **19**, 1–16.

30 H. Z. H Zhang, LZ Hao, JA Pan, Q Gao, JF Zhang, RK Kankala, SB Wang, AZ Chen, *J. Control. Release.*, 2021, **329**, 286–298.

31 W. L. W Liang, J Chen, L Li, M Li, X Wei, B Tan, Y Shang, G Fan, W Wang, *ACS Appl. Mater. Interfaces.*, 2019, **11**, 14619–14629.

32 I. T. Takatani-Nakase , M. Katayama , C. Matsui , K. Hanaoka , A. J. van der Vlies , K. Takahashi, *Mol. Biosyst.*, 2017, **13**, 1705–108.

33 L. P. X Sun, Y Wang, S Wen, K Huang, J Huang, X Chu, F Wang, *J. Nanobiotechnol.*, 2019, **19**, 40.

34 L. A. C. et al. Z Xiao, T Bonnard, A Shakouri-Motlagh, RAL Wylie, J Collins, J White, *Chem. Eur J.*, 2017, **23**, 11294–11300.

35 H. S. WC Lin, WY Pan, CK Liu, WX Huang, HL Song, KS Chang, MJ Li, *Biomaterials*, 2018, **182**, 289–298.

36 H. H. et al. Z Zheng, A Chen, Y Chen, J Chen, AA Albashari, J Li, J Yin, Z He, Q Wang, *J. Mater. Chem. B.*, 2019, **7**, 611–618.

37 Y. Z. Y Yu, Z Wang, Q Ding, X Yu, Q Yang, R Wang, Y Fang, W Qi, J Liao, W Hu, *Pharmaceutics*, 2021, **13**, 742.

38 A. V. D. V. U Hasegawa, *MedChemComm.*, 2015, **6**, 273–276.

39 Q. W. J Wu, Y Li, C He, J Kang, J Ye, Z Xiao, J Zhu, A Chen, S Feng, X Li, J Xiao, M Xian, *ACS Appl. Mater. Interfaces.*, 2016, **8**, 27474–27481.

40 Y. A. er al. J Wu, A Chen, Y Zhou, S Zheng, Y Yang, *Biomaterials*, 2019, **222**, 119398.

41 Q. W. X Zhao, L Liu, T An, M Xian, JA Luckanagul, Z Su, Y Lin, *Acta Biomater*, 2020, **104**, 85–94.

42 A. M. R Raggio, W Bonani, E Callone, S Dirè, L Gambari, F Grassi, *Biomater. Sci. Eng.*, 2018, **4**, 2956–2966.

43 S. M. A Mauretti, A Neri, O Kossover, D Seliktar, PD Nardo, *Macromol. Biosci.*, 2016, **16**, 847–858.

44 J. F. Q. et al. NV Dao, F Ercole, MC Urquhart, LM Kaminskas, CJ Nowell, TP Davis, *Biomater. Sci.*, 2021, **9**, 834–846.

45 N. G. Y Liu, F Yang, C Yuan, M Li, T Wang, B Chen, J Jin, P Zhao, J Tong, S Luo, *ACS Nano.*, 2017, **11**, 1509–1519.

46 P. H. T He, X Qin, C Jiang, D Jiang, S Lei, J Lin, WG Zhu, J Qu, *Theranostics.*, 2022, **10**, 2453–2462.

47 X. C. C Xie, D Cen, Z Ren, Y Wang, Y Wu, X Li, G Han, *Adv. Sci.*, 7AD, **7**, 1903512.

48 J. L. L Lin, H Qin, J Huang, H Liang, D Quan, *2018*, 9AD, **21**, 2942–2950.

49 T. D. F Ercole, FM Mansfeld, M Kavallaris, MR Whittaker, JF Quinn, ML Halls, *Biomacromolecules.*, 2016, **17**, 371–383.

50 Q. W. S Feng, Y Zhao, M Xian, *Acta Biomater.*, 2015, **27**, 205–213.

51 M. Zhou, Y. Qian, Y. Zhu and J. Matson, *Chem. Commun.*, 2020, **56**, 1085–1088.

52 J. M. Y Wang, Z Li, Y Shmidov, RJ Carrazzone, R Bitton, *J. Am. Chem. Soc*, 2020, **142**,

20058–20065.

53 J. Q. F Ercole, MR Whittaker, ML Halls, BJ Boyd, TP Davis, *Chem. Commun.*, 2017, **53**, 8030–8033.

54 N. V. Dao, F. Ercole, L. M. Kaminskas, T. P. Davis, E. K. Sloan, M. R. Whittaker and J. F. Quinn, *Biomacromolecules*, 2020, **21**, 5292–5305.

55 J. Du D Liu, Y Liao, EJ Cornel, M Lv, T Wu, X Zhang, L Fan, M Sun, Y Zhu, Z Fan, *Chem. Mater.*, 2021, **33**, 7972–7985.

56 M. Wan, Z. Liu, T. Li, H. Chen, Q. Wang, T. Chen, Y. Tao and C. Mao, *Angew. Chem. Int. Ed.*, 2021, **60**, 16139–16148.

57 E. Gazzano, I. Buondonno, A. Marengo, B. Rolando, K. Chegaev and et al J. Kopecka, *Cancer Lett.*, 2019, **456**, 29–39.

58 et al. Li J., Xie L., Li B., Yin C., Wang G., Sang W., *Adv. Mater.*, 2021, **33**, 2008481.

59 A. A. Yueqin Zheng, Bingchen Yu, Ladie Kimberly De La Cruz, Manjusha Roy Choudhury and B. Wang, *Med. Res. Rev.*, 2017, **00**, 1–44.

60 B. M. Kuljeet Kaur, Yin Wang, John, *Biomacromolecules*, 2020, **21**, 1171–1178.

61 Y. Qian, K. Kaur, J. C. Foster and J. B. Matson, *Biomacromolecules*, 2019, **20**, 1077–1086.

62 Y. Wang, K. Kaur, S. J. Scannelli, R. Bitton and J. B. Matson, *J. Am. Chem. Soc.*, 2018, **140**, 14945–14951.

63 J. B. M. Yun Qiana, Afnan Altamimib, c, Shaina Alston Yatesb, Santu Sarkarb, Matthew Cochranb, Mingjun Zhoua, Nicole Levi-Polyachenkob, *Biomater Sci*, 2020, **8**, 2564–2576.

64 W. Liang, J. Chen, L. Li, M. Li, X. Wei, B. Tan, Y. Shang, G. Fan, W. Wang and W. Liu, *ACS Appl. Mater. Interfaces*, 2019, **11**, 14619–14629.

65 A. Thamizhanban, K. Lalitha, G. P. Sarvepalli, C. U. Maheswari, V. Sridharan, J. B. B. Rayappan and S. Nagarajan, *J. Mater. Chem. B*, 2019, **7**, 6238–6246.

66 J. Wu, A. Chen, Y. Zhou, S. Zheng, Y. Yang, Y. An, K. Xu, H. He, J. Kang, J. A.

Luckanagul, M. Xian, J. Xiao and Q. Wang, *Biomaterials*, 2019, **222**, 119398.

67 C. R. Powell, K. M. Dillon and J. B. Matson, *Biochem pharmacol*, 2018, **176**, 110–123.

68 B. O. Okesola, M. P. Vieira, D. J. Cornwell, N. K. Whitelaw and D. K. Smith, *Soft Matter*, 2015, **11**, 4768–4787.

69 R. C. Deis and M. W. Kearsley, *Sweeten. Sugar Altern. Food Technol.*, 2012, 331–346.

70 A. Jouyban, M. A. A. Fakhree and A. Shayanfar, 2010, **13**, 524–535.

71 R. B. N. L. Kohl, in *Handbook of Natural Gas Transmission and Processing*, 2019, pp. 231–269.

72 E. J. Howe, B. O. Okesola and D. K. Smith, *Chem. Commun.*, 2015, **51**, 7451–7454.

73 C. C. Piras, A. K. Patterson and D. K. Smith, *Chem. - A Eur. J.*, 2021, **27**, 13203–13210.

74 K. Peng, T. Sottmann and C. Stubenrauch, *Mol. Physics, 2021, 119*.

75 B. Springs, C. Xie and J. Xia, A1, US 2006/0079720, 2006.

76 A. Das, P. K. Mandal, F. J. Lovas, C. Medcraft, N. R. Walker and E. Arunan, *Angew. Chemie - Int. Ed.*, 2018, **57**, 15199–15203.

77 Z. Yang, L. Feng, D. Jun-Bao, T. Chao-Shu, X. Guo-Heng and G. Bin, *Acta Physiol. Sininca*, 2012, **64**, 681–686.

CHAPTER 2B

PREPARATION OF POLYPHENYLENE SULFIDE IN CONFINED REACTION MEDIA

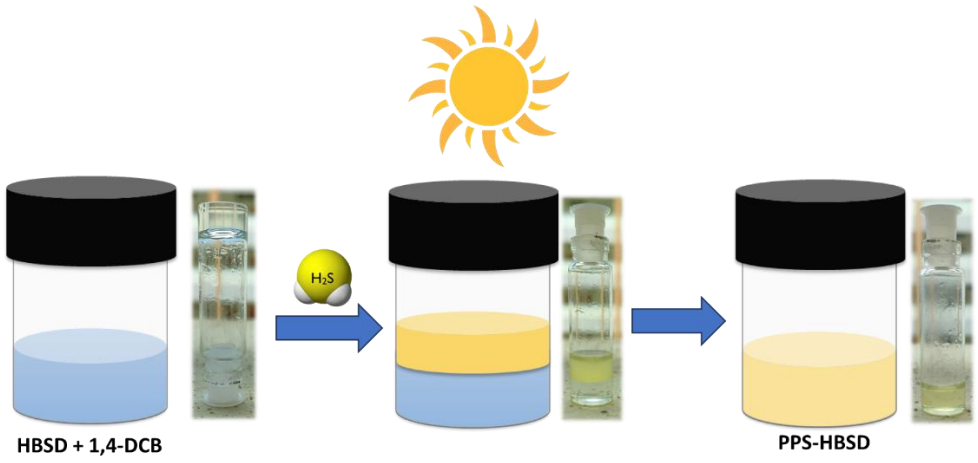

2B.1 Objective

This chapter aims to develop an environmentally friendly and energy-efficient synthesis method for polyphenylene sulfide (PPS) using a confined media approach, where H_2S entrapped in an oligo[1,3:2,4-(O-benzylidene)-D-sorbitol]-dialdehyde (HBSD)-N-methyl pyrrolidone (NMP) gel matrix reacts with 1,4-dichlorobenzene at mild temperatures, eliminating the need for high temperatures, pressures, and strong chemicals typically required in conventional PPS synthesis methods.

2B.2 Abstract

A sustainable, eco-friendly protocol for the synthesis of poly(p-phenylene sulfide) using a dibenzylidene sorbitol-derived oligomeric gel in N-methyl-2-pyrrolidone (NMP) as a confined medium. This approach leverages the H2S-entrapment properties of HBSD gels in NMP solvent, eliminating the need for sodium sulfide and reducing unwanted side reactions. The resulting PPS-HBSD composite exhibits enhanced thermal stability, mechanical strength, and self-healing properties. Characterization via FTIR, XRD, SEM, and rheology reveals the composite's unique supramolecular structure and potential for applications in advanced materials. This sustainable protocol offers a significant advancement in PPS synthesis, demonstrating the versatility of confined gel matrices in polymer synthesis.

2B.3 Introduction

The aerospace, automotive, and energy industries share a common need for high-performance materials that combine lightweight properties with high load-carrying capacity. As a result, engineering thermoplastics have garnered significant attention in these sectors. Specifically, poly(phenylene sulfide) (PPS), poly(ether-ether-ketone), poly(aryl-ether-ketone), and poly(ether-imide) have emerged as promising materials, owing to their exceptional mechanical properties, thermal stability, and resistance to chemical degradation. The use of these advanced thermoplastics is expected to play a crucial role in the development of next-generation components and systems, enabling the creation of lighter, more efficient, and more sustainable structures and devices.[1] PPS is one of the high-performance thermoplastic and semi-crystalline polymers. Its linear and rigid chemical structure, comprising alternating para-substituted rings of phenylene and sulfur atoms (Figure 2B.1), confers its distinctive characteristics. Specifically, PPS exhibits a high melting temperature, ranging from 270 to 290°C, a glass transition temperature of approximately 90°C, and a thermal decomposition temperature of around 508°C. Additionally, its coefficient of linear thermal expansion is 49 µm/m°C, making

it an ideal material for applications demanding high thermal stability and dimensional integrity.[2] Specifically, PPS demonstrates outstanding thermal stability, minimal thermal degradation[3], high flame resistance, superior mechanical properties (including high modulus, tensile strength, dimensional stability, and fatigue resistance), excellent chemical stability (resistance to solvents), and low moisture absorption.[4,5] Owing to its properties, PPS was widely used in aerospace,[6] automotive,[7] and wind energy.[8]

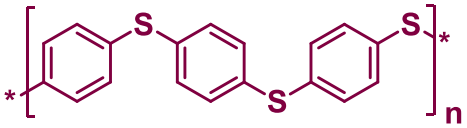

Polyphenylene sulfide

(2.6)

Figure 2B.1. Molecular structure of PPS.

The use of confined media to synthesize polymers has significantly influenced the reaction kinetics and polymer properties.[9] Nature's enzymatic polymerizations, which produce DNA and protein biopolymers, occur within confined and organized molecular-scale spaces, relying on specific noncovalent (e.g., hydrogen bonds) and covalent (e.g., peptide bonds) interactions.[10] Inspired by the exquisite control over hierarchical organization and assembly in natural systems, molecular engineers have long sought to replicate this control in synthetic materials. While synthetic materials still lag behind their natural counterparts in terms of complex multifunctionalities, Molecular engineering, guided by biological principles, enables precise control over the structure and assembly of synthetic materials across various length scales, allowing for the tuning of their molecular, nanoscopic, and macroscopic properties. By mimicking nature's strategies, researchers can design and engineer synthetic materials with tailored properties, bridging the gap between natural and synthetic systems. Various confined media have been extensively documented in the literature, including nanoparticles, micelles, zeolites, MOFs, enzymes, and gels, which offer unique environments for polymerization reactions[11,12] (Figure 2B.2).

Clasen in 1956 performed polymerization of dimethyl butadiene clatharated within thiourea.[13] Aida and Ting et al. showed that confined nanopore reactors with appropriate catalysts suppress chain transfer reactions, yielding linear polymers with ultrahigh molecular weights and exceptional strength.[14] Beers and co-workers observed that in confined media, the radical polymerization can be controlled, thereby limiting the chain transfer reaction and irreversible termination.[15] Bharathi and Moore discovered that the polymerization of AB_2

monomers in confined spaces yielded hyperbranched polymers with low polydispersity, indicating a high degree of molecular uniformity.[16] Jianxin et al. synthesized 2D sheets of functional conjugated poly(3,4-ethylenedioxythiophene) with controlled morphology and high crystallinity using micelles as confined media.[17] Demetrio and coworkers have synthesized polyacetylene in SiO_2 Zeolite, by using pressure as the only driving force.

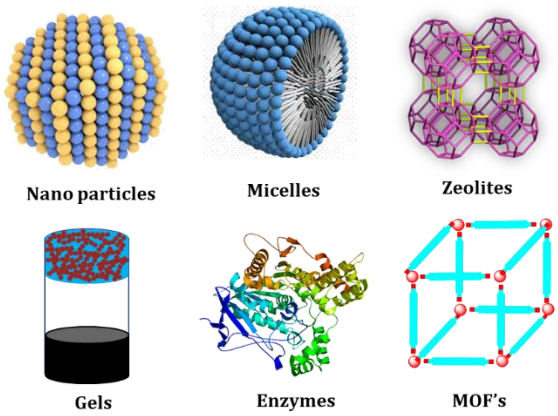

Figure 2B.2. Various confined media used for polymerization reactions

The sodium sulfide method is commonly employed for the preparation of PPS. This process involves the polymerization of sodium sulfide and p-dichlorobenzene (DCB) at an elevated temperature of 230-250°C and high pressure in the polar aprotic solvent N-methyl-2-pyrrolidone (NMP).[18] During the pre-polymerization stage, sodium sulfide undergoes hydrolysis to form sodium hydrosulfide (NaSH) and sodium hydroxide. The latter can react with NMP to produce sodium N-methyl-4-aminobutyrate (SMAB), which forms a complex SMAB-NaSH that is soluble in NMP at high temperatures.[19] This complex enables the dissolution of sulfur elements in the organic phase, facilitating their participation in the polymerization reaction. However, SMAB can also engage in nucleophilic substitution reactions with the chlorine atoms in DCB or the chlorine end-groups of PPS, leading to a decrease in DCB activity or the termination of PPS chain growth.[20] Understanding these reactions is crucial for optimizing the synthesis of PPS with desired properties. To overcome the side reactions of salt contaminants and harsh reaction conditions, PPS is synthesized in a gel-based confined media, using direct H_2S gas as a sulfur source.

2B.4 Results and Discussion

NMP is industrially used as a solvent for the synthesis of PPS. In the conventional method, large amounts of NMP are used for the polycondensation reaction between 1,4-DCB and Na_2S in the presence of a base (NaOH/ Na_2CO_3). NMP also stabilizes the sulfide anions generated in the reaction.[21] This study reports a new approach to the in situ formation of PPS polymers within a gel matrix, a previously unexplored strategy for the synthesis of PPS. To achieve this, an oligomeric derivative of dibenzylidene sorbitol (DBS), namely HBSD, was synthesized and reported in Chapter 2A. The characterization and gelation studies of HBSD are also given in Chapter 2A. Notably, the HBSD-NMP gel serves as a confined medium for PPS polymerization, enabling the trapping of H_2S gas within the gel matrix. This approach eliminates the need for Na_2S, thereby reducing salt contaminants and unwanted polymerizations during the reaction. This method offers a promising route to synthesize PPS polymers with improved purity and controlled architecture. The HBSD-NMP gel was subjected to co-gelation with 1,4-DCB and H_2S at room temperature to initiate polymerization. However, even after 3 days, no evidence of PPS formation was observed, suggesting that the expected polymerization reaction did not occur under these conditions.

Several mechanisms have been proposed for the polymerization such as the radical cation mechanism and $S_{RN}1$ mechanism, However, it is now widely accepted that the chain growth steps proceed through the S_NAr mechanism, forming a Meisenheimer complex as the transitional state. This mechanism involves a nucleophilic attack of the sulfide anion on the activated aromatic ring, leading to the formation of a Meisenheimer complex (rate-determining step), which then collapses to form a new carbon-sulfur bond. This process repeats, resulting in the growth of the polymer chain.[22]

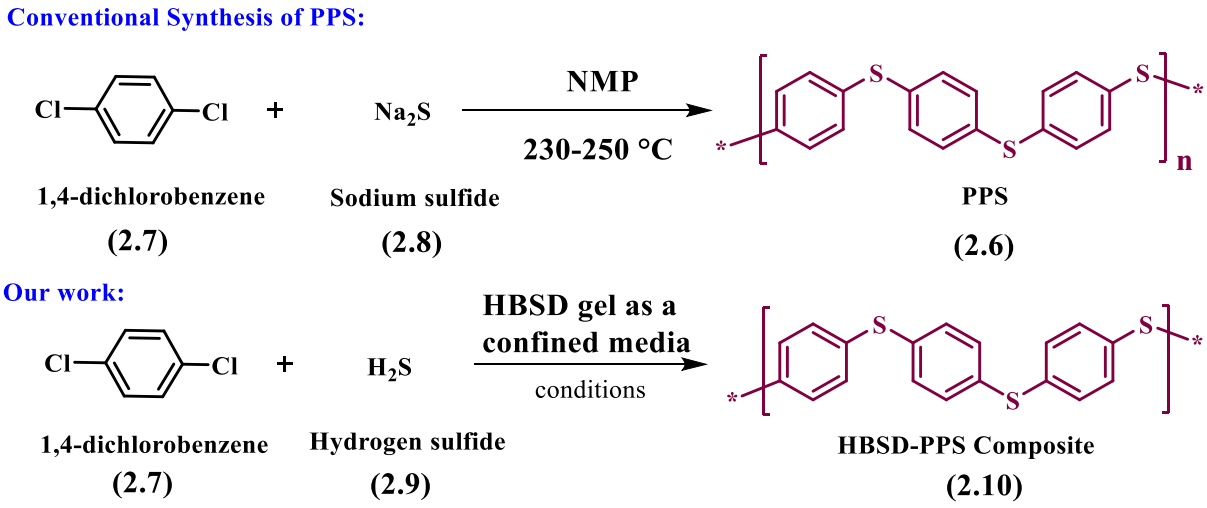

Scheme 2B.1. Synthesis of PPS

To enhance nucleophilicity and stabilize transition states, NaOH and Na_2CO_3 were added to the gel medium. However, despite these efforts, PPS formation was not observed. Interestingly, when the temperature was elevated to 50°C and maintained for 3 days, polymerization successfully occurred within the gel matrix, which is primarily confirmed by the formation of rigid pale-yellow gels exhibiting self-healing behaviour.

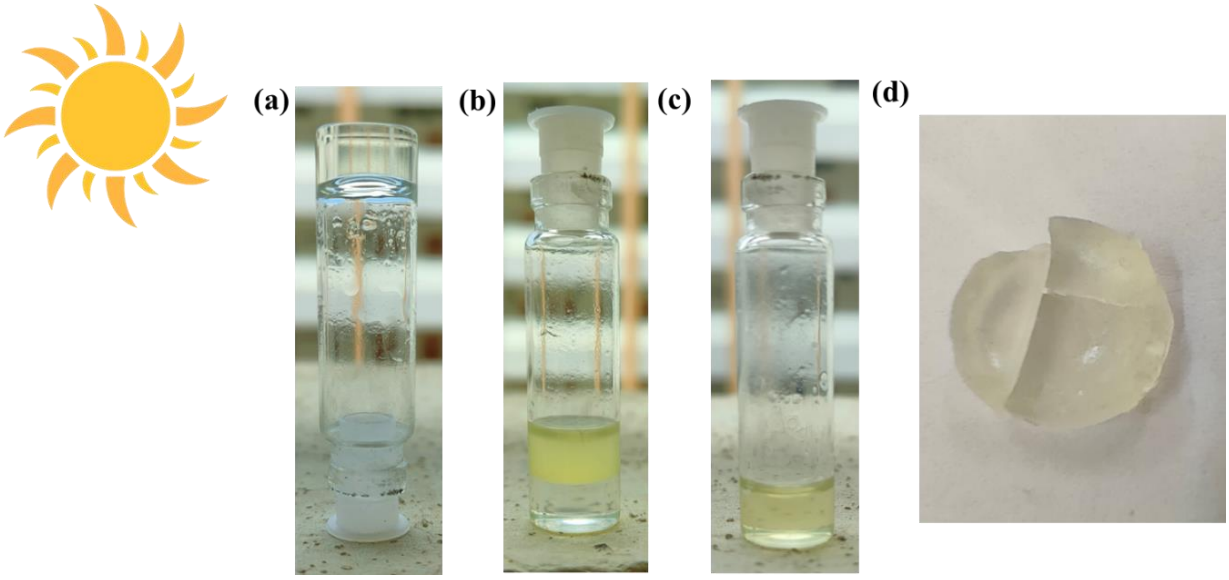

Figure 2B.3. (a) HBSD –NMP gel with 1,4- dichlorobenzene under sunlight; (b) addition of H_2S injected NMP solvent; (c) Formation of PPS-HBSD composite in gel under sunlight; (d) strong PPS composite gel showing self-healing properties.

Notably, identical results were obtained when the reaction was conducted in the gel medium under sunlight for 3 days, suggesting a facile and sustainable route to PPS synthesis. (Figure 2B.3) Formation of PPS in the gel matrix offers advantages like improved molecular weight control, reduced chain transfer reactions, increased polymer yield, enhanced polymer properties, simplified purification, reduced solvent usage, and improved safety.[23] The formed PPS-HBSD composite is confirmed by using FTIR, XRD, SEM, and rheological studies.

To study the flow properties of the gel, amplitude sweep, frequency sweep, and thixotropy studies were performed on the PPS-HBSD composite (Figure 2B.4). Intermolecular interactions governing the supramolecular architecture of the gels undergo deformation in response to stress or strain. By conducting strain amplitude sweep and angular frequency sweep experiments, the storage modulus (G') and loss modulus (G") can be determined, providing valuable insights into the gel's mechanical properties. Analyzing the changes in G' and G" as a function of strain amplitude and angular frequency reveals the gel's linear viscoelastic region, non-linear behaviour, relaxation mechanisms, and microstructure, ultimately shedding light on

its dynamics and behaviour under various conditions. Throughout the frequency sweep measurements of the PPS-HBSD gel, it was observed that the storage modulus G' consistently remained higher than the loss modulus G''; this indicates that PPS-HBSD gel exhibits stability and resilience towards external forces. The storage modulus G' values of PPS-HBSD have increased by multiple folds when compared to the storage modulus G' of HBSD gel (discussed in chapter 2A), this is attributed to the increase in gel strength due to the formation of PPS inside the gel (Figure 2B.4a). The amplitude sweep measurements demonstrate that the PPS-HBSD show gel-like behaviour (G'>G'') up to critical strain level 0.05%. After this point, a decrease in G' and G'' indicates the onset of fluid-like behaviour in the gels (Figure 2B.4b).

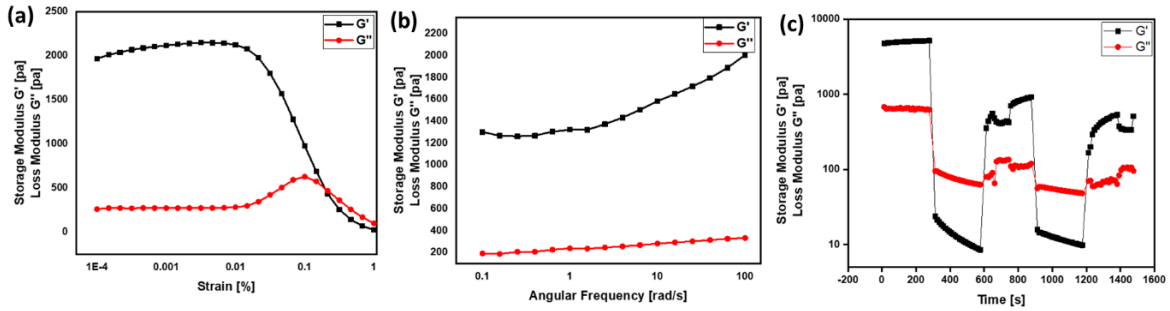

Figure 2B.4. Rheology studies of PPS-HBSD Hybrid gel (a) Amplitude sweep; (b) Frequency sweep; (c) Thixotropic studies

The thixotropic nature of gels reveals their ability to recover their structural integrity after being subjected to various strains. Subjecting the PPS-HBSD gel to a constant strain of 100% resulted in a decline in its strength. Upon reducing the strain to 0.1%, the gel's viscosity recovered, but with a slight reduction in the initial storage modulus value. This observation suggests that the poly(phenylene sulfide) (PPS) polymer forms a well-ordered structural architecture inside the gel matrix and when it is deformed, does not fully regain its original configuration upon strain removal (Figure 2B.4c). This incomplete recovery of storage modulus is attributed to the PPS structure interfering with the self-healing ability of the HBSD gel. This partially reversible behaviour was consistently observed through multiple cycles of strain ramp-up and ramp-down experiments.

FTIR spectral studies provided definitive evidence for the formation of PPS within the gel matrix (Figure 2B.5). The FTIR spectra exhibited distinctive absorption peaks at 1093 cm^{-1}, corresponding to the C-S stretching frequency, and 835 cm^{-1}, attributed to the deformation and stretching frequency of the C-H group in the 1,4-substituted benzene ring. Moreover,

characteristic peaks at 3409 cm^{-1} and 1694 cm^{-1} were observed, which are associated with the hydroxy and aldehyde groups of the HBSD molecules, respectively.

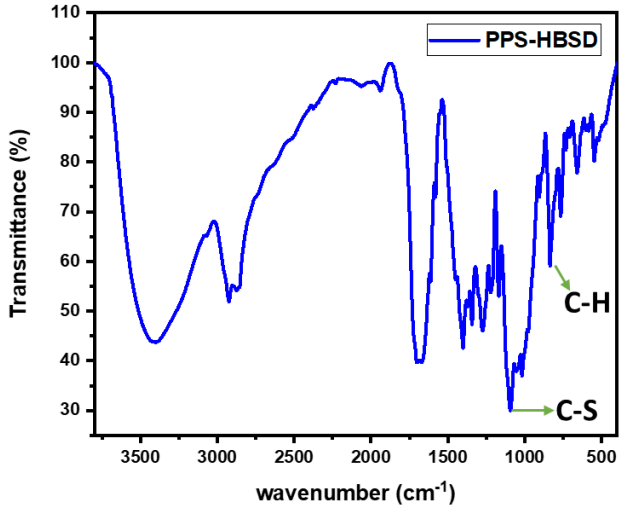

Figure 2B.5. FTIR spectra of PPS

The X-ray diffraction (XRD) pattern of the PPS-HBSD composite exhibited two distinct peaks at 19.03 and 20.8, corresponding to the (110) and (200) crystalline planes of the orthorhombic structure of PPS, respectively, when compared with the XRD peaks of HBSD gel. The calculated d-spacing values for these peaks were 4.73 Å and 4.35 Å, respectively, which are in good agreement with the expected values for the orthorhombic structure of PPS.[24] This confirms the presence of a crystalline phase with an orthorhombic structure in the gel matrix. The strong peak at 23.4 with a d-spacing value of 3.74 Å is attributed to the π-π stacking between phenyl groups of PPS and HBSD.

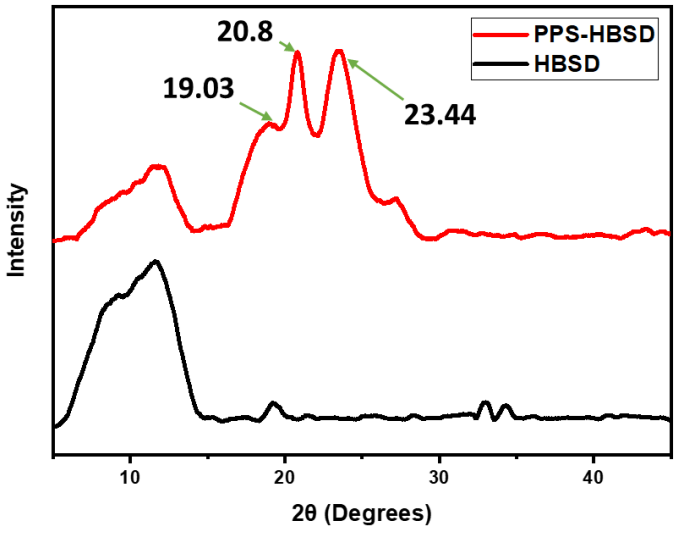

Figure 2B.6. XRD spectra of PPS-HBSD composite and HBSD gel.

The PPS-HBSD composite exhibits a unique morphology characterized by flakes-like structures, which are typically observed in polymer blends with phase separation as shown in Figure 2B.6 at different magnifications. This distinctive morphology is attributed to the presence of the two components, leading to the formation of distinct phases with different chemical and physical properties from the independent component. The flakes-like morphology of PPS-HBSD composites offers potential advantages for various applications, including advanced composites, coatings, and electronic materials.

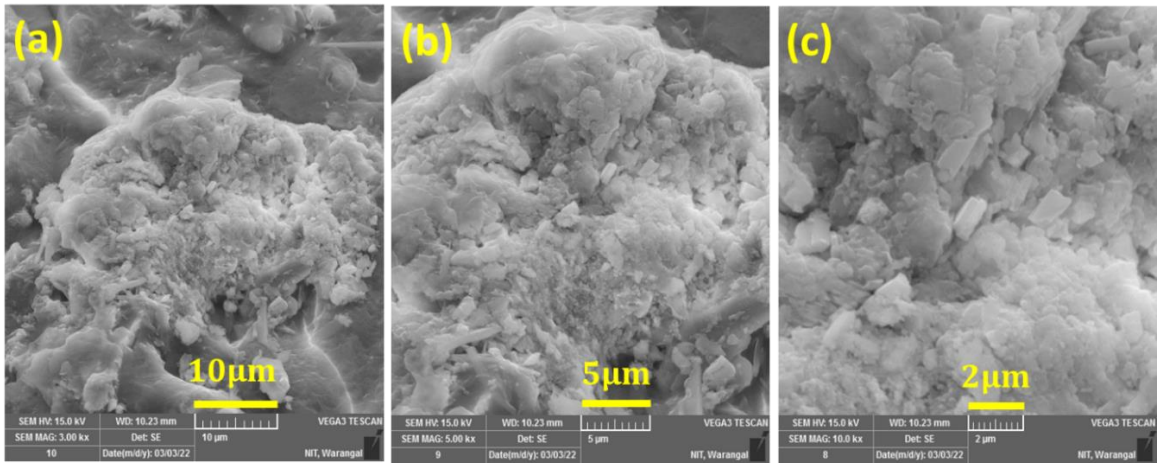

Figure 2B.7. SEM images of PPS-HBSD hybrid gel at (a)10µm; (b) 5µm; (c) 2µm.

2B.5 Experimental studies

2B.5.1 Materials and Methods

All the chemicals and solvents used for the synthesis of Diformyl dibenzylidene sorbitol and polyphenylene sulfide composite were purchased from commercial suppliers such as Merck, Aldrich, Himedia, and Avra chemicals and were used without purification. A detailed materials and methods, experimental procedure for rheological measurements, morphological analysis, and XRD is given in Chapter 2A.

2B.5.2 Procedure for the synthesis of PPS-HBSD composite

A gel was formed by dissolving 1.5 wt/v % of HBSD in NMP solvent, heating it to solubilize, and then allowing it to cool to room temperature. Through the co-gelation method, 1,4-dichlorobenzene (1 mmol) and H_2S gas were added/purged to the HBSD gel. The mixture was then exposed to sunlight for 3 days, followed by washing with water and chloroform, and finally drying under vacuum to obtain the PPS-HBSD composite.

2B.6 Conclusion

A sustainable protocol has been developed for the in-situ polymerization of 1,4-dichlorobenzene and H_2S to form PPS using HBSD gel in NMP as a confined media. This approach leverages the H_2S-entrapment properties of HBSD gels in NMP, enabling a more efficient and environmentally friendly synthesis of PPS. The formed PPS-HBSD composite was thoroughly characterized using FTIR, XRD, and SEM. Furthermore, the rheological properties of the composite gel were investigated, revealing its potential for applications in various fields. This innovative protocol offers a significant advancement in the synthesis of PPS in a confined media, generating a supramolecular structure composed of both LMWG and a polymer.

2B.7 References

1 C. Bonten, in *Plastics Technology*, 2019, pp. 65–246.

2 F. B. P. Zuo, A. Tcharkhtchi, M. Shirinbayan, J. Fitoussi, *Macromol. Mater. Eng.*, 2019, **304**, 1800686.

3 G. Wypych, *PPS poly(p-phenylene sulfide)*, 2012.

4 J. K. Fink, in *High performance polymers*, 2014, pp. 129–151.

5 A. D. Macallum, *J. Org. Chem*, 1948, **13**, 154–159.

6 S. Devaraju and M. Alagar, *Encycl. Mater. Compos.*, 2021, **1**, 947–959.

7 Y. G. T. Girijappa, M. Vinod Ayyappan, J. Puttegowda, Sanjay M. Rangappa, Parameswaranpillai and S. Siengchin, *Encycl. Mater. Plast. Polym.*, 2022, **4**, 103–111.

8 H. K. Jang, W. H. Choi, C. G. Kim, J. B. Kim and D. W. Lim, *Compos. Part B Eng.*, 2014, **56**, 178–183.

9 M. Tsotsalas, S. Begum, Z. Hassan and S. Bra, *Langmuir*, 2020, **36**, 10657–10673.

10 S. Zhang, *Nat. Biotechnol.*, 2003, **21**, 1171–1178.

11 Y. Chen, M. Zuo, Y. Chen, P. Yu, X. Chen, X. Zhang, W. Yuan, Y. Wu, W. Zhu and Y. Zhao, *Nat. Commun.*, 2023, **14**, 5229.

12 E. C. Santos, A. Angelini, D. Hürlimann, W. Meier and C. G. Palivan, *Chemistry (Easton).*, 2020, **2**, 470–489.

13 H. Clasen, *Zeitschrift fur Elektrochemie*, 1956, **60**, 982–987.

14 S. Chan, Y. Lin and C. Ting, *Macromolecules*, 2003, **36**, 8910–8912.

15 T. Wu, Y. Mei, T. Cabral, C. Xu and K. L. Beers, *J. Am. Chem. Soc.*, 2004, **126**, 9880–9881.

16 P. Bharathi and J. S. Moore, *J Am Chem Soc*, 1997, **7863**, 3391–3392.

17 X. Peng, J. Zhang, J. Zhou, S. Chen, Y. Jia, X. Han, X. Meng, C. W. Bielawski and J. Geng, *Angew. Chem. Int. Ed.*, 2023, **135**, e202301940.

18 J. T. J. Edmonds and H. W. J. Hill, *US Pat.*, 1967, 3354129.

19 D. R. Fahey and E. Ash, *Macromolecules*, 1991, **24**, 4242–4249.

20 A. P. Gies, J. F. Geibel and D. M. Hercules, *Macromolecules*, 2010, **43**, 943–951.

21 Y. J. Ou, X. M. Wang, C. L. Li, Y. L. Zhu and X. L. Li, *Earth Environ. Sci.*, 2017, **100**, 012036.

22 R. Guo and J. E. G. Mc, *Polym. Sci. A Compr. Ref.*, 2012, **5**, 377–430.

23 M. Shao, X. Yue and J. He, *Iran. Polym. J.*, 2020, **29**, 275–286.

24 M. Zhang, X. Wang, Y. Bai, Z. Li and B. Cheng, *Sci. Rep.*, 2017, **7**, 4443.

CHAPTER 3

REGIOSELECTIVE SYNTHESIS OF 4-ARYLAMINO-1,2-NAPHTHOQUINONES IN A CONFINED REACTION MEDIA USING LED LIGHT

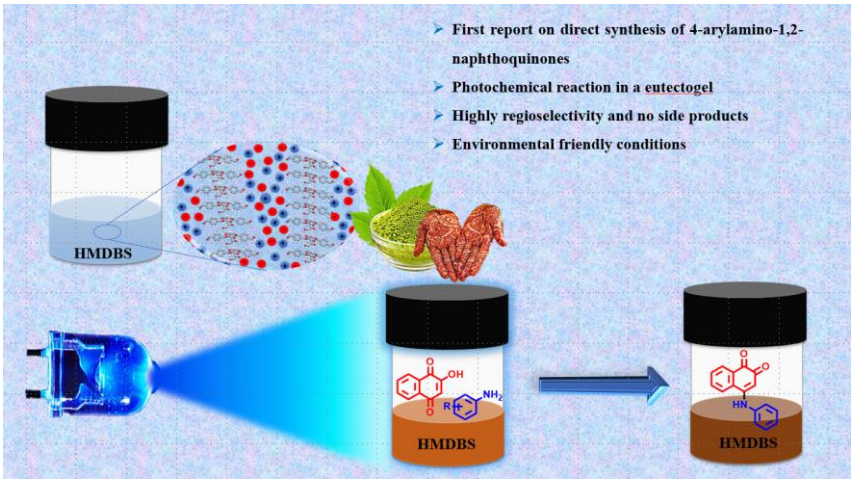

3.1 Objective

This chapter aims to develop a new, efficient, and regioselective synthetic protocol for 4-arylamino-1,4-naphthoquinones using a photochemical reaction in a confined eutectogel medium, using a modified natural compound, Lawsone (2-hydroxy-1,4-naphthoquinone), and various arylamines, under mild conditions, utilizing blue light irradiation, and exploring the potential of 4-(hydroxymethyl)-1,3:2,4-dibenzylidene-D-sorbitol (HMDBS) as a sustainable and versatile gelator for confined media reactions

3.2 Abstract

Predicting selectivity and conversion in a confined reaction medium under photochemical conditions is highly challenging as compared to the corresponding conventional synthesis. Herein, we report the use of a simple carbohydrate-derived eutectogel to facilitate LED-light-induced regioselective synthesis of 4-arylamino-1,2-naphthoquinones in good yield. This methodology, by including a reusable reaction medium, proved to have the potential of affording the regioselective formation of various desired products in good yields.

3.3 Introduction

Supramolecular assembly is a ubiquitous phenomenon in nature in which molecules spontaneously form aggregates via non-covalent interactions, which are intrinsically able to control selectivity, rate of conversion, and kinetics of a chemical process in biological systems.[1-4] It is surprising to see the existence of life in living things facilitated by the synthesis of precise organic molecules in confined reaction environments such as reactive pockets, bilayer or multilayer membranes, enzymes, micelles, vesicles, emulsions, gels, helical tubules, polyelectrolyte nanoparticles, Molecular Organic frameworks cells, and fibrillar network structures by bottom-up assembly process.[5-10] Even though ample of footprints of highly precise and well-programmed nature's assembly processes were documented in science, technology, and medicine,[11-15] the topic has been emerged as a discrete field of investigation because of its potential to enhance organic synthesis under sustainable reaction conditions. It is worth mentioning that the confined reaction environments obtained by self-assembling chiral natural molecules[16,17] could offer new clues in organic synthesis and enable the molecule under investigation to be tuned and controlled, which behave differently than the conventional chemical reactions. This is primarily attributed to the optimized molecular orientation and reduced molecular motion of the reactant species in gel media, which is in contrast to the more random and dynamic arrangement found in bulk solutions Nevertheless, in assembled natural

systems, the energy required for a chemical reaction is provided by light or self-generated nano-energy by means of mechanical movement of assembled layers assisted by pressure and flow velocity, i.e., photochemical and electrochemical reactions.[18,19] Supramolecular gels, characterized by high specific surface areas, stimuli-responsive reversibility, and favourable diffusion properties, have emerged as promising platforms to mimic the compartmentalization of complex natural systems. These gels can facilitate photochemical reactions that are otherwise challenging to perform. Additionally, their viscoelastic nature may help mitigate overconcentration and overheating effects, offering an advantage over more rigid systems. By harnessing the versatility and dynamic behaviour of supramolecular gels, researchers can develop innovative solutions for photochemical applications.[20]

3.3.1 Photochemical reactions in confined media

The supramolecular gels systems can be used as a reaction media for various photochemical reactions such as photodimerization, photooxidation, trifluoromethylation, triplet-triplet annihilation upconversion (TTA-UC) coupled to single electron transfer, etc.[21] For the first time, Maitra and co-workers demonstrated photodimerization of Acenaphthylene in supramolecular gels obtained by LMW bile acids as confined media. Photodimerization performed in gel media yielded 3-10 times higher syn/anti ratios when compared with aqueous or micellar solutions.[22] They also observed that the photo dimer rations are greatly influenced by the rheological properties of the gel when tested with different gelators. The higher the rigidity of the gel, the higher the product selectivity. (Figure 3.1)

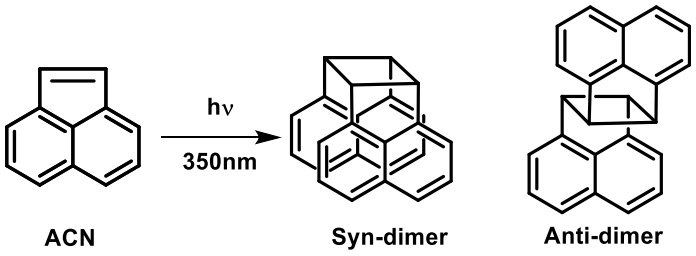

Scheme 3.1 Photodimerization of ACN in gel media

Shinkai et al. revealed that the photodimerization of anthracene carboxylic acid in a gelderived from 3,4,5-tris(n-dodecyloxy)benzoylamide substituted D-alanine yielded only syn and anti-product out of four different photo dimers obtained in solution phase.[23] Simon et al. successfully encapsulated Pd(II) mesoporphyrin IX and a UC chromophore 9,10-diphenylanthracene within a covalently cross-linked organogel, prepared from poly(vinyl alcohol) and hexamethylene diisocyanate in a DMF/DMSO-based solvent system. The

resulting material exhibited excellent mechanical integrity, high molecular mobility, and outstanding optical quality, with a transmittance of over 95% in the visible spectrum. Moreover, the cross-linked organogel provided effective protection against triplet state quenching by oxygen, leading to a significant enhancement in UC quantum yield from >0.6 under ambient conditions to 14% under oxygen-free conditions.[24] Schmidt et al. also demonstrated TTA-UC of DMDBS. This organogel served as a host matrix for the upconversion pair, consisting of palladium tetraphenyl porphyrin and 9,10-diphenylanthracene. The supramolecular architecture of the tetralin organogel provided a suitable platform for the TTA-UC process, showcasing the potential of such systems for upconversion applications.[25] Photo-oxidation,[26] and photoreduction can also be performed in gel media.

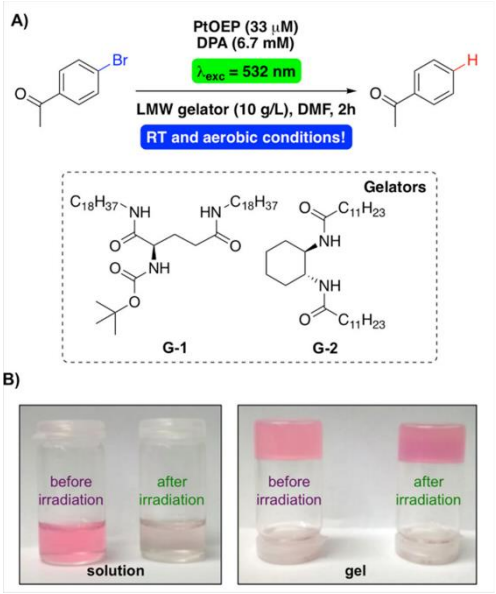

Figure 3.1. (A) Photoreduction of 4-bromoacetophenone performed in gel media. (B) Visual change in colour of the reaction performed in solution and gel media [adapted from ref 13].

As shown in Figure 3.1, upon laser irradiation at 532 nm, the reduction of *p*-bromoacetophenone to acetophenone is observed. Notably, the efficacy of this approach was also visually apparent. When the reaction was conducted in conventional aerobic conditions in DMF, the initial pink solution underwent complete decolorization upon irradiation, due to the decomposition of Platinum octaethylporphyrin by dissolved molecular oxygen. Whereas in the gel state, the pink coloration persisted unchanged (Figure 3.1), providing tangible evidence that the excited species are efficiently shielded from quenching by dissolved oxygen, thereby preserving the integrity of the upconversion process.[27]

A comprehensive method is introduced, based on the regioselective photochemical reaction in eutectogel. Naphthoquinones bearing a hydroxyl group on the quinone moiety, collectively known as lawsone. Lawsone, the simplest naturally occurring naphthoquinone, is readily obtained from the leaves of the Henna plant and is the primary contributor to the distinctive red-orange pigment properties. Traditionally, extracts of henna have been used as colouring agent for skin, hair, nails, and clothes for more than 5000 years, this is due to the Michael reaction of lawsone with the amino acids present on skin and amine or thiol groups of keratin present in hair.[28-30]

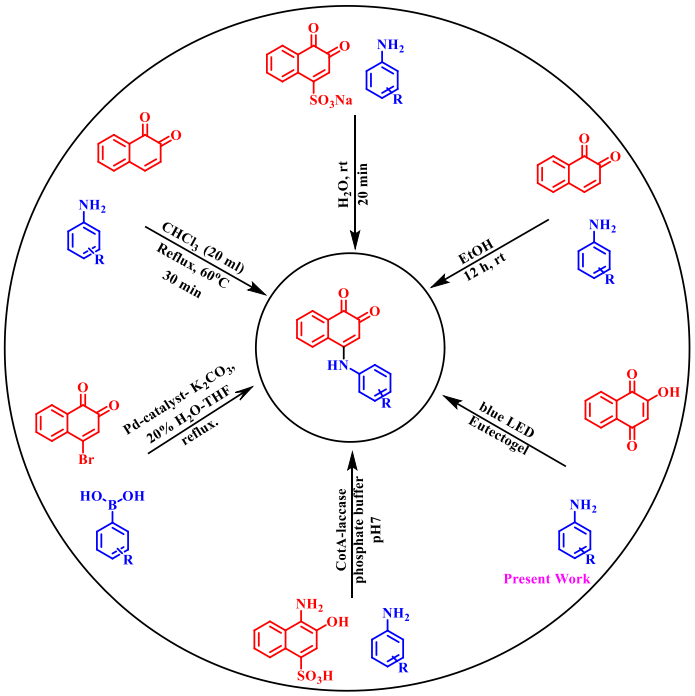

Figure 3.2. Various reaction conditions for the synthesis of 4-arylamino-1,2- Naphthoquinones reported in the literature.

The conceptual approach utilizes the use of one of the interesting natural compounds, Lawsone (2-hydroxy-1,4-naphthoquinone) as one of the starting materials, which displays a broad range of biological and pharmacological properties including antibacterial, antifungal, antiviral, wound healing, antiparasitic, tuberculostatic, anti-fertility, analgesic, anti-inflammatory, enzyme inhibitory, nematocidal, anticoagulant, and protein glycation inhibitory effects.[31-33] It is worth mentioning that the Lawsone displays a strong interaction with cellular components such as DNA, proteins, and lipids facilitated by oxidative and electrophilic behaviour. Specifically, the modification of Lawsone significantly alters its electrophilic potential and tunes its solubility and stability; hence, its modification is considered significant among researchers.[34] In recent years, the functionalization of 2-hydroxy-1,4-naphthoquinones

has gained broader interest in organic synthesis because of their potential biological property, diverse reactivity, bond-forming ability, and selectivity for constructing complex molecular structures. The existing reaction conditions for the synthesis of 2-hydroxy-1,4-naphthoquinones have been summarised in Figure 3.2.[35-38] Till date, regioselective access of 4-arylamino-1,4-naphthoquinones from naturally obtained lawsone is not reported.

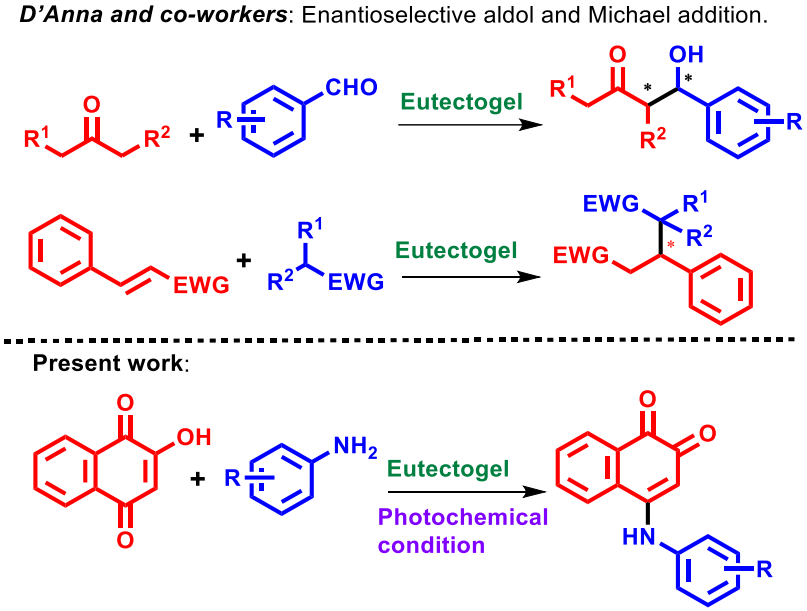

Figure 3.3. Examples of organic reactions in eutectogel and present work.

D'Anna co-workers reported a direct enantioselective formation of □-hydroxy ketones and C-C bond formation using aldol and Michael addition reactions using Eutectogel based on dibenzylidene sorbitol in DES (ChCl:Urea-1:2) in presence of L-Proline. (Figure 3.3).[43,44] In this chapter, photocatalyzed regioselective synthesis of 4-arylamino-1,2-Napthoquinones in confined reaction media has been developed using environmentally friendly conditions.

3.4 Results and Discussion

Firstly, by rationally introducing a flexible hydroxyl group into a well-known gelator, DBS, a 4-(hydroxymethyl)-1,3:2,4-dibenzylidene-D-sorbitol 3.4 (HMDBS) is generated in good yield. and confirmed using NMR, IR, and Mass spectral techniques.

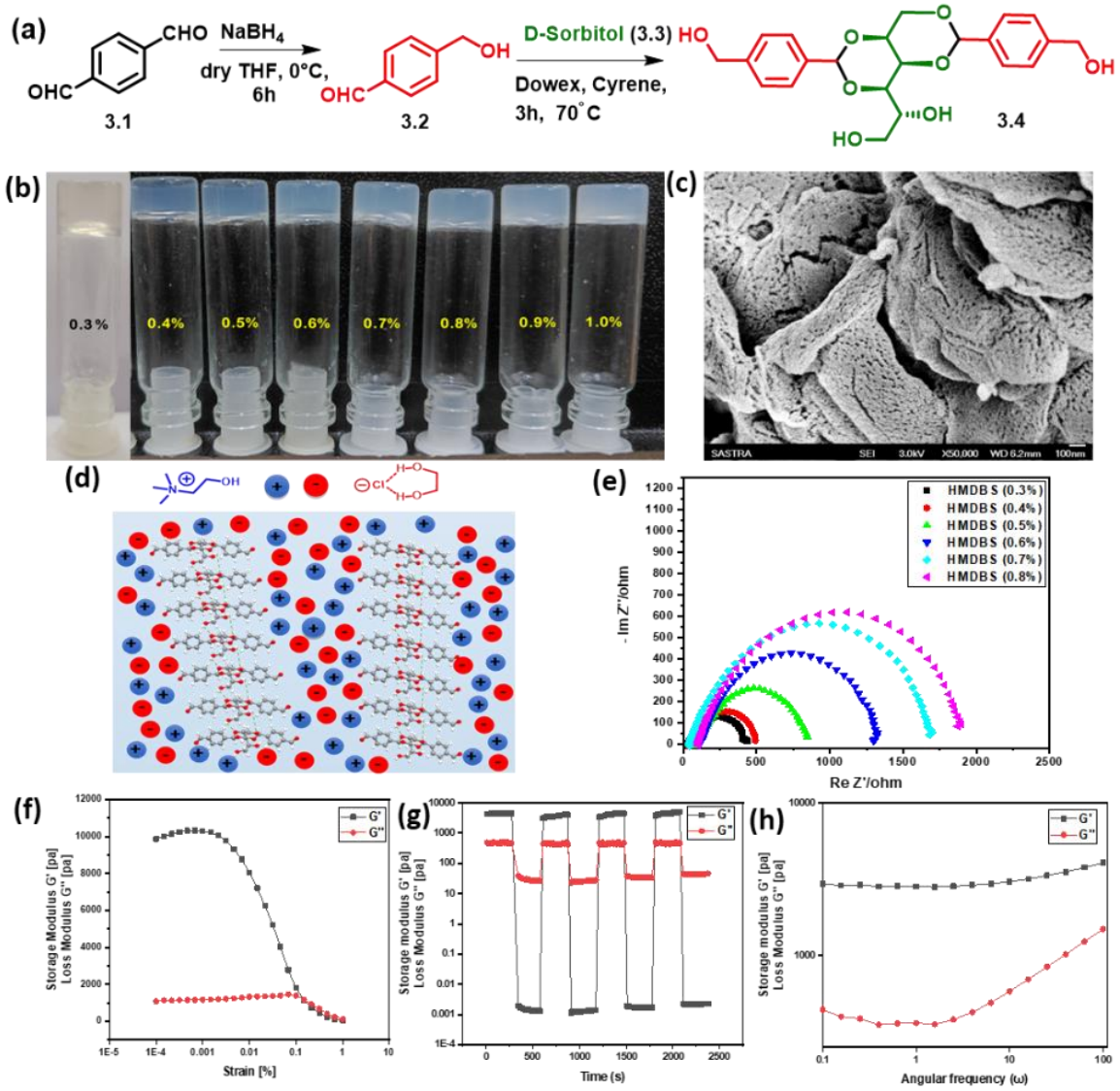

Figure 3.4. (a) Synthesis of HMDBS, 3.4. (b) Images of gel formed by HMDBS in ChCl:EG (1:3) ratio with increasing gelator concentration in wt/v. (c) SEM image of xerogel of HMDBS in ChCl:EG (1:3) at 0.3% wt/v. (d) Pictorial representation of the formation HMDBS eutectogel. (e) Electrochemical impedance measurements of HMDBS eutectogels at varying gelator concentration given in % wt/v. (f-h) Rheological studies of HMDBS eutectogels at 0.3% wt/v.

Terepthalaldehyde is reduced to hydroxymethyl benzaldehyde using $NaBH_4$ and further reacted with sorbitol to form a methyl hydroxy derivative of DBS(HMDBS) (Figure 3.2) using an optimized reaction condition mentioned in the previous chapter. The molecular assembly of HMDBS to form gel is tested by adding a known quantity of sample in a wide range of solvents by adopting "stable to inversion of a test tube" method (Table 3.1).[45] Gelation studies revealed the exceptional gelation behaviour in polar protic and aprotic solvents. In the literature precedents, DBS was identified as a good candidate for the formation of gel in DES.[46,47] Based on our expertise in the field of molecular assembly, a detailed investigation of intermolecular

interactions, and a balance of solvent and gelator interaction could bring new insight in this field. Even though there has been considerable development in the generation of conductive gel and gel electrolytes,[48,49] synthetic applications of eutectogel have not been much explored. To perform organic reactions in confined media, the gelation behaviour of HMDBS in DES is explored (Table 3.2). In the preliminary investigation, effective gelation of HMDBS in different DES such as EG:ChCl, PEG:ChCl, Glycerol:ChCl and Urea:ChCl is observed.

Table 3.1. Gelation studies of HMDBS in various solvents

I- Insoluble; G- Gel; S- Soluble; PS- Partial soluble.

S.No	Solvent	Gelation (CGC), (wt/v %)
1	Water	I
2	Methanol	I
3	Ethanol	I
4	Glycerol	G (0.4)
5	Ethylene glycol	G (0.6)
6	Tetrahydrofuran	S
7	Dimethyl sulfoxide	S
8	Dimethyl sulfoxide + water	G (0.4)
9	Acetone	I
10	1,4-dioxane	PS
11	Dimethyl formamide	G (0.6)
12	Polyethylene glycol	G (0.5)
13	Acetic acid	I
14	N-methyl pyrrolidone	I
15	1,2-Dichlorobenzene	I
16	Pyridine	I
17	n-Butanol	G (0.4)
18	Toluene	I
19	Benzyl alcohol	G (0.4)
20	Olive oil	I
21	Linseed oil	I
22	Dimethyl carbonate	I
23	Cyrene	I

Table 3.2. Gelation studies of HMDBS in Deep eutectic solvents

S.NO	Deep Eutectic solvents	Gelation(CGC wt/v)
1	Choline Chloride + Ethylene glycol (1:4)	G (0.3)
2	Choline Chloride + Ethylene glycol (1:3)	G (0.3)
3	Choline Chloride + Ethylene glycol (1.5:2)	G (1)

4	Choline Chloride + Glycerol (1:4)	G (0.4)
5	Choline Chloride + Glycerol (1:3)	G (0.5)
6	Choline Chloride + Glycerol (1.5:2)	G (1.3)
7	Choline Chloride + Urea (1:4)	G (0.6)
8	Choline Chloride + Urea (1:3)	G (0.6)
9	Choline Chloride + Urea (1.5:2)	G (1.5)
10	Choline Chloride + Polyethylene glycol (1:4)	Dense precipitation is observed
11	Choline Chloride + Polyethylene glycol (1:3)	Dense precipitation is observed
12	Choline Chloride + Polyethylene glycol (1.5:2)	Dense precipitation is observed

G-gel; I-insoluble

Generally, the properties of eutectogel are based on the intermolecular interactions displayed by the gelator, and the loading capability of DES and their interactions. Smith and co-workers reported that a higher loading of DBS ≥4.0% wt/v is required to form a gel in DES formed by ChCl:EG, which is attributed to the ionic nature of ChCl.[47] in the case of HMDBS, it is surprising to observe the formation of eutectogel at a lower loading of 0.3 % wt/v in ChCl:EG (1:3) ratio. A detailed investigation of the molecular structural aspects revealed that an introduction of hydroxymethyl group could enhance the gelation ability in the trend of more than 10 folds. Furthermore, the effect of additional loading of ChCl and EG in HMDBS eutectogel is tested. The increased ratio of ChCl (1.5:2) resulted in the increase of CGC to 1.0 % wt/v, which is due to the increased anionic character of eutectogel. However, the increased ratio of EG up to 1:4 ratio did not affect the CGC, whereas the gel-to-sol transition temperature (T_g) is substantially reduced. During the process of gelation, in addition to the complementary interaction between EG and ChCl, the free hydroxyl groups in the sorbitol backbone are also involved in the intermolecular H-bonding. Pleasingly, 4-hydroxymethyl benzylidene group of HMDBS did not interact with ChCl, but rather displayed intermolecular H-bonding with DES system and stabilized the assembled architecture. A phase diagram is obtained by determining Tg of HMDBS eutectogel with respect to gelator concentration is shown in Figure 3.5. A gradual increase in Tg was observed with an increase in the concentration of the gelator, and a trend of transparent to translucent was also observed (Figure 3.4b). As per Bunsen and Roscoe law, the photochemical reaction is directly proportional to the total energy irradiation, which is very much likely to be achieved in a transparent eutectogel, and hence our optimized condition for the formation of HMDBS eutectogel is 0.3% wt/v in 1:3 ratio of ChCl:EG.

Morphological studies of HMDBS eutectogel revealed the formation of a fibrillar network, wherein the DES is immobilized (Figure 3.4c). The practical utility and processability of eutectogel were identified using rheological measurements.[50] The larger value of elastic modulus, G' when compared to the viscous modulus, G'' revealed the robustness of the gel (Figure 3.4f&g). For catalysis applications, it is mandated to investigate the thixotropic behaviour, which deals with the rebuilding of intermolecular interaction by changing the strain. The same trend followed in the step strain experiment even after 3 cycles revealed the execution of the principle of microscopic reversibility (Figure 3.4h). Further, based on the electrochemical impedance measurements, XRD, and FTIR analysis, a plausible molecular packing in eutectogel is proposed (Figure 3.4d&e).

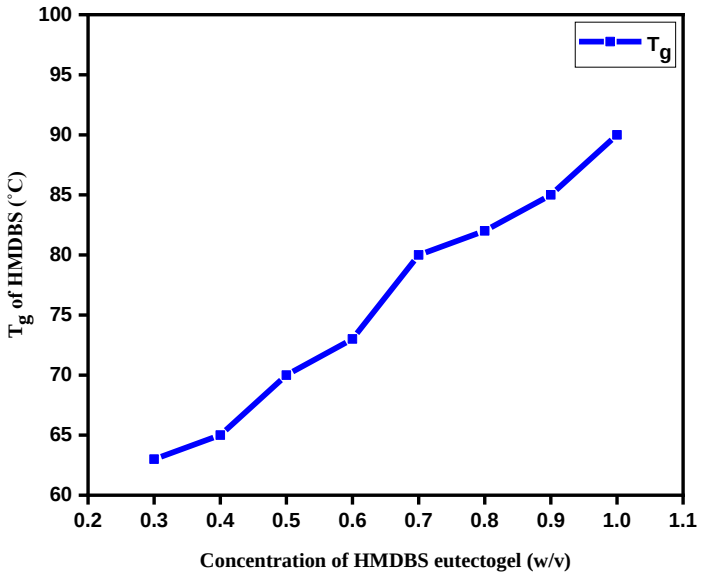

Figure 3.5. Transition temperature (T_g) values of HMDBS-ChCl: EG gels determined via test tube inversion experiments

In the conventional synthesis, the reaction of 2-hydroxy-1,4-naphthoquinone 5 with aniline generated 2-arylamino-1,4-naphthoquinone in good yield with several drawbacks, including harsh reaction conditions and by-product formation (Scheme 3.2a).[51] The reactivity of C1-C4 sites of compound 5 is almost similar towards nucleophiles, however, a proper functionalization or activation requires a suitable catalyst/additive. For example, the direct use of *p*-TSOH and TFA as a catalyst in water generated 2-arylamino-1,4-naphthoquinone in poor yield.[52] Our initial screening studies using the conventional method revealed that the use of polar protic solvents such as MeOH, EtOH, *i*-PrOH, and BuOH in the presence of $CuSO_4$

generated a mixture of products as identified by NMR spectral studies A direct reflux of compounds 5 and 6 in methanol delivered 2-methoxy-1,4-naphthoquinone as a major product and 4-arylamino-1,4-naphthoquinone derivatives as minor product with a traces of 2-arylamino-1,4-naphthoquinone as identified by TLC (Table 3.3)

Table 3.3. Optimization studies for 4-arylamino-1,2-naphthoquinones using conventional method

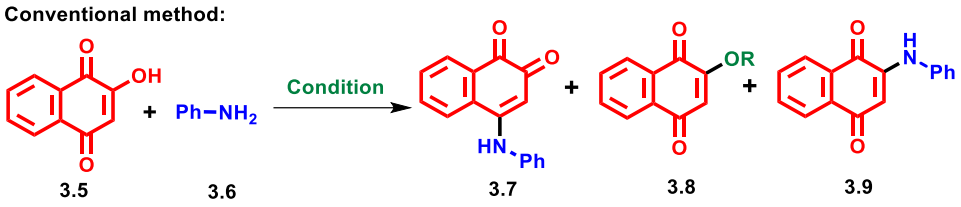

S.No	Catalyst	Condition	Solvent	Time (h)	3.7 (%)	3.8 (%)	3.9 (%)
1.	*p*-TSA	Reflux	MeOH	24	-	12	45
2.	TFA	Reflux	MeOH	12	traces	21	42
3.	$CuSO_4$	Reflux	MeOH/EtOH/BuOH, *i*-PrOH	24	traces	57	traces
4.	$ZnSO_4$	Reflux	MeOH	48	traces	traces	traces
5.	$MgSO_4$	Reflux	MeOH	48	-	-	-
6.	-	Reflux	MeOH	24	13	52	32

It is conclusive that the use of strong acid generates 2-arylamino-1,4-naphthoquinone and in the presence or absence of Lewis acid in protic solvents generates a mixture of products without any regioselectivity.[51,52] To attain regioselectivity in nucleophilic substitution reaction in Lawsone, this reaction is performed in eutectogel as a confined reaction media.

As a starting point to establish photochemical reaction in confined eutectogel media, a reaction between compound 3.5 and 3.6a was performed as a model substrate. To begin with, among the various eutectogels, gel formed by HMDBS in 0.3% wt/v in ChCl:EG (1:3) ratio has been selected as a confined media because of its transparency, lower CGC, a broad range of substrate solubility and easy work-up after the completion of the reaction. To execute our plan, firstly, the gel is formed by incorporating compound 3.5 and 3.6 with HMDBS by co-gelation or casting on gel method[44] and kept under direct sunlight for about 8h. Interestingly, the reaction was observed to yield 4-arylamino-1,4-naphthoquinone in 20% yield. The prolonged exposure to the sunlight for about 7 days furnished 35% yield. According to 1st law

of photochemistry and Bunsen-Roscoe law, the photochemical reaction is based on the λ_{abs} of substrate and λ_{em} of the light source and its dose. Further, NMR analysis revealed the formation of the desired product along with the unreacted starting materials. The irradiation of blue LED onto the preformed HMDBS eutectogel along with the reactants generated the desired 4-arylamino-1,4-naphthoquinones exclusively in excellent yields in 24h. Regioselective formation of 4-arylamino-1,4-naphthoquinones was characterised and confirmed by using NMR and HRMS techniques.

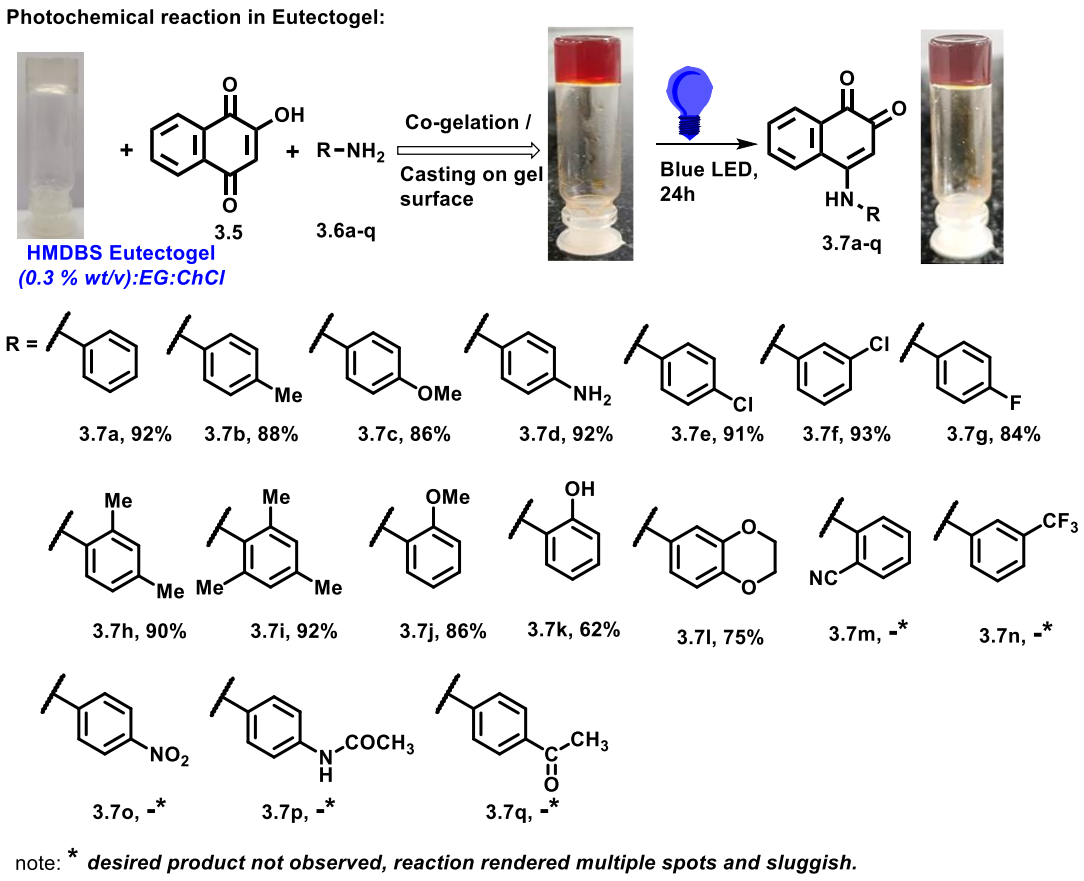

Scheme 3.2. Photochemical reaction of 2-hydroxy-1,4-naphthoquinone with various arylamines in eutectogel.

Having identified the optimized reaction condition, the generality and limitations of photochemical reaction have been evaluated by employing different aromatic amines with electron-donating and withdrawing substituents. Irrespective of the electronic effect, all the tested substrates delivered the expected 4-arylamino-1,4-naphthoquinones in 62-93% yields. It is worth mentioning that arylamines having moderately and strongly deactivating substituents did not furnish the desired product; it rendered multiple spots and sluggish (Scheme 3.2; compounds 3.7m-q). Employing aliphatic amines did not deliver the expected product under

the optimized condition, which may be due to less stability of amino radical formed during the course of the reaction, as identified by control experiments.

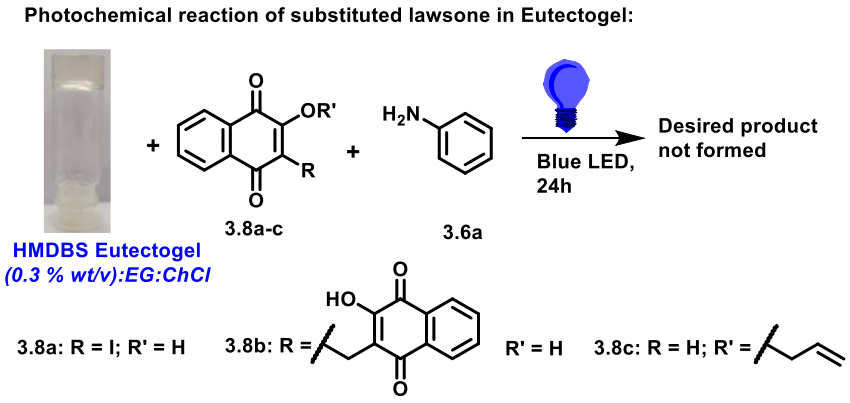

Scheme 3.3. Investigation of photochemical reaction of substituted lawsone with aniline.

Further, the investigation of the photochemical reaction of substituted lawsone derivatives, 3.8a-c with aniline 3.6a, did not furnish the desired product because of the bathochromic shift displayed by 3.8a and 3.8b, which does not match with the energy of the blue LED (Figure 3.6).

It is worth mentioning that substrate 3.8c absorbance is in line with the 2-hydroxy-1,4-naphthoquinone; however, it failed to furnish the desired product because of the absence of a free hydroxyl group at the C-2 position.

Several experiments were performed to probe the mechanistic insight of this transformation in addition to the literature precedents. Firstly, the effect of eutectogel gelator concentration in photochemical reaction is evaluated. As gelator concentration increases from 0.3 to 1.0 % wt/v, the rate of reaction decreases. In the case of 1.0 % wt/v eutectogel system, even after irradiation of blue LED for about 48h, a complete conversion was not observed, which may be because of the translucent nature of the gel, where in light could not penetrate.

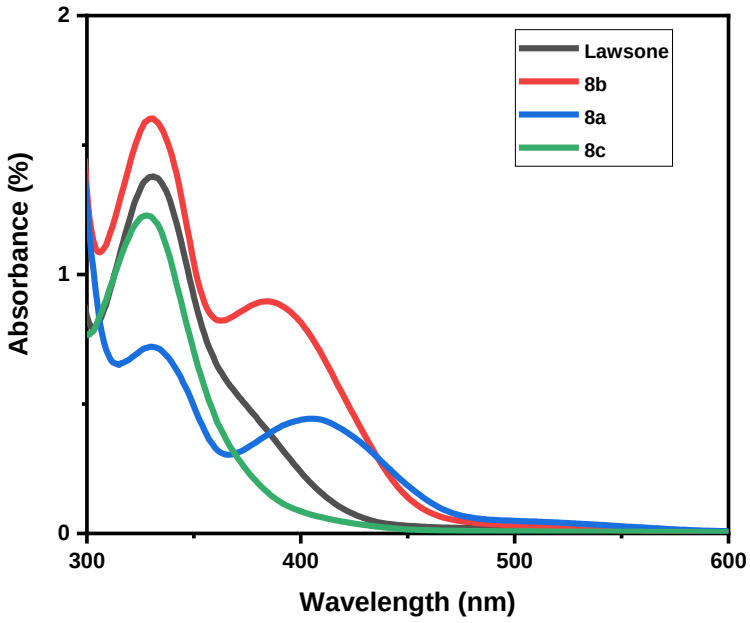

Figure 3.6. UV-vis spectra of lawsone, compound 3.8a, 3.8b, and 3.8c in THF.

It is worth mentioning that the direct use of DBS eutectogel system did not furnish the required product, due to the unavailability of a free H-bonding donor to stabilize the keto form of Lawsone. However, a trace of product formed in DBS system is due to the presence of free molecules present in the 3D fibrous network, which extends its arm for hydrogen bonding with the reactant. An attempt to synthesize the desired product in the solution phase using polar protic solvents and DES was not successful because of the competitive 2-O-alkylated and 2-arylaminated products. To identify the transformation proceeds via the ionic or radical pathway, a stoichiometric quantity of TEMPO was added on to the eutectogel under optimized conditions. The formation of traces of product with a complete recovery of substrates indicated the radical pathway-assisted transformation. The addition of benzoyl peroxide onto the HMDBS eutectogel with aniline in the absence of 2-hydroxy-1,4-naphthoquinone generated polyaniline, which supports the formation of an amino radical stabilized by mesomeric effect during the course of the reaction (Figure 3.7).

UV-vis studies were performed to obtain direct evidence of the involvement of radical mechanism. Before the onset of irradiation, UV-vis spectra were acquired at t = 0h for the reaction mixture. As shown in figure 3.8, lawsone displayed absorbance at 331 nm. Upon irradiation of reaction media with blue LED, a new peak centered at 459 nm appeared, and absorbance intensity increased with respect to time. The higher molar extinction coefficient of lawsone enables them as a probable photoinitiator, and the existence of an isosbestic point revealed the formation of new radical species.[32] Direct irradiation of reaction media in the

absence of arylamine could also furnish direct evidence for radical mechanism. As seen in Figure 3.8, with respect to time a decrease in the intensity of absorbance of lawsone with an isosbestic point revealed the existence of radical pathway. It is worth mentioning that the reaction did not proceed with aliphatic amines because of the lack of stability of amino radical formed. Control experiments and UV-vis studies supported that the benzyl hydroxyl group is essential for the stabilization of radical species, which in turn activate the C-4 carbonyl group of 2-hydroxy-1,4-naphthoquinone. Based on the experimental results, the possible mechanism is given in Figure 3.9.

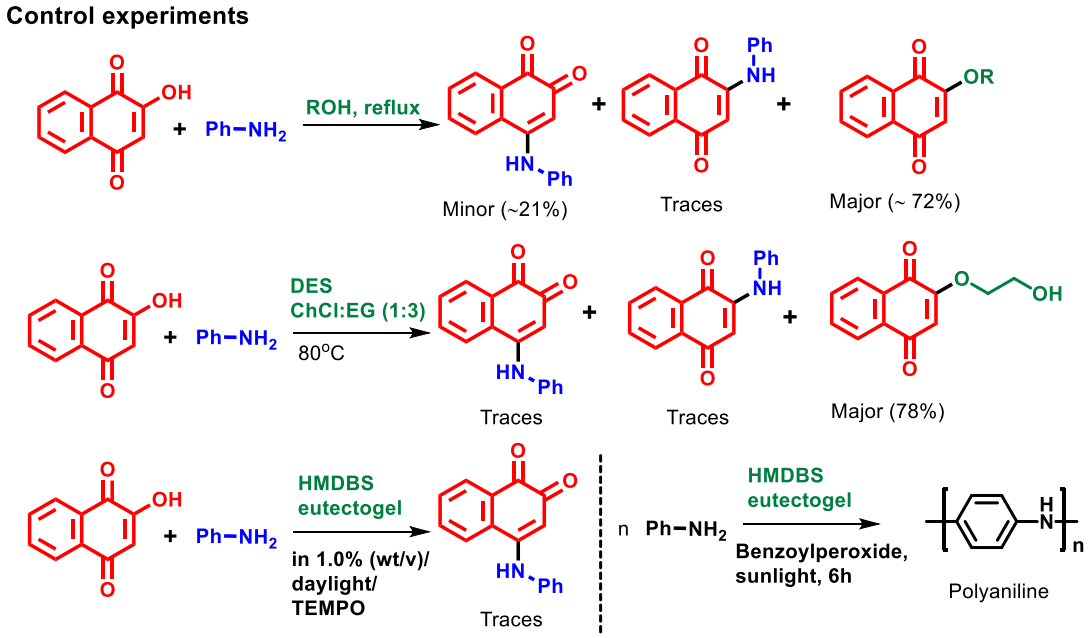

Figure 3.7. Control experiments for the synthesis of 4-arylamino-1,4-napthoqinones.

Upon exposure to blue LED irradiation, lawsone undergoes homolytic cleavage, generating highly reactive radicals that subsequently undergo radical stabilization. The radical formed at the 4-position of lawsone, a highly reactive oxygen-centered radical, abstracts a proton from the aryl amine, yielding a radical species of the aryl amine. This key step enables the formation of a covalent bond between the lawsone and aryl amine moieties.

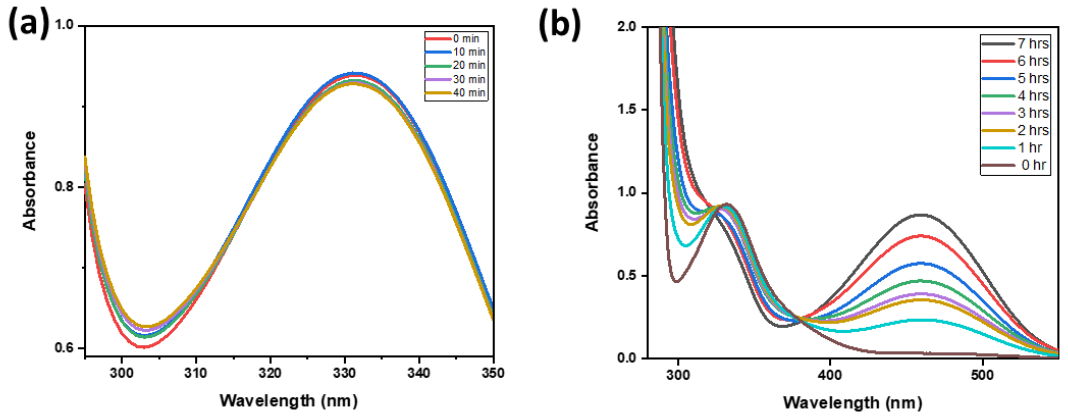

Figure 3.8. (a) UV-Vis spectra of lawsone under blue LED at different time intervals and (b) UV studies of the reaction mixture at different intervals.

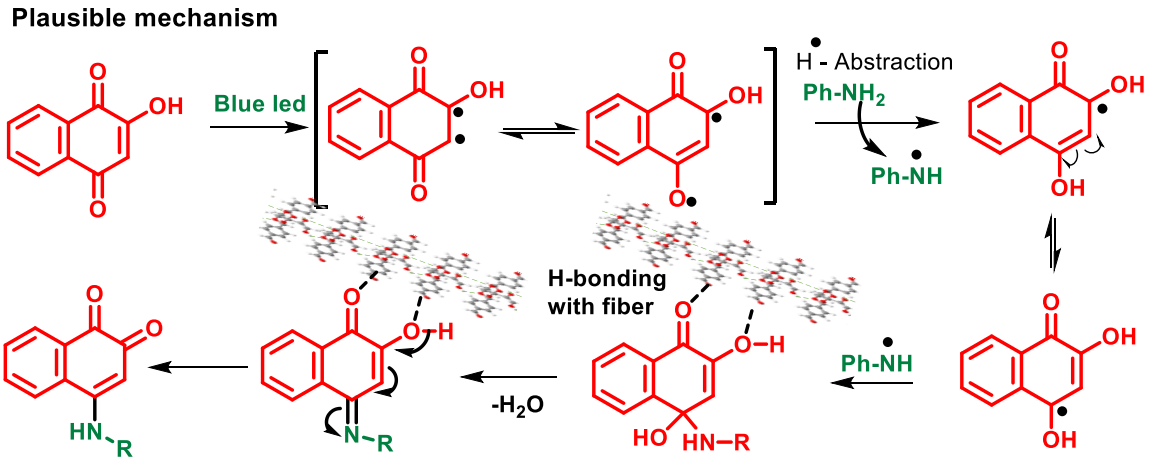

Figure 3.9. Plausible mechanism for the synthesis of 4-arylamino naphthoquinone

The lawsone radical and aryl amine radical then combine, followed by elimination, resulting in the formation of 4-arylamino-1,2-naphthaquinones. Notably, the keto groups at the 1 and 2 positions of the lawsone molecule are stabilized by hydrogen bonding with the fibers of the eutectogel, facilitating the generation of the desired product and enhancing the efficiency of the reaction.

3.5 Experimental section

3.5.1 General materials and methods

All reagents and solvents used for the synthesis of 4-(hydroxymethyl)-1,3:2,4-dibenzylidene-D-sorbitol, and 4-arylamino-1,2-napthoquinones were purchased from commercial suppliers such as Merck, Aldrich, Finar, SRL and Avra chemicals and were used without purification.

Materials and experimental methods for gelation studies, morphological analysis, rheological studies, and FTIR analysis are given in Chapter 2a.

3.5.2 Formation of deep eutectic gel

The deep eutectic solvent is prepared by mixing a suitable quantity of choline chloride ChCl (HBA) and Ethylene glycol/ Glycerol/ Urea (HBD) in a round bottom flask and stirred at 70 °C till a homogeneous solution is formed. To the formed DES, HMDBS gelator is added and heated till the gelator dissolves and left to stand for the gel formation.

3.5.3 Synthesis

3.5.3.1 Procedure for the synthesis of 4-hydroxymethyl benzaldehyde

To a stirred solution of terepthalaldehyde (1.0 eq) in dry THF at 0 ˚C, $NaBH_4$ (0.3 eq) is added in portions. The mixture was stirred for 6h. After completion of the reaction as identified by TLC, 1N HCl is added to the mixture and further stirred for 20 min. The solvent was removed under reduced pressure and the residue was extracted with ethyl acetate. Column chromatography was performed to obtain the pure product.

3.5.3.2 Procedure for the synthesis of 4-(hydroxymethyl)-1,3:2,4-dibenzylidene-D-sorbitol

To a stirred solution of D-Sorbitol (1 mmol) in Cyrene (10 mL) at rt under N_2 atmosphere, 4-hydroxymethyl benzaldehyde (2.1 mmol) and Dowex 50WX8 were added. The reaction mixture was stirred for about 24 h at 70 °C. After completion of the reaction as identified by TLC, the reaction mixture was allowed to cool down to room temperature. The formed precipitate is dissolved in hot cyrene and separates the catalyst by filtration. The cyrene solution is refrigerated for crystallization. The product is filtered, washed with water, and dried under a vacuum. The product was obtained as a white solid.

3.5.3.3 General Procedure for the synthesis of 4-arylamino-1,2-naphthoquinones

Lawsone (1 mmol) and amine (1.2 mmol) were incorporated in the HMDBS eutectogel by ether co-gelation method or cast-on gel surface method. In cast on gel surface method, a complete permeation of reactant was achieved after 12h at room temperature. After the incorporation of reactants, the gel vial is irradiated under blue LED for about 24 h. In order to follow the reaction progress, a small piece of gel is taken, dispersed in DCM, and analyzed with TCL. After completion of the reaction, the gel is placed in chloroform or hexane-

chloroform or chloroform-methanol mixture to extract the product, this process is repeated 3 times. The extracted mixture is evaporated under vacuum. Brown product thus obtained is crystalized in a mixture of solvents (Hexane-Ethyl acetate; Chloroform-Methanol, or a suitable solvents) and directly subjected to NMR analysis. Column chromatography is not performed.

3.6 Characterisation studies

3.6.1 ^{1}H-NMR, ^{13}C-NMR, and HRMS characterization data of synthesized compounds

Compound 3.2: 4-hydroxymethyl benzaldehyde

The product was obtained as a colour less liquid with 70% yield

^{1}H NMR (400 MHz, $CDCl_3$) δ: 9.86 (d, *J* = 1.6 Hz, 1H, OH), 7.74 (d, *J* = 7.9 Hz, 2H, Ar-H), 7.41 (d, *J* = 7.9 Hz, 2H, Ar-H), 4.68 (s, 2H, Ar-CH_2).

Compound 3.4: 4-(hydroxymethyl)-1,3:2,4-dibenzylidene-D-sorbitol

The product was obtained as a white solid with 86% yield

^{1}H NMR (400 MHz, DMSO-d_6) δ: 7.41 (t, *J* = 8.1 Hz, 4H, Ar-H), 7.31 (dd, *J* = 8.1, 1.6 Hz, 4H, Ar-H), 5.64 (s, 2H, acetal-H), 5.21 (s, 2H, benzylic-OH), 4.83 (s, 1H, Sac-H), 4.50 (s, 4H, Ar-CH_2), 4.21 – 4.11 (m, 3H, Sac-H), 3.93 (d, *J* = 1.7 Hz, 1H, Sac-H), 3.83 (dd, *J* = 9.2, 1.7 Hz, 1H, Sac-H), 3.76 (d, *J* = 6.4 Hz, 1H, Sac-H), 3.59 (dd, *J* = 11.3, 2.3 Hz, 1H, Sac-H), 3.43 (dd, *J* = 11.2, 5.1 Hz, 2H, Sac-H).

^{13}C NMR (100 MHz, DMSO-d_6) δ: 143.39, 143.29, 137.64, 137.38, 126.40, 126.38, 126.36, 126.34, 99.84, 99.78, 78.20, 78.12, 70.55, 69.78, 68.89, 68.20, 63.12.

HRMS (ESI, m/z): $C_{22}H_{26}O_8$, $[M+H]^+$ Calculated: 419.1706; $[M+H]^+$ found: 419.1704.

Compound 3.7a: 4-(phenylamino)-naphthalene-1,2-dione

The product was obtained as a brown solid with a 92% yield.

^{1}H NMR (400 MHz, $CDCl_3$) δ: 8.05 (t, *J* = 6.3 Hz, 2H, Ar-H), 7.69 (t, *J* = 7.6 Hz, 1H, Ar-H), 7.63 – 7.57 (m, 1H, Ar-H), 7.50 (s, 1H, NH), 7.35 (t, *J* = 7.8 Hz, 2H, Ar-H), 7.21 (dd, *J* = 8.0 Hz, 2H, Ar-H), 7.15 (t, *J* = 7.4 Hz, 1H Ar-H), 6.35 (s, 1H, Olefin-H).

^{13}C NMR (100 MHz, $CDCl_3$) δ: 183.97, 182.09, 144.75, 137.45, 134.95, 133.24, 132.38, 130.38, 129.72, 126.55, 126.19, 125.65, 122.64, 103.41.

HRMS(ESI m/z): $C_{16}H_{11}NO_2$, $[M+H]^+$ Calculated: 250.0868, $[M+H]^+$ Found: 250.0869**.**

Compound 3.7b: 4-(p-tolylamino)naphthalene-1,2-dione

The product was obtained as a brown solid with an 88% yield.

^{1}H NMR (400 MHz, $CDCl_3$) δ: 8.10 (m, *J* = 7.6, 3.0, 1.3 Hz, 2H, Ar-H), 7.75 (td, *J* = 7.6, 1.3 Hz, 1H, Ar-H), 7.65 (td, *J* = 7.5, 1.4 Hz, 1H, Ar-H), 7.52 (s, 1H, NH), 7.22 (d, *J* = 8.2 Hz, 2H, Ar-H), 7.16 (d, *J* = 8.4 Hz, 2H, Ar-H), 6.35 (s, 1H, Olefin-H), 2.36 (s, 3H, Ar-CH_3).

^{13}C NMR (100 MHz, $CDCl_3$) δ: 183.86, 182.16, 145.07, 135.66, 134.89, 134.77, 133.34, 132.26, 130.42, 130.25, 126.49, 126.16, 122.75, 103.04, 20.99.

Compound 3.7c: 4-((4-methoxyphenyl)amino)naphthalene-1,2-dione

The product was obtained as a brown solid with an 86% yield.

^{1}H NMR (400 MHz, $CDCl_3$) δ: 8.11 (m, *J* = 7.6, 4.0, 1.3 Hz, 2H, Ar-H), 7.75 (td, *J* = 7.5, 1.4 Hz, 1H, Ar-H), 7.66 (td, *J* = 7.5, 1.4 Hz, 1H, Ar-H), 7.44 (s, 1H, NH), 7.20 (d, *J* = 8.9 Hz, 2H, Ar-H), 6.95 (d, *J* = 9.0 Hz, 2H, Ar-H), 6.22 (s, 1H, Olefin-H), 3.83 (s, 3H, O-CH_3).

^{13}C NMR (100 MHz, $CDCl_3$) δ: 183.75, 182.19, 157.70, 145.70, 134.89, 133.42, 132.21, 130.44, 130.04, 126.45, 126.16, 124.87, 114.93, 102.55, 55.58.

Compound 3.7d: 4-((4-aminophenyl)amino)naphthalene-1,2-dione

^{1}H NMR (400 MHz, DMSO-d_6) δ: 9.03 (s, 1H, NH), 8.09 (d, *J* = 7.5 Hz, 1H, Ar-H), 7.99 (d, *J* = 7.5 Hz, 1H, Ar-H), 7.89 (t, *J* = 7.6 Hz, 1H, Ar-H), 7.81 (t, *J* = 7.5 Hz, 1H, Ar-H), 7.07 (d, *J* = 8.7 Hz, 2H, Ar-H), 6.68 (d, *J* = 8.7 Hz, 2H, Ar-H), 5.91 (s, 1H, Olefin-H), 5.28 (s, 2H, NH_2).

^{13}C NMR (100 MHz, DMSO-d_6) δ: 182.36, 147.64, 135.20, 133.66, 132.65, 131.05, 130.44, 126.41, 125.70, 122.53, 119.77, 114.92, 101.27.

HRMS(ESI m/z): $C_{16}H_{12}N_2O_2$, $[M+H]^+$ Calculated: 265.0977, $[M+H]^+$ Found: 265.0979**.**

Compound 3.7e: 4-((4-chlorophenyl)amino)naphthalene-1,2-dione

The product was obtained as a brown solid with a 91% yield.

^{1}H NMR (400 MHz, $CDCl_3$) δ: 8.13 (d, *J* = 8.2 Hz, 2H, Ar-H), 7.78 (s, 1H, Ar-H), 7.69 (s, 1H, Ar-H), 7.52 (s, 1H, NH), 7.40 (d, *J* = 8.1 Hz, 2H, Ar-H), 7.27 – 7.17 (m, 2H, Ar-H), 6.37 (s, 1H, Olefin-H).

^{13}C NMR (100 MHz, $CDCl_3$+DMSO-d_6) δ: 183.26, 181.85, 146.09, 137.37, 135.01, 133.03, 132.76, 130.77, 129.73, 129.49, 126.47, 125.73, 125.28, 103.03.

HRMS(ESI m/z): $C_{16}H_{10}ClNO_2$, $[M+H]^+$ Calculated: 284.0478, $[M+H]^+$ Found: 284.0477**.**

Compound 3.7f: 4-((3-chlorophenyl)amino)naphthalene-1,2-dione

The product was obtained as a brown solid with a 93% yield.

^{1}H NMR (400 MHz, $CDCl_3$) δ: 8.05 (m, *J* = 7.5, 4.9, 1.3 Hz, 2H, Ar-H), 7.71 (td, *J* = 7.6, 1.4 Hz, 1H, Ar-H), 7.62 (td, *J* = 7.6, 1.4 Hz, 1H, Ar-H), 7.47 (s, 1H, NH), 7.28 (t, *J* = 8.0 Hz, 1H, Ar-H), 7.22 (t, *J* = 2.1 Hz, 1H, Ar-H), 7.14 – 7.09 (m, 2H, Ar-H), 6.36 (s, 1H, Olefin-H).
^{13}C NMR (100 MHz, $CDCl_3$+DMSO-d_6) δ: 181.72, 134.81, 132.96, 132.55, 130.59, 126.48, 125.79, 125.17, 124.06, 123.21, 122.27, 103.55.
HRMS(ESI m/z): $C_{16}H_{10}ClNO_2$, $[M+H]^+$ Calculated: 284.0475, $[M+H]^+$ Found: 284.0477**.**

Compound 3.7g: 4-((4-fluorophenyl)amino)naphthalene-1,2-dione

The product was obtained as a brown solid with an 84% yield.

^{1}H NMR (400 MHz, $CDCl_3$) δ: 8.11 (t, *J* = 7.0 Hz, 2H, Ar-H), 7.72 (dt, *J* = 36.7, 7.5 Hz, 2H, Ar-H), 7.46 (s, 1H, NH), 7.29 – 7.22 (m, 2H, Ar-H), 7.13 (t, *J* = 8.4 Hz, 2H, Ar-H), 6.25 (s, 1H, Olefin-H).
^{13}C NMR (100 MHz, $CDCl_3$) δ: 183.86, 181.97, 145.32, 135.00, 133.22, 132.43, 130.36, 126.55, 126.24, 125.07, 124.99, 116.77, 116.55, 103.14.

Compound 3.7h: 4-((2,4-dimethylphenyl)amino)naphthalene-1,2-dione

The product was obtained as a brown solid with a 90% yield.

^{1}H NMR (400 MHz, $CDCl_3$) δ: 8.11 (m, *J* = 9.4, 7.7, 1.0 Hz, 2H, Ar-H), 7.75 (td, *J* = 7.5, 1.3 Hz, 1H, Ar-H), 7.66 (td, *J* = 7.5, 1.3 Hz, 1H, Ar-H),7.27(s,1H, NH) 7.17 – 7.04 (m, 3H, Ar-H), 5.90 (s, 1H, Olefin-H), 2.34 (s, 3H, Ar-CH_3), 2.24 (s, 3H, Ar-CH_3).
^{13}C NMR (100 MHz, $CDCl_3$) δ: 183.71, 182.24, 146.16, 136.90, 134.87, 133.49, 133.13, 132.70, 132.20, 132.05, 130.53, 127.74, 126.39, 126.18, 124.93, 102.90, 20.99, 17.67.

Compound 3.7i: 4-((2,4,6-trimethylphenyl)amino)naphthalene-1,2-dione

The product was obtained as a brown solid with a 92% yield.

^{1}H NMR (400 MHz, $CDCl_3$) δ: 8.15 – 8.07 (m, 2H, Ar-H), 7.74 (d, *J* = 1.3 Hz, 1H, Ar-H), 7.66 (td, *J* = 7.5, 1.2 Hz, 1H, Ar-H), 7.04(s, 1H, NH), 6.95 (s, 2H, Ar-H), 5.38 (s, 1H, Olefin-H), 2.31 (s, 3H, Ar-CH_3), 2.16 (s, 6H, Ar-CH_3).
^{13}C NMR (100 MHz, $CDCl_3$) δ: 183.51, 182.10, 146.92, 137.93, 135.43, 134.82, 133.65, 132.13, 130.92, 130.69, 129.48, 126.30, 126.21, 102.66, 20.96, 17.92.

Compound 3.7j: 4-((2-methoxyphenyl)amino)naphthalene-1,2-dione

The product was obtained as a brown solid with an 86% yield.

^{1}H NMR (400 MHz, $CDCl_3$) δ: 8.13 (s, 2H, Ar-H), 7.72 (dt, *J* = 36.5, 7.0 Hz, 2H, Ar-H), 7.49 – 7.39 (m, 1H, Ar-H), 7.22 – 7.11 (m, 1H, Ar-H), 7.01 (dt, *J* = 13.2, 5.7 Hz, 2H, Ar-H), 6.48 (s, 1H, Olefin-H), 3.91 (s, 3H, Ar-OCH_3).
^{13}C NMR (100 MHz, $CDCl_3$) δ: 184.00, 182.14, 151.18, 143.99, 134.78, 133.33, 132.30, 126.98, 126.54, 126.13, 125.48, 121.08, 120.92, 111.17, 103.63, 55.78.

Compound 3.7k: 4-((2-hydroxyphenyl)amino)naphthalene-1,2-dione

The product was obtained as a brown solid with a 62% yield.

^{1}H NMR (400 MHz, $CDCl_3$+DMSO) δ: 9.65 (s, 1H, NH), 8.15 – 8.03 (m, 3H, Ar-H), 7.81 – 7.73 (m, 1H, NH), 7.71 – 7.65 (m, 1H, Ar-H), 7.33 (d, *J* = 7.1 Hz, 1H, Ar-H), 7.07 – 6.97 (m, 2H, Ar-H), 6.93 – 6.85 (m, 1H Ar-H), 6.29 (s, 1H, Olefin-H).
^{13}C NMR (100 MHz, $CDCl_3$+DMSO) δ: 183.52, 181.97, 149.92, 144.70, 134.72, 133.29, 132.27, 130.55, 126.40, 126.04, 125.83, 125.51, 122.17, 119.71, 116.32, 102.93.

Compound 3.7l: 4-((3,4-ethylenedioxyphenyl)amino)naphthalene-1,2-dione

The product was obtained as a brown solid with a 75% yield.

^{1}H NMR (400 MHz, $CDCl_3$) δ: 8.10 (dt, *J* = 7.5, 1.7 Hz, 2H, Ar-H), 7.75 (td, *J* = 7.6, 1.3 Hz, 1H, Ar-H), 7.65 (td, *J* = 7.6, 1.3 Hz, 1H, Ar-H), 7.40 (s, 1H, NH), 6.89 (d, *J* = 8.6 Hz, 1H, Ar-H), 6.81 (d, *J* = 2.5 Hz, 1H, Ar-H), 6.74 (dd, *J* = 8.6, 2.5 Hz, 1H, Ar-H), 6.29 (s, 1H, Olefin-H), 4.28 (s, 4H, Ar-O-CH_2).
^{13}C NMR (100 MHz, $CDCl_3$) δ**:**183.78, 182.11, 145.38, 144.07, 141.75, 134.86, 133.35, 132.22, 130.72, 130.42, 126.45, 126.13, 118.02, 116.58, 112.47, 102.89, 64.41, 64.33.

Compound 3.8a: 2-methoxynaphthalene-1,4-dione

The product was obtained as a brown solid with a 92% yield.

^{1}H NMR (400 MHz, $CDCl_3$+DMSO-d_6) δ: 8.00 (dd, *J* = 17.0, 7.1 Hz, 2H, Ar-H), 7.70 (m, *J* = 7.5 Hz, 2H, Ar-H), 6.16 (s, 1H, Olefin-H), 3.85 (s, 3H, O-CH_3).
^{13}C NMR (100 MHz, $CDCl_3$+DMSO-d_6) δ: 184.58, 179.95, 160.39, 134.39, 133.40, 131.95, 130.98, 126.49, 126.00, 109.95, 56.52.
HRMS(ESI m/z): $C_{11}H_{18}O_3$, $[M+H]^+$ Calculated: 189.0551, $[M+H]^+$ Found: 189.0559**.**

Compound 3.8b: 2-ethoxynaphthalene-1,4-dione

The product was obtained as a brown solid with an 80% yield.

^{1}H NMR (400 MHz, $CDCl_3$) δ: 8.08 – 7.99 (m, 2H, Ar-H), 7.70 – 7.61 (m, 2H, Ar-H), 6.08 (s, 1H, Olefin-H), 4.03 (q, *J* = 7.0 Hz, 2H, O-CH_2), 1.46 (t, *J* = 7.0 Hz, 3H, CH_3).

^{13}C NMR (100 MHz, $CDCl_3$) δ: 185.08, 180.21, 159.72, 134.25, 133.28, 132.01, 131.15, 126.71, 126.12, 110.21, 65.35, 13.93.

HRMS(ESI m/z): $C_{12}H_{10}O_3$, $[M+H]^+$ Calculated: 203.0708, $[M+H]^+$ Found: 203.0708**.**

Compound 3.8c: 2-isopropoxynaphthalene-1,4-dione

The product was obtained as a brown solid with a 78% yield.

^{1}H NMR (400 MHz, $CDCl_3$) δ: 8.03 (m, *J* = 16.8, 7.2, 1.1 Hz, 2H, Ar-H), 7.69 – 7.61 (m, 2H, Ar-H), 6.07 (s, 1H, Olefin-H), 4.50 (m, *J* = 6.1 Hz, 1H, O-C*H*), 1.38 (d, *J* = 6.1 Hz, 6H, CH_3).

^{13}C NMR (100 MHz, $CDCl_3$) δ: 185.25, 180.53, 158.70, 134.18, 133.21, 131.96, 131.29, 126.70, 126.04, 110.50, 72.46, 21.18.

Compound 3.8d: 2-butoxynaphthalene-1,4-dione

The product was obtained as a brown solid with a 98% yield.

^{1}H NMR (400 MHz, $CDCl_3$) δ: 8.02 (m, *J* = 17.0, 7.2, 1.3 Hz, 2H, Ar-H), 7.69 – 7.60 (m, 2H, Ar-H), 6.08 (s, 1H, Olefin-H), 3.94 (t, *J* = 6.6 Hz, 2H, O-C*H*$_2$), 1.81 (m, *J* = 9.1, 7.8, 6.5 Hz, 2H, alkyl(CH_2)), 1.50 – 1.38 (m, 2H, Alkyl(CH_2)), 0.92 (t, *J* = 7.4 Hz, 3H, Alkyl(CH_3)).

^{13}C NMR (100 MHz, $CDCl_3$) δ: 185.09, 180.16, 159.92, 134.21, 133.25, 132.02, 131.18, 126.66, 126.10, 110.17, 69.38, 30.24, 19.12, 13.70.

3.4.2 ^{1}H-NMR, ^{13}C-NMR, and HRMS spectra of a few synthesized compounds

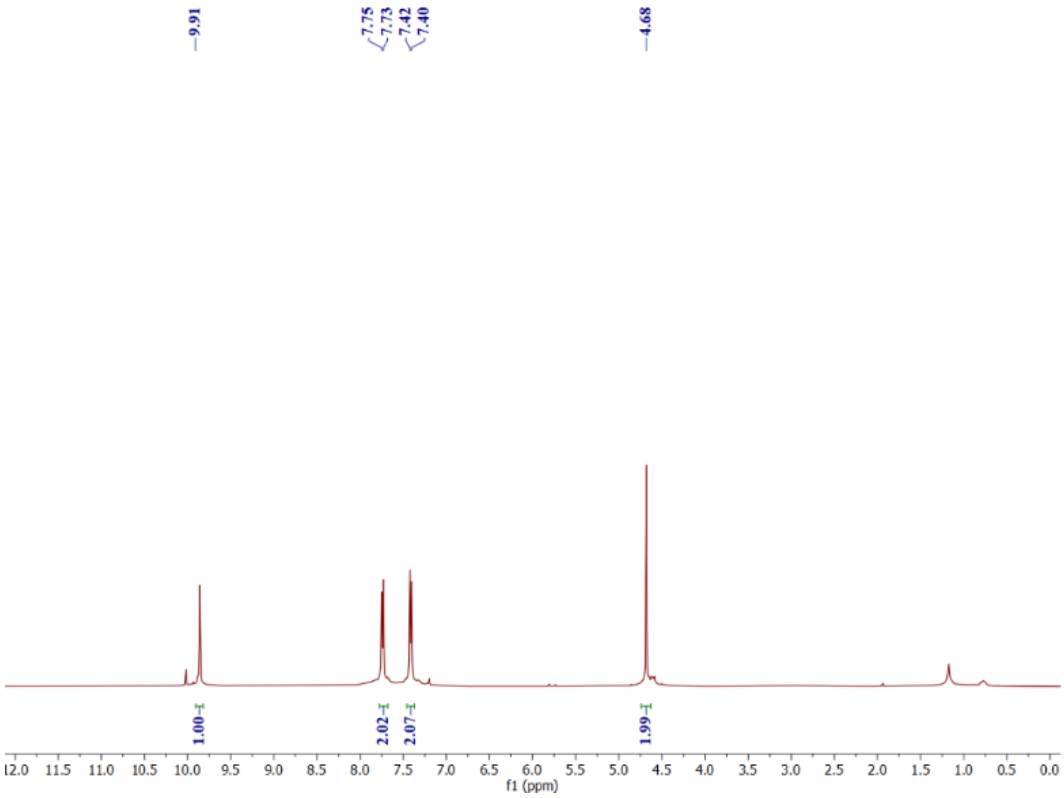

Figure 3.10. ^{1}H NMR (400MHz) Spectrum of HMBA **3.2** in $CDCl_3$ at 28 °C.

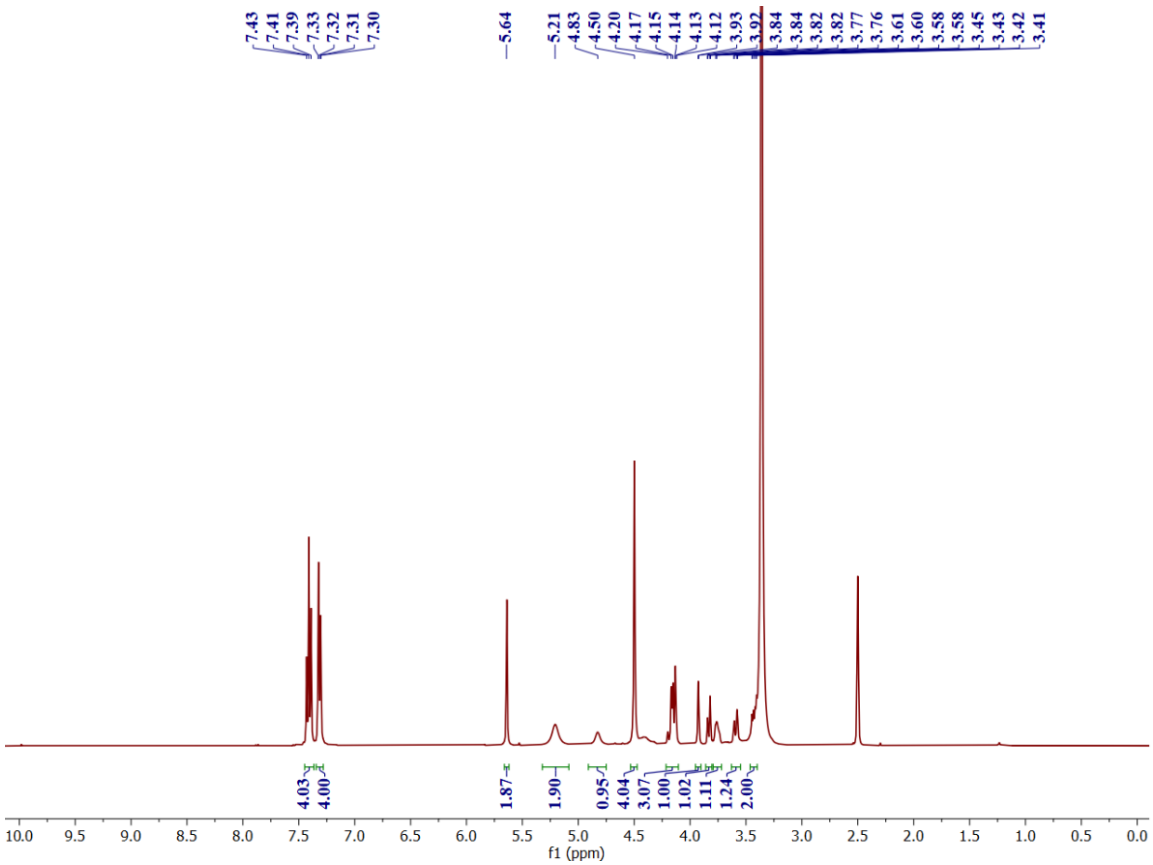

Figure 3.11. ^{1}H NMR (400MHz) Spectrum of HMDBS **3.4** in DMSO-d_6 at 28 °C.

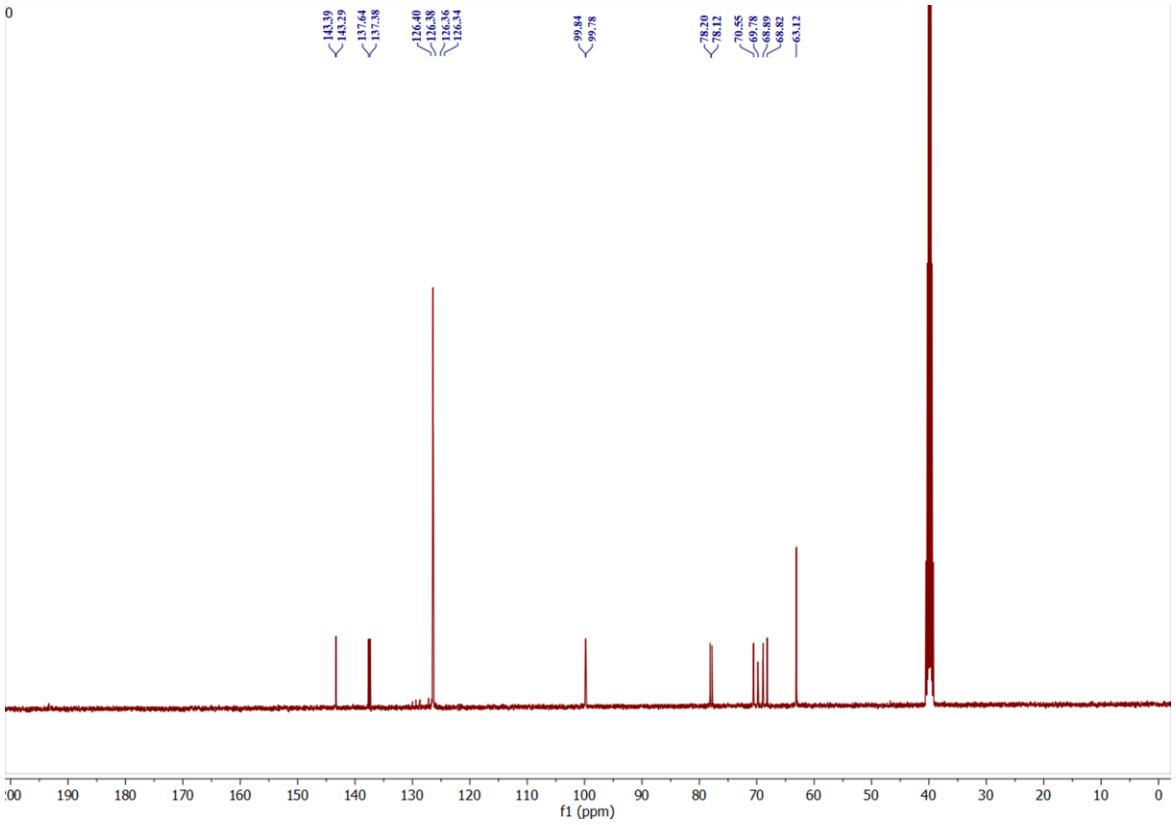

Figure 3.12. ^{13}C NMR (100 MHz) Spectrum HMDBS **3.4** in DMSO-d_6 28 °C.

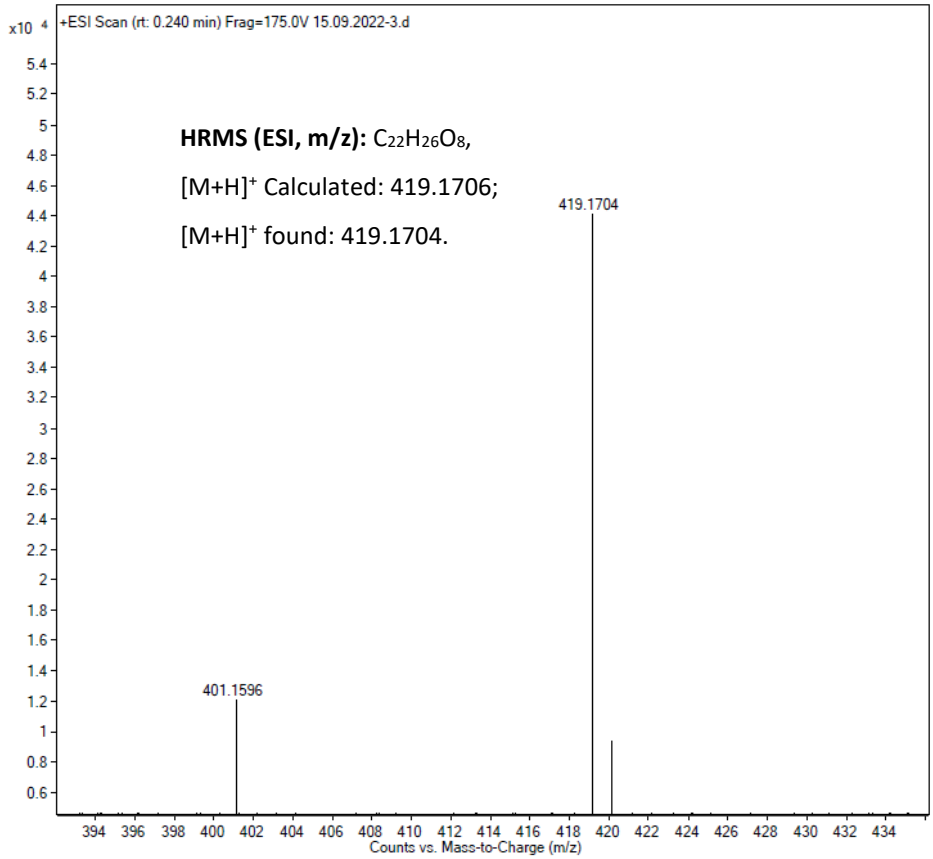

Figure 3.13 HRMS Spectrum of HMDBS **3.4**.

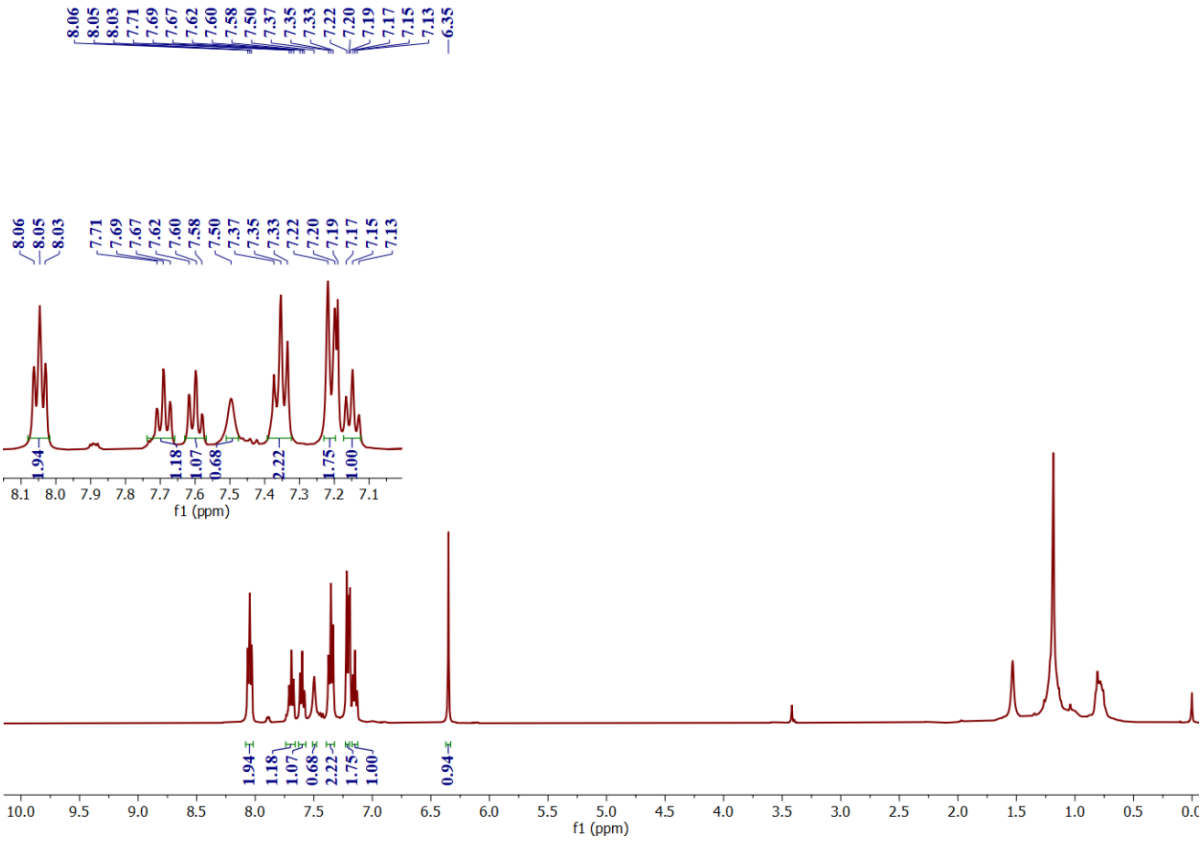

Figure 3.14. ^{1}H NMR (400MHz) Spectrum of **3.7a** in $CDCl_3$ at 28 °C.

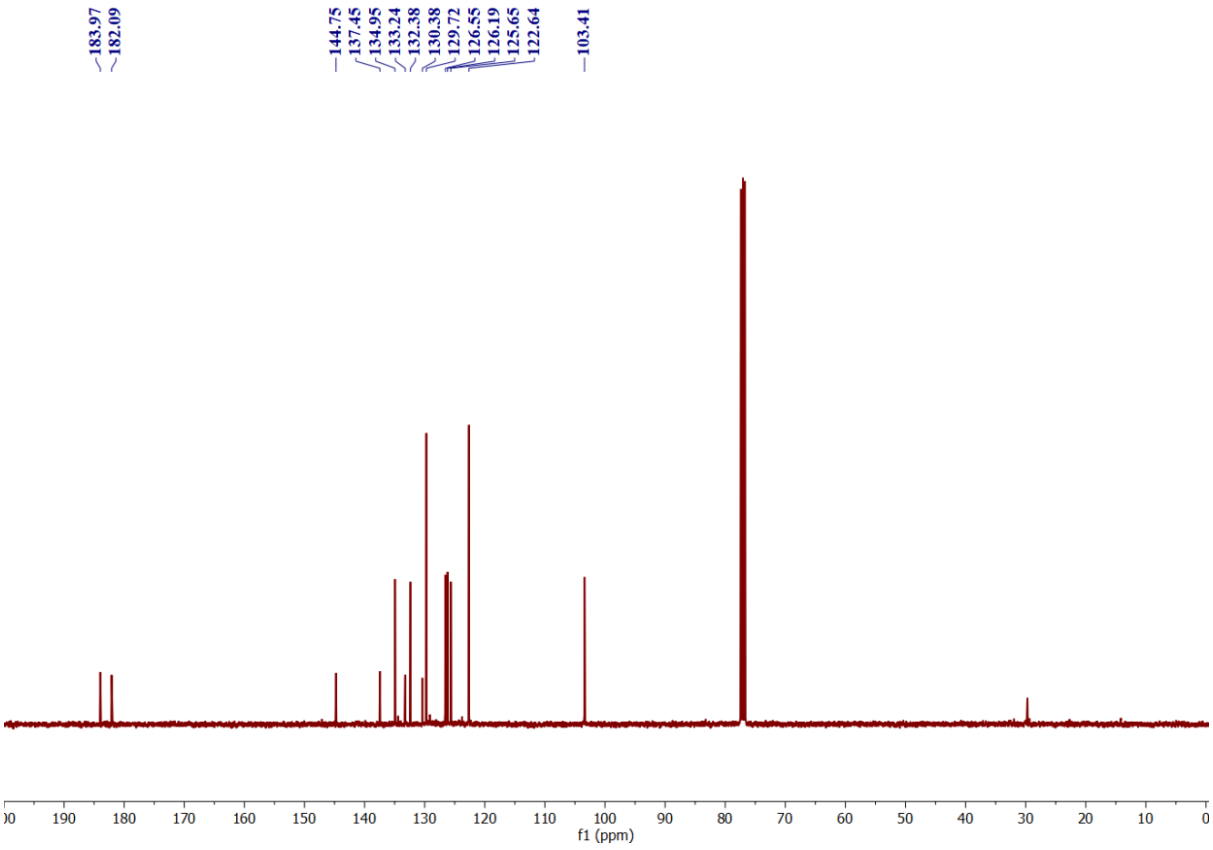

Figure 3.15. ^{13}C NMR (100 MHz) Spectrum of **3.7a** in $CDCl_3$ at 28 °C.

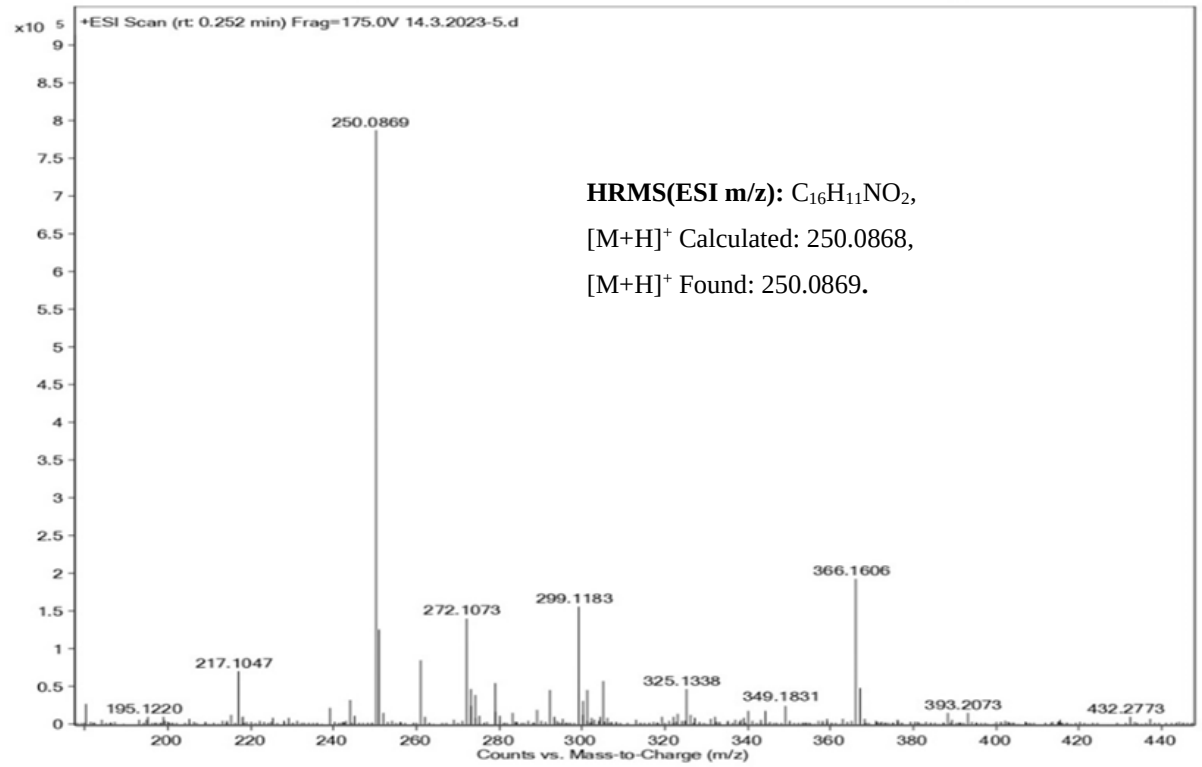

Figure 3.16. HRMS Spectrum of **3.7a**.

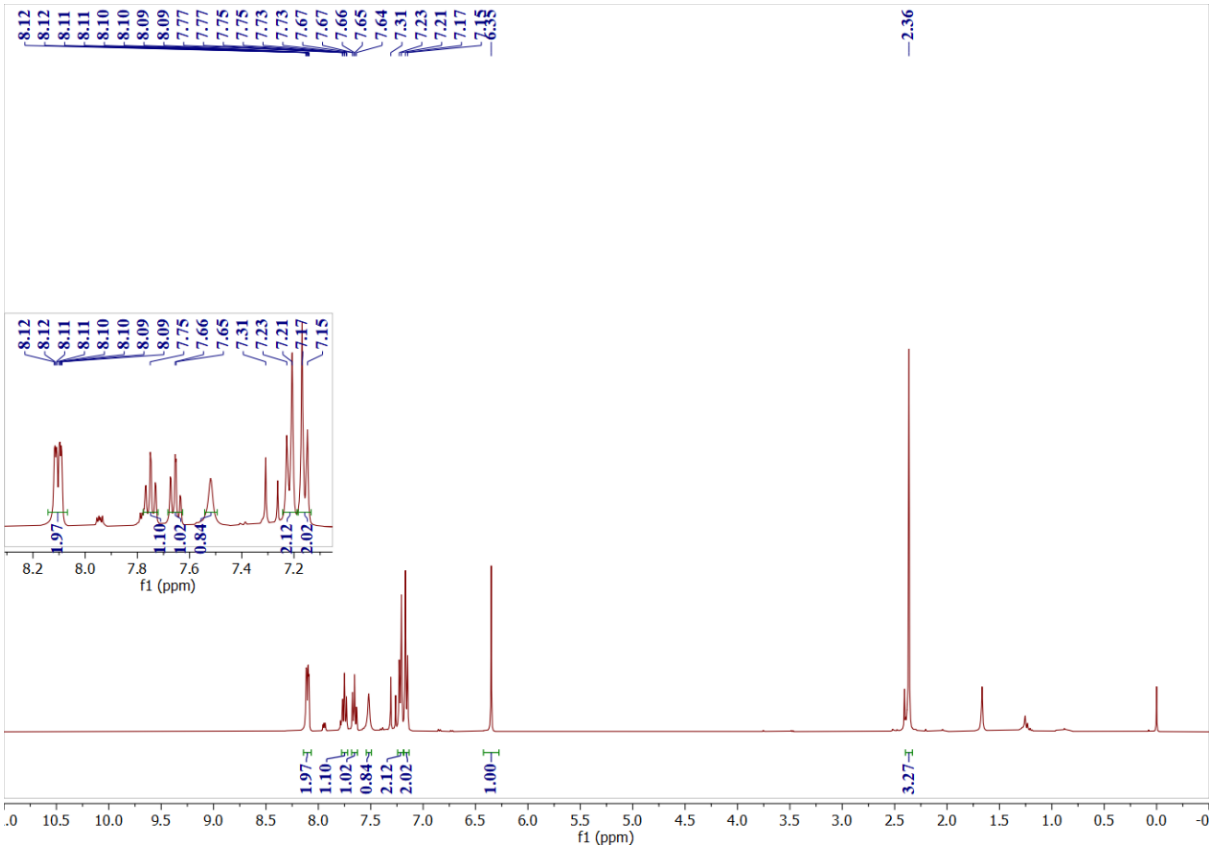

Figure 3.17. ^{1}H NMR (400MHz) Spectrum of **3.7b** in $CDCl_3$ at 28 °C.

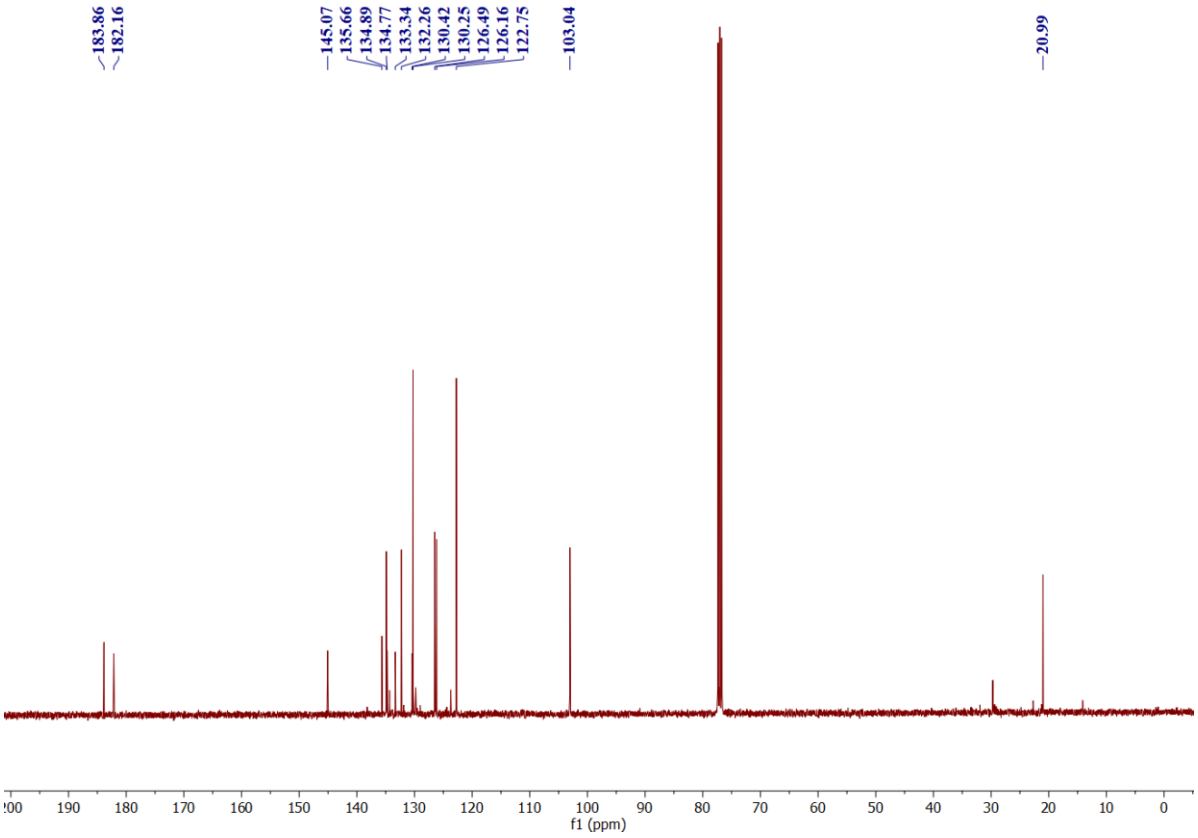

Figure 3.18. ^{13}C NMR (100 MHz) Spectrum of **3.7b** in $CDCl_3$ at 28 °C.

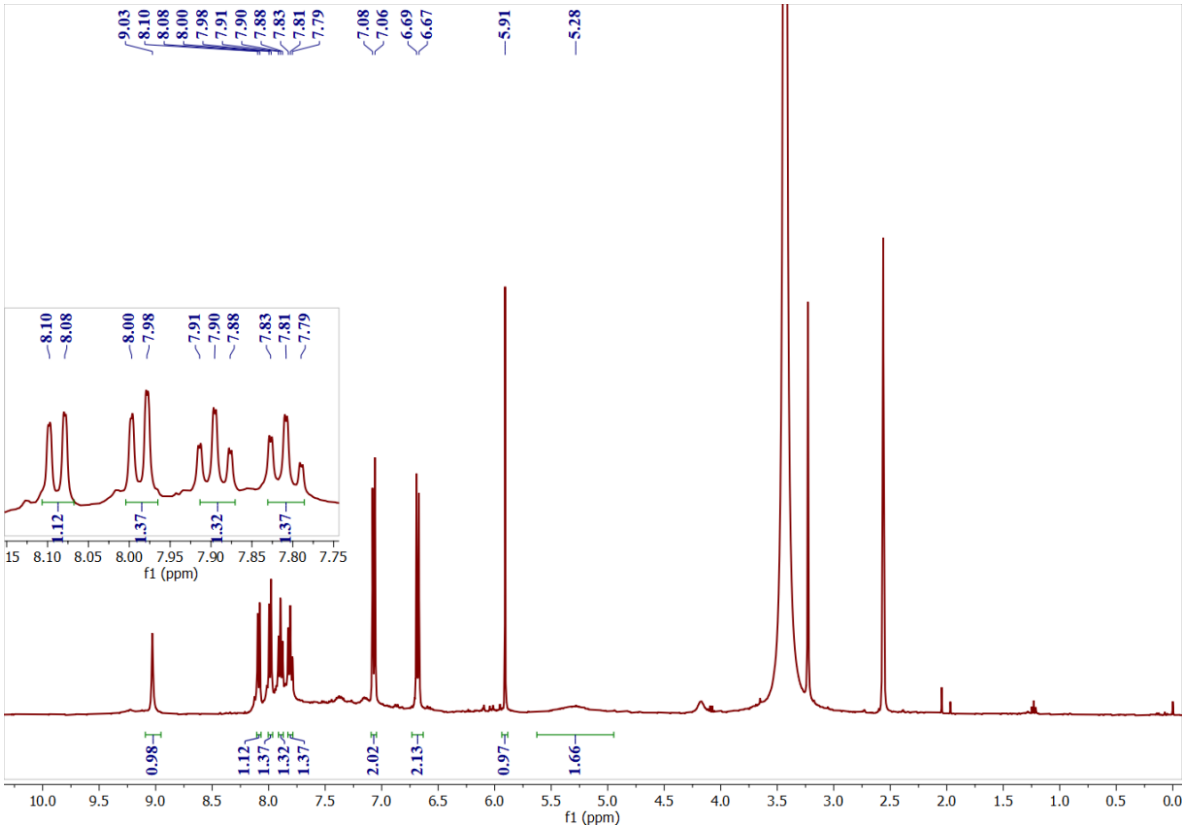

Figure 3.19. ^{11}H NMR (400MHz) Spectrum of **3.7d** in DMSO-d_6 at 80 °C.

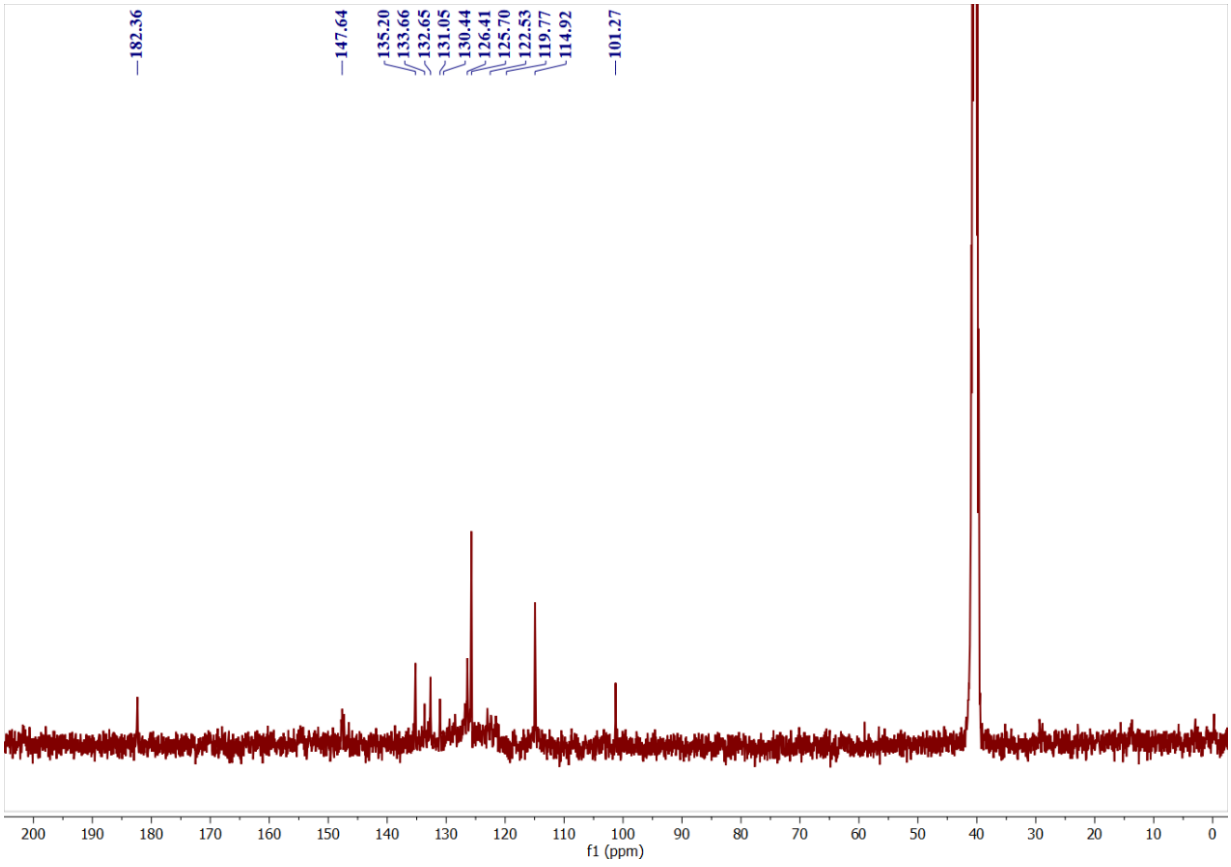

Figure 3.20. ^{13}C NMR (100 MHz) Spectrum of **3.7d** in DMSO-d_6 at 80 °C.

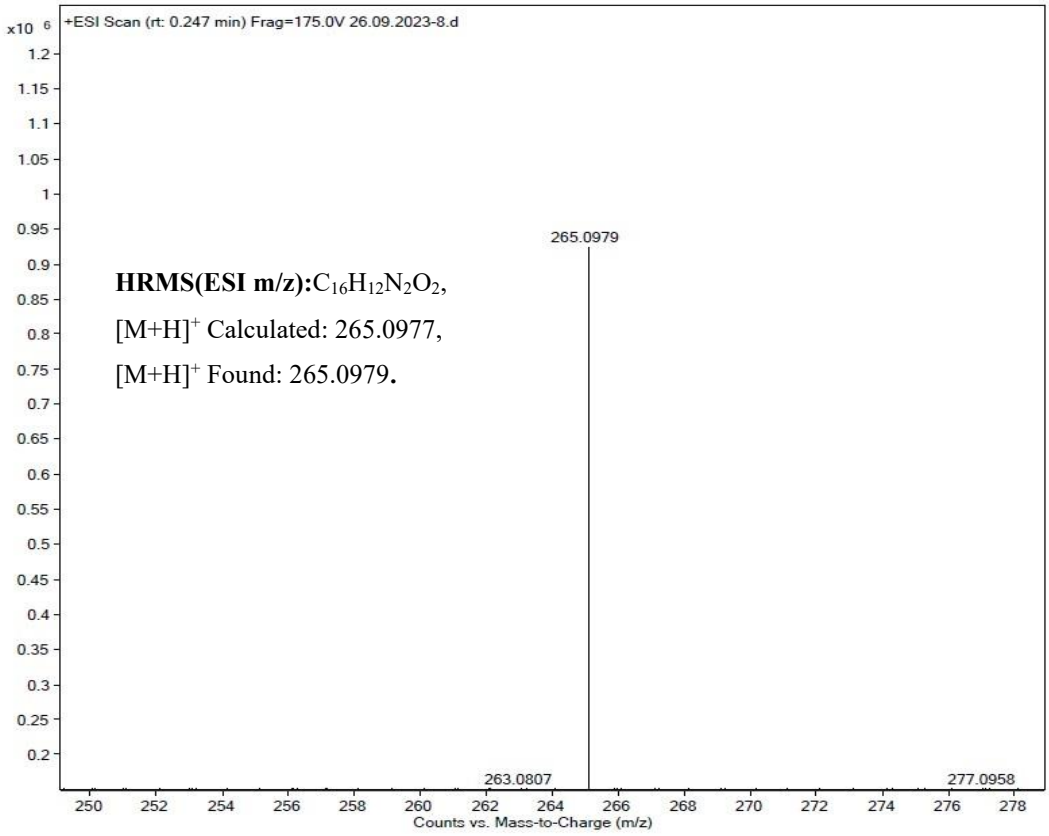

Figure 3.21. HRMS Spectrum of **3.7d**.

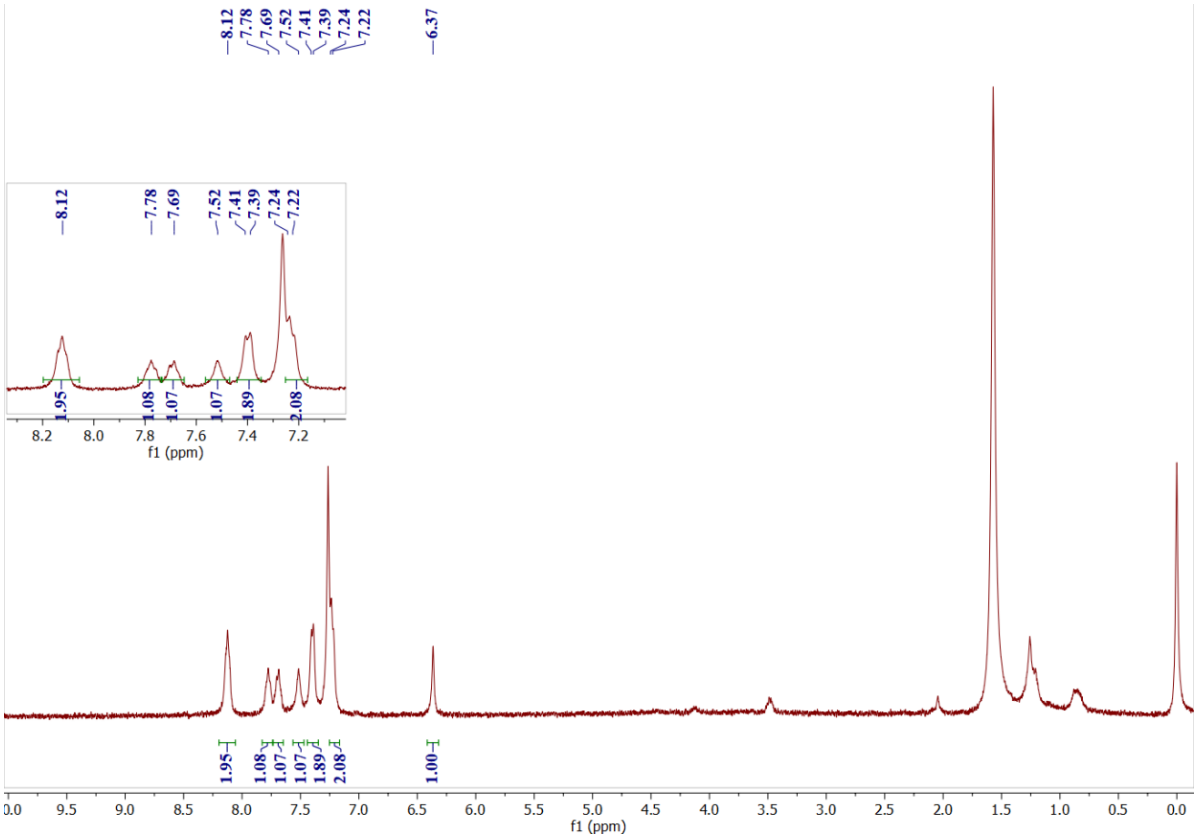

Figure 3.22. ^{1}H NMR (400MHz) Spectrum of **3.7e** in $CDCl_3$ at 28 °C.

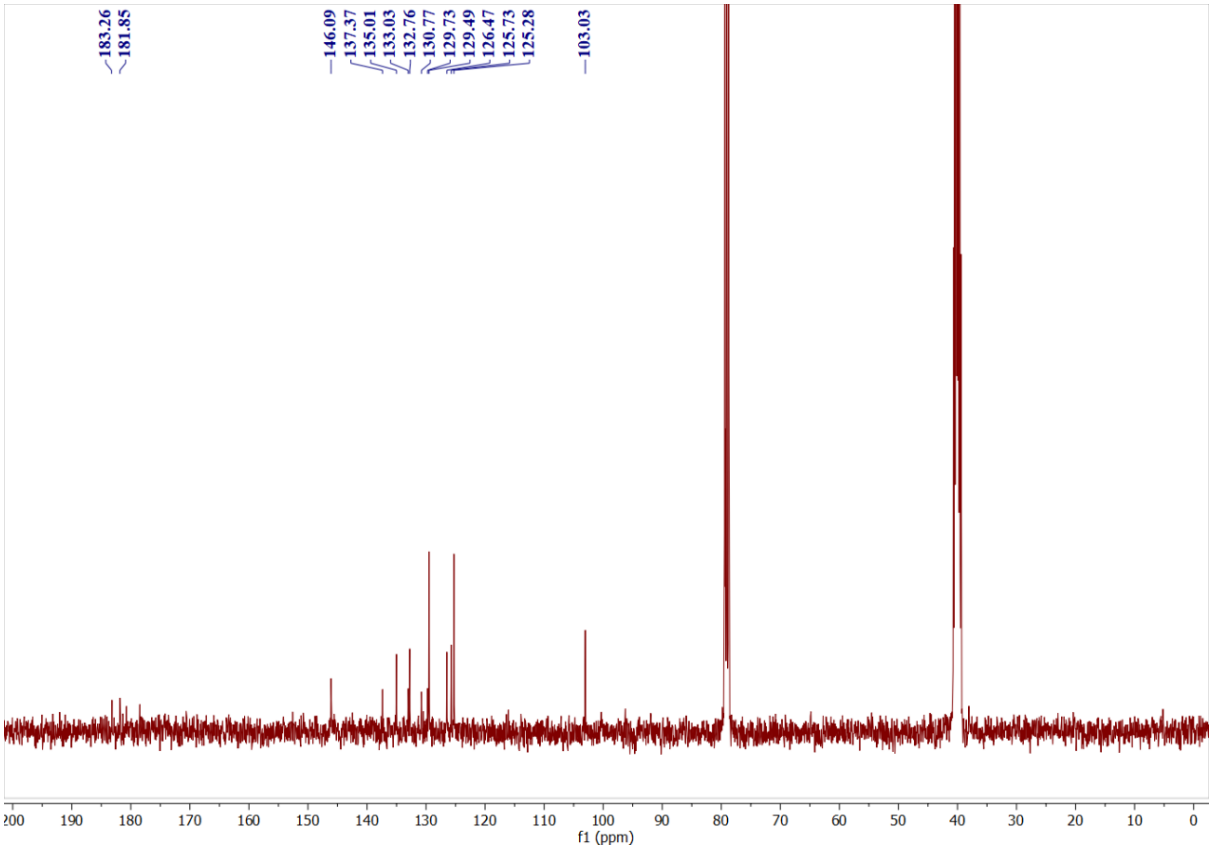

Figure 3.23. ^{13}C NMR (100 MHz) Spectrum of **3.7e** in $CDCl_3$+DMSO-d_6 at 28 °C.

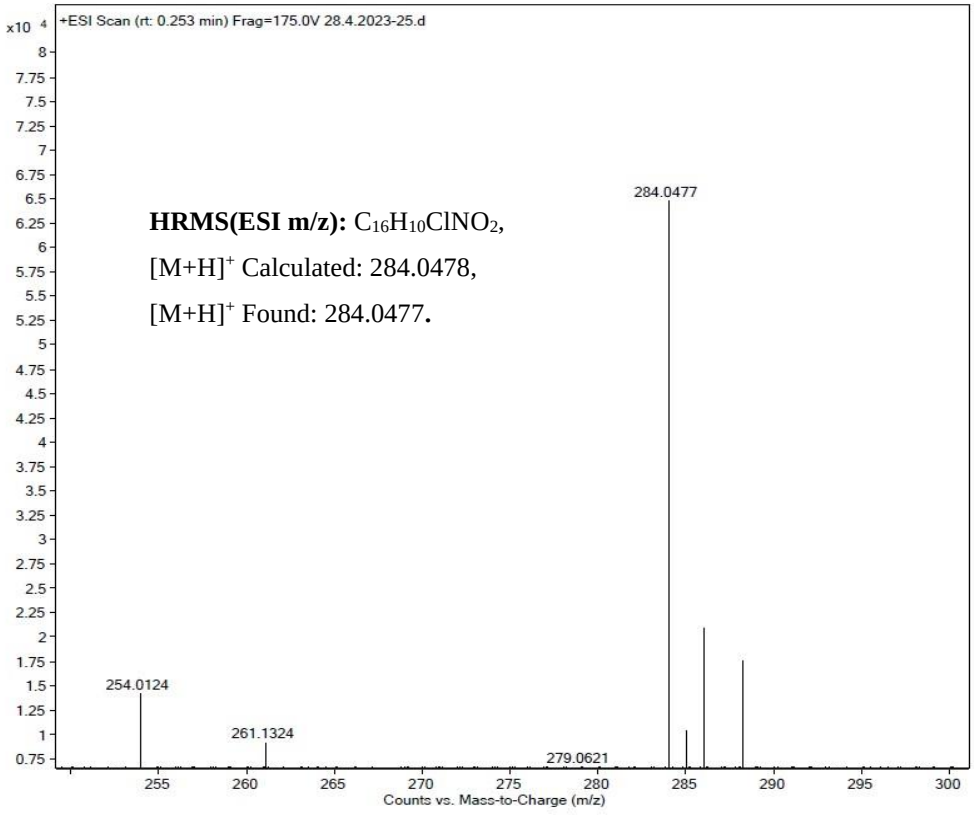

Figure 3.24. HRMS Spectrum of **3.7e**.

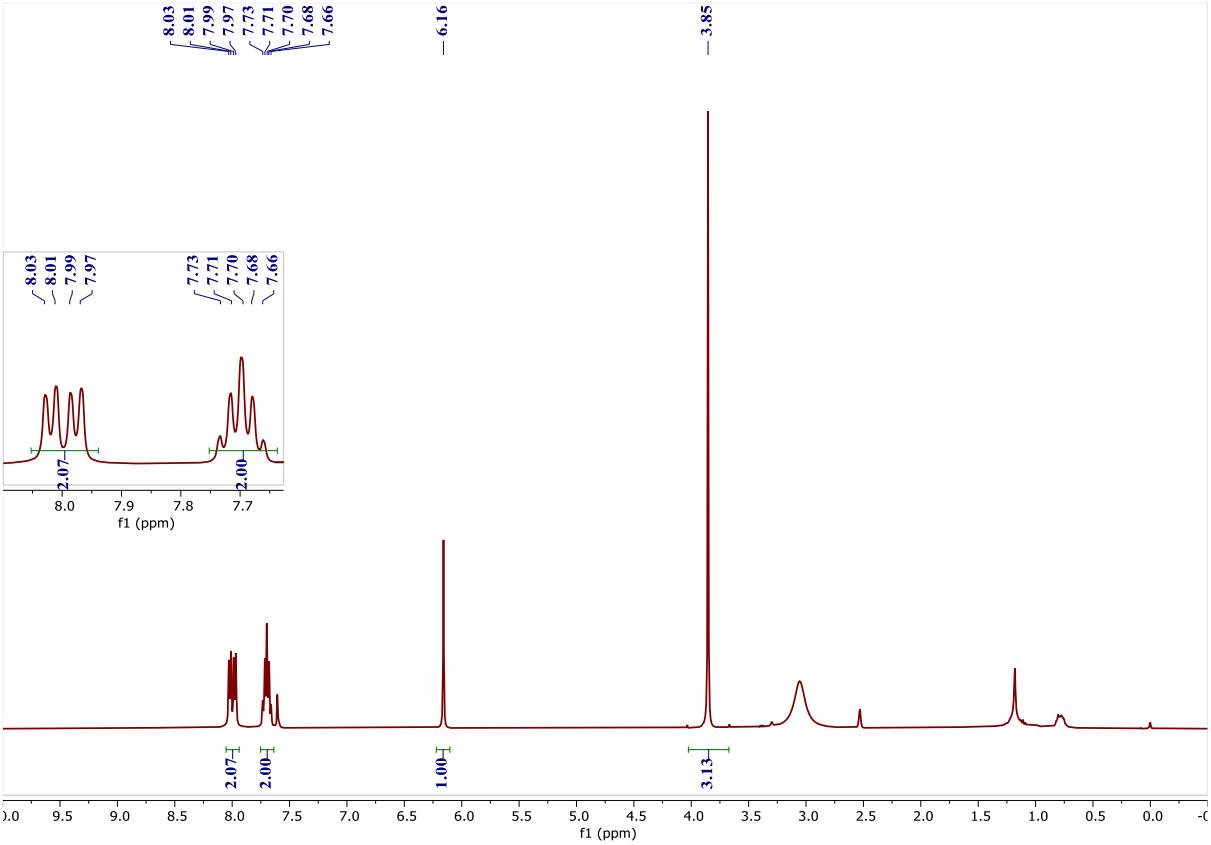

Figure 3.25. ^{1}H NMR (400MHz) Spectrum of **3.8a** in $CDCl_3$+DMSO-d_6 at 28 °C.

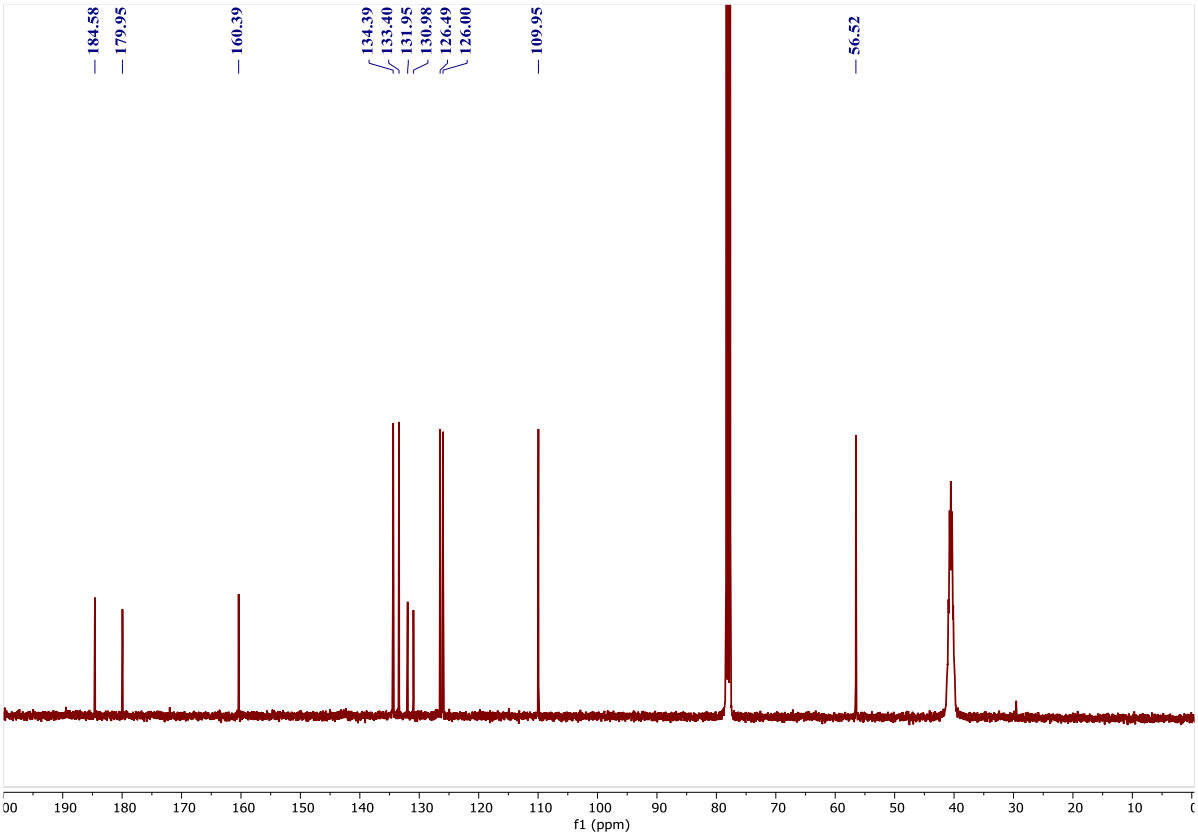

Figure 3.26. ^{13}C NMR (100 MHz) Spectrum of **3.8a** in $CDCl_3$+DMSO-d_6 at 28 °C.

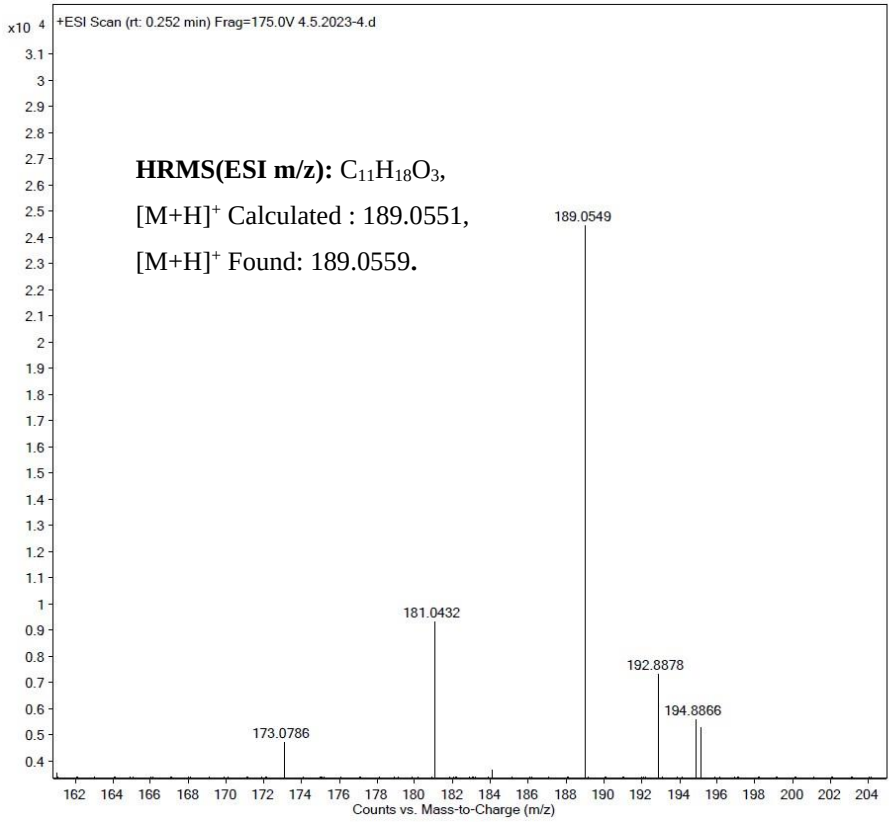

Figure 3.27. HRMS Spectrum of **3.8a**.

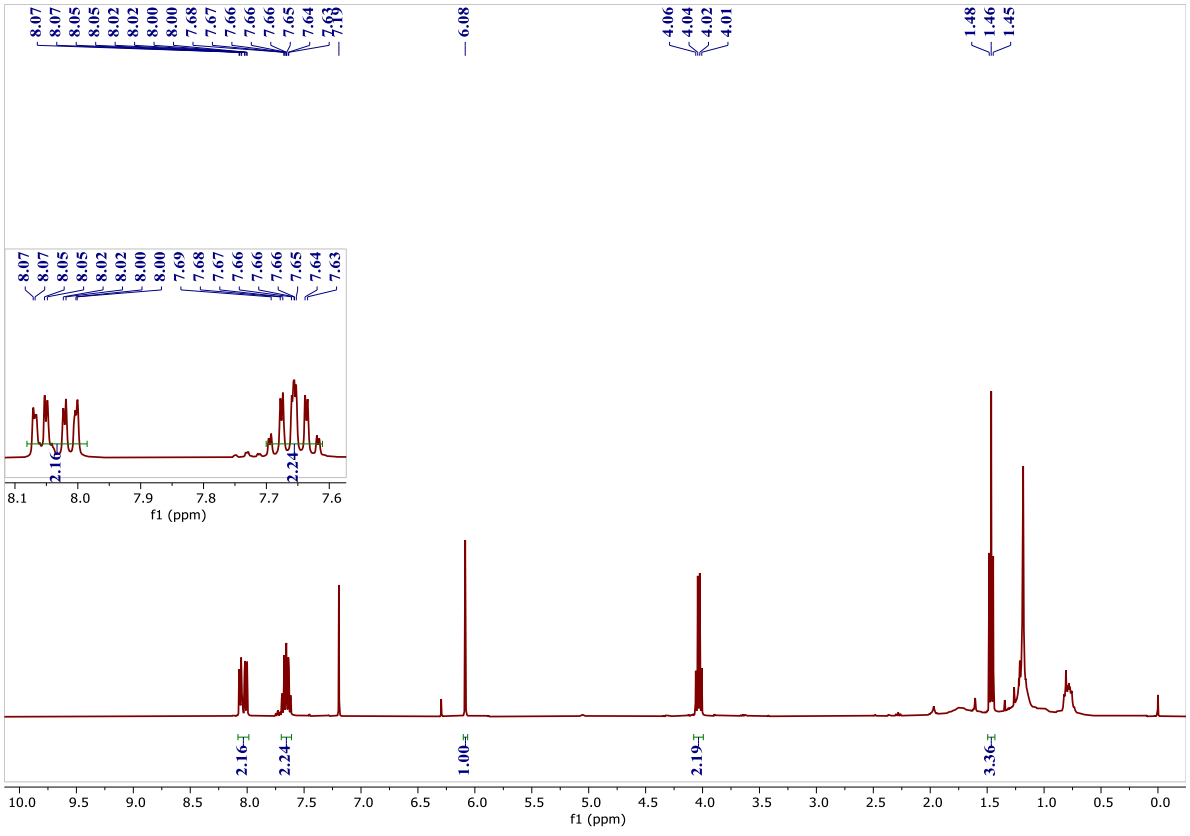

Figure 3.28. ^{1}H NMR (400MHz) Spectrum of **3.8b** in $CDCl_3$ at 28 °C.

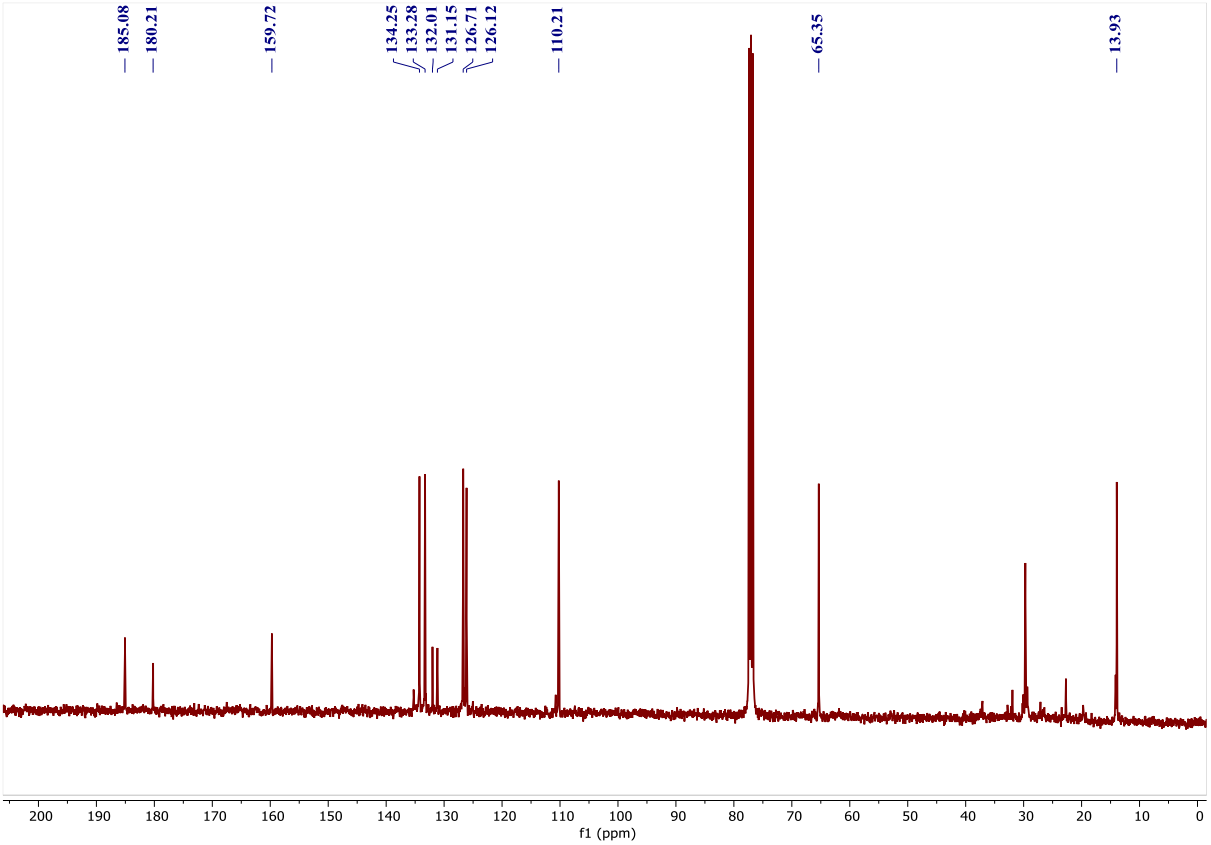

Figure 3.29. ^{13}C NMR (100 MHz) Spectrum of **3.8b** in $CDCl_3$ at 28 °C.

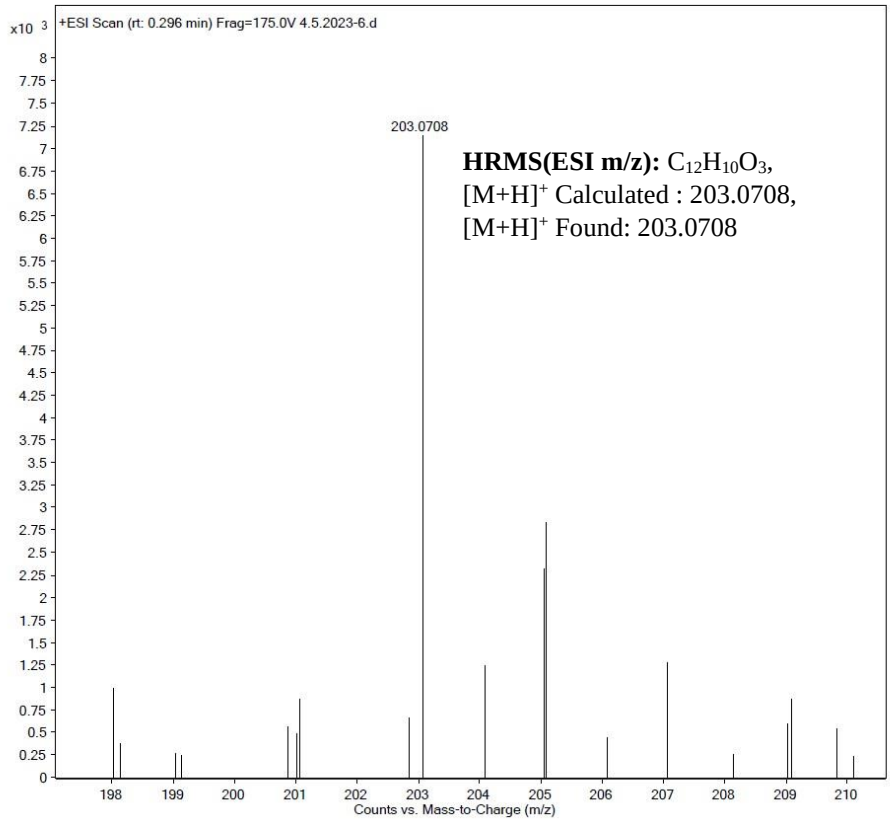

Figure 3.30. HRMS Spectrum of **3.8b**.

3.7 Conclusion

In Summary, a new DBS derivative (MHDBS) is synthesized and studied its gelation properties as eutectogel. Utilizing this eutectogel as a confined reaction media, regioselective synthesis of 4-arylamino-1,2-naphthoquinones is successfully achieved through a photochemical reaction. This innovative approach leverages the unique properties of the 3D fibrous network of the transparent gel, which, under photochemical conditions, exhibited unprecedented precision and control over the reaction outcome. Notably, the eutectogel medium showed better results than conventional methods in terms of regioselectivity, yielding exclusively the desired 4-arylamino-1,2-naphthoquinones. Control experiments provided valuable insights into the underlying mechanisms, confirming the exclusive formation of the products via a radical mechanism.

3.8 References

1. G. Brancato, F. Coutrot, D. A. Leigh, A. Murphy, J. K. Y. Wong and F. Zerbetto, *Proc. Natl. Acad. Sci. U. S. A.*, 2002, **99**, 4967–4971.
2. P. Xing and Y. Zhao, *Acc. Chem. Res.*, 2018, **51**, 2324.
3. M. Weißenfels, J. Gemen and R. Klajn, *Chem*, 2021, **7**, 23.
4. T. J. Longo, N. A. Shumovskyi, B. Uralcan, S. V. Buldyrev, M. A. Anisimov and P. G. Debenedetti, *Proc. Natl. Acad. Sci. U. S. A.*, 2022, **120**, 1, e2215012120.
5. B. Maity, K. Fujita and T. Ueno, *Curr. Opin. Chem. Biol*., 2015, **25**, 88.
6. I. Sinha and P. S. Mukherjee, *Inorg. Chem.*, 2018, **57**, 4205
7. M. Petroselli, Y. Q. Chen, J. Rebek and Y. Yu, *Green Synth. Catal.,* 2021, **2**, 123.
8. A. Ziogas, G. Kolb, M. O'Connell, A. Attour, F. Lapicque, M. Matlosz and S. Rode, *J. Appl. Electrochem*., 2009, **39**, 2297.
9. B. Maiti, A. Abramov, R. Pérez-Ruiz and D. Díaz, *Acc. Chem. Res.,* 2019, **52**, 1865.
10. A. Ziogas, G. Kolb, M. O'Connell, A. Attour, F. Lapicque, M. Matlosz and S. Rode, *J. Appl. Electrochem*., 2009, **39**, 2297.
11. G. M. Whitesides and B. Grzybowski, *Science,* 2002, **295**, 2418.

12. D. T. Bong, T. D. Clark, J. R. Granja and M. Reza Ghadiri, *Angew. Chem., Int. Ed*., 2001, **40**, 988.

13. V. Balzani, A. Credi, F. M. Raymo and J. F. Stoddart, *Angew. Chem., Int. Ed.*, 2000, **39**, 3348.

14. J.-M. Lehn, *Angew. Chem., Int. Ed*., 1990, **29**, 1304.

15. B. Jeong and A. Gutowska, *Trends Biotechnol*., 2002, **20**, 305.

16. L. Zhang, L. Qin, X. Wang, H. Cao and M. Liu, *Adv. Mater.*, 2014, **26**, 6959.

17. M. F. M. Sciacca, et al., *ACS Chem. Neurosci.*, 2017, **8**, 1767. 5.

18. M. Oliva, G. A. Coppola, E. V. Van der Eycken and U. K. Sharma, *Adv. Synth. Catal.*, 2021, **363**, 1810.

19. P. R. D. Murray, et al., *Chem. Rev*., 2022, **122**, 2017.

20. B. Maiti, A. Abramov, R. Pérez-Ruiz, D. D. Díaz, *Acc. Chem. Res*., 2019, **52**, 7, 1865-1876

21. C. Mao, Z. Mingjiang, J. Jeremiah A, *Chem. Rev*., 2016, **116**, 10167-10211

22. B. Shreedhar; M. Uday, *Molecules*, 2007, **12**, 9, 2181-2189.

23. D. Arnab; F. Norifumi; H. Shuichi; S. Kazuki; S. Seiji, *Chem. Comm.*, 2009, **16**, 2100-2103.

24. R. Vadrucci, C. Weder, Y. C. Simon, Y. C, *Mater. Horiz*., 2015, **2**, 120– 124.

25. K. Sripathy, R. W. Macqueen,J. R. Peterson, Y. Y. Cheng, M. Dvorak, D. R. McCamey, N. D. Treat, N. Stingelin, T. W. Schmidt, *J. Mater. Chem. C*, 2015, **3**, 616– 622.

26. J. Bachl, A. Hohenleutner, B. B. Dhar, C. Cativiela, U. Maitra, B. König, D. Díaz Díaz, *J. Mater. Chem. A.*, 2013, **1**, 4577– 4588.

27. M. Häring, R. P. Pérez-Ruiz, A. Jacobi von Wangelin, D. Díaz Díaz, *Chem. Commun*., 2015, **51**, 16848– 16851.

28. H. B. Singh, K. A. *Bharati, Handbook of Natural Dyes and Pigments*, Elseiver, 2014.

29. P. Babula, V. Adam, L. Havel and R. Kizek, *Curr. Pharm. Anal.*, 2009, **5**, 47.

30. M. A. Pasha, K. Anebouselvy and D. B. Ramachary, *Tetrahedron*, 2022, **117**, 132793..

31. R. Sagar, U. Shankar, A. Khanna, K. Singh and G. Tiwari, *SynOpen*, 2023, **7**, 619.

32. Chaudhary and J. M. Khurana, *Curr. Org. Chem.*, 2015, **20**, 1314.

33. H. Tseng, C. K. Lin, Y. L. Chen, C. K. Tseng, J. Y. Lee, J. C. Lee, *Eur. J. Med. Chem.*, 2018, **143**, 970–982.

34. C, H. Tseng, C. M. Cheng, C. C, Tzeng, S. I. Peng, C. L. Yang, Y. L. Chen, *Bioorganic Med. Chem.*, 2013, **21**, 2, 523–531.

35. P. Singh, A. Baheti, K. R. J Thomas, *J. Org. Chem.*, 2011, **76**, 15, 6134–6145.

36. R. A. Urbanek, S. J. Suchard, G. B. Steelman, K. S. Knappenberger, L. A. Sygowski, C. A. Veale, M. J. Chapdelaine, *J. Med. Chem.*, 2001, **44**, 11, 1777–1793.

37. L. M. Gornostaev, T. A. Rukovets, E. V. Arnold, Y. G. Khalyavina, Y. V. Gatilov, *Russ. J. Org. Chem*., 2018, **54**, 1, 78–86.

38. C. Sousa, I. Santos, M. F. M. M. Piedade,L. O. Martins, M. P. Robalo, Adv. *Synth. Catal*. 2020, **362**, 16, 3380–3387.

39. B. B. Hansen, S. Spittle, B. Chen, D. Poe, Y. Zhang, J. M. Klein, A. Horton, L. Adhikari, T. Zelovich, B. W. Doherty, B. Gurkan, E. J. Maginn, A. Ragauskas, M. Dadmun, T. A. Zawodzinski, G. A. Baker, M. E. Tuckerman, R. F. Savinell an J. R. Sangoro, *Chem. Rev*., 2021, **121**, 1232.

40. D. Yu, Z. Xue and T. Mu, *Chem. Soc. Rev*., 2021, **50**, 8596.

41. A. Bjelic, B. Hočevar, M. Grilc, U. Novak and B. Likozar, *Rev. Chem. Eng*., 2022, **38**, 243.

42. M. M. Cajnko, F. A. Vicente, U. Novak and B. Likozar, *Green Chem.*, 2023, **25**, 9045.

43. B. Saavedra, A. Meli, C. Rizzo, D. J. Ramón and F. D'Anna, *Green Chem.*, 2021, **23**, 6555.

44. C. Rizzo, S. Marullo, M. Benaglia and F. D'Anna, *European J. Org. Chem.*, 2023, **26**, e202300263

45. S. R. Jadhav, P. K. Vemula, R. Kumar, S. R. Raghavan and G. John, *Angew. Chemie. Int. Ed.*, 2010, **49**, 7695.

46. B. O. Okesola, V. M. P. Vieira, D. J. Cornwell, N. K. Whitelaw and D. K. Smith, *Soft Matter*, 2015, **11**, 4768.

47. J. Ruiz-Olles, P. Slavik, N. K. Whitelaw and D. K. Smith, *Angew. Chemie. Int. Ed.*, 2019, **58**, 4173.

48. Y. Shi, J. Zhang, L. Pan, Y. Shi and G. Yu, *Nano Today*, 2016, **11**, 738.

49. S. Ma, J. Xu, S. Sohrabi and J. Zhang, *J. Mater. Chem. A*, 2023, **11**, 11572.

50. K. Lalitha, V. Sridharan, C. U. Maheswari, P. K. Vemula and S. Nagarajan, *Chem. Commun.*, 2017, **53**, 1538.

51. S. Mahajan, S. Khullar, S. K. Mandal and I. P. Singh, *Chem. Commun.*, 2014, **50**, 10078.

52. C. Elian, V. Brezová, P. Sautrot-Ba, M. Breza and D. L. Versace, *Polymers* (Basel), 2021, **13**, 2015

53. C. Elian, V. Brezová, P. Sautrot-Ba, M. Breza, D. L. Versace, *Polymers*, 2021, ***13***, 2015

CHAPTER 4

SYNTHESIS OF TETRAZOLE BENZYLIDENE-D-SORBITOL IN A CONFINED REACTION MEDIA: APPLICATION IN THE GENERATION OF METALLOGELS

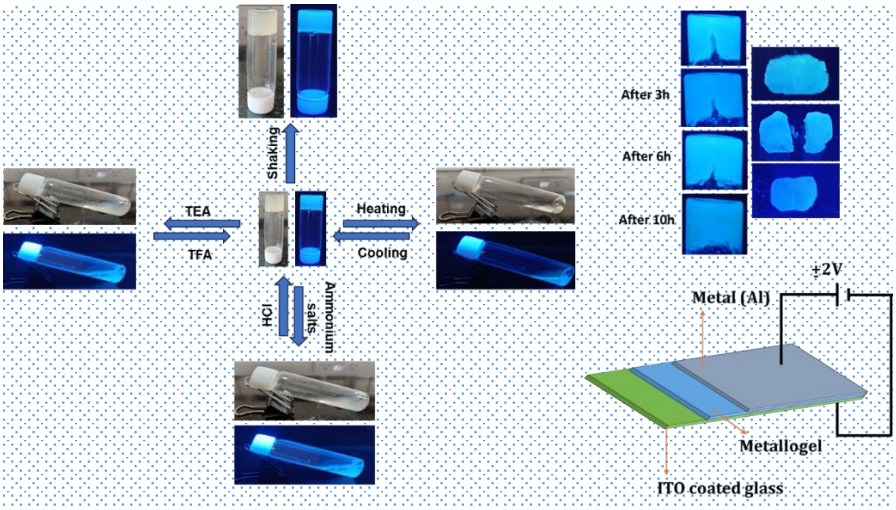

4.1 Objective

This chapter aims to design, synthesize, and characterize novel tetrazole-based dibenzylidene sorbitol (DBS) derivatives as low molecular weight gelators (LMWGs) for the formation of supramolecular metallogels with transition and lanthanide metals and to explore their potential applications in stimuli-responsive, self-healing, and photo-responsive materials, particularly in the development of semiconducting Schottky diodes.

4.2 Abstract

A new class of supramolecular metallogels has been developed through the synthesis of tetrazole-functionalized dibenzylidene sorbitol (DBS) derivatives, which exhibit efficient gelation in various solvents. The derivatives, MTZDBS and DTZDBS, exhibit efficient gelation in polar protic solvents and deep eutectic solvents. Metallogels formed with DTZDBS and Eu(III) ions demonstrate stimuli-responsive and self-healing properties, with potential applications in optoelectronic devices. Rheological, FTIR, SEM, and UV-vis studies reveal the metallogels' structural and optical properties. Notably, the EuTZDBS metallogel-based Schottky diode exhibits enhanced charge transfer under light irradiation, indicating promising photo-responsive behavior. This study expands the scope of sugar-based metallogels and highlights their potential in advanced materials applications

4.3 Introduction

A brief introduction to confined reaction media is provided in the previous chapters. Metallogels, a class of gels that incorporate metal as an essential structural component, have garnered significant attention in recent years. Metallogel formation is driven by a combination of supramolecular interactions, including metal-ligand, metal-solvent, metal-counter anion, and bulk solvent interactions.[1] These interactions work together to control the self-assembly process, resulting in metallogels with unique properties and functionalities.[2] A significant milestone was achieved by Xu and co-workers, who designed and synthesized a Pd^{2+} coordination polymer metallogel[3]. The incorporation of metal into gels can impart additional properties, including colour, charge transfer, fluorescence, rheological behaviour, magnetism, helicity, stimuli-responsiveness, nanofabrication, conductance, and catalysis.[4–13] Researchers have made attempts to adopt rational approaches to design metallogelators by incorporating aromatic linkers, steroid-based fragments,[14] and higher alkyl chains into the coordination complexes.[15–18] These metallogels possess different nanostructures based on their interactions with metal ions such as nanofibers, nanotubes and nanovesicles.[19–22] For example, alginic acid,

a polysaccharide forms hydrogels with divalent cations like Ca^{+2} by interacting with its acid groups.[23,24] Terpyridines have been extensively studied as ligands for metallogels because of their ability to form strong coordination complexes with d- and f-block metals for electronic applications.[25,26] Sulfur atoms are also used for forming coordination bonds along with C, N, and O atoms to obtain metallogels. Metallophillic hydrogels have been developed through the self-assembly of metal-thiolate complexes.[27] Gosh et al. demonstrated that electrostatic interactions can also be used to form metallogels, by using positively charged Mg^{+2} to undergo crosslinking with negatively charged polymeric counter ions such as poly(3,4-ethylenedioxythiophene) and poly(sodium-p-styrene sulfonate).[28,29] Bunzen et al. used a subcomponent self-assembly approach to obtain complex architectures from simple molecules.[30,31] Additionally, metal NPs can be introduced to the self-assembling gelators or polymer to obtain metallogels, but their stability depends upon the size distribution of NPs, solvent and preparation methods.[32]

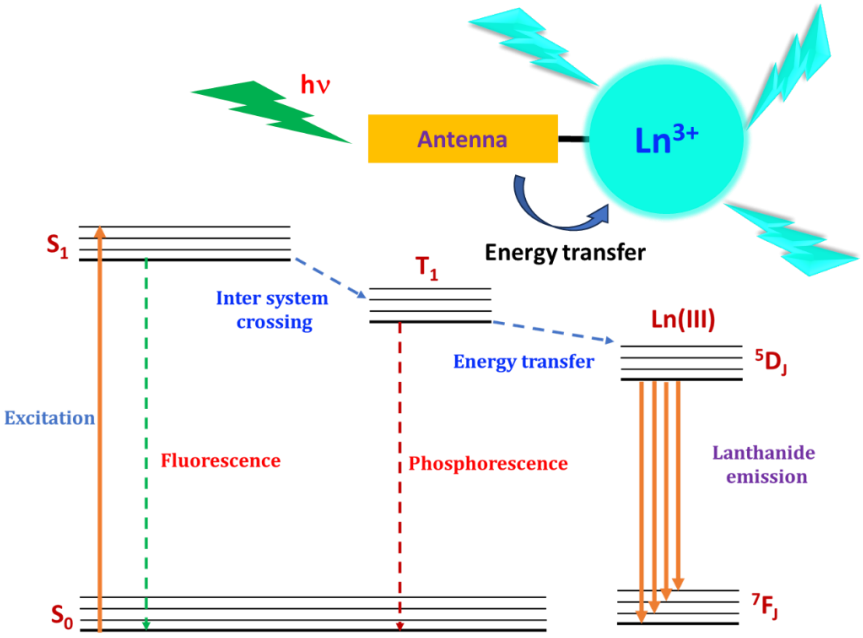

Figure 4.1. Demonstration of antenna effect in lanthanide metallogels.

Owing to their unique photoluminescence properties, such as stable and sharp emission peaks, long luminescence lifetime (in the millisecond range), resistance to photobleaching, and intense luminescence and high quantum yields, lanthanide ions have gained significant interest in forming metallogels.[33] The intense luminescence in lanthanide-based gels arises due to the 'antenna effect', where organic sensitizers/ligands act as antennas to facilitate the excitation of Ln(III) ions. The process involves the antenna absorbing electromagnetic radiation (UV) light,

and gas exited from the ground state (S_0) to the higher energy singlet state (S_1), followed by intersystem crossing, a non-radiative process to the longer-lived triplet state T_1 ($S_1 \rightarrow .T_1$). The triplet state then non-radiatively transfers energy to the Ln(III) ion (Figure 4.1).[34]

Lanthanide metallogels demonstrate applications such as chemical sensors,[35], bio-sensors[36], optoelectronic devices[37], luminescent films[38], self-healing materials[39] and stimuli-responsive materials[40] (Figure 4.2). Lanthanide metallogels are prepared by combining the LMWG's with lanthanide metals that can act as sensors[41] and self-healing luminescent materials.[39,42,43] Triazine-based metallogels formed with Tb^{3+} act as biosensors.[44] Maitra and coworkers used sodium cholate to form strong luminescent metallogels with lanthanides by incorporating various sensitizers such as pyrene and dihydroxy naphthalene and used them for the detection of lipase and β-glucosidase.[45–48] Various coordinating units have been extensively investigated for the formation of luminescent lanthanide metallogels.[40,49–59] In this chapter, the tetrazole derivative of DBS has been used to form metallogels with Eu^{3+}, which demonstrated stimuli-responsive, self-healing and Schottky diode properties. The ability to incorporate reactive sites within the metallogel network opens doors for efficient and selective reactions within a confined environment.

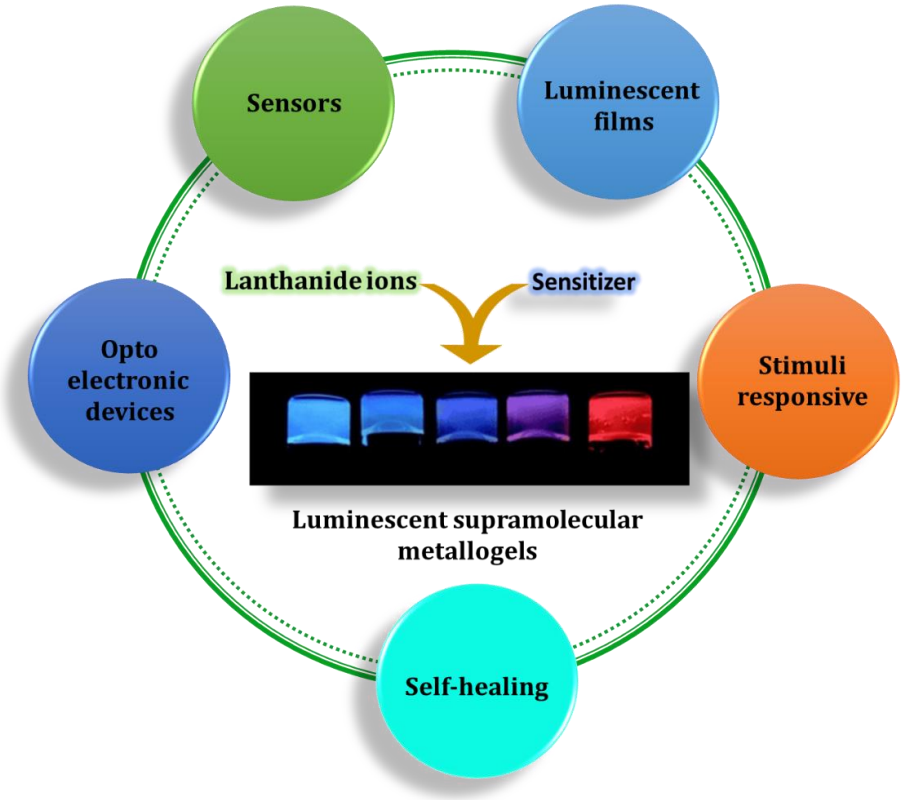

Figure 4.2. Applications of Lanthanide metallogels.

4.4 Results and Discussion

Tetrazoles are emerging as promising ligands for metallogel construction due to their unique properties and nitrogen-rich environment offer multiple binding sites, facilitating efficient cross-linking and complex formation with metal ions, making them ideal building blocks for metallogel formation. Tetrazoles can be strategically constructed to include functionalities like aromatic moieties or hydrogen bond donors/acceptors. These functionalities facilitate self-assembly via π-π stacking and hydrogen bonding. This ability empowers researchers to precisely adjust the properties of the metallogel beyond self-assembly, encompassing solubility and responsiveness to external stimuli (such as light and pH).[60] Nitriles are the common precursors for the synthesis of tetrazoles through [3+2] azide-nitrile cycloaddition reaction. As DBS is known for its exceptional gelation properties, a nitrile derivative of DBS has been synthesised in good yields by reacting *p*-cyanobenzaldehyde and sorbitol using Amberlyst as a catalyst in MeCN solvent (Scheme 4.1). The reaction conditions were previously optimized, which were discussed in Chapter 2. The formed product is characterised by NMR and HRMS techniques.

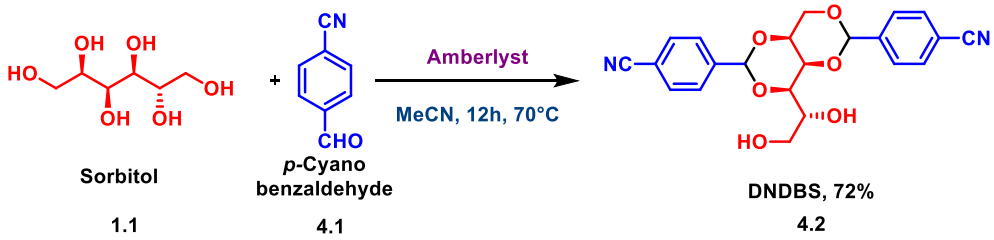

Scheme 4.1. Synthesis of Dinitrile dibenzylidene sorbitol (DNDBS)

Gelation studies have been performed on DNDBS using various solvents by the stable-to-inversion method, which involves dissolving the gelator in a suitable solvent through heating, followed by cooling to room temperature. During cooling, a bottom-up assembly of molecules occurs, driven by hydrogen bonding and π-π interactions, that enables the formation of the desired architecture with high precision and error correction capabilities. It is observed that DNDBS could be able to form gels in DMF, ethylene glycol (EG), benzyl alcohol, PEG 400 and triethylene glycol. Interestingly, DNDBS could be able to form a gel in DES. DNDBS successfully formed eutectogels in ChCl:EG and ChCl: Glycerol mixtures (Table 4.1).

Table 4.1. Gelation studies of DNDBS

S.NO	Solvent	Gelation	CGC (wt/v %)
1	DMSO	S	-
2	H_2O	NS	-
3	DMF	G	1
4	NMP	S	-
5	Ethylene Glycol	G	0.8
6	THF	S	-
7	Toluene	NS	-
8	Acetone	NS	-
9	1,2-Dichlorobenzene	PG	1.5
10	Benzyl Alcohol	G	1.0
11	MEOH	NS	-
12	PEG 400	G	1.0
13	Dimethyl carbonate	NS	-
14	ETOH	NS	-
16	Triethylene Glycol	G	1.0
17	Dimethoxy ethane	NS	-
18	Glycerol	G	1.0
19	DCM	NS	-
20	1,4-Dioxane	S	-
21	Paraffin Oil	NS	-
22	Linseed oil	NS	-
23	CCl_4	NS	-
24	Acetic acid	NS	-
25	MeCN	NS	-
26	Dichloroethane	NS	-
27	Cyclohexane	NS	-
28	ChCl:EG	G	1.0
29	ChCl: Glycerol	G	1.2

I–Insoluble; G-Gel; S-Soluble; PG-Partial gelation.

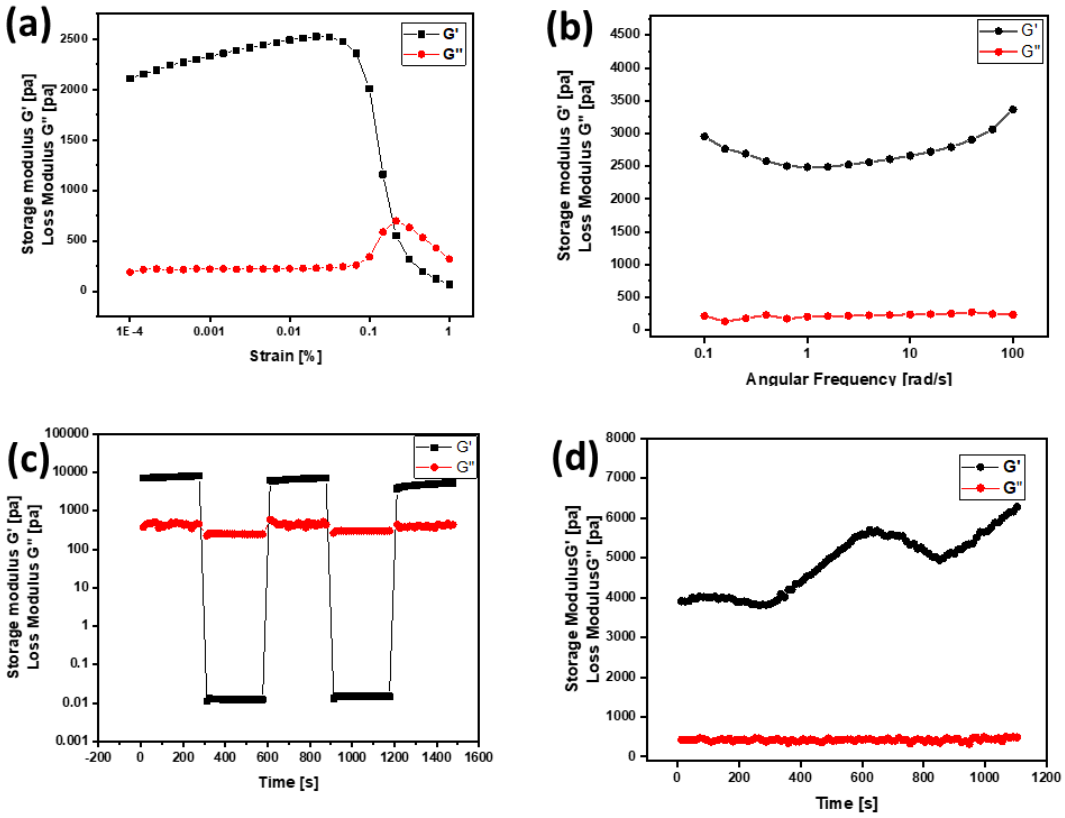

Figure 4.3. Rheological studies of DNDBS eutectogel (a) Amplitude sweep; (b) Frequency sweep; (c) Thixotropy; (d) temperature ramp-up and ramp-down experiment.

The mechanical properties of the DNDBS gel formed in the eutectogel ChCl: EG (1:2) were examined through the analysis of its viscoelastic characteristics utilizing a Rheometer. Gels experience deformation in reaction to stress or strain, which is contingent on the intermolecular interactions dictating the supramolecular structure. The exploration of flow properties of the gel concerning strain amplitude sweep and angular frequency sweep in relation to storage modulus (G') and loss modulus (G'') holds significant importance for applications in organic materials. The frequency sweep measurements of the DNDBS gel depicted in Figure 4.3 consistently revealed that the storage modulus G' surpassed the loss modulus G'', suggesting that the DNDBS gel demonstrates stability and resistance to external forces. The amplitude sweep measurements clearly illustrate the gel-like behaviour of DNDBS, where G' is greater than G'' up to a critical strain level of 0.02%. Subsequently, a decline in both G' and G'' signifies the transition to fluid-like behaviour in the gels. Following an evaluation of the gel's ability to withstand external forces. Examination of their processability was carried out through continuous temperature ramp-up and ramp-down experiments spanning from 23°C to 55°C. This investigation reveals that the gels disintegrate upon heating and subsequently reform the

gel network upon cooling, facilitated by reversible non-covalent interactions. The thixotropic behaviour exhibited by gels offers valuable insights into their ability to restore the structural integrity that may have been compromised as a result of subjecting the gel to various % of strain. Following the imposition of a consistent 100% strain, the DNDBS gel exhibited a decline in its strength, which was then reversed upon reducing the strain to 0.1%, leading to a restoration of the gel's original viscosity. A series of three consecutive cycles involving incremental strain application and subsequent relaxation revealed a progressive decline in the structural integrity of the gel concurrent with the increase in strain. Nevertheless, the gel promptly returned to its initial state once the strain was alleviated back to 0.1%.

The involvement of functional groups in the process of self-assembly can be investigated using FTIR spectroscopy. The FTIR spectra of the amorphous and Xerogels of DNDBS are shown in Figure 4.4. DNDBS in an amorphous state displays an OH-stretching frequency at 3373 cm^{-1} and a stretching frequency of C=C in the aromatic group at 1615 cm^{-1}. After undergoing self-assembly, xerogels of DNDBS displayed an OH-stretching frequency at 3413 cm^{-1} and a stretching frequency of C=C in the aromatic group at 1654 cm^{-1}. which confirms the involvement of OH groups and aromatic groups in self-assembly of molecules into 3D architectures.

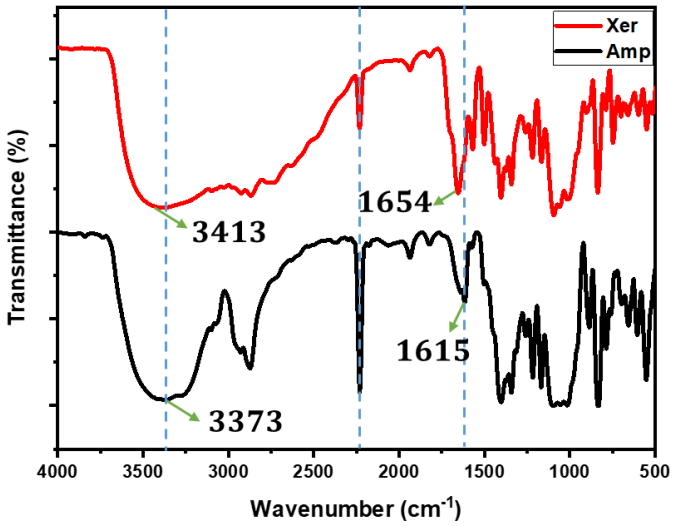

Figure 4.4. Comparison of IR spectra of xerogel and amorphous DNDBS

The distinctive characteristics of DES, including their simple preparation, cost-effectiveness, stability, non-volatility, minimal toxicity, and strong biodegradability, underscore their potential for sustainable solvent utilization.[61] Eutectogels contain liquid DES components entrapped within a 3D network structure formed by the gelator. This network behaves like a

microscopic cage, confining the reactants within proximity. This confinement significantly influences the reaction pathways, favouring specific products, and potentially leading to higher selectivity for the target. Eutectogels have been used as a confined medium for various chemical transformations, which are discussed in the Chapter 3.[62]

The azide-nitrile cycloaddition reactions are best suited to be performed in confined media, as the proximity of azide and alkyne moieties in the self-assembled state will increase the rate of the reaction. The synthesis of triazoles by azide-alkyne cycloaddition reaction using gels as confined media has previously been explored.[63] This is the first report of the synthesis of tetrazoles by azide-nitrile cycloaddition reaction in a confine media, by reacting DNDBS with sodium azide (Scheme 4.2). From the FTIR study, it is observed that the peak at 2231 cm^{-1} representing C≡N stretching frequency has not undergone any shift upon self-assembly, hence, the pendant nitrile groups on DBS are available for further modification.

Interestingly, this reaction yielded two products, mono tetrazole dibenzylidene sorbitol (MTZDBS) and ditetrazole dibenzylidene sorbitol (DTZDBS). Generally, high temperatures are required for the formation of tetrazoles in conventional conditions. However, in confined media, the formation of tetrazoles is observed at lower temperatures, which signifies the advantage of confined reaction media. By using different solvents, reagents, and varying time and temperature, optimization studies have been performed for the cycloaddition reaction of DNDBS and NaN_3 in confined media (Table 4.2).

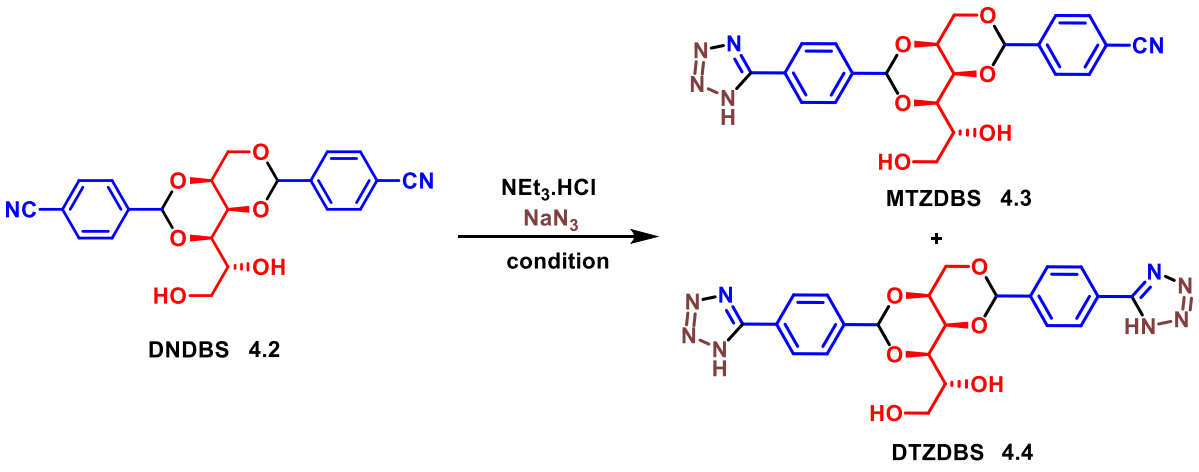

Scheme 4.2. Synthesis of MTZDBS and DTZDBS.

Table 4.2. Optimisation studies for the synthesis of MTZDBS and DTZDBS.

S.No	Gel/Solvent	Reagent	Temp [°C]	Time [h]	MTZDBS [%]	DTZDBS [%]
1	Ethylene Glycol	TEA	60	24	42	-
2	DES (ChCl+EG(1:4))	TEA	rt	24	traces	-
3	DES(ChCl+EG(1:4))-Gel medium	TEA	60	24	65	-
4	DES(ChCl+EG(1:4))-Gel medium	TEA	60	48	78	-
5	DES(ChCl+EG(1:3))- Gel medium	TEA	60	48	83	-
6	DES(ChCl+EG(1:2))- Gel medium	TEA	60	48	89	-
7	DES(ChCl+EG(1:2))- Gel medium	TEA	60	72	74	traces
8	DES(ChCl+EG(1:2))-solution *	TEA	120	24	83	traces
9	DES(ChCl+EG(1:2))- solution *	TEA	120	36	40[a]	25[a]
10	DES(ChCl+EG(1:2))- solution*	TEA	120	48	25[a]	55[a]
11	DES(ChCl+EG(1:2))- solution*	TEA	120	72	traces	76

a= Yields obtained from crude NMR, * - Gel to sol transition occurred at 120 °C, and reaction occurred in solution phase.

From the optimization studies, it is observed that less yields of MTZDBS and no formation of DTZDBS has been observed when the reaction was performed in the gel formed in ethylene glycol at rt. The yield of MTZDBS increased to 89%, when the reaction performed in eutectogel formed in ChCl:EG (1:2) at 60°C (entry 6, table 4.2). Eutectic solvent in the system displays a dual interaction behaviour with the azide ion via electrostatic interaction and H-bonding. These combined interactions likely lead to a more effective formation of ion pairs between choline chloride and azide. Consequently, the local concentration of available azide ions in solution could potentially increase.[64] The formation of DTZDBS is not observed even when the reaction duration is prolonged to 3 days at 60°C in confined media. This result revealed that in the assembled state, only one -CN group was exposed out for the reaction to occur. However, at 120°C, the gel-to-sol transition occurs by disassembly of molecules. As the temperature further increased to 120°C, the gel media is converted into to liquid state due to the disruption of H-bonding at high temperatures and when the reaction is continued for 3 days, 76% yield of DTZDBS is observed (entry 11, table 4.2). Both mono and tetrazole DBS derivatives have been confirmed using NMR and HRMS techniques. In, ^{1}H-NMR, MTZDBS

and DTZDBS are differentiated by the downfield shift of the aromatic protons adjacent to the tetrazole moiety. This is due to the deshielding effect of the tetrazole ring.

The formation of ditetrazole is further confirmed by comparing the FTIR spectra of DNDBS and DTZDBS. The absence of C≡N stretching at 2231 cm^{-1} and a new stretching frequency at 1567 cm^{-1} corresponds to C=N in the FTIR confirms the formation of DTZDBS (Figure 4.5). The self-assembly of MTZDBS and DTZDBS has been investigated by performing gelation studies by stable-to-inversion method, and it is observed that both of them show similar gelation. MTZDBS and DTZDBS formed gels in polar solvents such as DMF, DMF+H_2O, ethylene glycol and glycerol (Table 4.4).

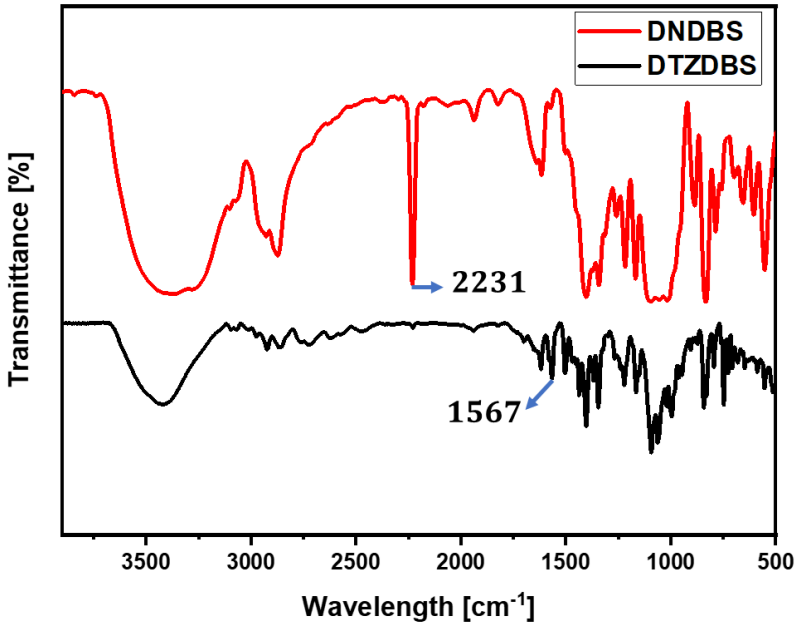

Figure 4.5. Comparison of IR spectra of DNDBS and DTZDBS

Table 4.3. Gelation studies of MTZDBS and DTZDBS

S.No	Solvent	Gelation CGC (wt/v %)	
		MTZDBS	DTZDBS
1	DMSO	S	S
2	DMSO+H_2O	PG	PG
3	H_2O	NS	NS
4	DMF	G (0.8)	G (0.5)
5	DMF+H_2O	G (1.2)	G (0.8)
6	NMP	S	S

7	Ethylene Glycol	G (0.8)	G (0.5)
8	THF	NS	NS
9	Toluene	NS	NS
10	Acetone	NS	NS
11	1,2-Dichlorobenzene	NS	NS
12	Benzyl Alcohol	NS	NS
13	MeOH	NS	NS
14	PEG 400	G (1)	G (1)
15	Dimethyl carbonate	NS	NS
16	EtOH	NS	NS
17	Diethyl Ether	NS	NS
18	Glycerol	G (0.8)	G (1)
19	Dimethoxy ethane	NS	NS
20	DCM	NS	NS
21	1,4-Dioxane	NS	NS
22	Paraffin Oil	NS	NS
23	Linseed oil	NS	NS
24	CCl_4	NS	NS
25	Acetic acid	NS	NS
26	MeCN	NS	NS
27	Dichloroethane	NS	NS
28	Cyclohexane	NS	NS

I–Insoluble; G-Gel; S-Soluble; PG-Partial gelation

The formation of gels in a solvent mixture of DMF and H_2O provides an opportunity to investigate the fabrication of metallogels. Metallogels can be generated by various protocols such as heating-cooling, sonication, microwave, and room-temperature gelation.[65] Tetrazoles are well-known ligands in coordination polymer chemistry. The gelation ability of DTZDBS is tested with different metal acetates such as Co^{2+}, Ni^{2+}, Co^{2+} and Zn^{2+} by using the sonication method, where DTZDBS, dissolved in DMF and metal ions dissolved in H_2O are mixed and sonicated for 1 minute to form strong metallogels (Figure 4.6).

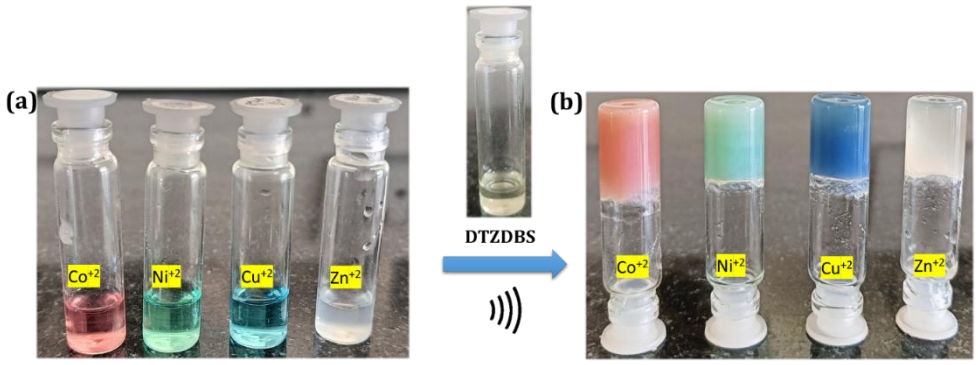

Figure 4.6. (a) metal acetate solutions in water (b) metallogels formed after mixing metal solutions with DTZDBS gelator in DMF

Further, the optimization of metallogel formation revealed that strong metallogels are formed when an equal ratio of DMF:H_2O and equal concentrations of the gelator and metal ions are used. The formation of metallogels relies on the balance between the metal ions and gelator molecules, excess of either will lead to the formation of incomplete networks or hindering crosslinking between the complexes thereby disrupting the self-assembly process. Metallogels formed by the tetrazole-based ligands demonstrate dynamic properties and act as important tools for the construction of complex ordered structures. In terms of magnetic and spectroscopic behaviour, lanthanide metals exhibit interesting properties, when compared to the 3d-transition metals. Ln^{3+} ions function as hard Lewis acids and are capable of interacting with donor atoms preferentially with O, N, and S atoms, leading to the formation of lanthanide-based complexes. Additionally, Ln^{3+} ions have a tendency to create complexes with higher coordination numbers and greater flexibility in their coordination mode, allowing for easier ligand exchange compared to other 3d-transition metals. Consequently, these lanthanide complexes demonstrate distinct physicochemical properties.[59]

The versatile coordination modes of tetrazole ligands with Eu^{3+} facilitate the Eu^{3+}-based metallogelation.[66] Using the sonication method, EuDTZDBS metallogels have been formed by mixing, DTZDBS gelator in DMF and Eu^{3+} in water (Figure 4.7).

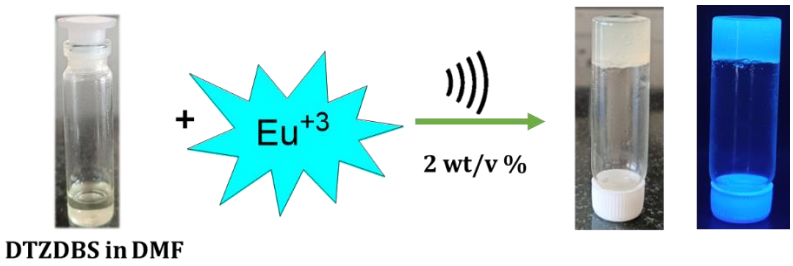

Figure 4.7. Formation of EuDTZDBS metallogel.

To investigate the rheological properties of the metallogels, amplitude and frequency sweep studies have been performed. In frequency sweep studies, the metallogel consistently revealed that the storage modulus G' is greater than the loss modulus G''; suggesting that the EuDTZDBS gel demonstrates stability and resistance to external forces. The amplitude sweep measurements clearly illustrate the gel-like behaviour of EuDTZDBS, where G' is greater than G'' up to a critical strain level of 2.15%. Subsequently, a decline in both G' and G'' signifies the transition to fluid-like behaviour in the gels (Figure 4.8).

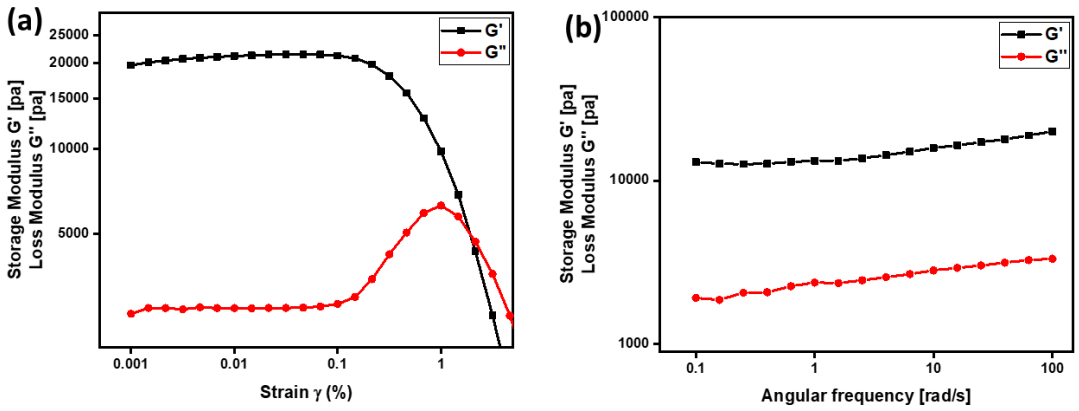

Figure 4.8. Rheological studies of EuDTZDBS gel (a) Amplitude sweep and (b) Frequency sweep.

The morphology of the metallogels is studied using SEM analysis, and the xerogel of EuDTZDBS metallogel revealed that crosslinked microfibrillar sheet-like architecture (Figure 4.9a). Further, FTIR analysis revealed the coordination of Eu^{3+} with DTZDBS in the metallogel (Figure 4.9b).

Stimuli-responsive nature of the EuDTZDBS metallogels has been investigated under various conditions. The metallogel demonstrated good mechanical stability, withstanding external mechanical forces as it resisted breakdown into a sol state even after vigorous shaking, thereby showcasing its robust gel-like properties. The metallogels exhibited Thermoreversibility behaviour, undergoing a reversible sol-gel transition upon temperature variation, where they get dissolved into a clear solution upon heating due to the disruption of weak non-covalent interactions and regained its gel state upon cooling by regeneration of the non-covalent interaction through self-assembly process, demonstrating a robust and reversible thermal response.

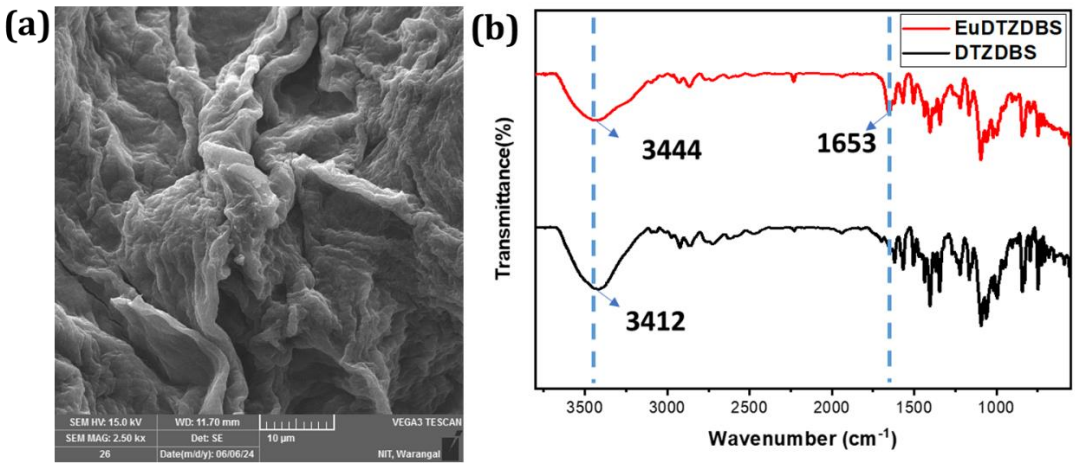

Figure 4.9. (a) SEM image of EuDTZDBS at 10µm and (b) Comparison of FTIR spectra of DTZDBS and EuDTZDBS

The metallogels were tested for their response to various salts, including NH_4OAc, NH_4OH, NaI, NaBr, NaCl, NaF, $NaHCO_3$, and $NaHSO_4$. Notably, the addition of ammonium salts (NH_4OAc and NH_4OH) induced a sol-gel transition, converting the metallogel to a sol state. However, upon subsequent addition of HCl to the resulting sol, the gel state was restored, demonstrating a reversible sol-gel transition. The gel-to-sol transition in the presence of ammonium salts can be attributed to a combination of factors. Ammonium ions disrupt the hydrogen bonding network between the metallogel components, and compete with metal-ligand bonds through ion-dipole interactions, potentially destabilizing the gel structure, leading to the breakdown of the gel and the addition of HCl displaces the ammonium ions from interfering in the metal-ligand interactions, thereby regenerating the gel. This observation highlights the metallogels sensitivity to specific ions. Upon addition of triethyl amine (TEA), the metallogel transforms into a sol state, likely due to disruption of hydrogen bonding and coordination with metal centers. However, the subsequent introduction of trifluoroacetic acid (TFA) induces a reversal of this process, reforming the gel state. This observation suggests that TFA re-establishes the hydrogen bonding network, protonates ligands, and displaces coordinated TEA, restoring the original metal-ligand bonds and gel structure. The metallogel EuDTZDBS exhibits a multifaceted responsive behaviour, demonstrating reversible thermo-, ion-, and pH-responsive properties, highlighting its potential for stimuli-responsive applications (Figure 4.10).

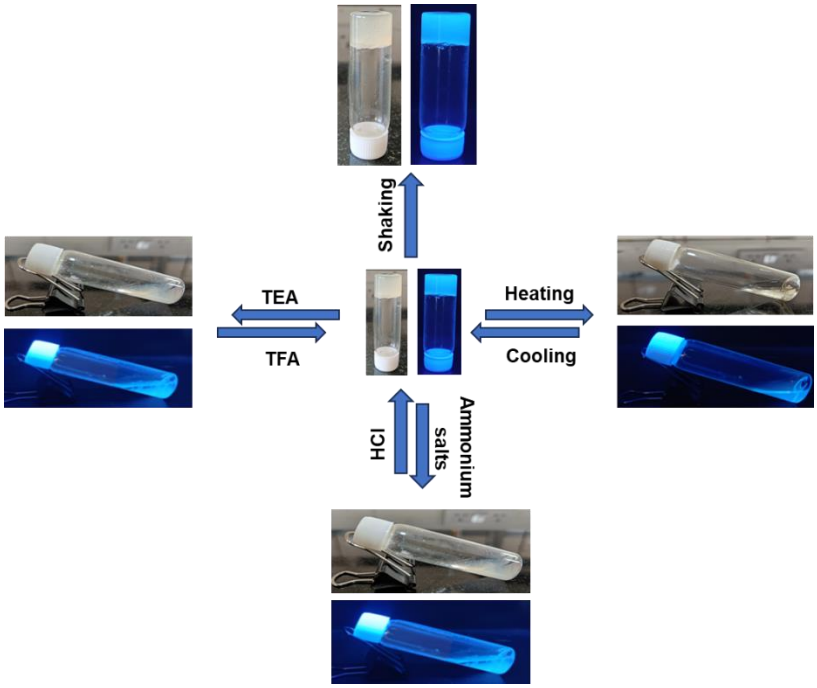

Figure 4.10. Stimuli-responsive properties of EuDTZDBS metallogels in visible light and UV light

The key advantage of LMWG lies in the reversible nature of their non-covalent interactions, which enables the gels to heal and recover to their original structure following deformation.

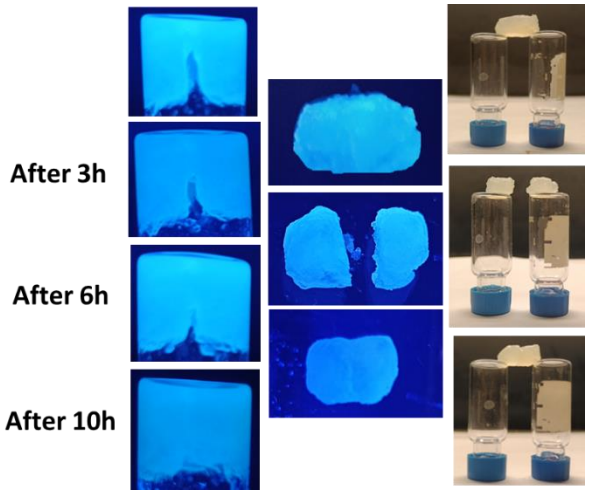

Figure 4.11. Demonstration of self-healing ability of EuDTZDBS metallogels in UV and visible light.

The self-healing ability of the metallogel was investigated by intentionally inflicting damage through cutting. Notably, the gel demonstrated autonomous self-healing, as the cut disappeared spontaneously within a few hours without the need for external stimuli. Furthermore, when the gel was severed into two separate pieces and placed in close proximity, the blocks spontaneously recombined, highlighting the metallogel's remarkable self-healing ability (Figure 4.11)

The photophysical properties of the synthesized metallogels were investigated using UV-vis spectrometry. UV spectra of the metallogels have been recorded from 360-600nm, as shown in Figure 4.12 (inset). The optical band gap was obtained from the careful analysis of the Tauc's plot obtained from the UV spectrum, using the equation:

$$\alpha h\nu = A(h\nu - E_g)^n$$

where α is the absorption coefficient, h is Planck's constant, ν is the frequency of light, A is energy dependent constant (taken as 1), Eg is the band gap, and n is the electron transition process-dependent constant (for direct transition n = 1/2). From Figure 4.12, it is observed that the material has a direct optical band gap of 4.357 eV. The presence of a wide band gap confirms the semiconducting nature of the metallogels and it inspires to further investigate the charge transfer properties of the metallogel. These unique properties of Wide bandgap semiconductors enable them to find application in power electronics, aerospace, and automotive industries, where high performance and reliability are paramount.[67,68]

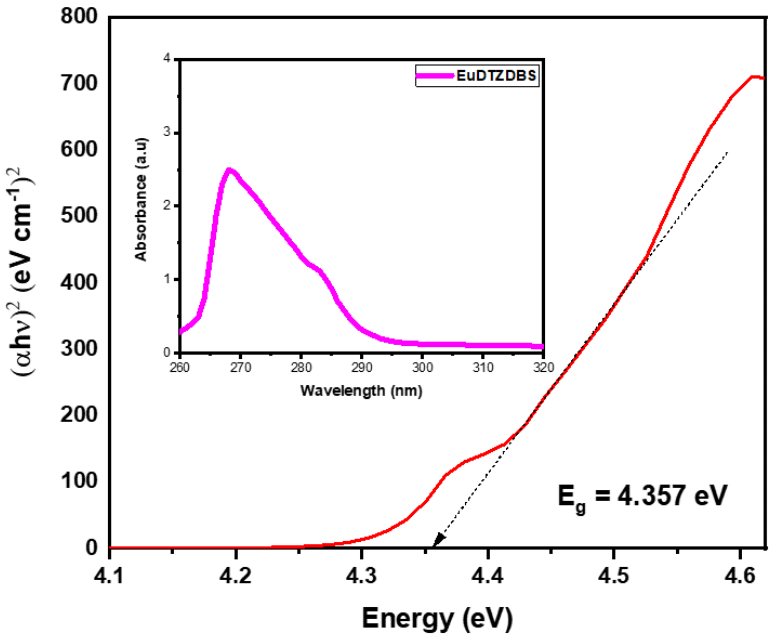

Figure 4.12. Tauc's plot of EuDTZDBS and UV-Vis spectrum of EuDTZDBS (Inset)

To investigate the charge transport characteristics of the metallogels, a metal-semiconductor junction as a thin film device was fabricated. The device architecture consisted of coating the metallogel material on ITO-coated glass, which served as the substrate as well as a cathode. Subsequently, an aluminium metal layer was deposited on top of the metallogel layer, acting as the anode. This sandwich structure enabled the formation of a metal-semiconductor junction, allowing for the study of charge transport properties across the interface. The resulting device

was then characterized to elucidate the metallogel's semiconducting behaviour, charge carrier mobility, and potential applications in electronic devices. The current-voltage (I-V) behaviour is investigated for the fabricated junction diode with a bias voltage applied in the range of ±2 V at ambient temperature (28°C). The I-V studies were performed under light and dark conditions, to check its photo-responsive properties. The conductivity of the junction diode is calculated to be 6.25 x 10^{-5} Sm^{-1} which signifies EuDTZDBS as a typical semiconductor material. The I–V graph of metallogels thin film device (Figure 4.13) exhibits nonlinear rectifying behaviour, which indicates the formation of a Schottky barrier diode at the Al/metallogel boundary. Hence, the fabricated diode can be called a Schottky diode.

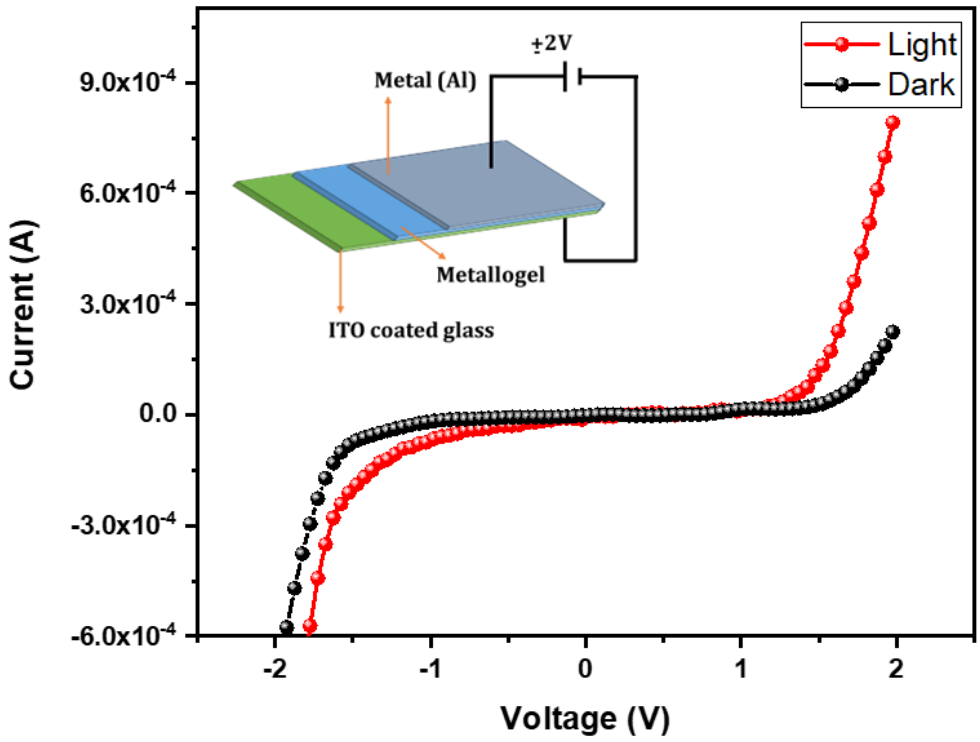

Figure 4.13. I-V characteristic curves in light and dark conditions. Fabrication of Schottky diode (Inset).

Notably, the device exhibited a significant increase in current generation under light conditions compared to dark conditions. This phenomenon is attributed to the photo-induced energy transfer from the tetrazole ring to the metal ion, which enhances the charge transport properties of the metallogel. In contrast, under dark conditions, the energy transfer is relatively low, resulting in reduced current generation at the same potential. This observation highlights the photo-responsive behaviour of the metallogel-based device, suggesting its potential applications in photovoltaic and optoelectronic devices. It is worth mentioning that the metallogel-based device, fabricated in this study, exhibits a self-healing Schottky diode property.

4.5 Experimental section

4.5.1 Materials and Methods

Materials and experimental methods for gelation studies, morphological analysis, rheological studies, and FTIR analysis are given in Chapter 2a

4.5.2 Synthesis

4.5.2.1 Synthesis of DNDBS

To a stirred solution of D-Sorbitol (1 mmol) in acetonitrile (10 mL) at rt under N_2 atmosphere, *p*-Cyanobenzaldehyde (2 mmol) and Amberlyst were added. The reaction mixture was stirred for another 24 h at reflux conditions. After completion of the reaction confirmed by TLC, the reaction mixture was allowed to cool down to room temperature. The formed precipitate is dissolved in hot cyrene and separated the catalyst by filtration. The cyrene solution is refrigerated for crystallization. The product is filtered, washed with water, and dried under a vacuum. The product was obtained as a white solid.

4.5.2.2 Synthesis of MTZDBS

To the hot solution of DNDBS (1 equiv) in ChCl:EG (1:2) DES, 0.2 equiv. of TEA and 3 equiv. of NaN_3 is added and allowed to form a gel under the co-gelation method. The formed gel is subjected to 60°C temperature and the reaction proceeded for 48 h. After completion of the reaction, the gel is placed in a beaker containing an acidic buffer and stirred for 5 minutes. The obtained precipitate is filtered and washed with hot THF. The precipitate is dried under a vacuum to obtain a pale-yellow solid.

4.5.2.3 Synthesis of DTZDBS

To the solution of DNDBS (1 equiv.) in ChCl:EG (1:2) DES, 0.2 equiv. of TEA and 3 equiv. of NaN_3 is added and heated to 120°C for 72 h. After completion of the reaction, the hot solution is poured into a beaker containing an acidic buffer. The obtained precipitate is filtered and washed with hot THF. The precipitate is dried under a vacuum to obtain a pale-yellow solid.

4.5.3 Fabrication of metallogel

To a 2wt/v % of DTZDBS dissolved in 1mL DMF in a vial, an equal concentration of respective metal ion solution in 1mL of water is added and kept in sonication for 1min to obtain strong metallogels.

4.5.4 Fabrication of Schottky diode

To fabricate a metallogel-based thin film device, ITO coated glass substrate is washed using an ultrasonic cleaner in a soap solution, and deionized water followed by isopropanol and acetone for 10 minutes each. After washing the ITO glass substrates are subjected to annealing at 70 °C in the presence of N_2 for 10 minutes. The metallogel is coated on the ITO glass using the drop casting method. Aluminium is used as a metal electrode. To perform the electrical measurement, the Schottky diode is formed by sandwiching the metallogel film between the ITO glass and aluminium metal. All the Electrical properties were obtained by analysing the device's current-voltage (I–V) characteristics using a Keithley Source meter (model no. 2401) with a two-probe method. The device fabrication and measurement studies are performed at ambient temperature (28 °C).

4.6 Characterisation studies

4.6.1 ^{1}H-NMR, ^{13}C-NMR, and HRMS characterization data of synthesized compounds

DNDBS: The product was obtained as a white solid with a 72% yield.

^{1}H NMR (400 MHz, DMSO-d_6) δ: 7.87 (3, J = 8.6 Hz, 4H), 7.71 – 7.60 (m, 4H), 5.77 (s, 2H), 4.96 (s, 1H), 4.50 (s, 1H), 4.22 (dd, J = 8.7, 1.7 Hz, 2H), 4.02 (s, 1H), 3.91 (dd, J = 9.3, 1.8 Hz, 1H), 3.78 (s, 1H), 3.71 (s, 1H), 3.60 (t, J = 12.5 Hz, 2H).

^{13}C NMR (100 MHz, DMSO-d_6) δ:143.80, 143.54, 133.87, 132.85, 132.79, 132.68, 132.48, 131.35, 128.86, 127.88, 127.71, 127.48, 126.35, 119.15, 111.86, 99.02, 97.89, 78.48, 71.16, 69.93, 68.76, 68.34, 67.38.

HRMS (ESI, m/z): $C_{22}H_{20}N_2O_6$; $[M+H]^+$ calculated : 431.1219; $[M+H]^+$ found : 431.1218

MTZDBS: The product was obtained as a pale brown solid with 89% yield.

^{1}H NMR (400 MHz, DMSO-d_6) δ: 8.07 (dt, J = 8.4, 3.3 Hz, 2H), 7.93 – 7.85 (m, 2H), 7.73 – 7.62 (m, 4H), 5.78 (d, J = 5.4 Hz, 2H), 4.93 (s, 1H), 4.29 – 4.19 (m, 3H), 4.03 (s, 1H), 3.92 (m, J = 9.3, 4.6, 1.6 Hz, 1H), 3.81 (m, J = 10.4, 5.8, 3.2 Hz, 2H), 3.63 (m, J = 11.0, 5.4, 2.2 Hz, 2H), 3.49 (m, J = 11.4, 7.8, 5.6 Hz, 1H).

^{13}C NMR (100 MHz, DMSO- d_6) δ: 156.34, 143.87, 143.62, 141.40, 141.11, 132.69, 132.62, 127.59, 127.51, 127.47, 127.09, 127.03, 111.86, 99.15, 98.55, 77.99, 70.66, 69.83, 68.94, 68.07, 63.05.

HRMS (ESI, m/z): $C_{22}H_{21}N_5O_6$; $[M+H]^+$ calculated : 452.1570; $[M+H]^+$ found : 452.1553

DTZDBS: The product was obtained as a pale brown solid with 76% yield.

^{1}H NMR (400 MHz, DMSO-d_6) δ 8.09 (dd, J = 8.4, 2.6 Hz, 4H), 7.70 (t, J = 8.7 Hz, 4H), 5.79 (s, 2H), 4.92 (s, 1H), 4.43 (s, 1H), 4.31 – 4.19 (m, 3H), 4.04 (d, J = 1.8 Hz, 1H), 3.93 (dd, J = 9.3, 1.7 Hz, 1H), 3.83 (m, J = 5.6, 2.2 Hz, 1H), 3.65 (dd, J = 11.5, 2.2 Hz, 1H), 3.52 (d, J = 5.4 Hz, 1H).

^{13}C NMR (100 MHz, DMSO-d_6) δ :162.78, 155.81, 141.81, 141.53, 128.15, 127.60, 127.24, 127.16, 99.13, 78.09, 70.66, 69.83, 69.03, 68.12, 63.07.

HRMS (ESI, m/z) : $C_{22}H_{20}N_8O_6$; $[M+H]^+$ calculated: 495.1740; $[M+H]^+$ found : 495.1740.

4.6.2 ^{1}H, ^{13}C-NMR and HRMS spectra of synthesized compounds

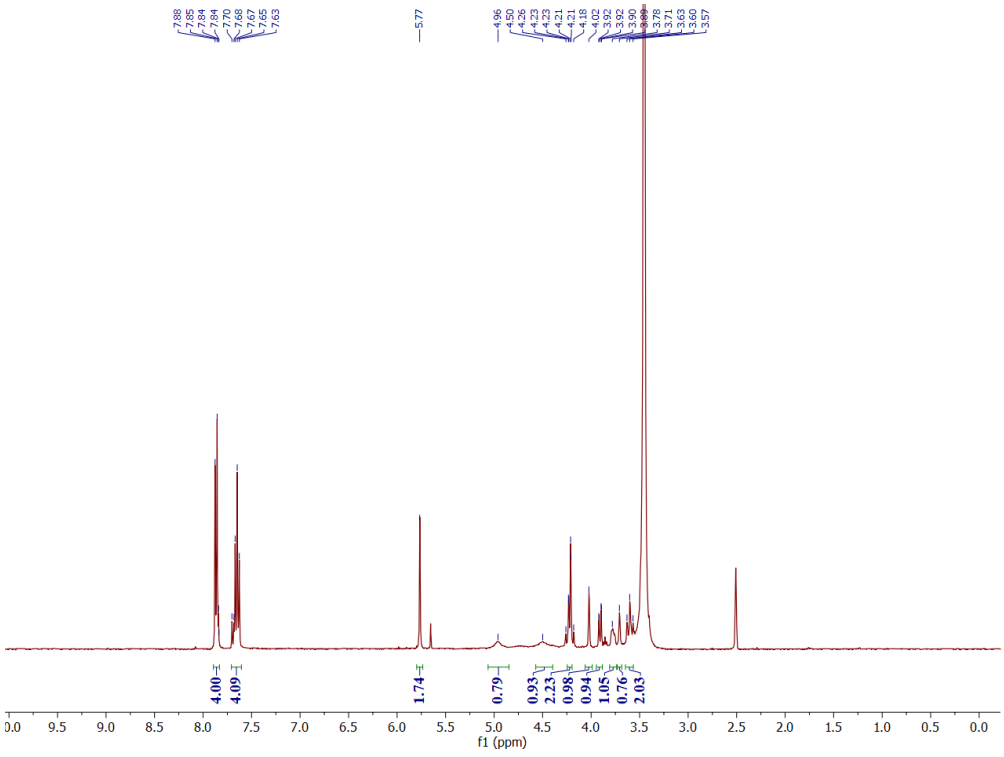

Figure 4.14. ^{1}H NMR (400MHz) Spectrum of DNDBS in DMSO-d_6 at 28 °C.

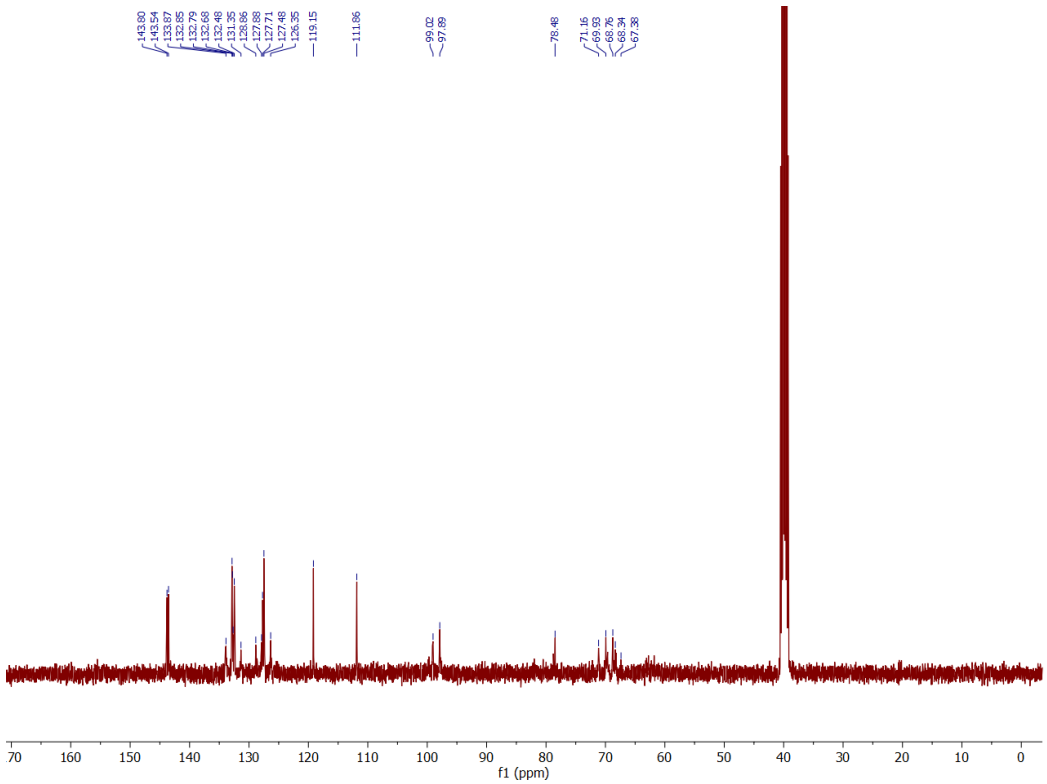

Figure 4.15. ^{13}C NMR (100MHz) Spectrum of DNDBS in DMSO-d_6 at 28 °C.

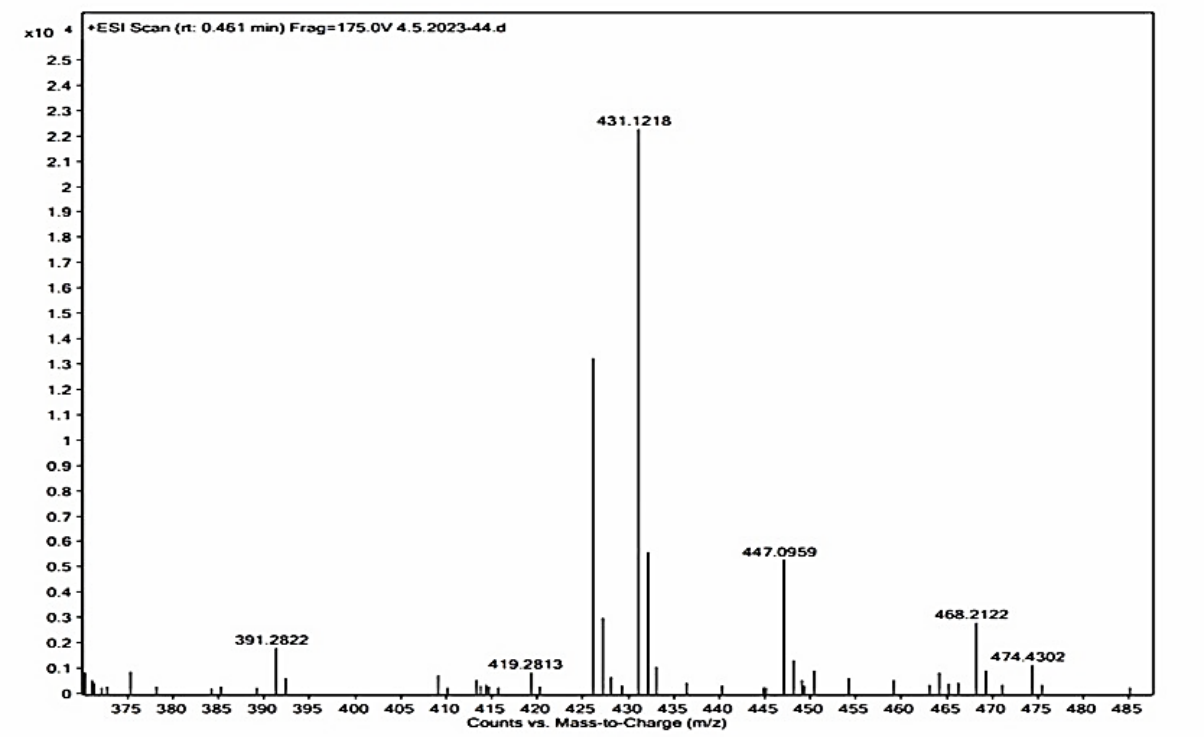

Figure 4.16. HRMS Spectrum of DNDBS.

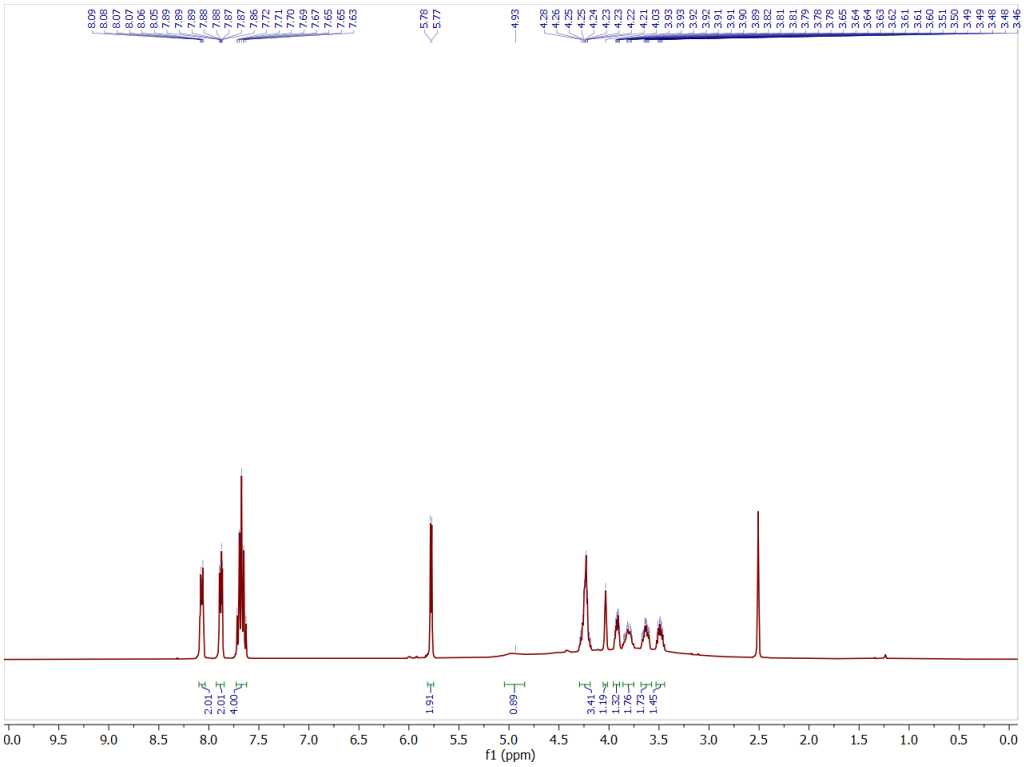

Figure 4.17. ^{1}H NMR (400MHz) Spectrum of MTZDBS in DMSO-d_6 at 28 °C.

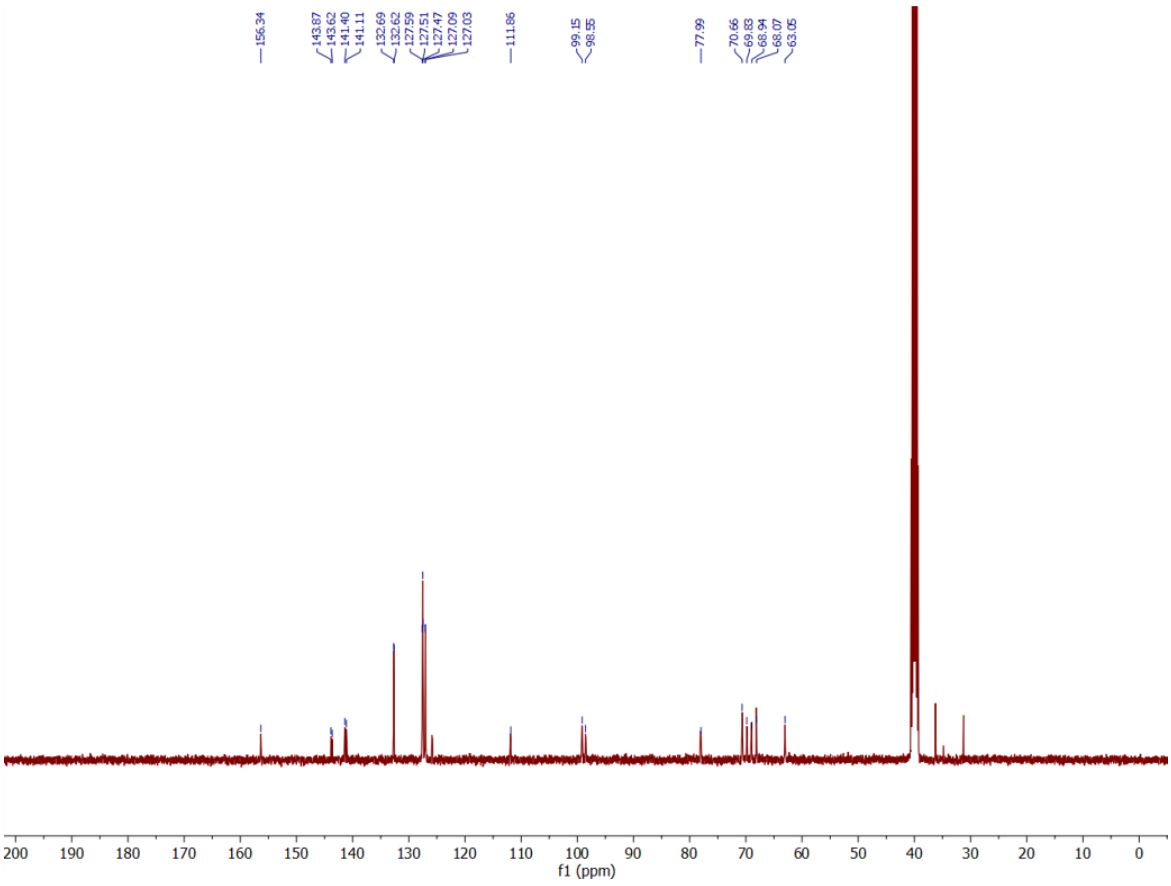

Figure 4.18. ^{13}C NMR (100MHz) Spectrum of MTZDBS in DMSO-d_6 at 28 °C.

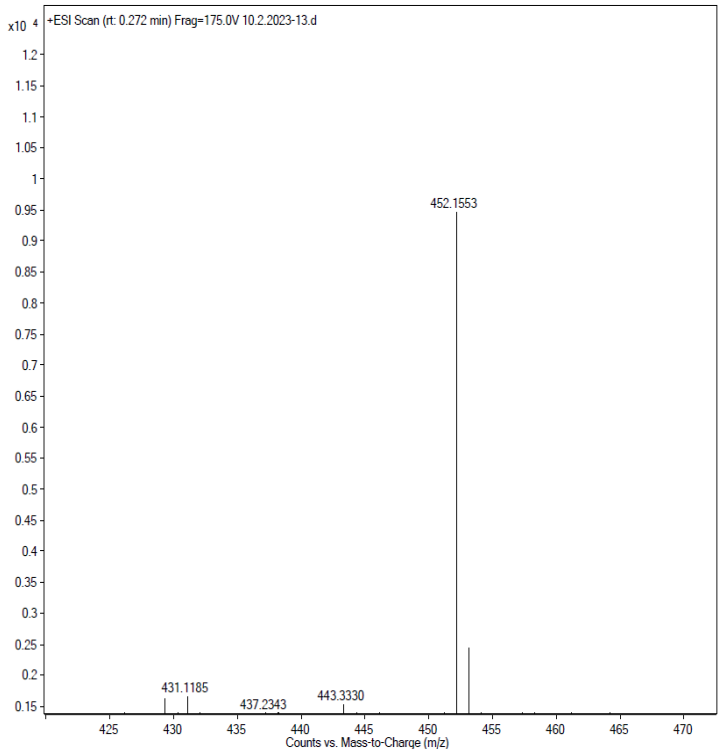

Figure 4.19. HRMS Spectrum of MTZDBS.

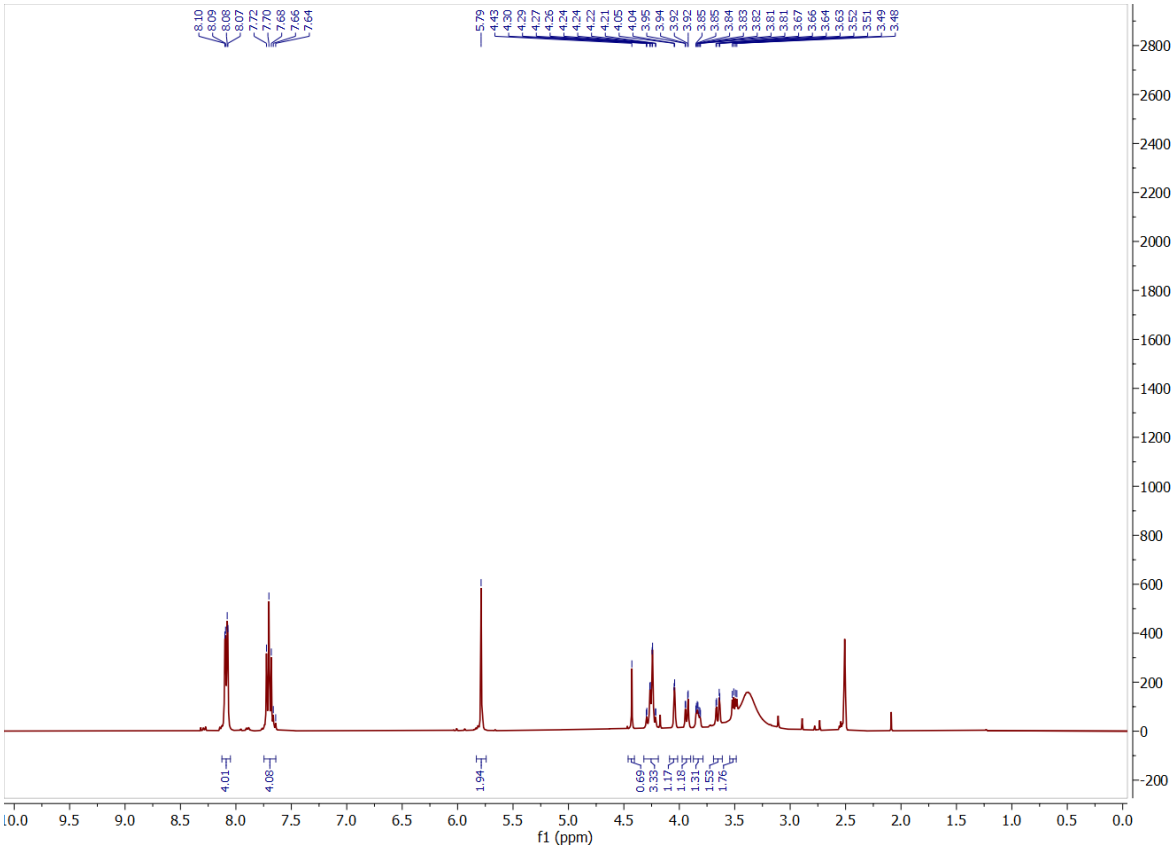

Figure 4.20. ^{1}H NMR (400MHz) Spectrum of DTZDBS in DMSO-d_6 at 28 °C.

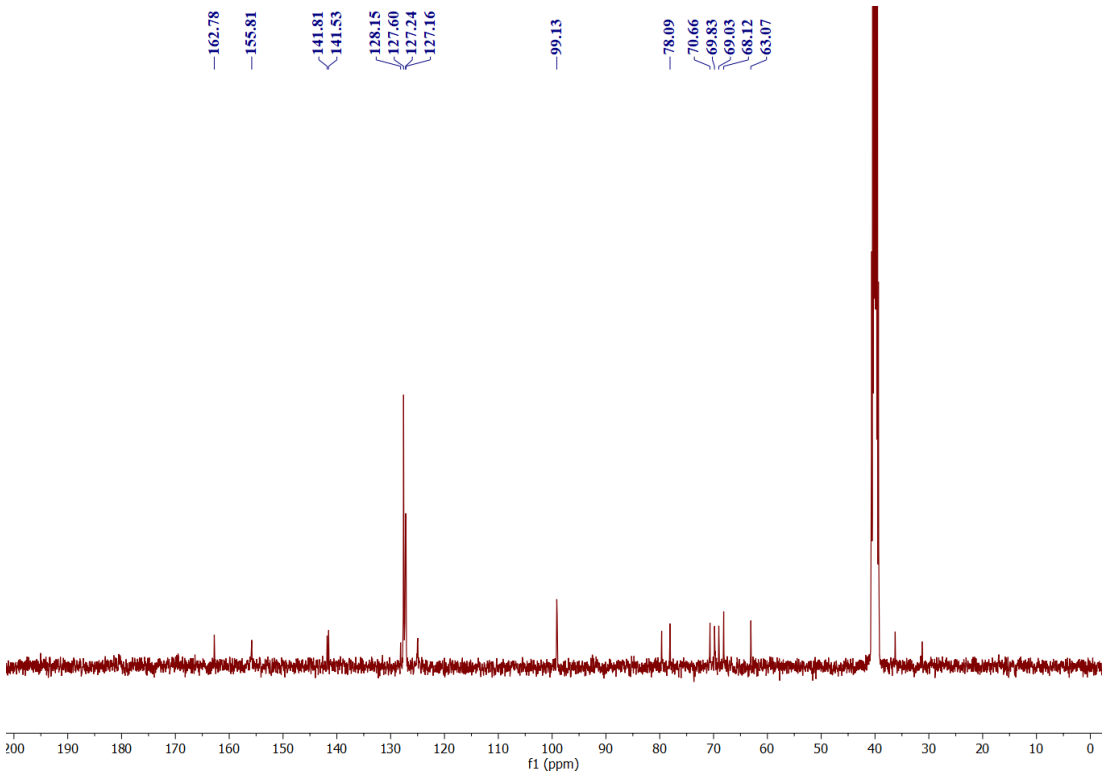

Figure 4.21. ^{13}C NMR (100MHz) Spectrum of DTZDBS in DMSO-d_6 at 28 °C.

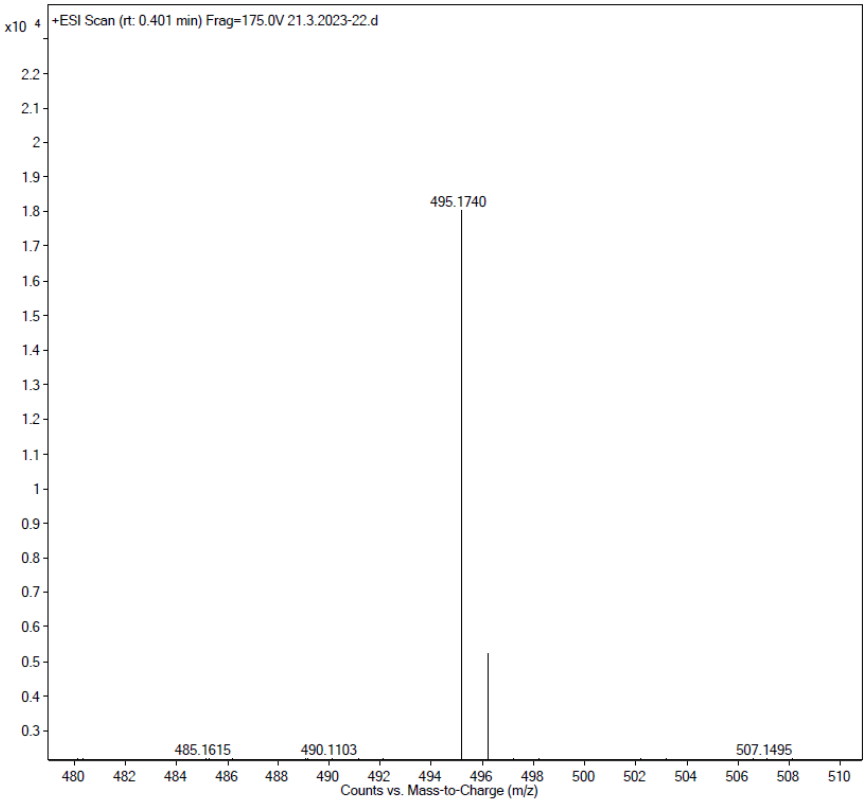

Figure 4.22. HRMS Spectrum of DTZDBS.

4.7 Conclusion

In this chapter, DNDBS were synthesized using the reaction conditions optimized in previous chapters in good yield. Using the confined reaction media approach, MTZDBS and DTZDBS were synthesized from DNDBS and sodium azide. The formed products are characterized using NMR, HRMS, and FTIR studies. Self-assembly studies revealed that MTZDBS and DTZDBS could able to form gel in various solvents. The formation of various metallogels from DTZDBS were presented in this chapter. One of the metallogels, Eu^{3+}-DTZDBS, is further for its charge transport ability, and the result revealed the potential in the fabrication of a self-healable, stimuli-responsive Schottky diode.

4.8 References

1 P. Dastidar, S. Ganguly and K. Sarkar, *Asian Chem. Editor. Soc.*, 2016, **11**, 2484–2498.

2 A. V. Lipowitz, *Leibigs Ann. Chem.*, 1841, **38**, 257–368.

3 B. Xing, M. Choi and B. Xu, *Chem. Commun.*, 2002, 362–363.

4 A. Fortunato and M. Mba, *Gels*, 2021, **7**, 85.

5 X. Ma, Y. Wang, Y. Lai, T. Ren, J. Tang, Y. Gao, Y. Geng and J. Zhang, *Soft Matter*, 2022, **18**, 9283–9290.

6 G. Yang, S. Li, N. Li, P. Zhang, C. Su, L. Gong, B. Chen, C. Qu, D. Qi, T. Wang and J. Jiang, *Angew. Chem. Int. Ed.*, 2022, **61**, e202205585.

7 F. Fages, *Angew. Chem. Int. Ed.*, 2006, **45**, 1680–1682.

8 W. S. Compel, *Dalt. Trans.*, 2016, **45**, 4509–4512.

9 M. K. Dixit, D. Chery, C. Mahendar, M. K. Dixit, D. Chery, C. Mahendar, C. Bucher, M. K. Dixit, D. Chery, C. Bucher and M. Dubey, *Inorg. Chem. Front.*, 2020, **7**, 991–1002.

10 T. Zhao, S. Chen, K. Kang, J. Ren and X. Yu, *Langmuir*, 2022, **38**, 1398–1405.

11 S. Majumdar, S. Sil, R. Sahu, M. Ghosh, G. Lepcha, A. Dey, S. Mandal, P. Pratim and B. Dey, *J. Mol. Liq.*, 2021, **338**, 116769.

12 A. De and R. Mondal, *ACS Omega*, 2018, **3**, 6022–6030.

13 Q. Lin, T. Lu, X. Zhu, B. Sun, Q. Yang and T. Wei, *Chem. Commun.*, 2015, **51**, 1635–1638.

14 P. S. L. Gelators, T. Tu, W. Fang, X. Bao, X. Li and K. H. Dötz, *Angew. Chem. Int. Ed.*, 2011, **123**, 6731–6735.

15 A. Y. Tam, K. M. Wong and V. W. Yam, *J. Am. Chem. Soc*, 2009, **131**, 6253–6260.

16 S. Yoon, W. J. Kwon, L. Piao, S. Kim, L. G. Chem and Y. Daejeon, *Langmuir*, 2007, **23**, 8295–8298.

17 G. R. Desiraju, *Angew. Chem. Int. Ed.*, 1995, **34**, 2311–2327.

18 Pathik Sahoo, V. G. Puranik, A. K. Patra and P. U. Sastryc and P.i Dastidar, *Soft Matter*, 2011, **7**, 3634–3641.

19 B. Adhikari, R. Afrasiabi and H. Kraatz, *Organometallics*, 2013, **32**, 5899–5905.

20 R. Afrasiabi and H.-B. Kraatz, *Chem. Eur J.*, 2013, **19**, 158623–15871.

21 Z. Sun, Z. Li, Y. He, R. Shen, L. Deng, M. Yang, Y. Liang and Y. Zhang, *J Am Chem Soc*, 2013, **135**, 13379–13386.

22 K. Liu, S. Zang, R. Xue, J. Yang, L. Wang, J. Huang and Y. Yan, *ACS Appl. Mater. Interfaces.*, 2018, **10**, 4530–4539.

23 R. A. Green, S. Baek, L. A. Poole-warren, P. J. Martens, R. A. Green, S. Baek, L. A. Poole-warren, P. J. Martens, R. A. Green, S. Baek, L. A. Poole-warren and P. J. Martens, *Sci. Technol. Adv. Mater*, 2010, **11**, 014107.

24 Z. Sun, F. Lv, L. Cao, L. Liu, Y. Zhang and Z. Lu, *Angew. Chem. Int. Ed.*, 2015, **54**, 7944–7948.

25 O. Kotova, R. Daly, C. M. G. dos Santos, M. Boese, P. E. Kruger, J. J. Boland and T. Gunnlaugsson, *Angew. Chem. Int. Ed.*, 2012, **51**, 7208–7212.

26 X. Yu, Z. Wang, Y. Li, L. Geng, J. Ren and G. Feng, *Inorg. Chem.*, 2017, **56**, 7512–7518.

27 P. Casuso, P. Carrasco, I. Loinaz, H. J. Grande and I. Odriozola, *Org. Biomol. Chem.*, 2010, **8**, 5455–5458.

28 S. Ghosh, J. Rasmusson and O. Inganäs, *Adv. Mater.*, 1998, **10**, 1097–1099.

29 S. Ghosh and O. Inganäs, *Adv. Mater.*, 1999, **11**, 1214–1218.

30 H. Bunzen, Onappa, E. Kalenius, S. Hietala and E. Kolehmainen, *Chem. Eur J.*, 2013, **19**, 12978–12981.

31 M. Tao, K. Xu, S. He, H. Li, L. Zhang, X. Luo and W. Zhong, *Chem. Commun.*, 2018, **54**, 4673–4676.

32 M. Cametti and Zoran Dzolic, *Chem. Commun.*, 2014, **50**, 8273–8286.

33 D. R. Dreyer, S. Park, C. W. Bielawski and R. S. Ruoff, *chem. Soc. Rev.*, 2010, **39**, 189–227.

34 N. Jiang, R. Wang, X. You and Y. Geng, *J. Mater. Chem. C.*, 2021, **9**, 13331–13337.

35 K. M. Orcutt, W. S. Jones, A. Mcdonald, D. Schrock and K. J. Wallace, *sensors*, 2010, **10**, 1326–1337.

36 C. Wang, Q. Han, P. Liu, G. Zhang, L. Song, X. Zou and Y. Fu, *ACS Sensors*, 2021, **6**, 252–258.

37 J. Yago, R. Silva, L. Lourenc, F. Gabriel, M. Mauricio, I. Bezerra, V. Alves, J. Nunes, D. S. Ferro, E. Barreto, I. Ta, W. M. De Azevedo and S. Alves, *ACS Appl. Mater. Interfaces.*, 2017, **9**, 16458–16465.

38 N. Alam, S. Mondal, S. Sahoo and D. Sarma, *ACS Appl. Mater. Interfaces.*, 2023, 1201–1212.

39 M. Martnez, O. Kotova, M. E. Mo, A. P. Bell, T. Mccabe, J. J. Boland and G. T, *J Am Chem Soc*, 2015, **137**, 1983–1992.

40 X. Tao, X. Chen, T. Chen, G. Du, Y. Wang and Q. Li, *Colloids Surfaces A Physicochem. Eng. Asp.*, 2022, **634**, 127910.

41 Y. Yang, W. Liu, Q. Zhong, J. Zhang, B. Yao, X. Lian and H. Niu, *ACS Appl. Nano Mater.*, 2021, **4**, 4735–4745.

42 Q. Zhou, X. Dong, J. Yuan, B. Zhang, S. Lu, Y. Xiong, Y. Liao, Q. Wang, Y. Yang and H. Wang, *J. Mol. Liq.*, 2019, **292**, 111373.

43 M. Xue, M. Chen, W. Chang, R. Chen and P. Li, *Colloid Polym. Sci.*, 2020, **298**, 233–241.

44 B. Zhang, X. Dong, Y. Xiong, Q. Zhou, S. Lu, Y. Liao, Y. Yang and H. Wang, *Dalt. Trans.*, 2020, **49**, 2827–2832.

45 T. Gorai and U. Maitra, *Angew. Chem. Int. Ed.*, 2017, **56**, 10730–10734.

46 S. Bhowmik and U. Maitra, *Chem. Commun.*, 2012, **48**, 4624–4626.

47 S. Banerjee, R. Kandanelli, S. Bhowmik and U. Maitra, *Soft Matter*, 2011, **7**, 8207–8215.

48 S. Bhowmik, S. Banerjee and U. Maitra, *Chem. Commun.*, 2010, **46**, 8642–8644.

49 T. S. Mahapatra, H. Singh, A. Maity, A. Dey, S. K. Pramanik, E. Suresh and A. Das, *J. Mater. Chem. C*, 2018, **6**, 9756–9766.

50 R. Kyarikwal, N. Malviya, A. Chakraborty and S. Mukhopadhyay, *ACS Appl. Mater. Interfaces*, 2021, **13**, 59567–59579.

51 H. Yang, A. Wang, L. Zhang, X. Zhou, G. Yang, Y. Li, Y. Zhang, B. Zhang and Y. Feng, *New J. Chem.*, 2017, **41**, 15173–15179.

52 J. B. Beck and S. J. Rowan, *J Am Chem Soc*, 2003, **125**, 13922–13923.

53 P. Sutar, V. M. Suresh and T. K. Maji, *Chem. Commun.*, 2015, **51**, 9876–9879.

54 P. Chen, Q. Li, S. Grindy and N. Holten-andersen, *J Am Chem Soc*, 2015, **137**, 11590–11593.

55 J. Wang, S. Sun, B. Wu, L. Hou, P. Ding, X. Guo, M. A. C. Stuart and J. Wang, *Macromolecules*, 2019, **52**, 8643–8650.

56 A. A. Jawad, N. R. Jber, B. S. Rasool and A. K. Abbas, *Al-Nahrain J. Sci.*, 2023, **26**, 1–7.

57 F. Y. Vahora, M. C. Makwana, M. K. Mishra and K. M. Vyas, *Chem. Eng. J.*, 2024, **488**, 150806.

58 J. H. Lee, Y. E. Baek, K. Y. Kim, H. Choi and J. H. Jung, *Supramol. Chem.*, 2016, **0278**, 1–4.

59 N. Malviya, R. Ranjan, C. Sonkar, S. M. Mobin and S. Mukhopadhyay, *ACS Appl. Nano Mater.*, 2019, **2**, 8005–8015.

60 S. Sarkar, S. Dutta, S. Chakrabarti, P. Bairi and T. Pal, *ACS Appl. Mater. Interfaces.*, 2014, **6**, 6308–6316.

61 K. Aruchamy, S. Ramasundaram, S. Divya, M. Chandran, Y. Kyusik and Tae H Oh, *Gels*, 2023, **9**, 585.

62 B. Saavedra, A. Meli, C. Rizzo, D. J. Ramón and F. D'Anna, *Green Chem.*, 2021, **23**, 6555–6565.

63 B. P. Krishnan and K. M. Sureshan, *J. Am. Chem. Soc.*, 2017, **139**, 1584–1589.

64 S. C. Sarngadharan, J. Aronson, C. Gelbaum, K. Gri, J. Faris, A. B. Moihdeen, M. Patel, M. Malone, K. Richman, C. A. Eckert, C. L. Liotta and P. Pollet, *Org. Process Res. Dev.*, 2022, **26**, 1432–1441.

65 B. C. Roy and T. Singha Mahapatra, *Soft Matter*, 2023, **19**, 1854–1872.

66 Y. Ma, F. Yu, S. Zhang, P. She, S. Liu, W. Huang and Q. Zhao, *CCS Chem.*, 2021, **2**, 2437–2444.

67 L. C. Tien and C. H. Ho, in *Gallium Oxide: Technology, Devices and Applications*, Elsevier Inc., 2018, pp. 67–90.

68 A. Yoshikawa, H. Matsunami and Y. Nanishi, in *Wide Bandgap Semiconductors: Fundamental Properties and Modern Photonic and Electronic Devices*, 2007, pp. 1–24.

Conclusion and Future Perspectives

A series of DBS derivatives were synthesized and studied its self-assembly behaviour. These derivatives displayed potential in forming organogel and eutectogel. The use of gel as a confined medium for various organic reactions is demonstrated. Advanced soft materials, such as stimuli-responsive H_2S delivery systems and self-healing Schottky diode were fabricated. Assembled soft materials derived from DBS derivatives can also be explored in drug delivery, solid-state electrolytes, confined reaction media, and flexible electronics.

List of Publications

1. **Facile Synthesis and Self-Assembly of Pharmaceutically Important Oligobenzylidine-D-Sorbitol Dialdehydes: Direct Encapsulation and Stimuli Responsive Delivery of H_2S.**

   Vara Prasad Rebaka, Yogendra Kumar, Tohira Banoo, Arun Kumar Rachamalla and Nagarajan Subbiah, *Mater. Adv.*, 2024, **5**, 5471.

2 **Regioselective synthesis of 4-arylamino-1, 2-naphthoquinones in eutectogel as a confined reaction medium using LED light.**

Vara Prasad Rebaka, Yogendra Kumar, R Arun Kumar, Tohira Banoo and Subbiah Nagarajan, *Org. Biomol. Chem*., 2024, **2**, 3876-3881.

3 **Sophorolipids and rhamnolipids as a biosurfactant: Synthesis and applications**

Rebaka Vara Prasad, Rachamalla Arun Kumar, Devendra Sharma, Atul Sharma, Subbiah Nagarajan,, Green Sustainable Process for Chemical and Environmental Engineering and Science, *Elsevie*r, 2021, Pages 423-472.

4 **State of the Art and New Perspectives in Oleogels and Applications**

Vara Prasad Rebaka, Arun Kumar Rachamalla, Srishti Batra, Nagarajan Subbaiah, Sustainable Green Chemical Processes and their Allied Applications. Nanotechnology in the Life Sciences. *Springer*, 2020, Pages:151-182.

5 **Anti-biofilm activities against food pathogens**

Rachamalla Arun Kumar, Rebaka Vara Prasad, Subbaiah Nagarajan, Applications of Next Generation Biosurfactants in the Food Sector, *Academic Press*, 2023, Pages 479-508.

6 **Glycolipid-Based Oleogels and Organogels: Promising Nanostructured Structuring Agents**

Ayyapillai Thamizhanban, Srikanth Balaji, Krishnamoorthy Lalitha, Yadavali Siva Prasad, R. Vara Prasad, R. Arun Kumar, C. Uma Maheswari, Vellaisamy Sridharan, and Subbiah Nagarajan. *J. Agric. Food Chem.*, 2020, **68**, 50, 14896-14906.

7 **A facile synthesis of amphiphilic N-glycosyl naphthalimides and fabrication of flexible semiconductors using molecular self-assembly**

Arun Kumar Rachamalla, Vara Prasad Rebaka, Tohira Banoo, Ravinder Pawar, Mohmmad Faizan, Krishnamoorthy Lalitha and Subbiah Nagarajan. *Green Chem.*, 2022, **24**, 2451-2463.

8 **Electronically Robust Self-Assembled Supramolecular Gel as a Potential Material in Triboelectric Nanogenerator**

Arun Kumar Rachamalla, Supraja Potu, Vara Prasad Rebaka, Tohira Banoo, Yogendra Kumar, Dr. C. Uma Maheswari, Dr. Vellaisamy Sridharan, Dr. Rakesh Kumar Rajaboina, Dr. Subbiah Nagarajan, *Chem. Eur. J.*, 2023, **29**, e202301076.

9 **A high performance triboelectric nanogenerator using assembled sugar naphthalimides for self-powered electronics and sensors**

Arun Kumar Rachamalla, Madathil Navaneeth, Tohira Banoo, Deepshikha, Vara Prasad Rebaka, Yogendra Kumar, Rakesh Kumar Rajaboina, Subbiah Nagarajan, *J. Chem. Eng.*, 2024, **490**, 151800.

10 **Hybrid hydrogels derived from renewable resources as a smart stimuli responsive soft material for drug delivery applications**

Vandana Singh, Yadavali Siva Prasad, Arun Kumar Rachamalla, Vara Prasad Rebaka, Tohira Banoo, C.Uma Maheswari, Vellaisamy Sridharan, Krishnamoorthy Lalitha, and Subbiah Nagarajan. *RSC Adv*., 2022, **12**, 2009.

11 **Supramolecular gels of gluconamides derived from renewable resources:Antibacterial and anti-biofilm applications**

Yadavali Siva Prasad, S. Manikandan, Krishnamoorthy Lalitha, Miryala Sandeep, R. Vara Prasad, R. Arun Kumar, C.S. Srinandan, C. Uma Maheswari, Vellaisamy Sridharan, Subbiah Nagarajan . *Nano Select*., 2020; **1**,510–524.

12 **Self-assembling nanoarchitectonics of twisted nanofibers of fluorescent amphiphiles as chemo-resistive sensor for methanol detection**

Vandana Singh, Ayyapillai Thamizhanban, Krishnamoorthy Lalitha, Dinesh Kumar Subbiah, Arun Kumar Rachamalla, Vara Prasad Rebaka, Tohira Banoo, Yogendra

Kumar, Vellaisamy Sridharan, Asrar Ahmad, Uma Maheswari Chockalingam, John Bosco Balaguru Rayappan, Azmat Ali Khan, Subbiah Nagarajan, 2023, *Gels*, **9**, 6, 442.